RIGA TECHNICAL UNIVERSITY

Armands Šenfelds

RESEARCH AND DEVELOPMENT OF DC MICROGRIDS FOR ROBOTIC MANUFACTURING

Doctoral Thesis

RTU Press
Riga 2023

RIGA TECHNICAL UNIVERSITY
Faculty of Electrical and Environmental Engineering
Institute of Industrial Electronics and Electrical Engineering

Armands Šenfelds
Doctoral Student of the Study Programme
"Computerised Control of Electrical Technologies"

RESEARCH AND DEVELOPMENT OF DC MICROGRIDS FOR ROBOTIC MANUFACTURING

The Doctoral Thesis

Scientific supervisor
Academician Professor Dr. habil. sc. ing
LEONĪDS RIBICKIS

RTU Press
Riga 2023

Šenfelds, A. Research and Development of DC Microgrids for Robotic Manufacturing. Summary of the Doctoral Thesis. Riga: RTU Press, 2023. 202 p.

Published in accordance with the decision of the Promotion Council "RTU P-14" of 4 October 2023, Minutes No. 04030-9.12.2/6.

The Thesis was supported by the European Social Fund within Project No. 8.2.2.0/20/I/008, "Strengthening of PhD students and academic personnel of Riga Technical University and BA School of Business and Finance in the strategic fields of specialization" of the Specific Objective 8.2.2 "To Strengthen Academic Staff of Higher Education Institutions in Strategic Specialization Areas" of the Operational Programme "Growth and Employment".

Cover picture generated by openAI DALL-E/ChatGPT 4.0

DOCTORAL THESIS PROPOSED TO RIGA TECHNICAL UNIVERSITY FOR THE PROMOTION TO THE SCIENTIFIC DEGREE OF DOCTOR OF SCIENCE

To be granted the scientific degree of Doctor of Science (Ph. D.), the present Doctoral Thesis has been submitted for the defence at the open meeting of RTU Promotion Council on 29 December 2023 11.30 at the Faculty of Electrical and Environmental Engineering of Riga Technical University, 12/1 Āzenes Street, Room 212.

OFFICIAL REVIEWERS

Associate Professor Senior Researcher Dr. sc. ing. Jānis Zaķis
Riga Technical University

Prof. Dr. Ir. Rik W. De Doncker,
RWTH Aachen University, Germany

Senior Researcher PhD Toomas Vaimann
Tallinn University of Technology, Estonia

DECLARATION OF ACADEMIC INTEGRITY

I hereby declare that the Doctoral Thesis submitted for review to Riga Technical University for promotion to the scientific degree of Doctor of Science (Ph. D.) is my own. I confirm that this Doctoral Thesis has not been submitted to any other university for promotion to a scientific degree.

Armands Šenfelds ……. (signature)

Date: ……

The Doctoral Thesis has been prepared as a thematically united collection of scientific publications. It consists of a summary and 19 publications, and 1 patent. Publications have been written in English. The total number of publication pages is 202.

ACKNOWLEDGMENTS

I would like to express my deepest gratitude to my scientific supervisor, academician Professor Dr. habil. sc. ing. Leonīds Ribickis for his guidance, motivation and support in the scientific work.

I would also like to thank all employees of the RTU Institute of Industrial Electronics and Electrical Engineering, in particular Professor Ivars Raņķis, Professor Peteris Apse-Apsītis, Associate Professor Dāvis Meike for experience-based advice during the preparation of the Thesis, researchers Ansis Avotiņš, Mārcis Priedītis, Genadijs Zaļeskis for the support during the experimental research phase, my students Artūrs Paugurs and Oskars Bormanis, and researcher Kristaps Vītols for motivational discussions and excellent management of laboratory technical equipment.

During the research development phase, the time and support given by family and parents has been invaluable –, thank you very much!

CONTENTS

GENERAL OVERVIEW OF THE THESIS

Topicality of the research

Automated manufacturing developments are closely linked to the use of industrial robot equipment. According to research by the International Federation of Robotics (IFR), the annual number of newly installed robots globally reaches a historical high and exceeds half a million units. The total number of industrial robot machines worldwide in 2022 is estimated at 3,903,633 units, an annual increase of 12 %[1]. The total number of robots in Europe is estimated at 728,390 units, with a steady annual growth trend of 6 % [2]. Given that electricity is the primary energy source for modern and robotic production processes, the need for energy-efficient electricity supply solutions remains relevant. In the context of the possible transfer of production processes from Asia to the European region and higher electricity costs, initiatives to implement optimal energy technologies have a direct economic benefit. Public willingness and determination to change the structure of existing energy sources and move towards climate-neutral solutions also define new cooperation models and require a more flexible approach to developing electric energy management systems for production purposes. According to the road map defined by the European Commission Green Deal [3] to become a climate-neutral continent by 2050, programmes that contribute to changing energy systems in the production sector [4] have been created. Combinations of new renewable energy sources with energy storage, electromobility and efficient lighting and heating consumption promote the interest of engineers when considering combining or replacing existing AC infrastructure with DC electricity transmission technology [5]. The Thesis explores and demonstrates solutions for energy-efficient and flexible use of electrical energy in robotic production conditions by introducing DC electrical power transmission elements.

Main hypotheses and objectives

Hypotheses

1. Energy efficiency can be improved for industrial robot applications by utilizing electric energy recovery and reuse.
2. DC-type power supply solutions are suitable for implementing dynamic energy exchange processes.
3. DC microgrid is suitable for implementing energy-efficient robotic production systems.

Objectives

1. Analyse existing industrial robot technology as typical electric drive systems and explore new methods for practical energy recovery that are possible in realizing robotic manipulator motion tasks.
2. Explore improvements in the energy efficiency and functionality parameters of new robotic manufacturing plants using DC type power supply solutions and equipment.

In order to achieve the Thesis objectives, the following tasks were assigned:

- Analyse the operation of typical AC robot drive systems and define the characteristic parameters for controlling the process of dissipating braking energy.
- Development of modification solutions for existing robot drive system functionality for the energy recovery, storage and redistribution of braking energy in multi-robot systems.
- Develop examples of a local DC microgrid solution for the total power supply of a robotic manufacturing process in the form of laboratory equipment and mathematical computer models.
- Explore new operating modes and analyse the efficiency of key nodes on the DC microgrid.

Research tools and methods

Several methods have been used to analyse electrical systems and develop and test new solutions. Fluke, N4L power analyser, measurement equipment, and laboratory oscilloscopes have been used to obtain data characterizing electrical measurement and operating mode. The Data Translation universal DAQ platform is used to record data by adding appropriate auxiliary current and voltage measurement equipment.
Mathematical data processing and analysis have been performed using Matlab and Excel tools. Simulink, LTSpice, and PSpice tools have been used for the physical modelling of electrical circuits and systems. Printed circuit boards have been designed using Eagle and OrCAD software. Assembly of equipment and prototype design have been developed using SolidWorks and FreeCAD tools.
Laboratory setup and tailored power flow measurement equipment for time-synchronized data have been installed for conducting physical experiments, and controlled DC power flow and load test benches have been developed.

Scientific novelty

- Development of new interconnection circuit power electronic topologies for industrial robots and centralized storage systems.
- Development of a new solution for the physical replication of dynamic power profiles of electrical equipment in the DC microgrid at the laboratory scale.
- Developed and experimentally tested computer model of electrical drive systems and their interconnections for industrial robots.
- An equivalent computer model developed for the DC microgrid centralized AC/DC converter.
- A time-based analysis technique has been developed to obtain the required power and current parameters for cyclic processes to scale the electrical system and select equipment.

Practical novelties

The interconnection topology of industrial robots and centralized storage facilities and prototypes of equipment for the development of modular energy recovery systems have been developed and patented.
A detailed and time-synchronized data set of electrical energy flow measurements in an industrial DC microgrid with 13 measuring points has been obtained.
Analysis of DC microgrid power flows and determination of the amount and efficiency of recovered energy in an actual production process have been carried out.
New experimental testing facilities have been established to emulate the equivalent power profiles of different industrial consumers in real-time on the DC microgrid and study related effects.

Practical significance of the research

An experimental analysis has been carried out on a real DC microgrid, confirming the hypothesis of reuse of recovered energy.
A demonstration and experimental testing system of the DC microgrid at the laboratory level has been established.
In-depth knowledge of the introduction of DC microgrids for manufacturing purposes and the electrical design of industrial robot systems has been acquired throughout the research.

Structure and scope of the Thesis

The Thesis has been written in the form of a thematically unified set of scientific publications on the use of DC electrical systems and related elements to improve the performance of industrial robot installations. The Thesis has four chapters presenting the study of existing industrial robot electric drive systems, their modifications with DC interconnection elements, and the application of a full DC microgrid and a practical demonstration for robotic production.

Approbation of the Thesis

The summary of the Thesis comprises 19 publications and 1 patent. The results of the thesis work were presented in 12 conferences and 3 scientific journals.

1. Stupāns, A., Maksimkins, P., **Šenfelds, A.,** Ribickis, L. Industrial Robot Energy Consumption Analysis for Gravity-induced Opposing Force Minimization. In: *2022 7th IEEE International Energy Conference (ENERGYCON 2022*), Latvia, Riga, 9–12 May 2022. Piscataway: IEEE, 2022, pp.678-682. DOI 10.1109/ENERGYCON53164.2022.9830240
2. **Šenfelds, A**. Analysis of Motion Modelling Approaches for Industrial Robot Applications. In: *2019 IEEE 7th Workshop on Advances in Information, Electronic and Electrical Engineering (AIEEE 2019): Proceedings*, Latvia, Liepaja, 15–16

November 2019. Piscataway: IEEE, 2019, pp. 145–148. DOI 10.1109/AIEEE48629.2019.8977112

3. Apse-Apsitis, P., Vitols, K., Grinfogels, E., **Senfelds, A.,** Avotins, A. Electricity meter sensitivity and precision measurements and research on influencing factors for the meter measurements. In: *IEEE Electromagnetic Compatibility Magazine*, vol. 7, no. 2, pp. 48–52 DOI 10.1109/MEMC.2018.8410661
4. **Šenfelds, A**., Avotiņš, A., Apse-Apsītis, P., Grīnfogels, E., Ribickis, L. Investigation on Power Quality Parameters of Industrial 600V DC Microgrid Hardware. In: *2018 20th European Conference on Power Electronics and Applications (EPE'18 ECCE Europe): Proceedings*, Latvia, Riga, 17–21 September 2018. ISBN 978-907581528-3
5. **Šenfelds, A**., Apse-Apsītis, P., Avotiņš, A., Ribickis, L., Hauf, D. Industrial DC Microgrid Analysis with Synchronous Multipoint Power Measurement Solution. In: *2017 19th European Conference on Power Electronics and Applications (EPE '17 ECCE Europe): Proceedings*, Poland, Warsaw, 11–14 September 2017. Piscataway, NJ: IEEE, 2017, pp.3685-3690 DOI 10.23919/EPE17ECCEEurope.2017.8099322
6. Paugurs, A., **Šenfelds, A.**, Ribickis, L. Impact of Industrial Robot Tool Mass on Regenerative Energy. In: *Proceedings of 19th European Conference on Power Electronics and Applications, EPE'17 ECCE Europe*, Poland, Warsaw, 11–14 September 2017. Piscataway: IEEE, 2017, pp. 1–6. DOI 10.23919/EPE17ECCEEurope.2017.8099185
7. Grēbers, R., Gadaleta, M., Paugurs, A., **Šenfelds, A**., Avotiņš, A., Pellicciari, M. Analysis of the Energy Consumption of a Novel DC Power Supplied Industrial Robot. *Procedia Manufacturing*, 2017, Vol. 11, pp. 311–318. DOI 10.1016/j.promfg.2017.07.111
8. **Šenfelds, A**., Bormanis, O., Paugurs, A. Analytical Approach for Industrial Microgrid Infeed Peak Power Dimensioning. In: *2016 57th International Scientific Conference on Power and Electrical Engineering of Riga Technical University (RTUCON 2016): Proceedings*, Latvia, Riga, 13–14 October 2016. Piscataway, NJ: IEEE, 2016, pp. 328–331. DOI 10.1109/RTUCON.2016.7763140
9. **Šenfelds, A.**, Bormanis, O., Paugurs, A. Modelling of AC/DC Power Supply Unit for DC Microgrid. In: *Advances in Information, Electronic and Electrical Engineering (AIEEE 2015):Proceedings of the 2015 IEEE 3rd Workshop*, Latvia, Riga, 13–14 November 2015. Piscataway: IEEE, 2015, pp. 81–84. DOI 10.1109/AIEEE.2015.7367294
10. **Šenfelds, A.** Analysis of Cyclic DC Load Currents for Intelligent Electrical Protection. In: *2015 56th International Scientific Conference on Power and Electrical Engineering of Riga Technical University (RTUCON):Proceedings*, Latvia, Riga, 14–14 October 2015. Riga: Riga Technical University, 2015, pp. 165–168. DOI 10.1109/RTUCON.2015.7343162
11. Paugurs, A., **Šenfelds, A**. Design of a Motor Drive System for Bidirectional DC Power Flow Control. In: *2015 56th International Scientific Conference on Power and Electrical Engineering of Riga Technical University (RTUCON*), Latvia, Riga, 14–14 October 2015. Riga: 2015, pp. 265–268. DOI 10.1109/RTUCON.2015.7343145
12. **Šenfelds, A**., Vorobjovs, M., Meike, D., Bormanis, O. Power Smoothing Approach within Industrial DC Microgrid with Supercapacitor Storage for Robotic Manufacturing Application. In: *2015 IEEE International Conference on Automation*

Science and Engineering (CASE 2015):Automation for a Sustainable Future: Proceedings, Sweden, Gothenburg, 24–28 August 2015. Piscataway: IEEE, 2015, pp. 1333–1338. DOI 10.1109/CoASE.2015.7294283

13. Apse-Apsītis, P., **Šenfelds, A.**, Avotiņš, A., Paugurs, A., Priedītis, M. Power Measurement and Data Logger with High-Resolution for Industrial DC-Grid Application. In: *Power Electronics and Applications (EPE'17 ECCE Europe), 2017 19th European Conference* , 2015, Vol. 9, pp. 36–42. DOI 10.1515/ecce-2015-0010
14. **Šenfelds, A.**, Paugurs, A. Electrical Drive DC Link Power Flow Control with Adaptive Approach. In: *2014 55th International Scientific Conference on Power and Electrical Engineering of Riga Technical University (RTUCON): Proceedings*, Latvia, Riga, 14–14 October 2014. Riga: RTU Press, 2014, pp. 30–33. DOI 10.1109/RTUCON.2014.6998195
15. Meike, D., **Šenfelds, A.**, Ribickis, L. Power Converter for DC Bus Sharing to Increase the Energy Efficiency in Drive Systems. In: *IECON 2013 – 39th Annual Conference of the IEEE Industrial Electronics Society: Proceedings*, Austria, Vienna, 10–13 November 2013. Piscataway, NJ: IEEE, 2013, pp. 7197–7202. DOI 10.1109/IECON.2013.6700329
16. Priedītis, M., Meike, D., **Šenfelds, A.** Micro Controller Unit Process Time Sharing and Digital Filter Analysis in Industrial Energy Exchange System. Power and Electrical Engineering. Vol. 31, 2013, pp. 106–111. ISSN 14077345
17. **Šenfelds, A.**, Meike, D. Industrial Shared DC Bus Application: Common Ground Current Observation. In: *54th International Scientific Conference of Riga Technical University. Section of Power and Electrical Engineering: Digest Book and Electronic Proceedings*, Latvia, Riga, 14–14 October 2013. Riga: RTU Press, 2013, pp. 11–13. ISBN 978-9934-10-470-1
18. **Šenfelds, A.**, Raņķis, I. Common Node Circular Current Examination in Shared DC Bus Power System. In: *13th International Symposium "Topical Problems in the Field of Electrical and Power Engineering. Doctoral School of Energy and Geotechnology II"*, Estonia, Pärnu, 14–19 January 2013. Pärnu: Elektriajam, 2013, pp. 85–88. ISBN 978-9985-69-054-3
19. Raņķis, I., Meike, D., **Šenfelds, A.** Utilization of Regeneration Energy in Industrial Robots System. *Enerģētika un elektrotehnika*. No. 31, 2013, pp. 95–100. ISSN 14077345
20. Lebrecht, M., Meike, D., Rankis, I., **Senfelds, A.** Produktionsanordnung mit wenigstens zweiAntriebssystemen. German Patent DE 10 2013 010 462 A1, Patent publication date: 27.03.2014

INTRODUCTION

Without highly automated technological solutions, a state-of-the-art manufacturing process that creates high-added value physical products of many units is hard to imagine. Industrial robot equipment is often used in processes characterized by product type repeatability, precise assembly conditions, hazards to humans and harmful conditions. An industrial robot is a complex machine that provides a computer-controlled process through an electromechanical system. It often uses electrical energy for its operations and fits into the broader production organization and necessary material and energy supply system. Developments related to the impact of geopolitical processes and significant increases in energy prices have contributed to the need for a new approach, diversifying energy sources, promoting system flexibility and efficient end use of energy, for which incentives are being developed [6]. Given the extensive process of introducing new technologies from an experimental prototype to fully defined everyday applications and the application of related standards and regulations, several focus groups and associations of engineers have emerged, as well as research projects AREUS [7] and DC Industrie [8], to promote the practical implementation of DC systems.

Given that DC systems can benefit from a wide range of applications from large-scale power generation and transmission, such as offshore wind farms and HVDC high-voltage direct current transmission lines, to, for example, a single power supply standard for domestic appliances, USB-C[9], organizations have developed with an intent to explore targeted applications. The Current OS Foundation [10] and DC systems [11] want to promote high-end, low-voltage DC applications and implement the relevant system management and coordination standards. The research organization FEN – Flexible Electrical Networks [12] – is promoting the deployment of DC system applications for the application of distribution and transmission networks to deploy future flexible energy systems. The activities and applications carried out in the Thesis are related to a large extent to the scope of the recently established ODCA – Open DC Alliance – for the exploration of industrial DC products and solutions. Given that DC industrial networks are entering the development phase as long-term investment projects for practical applications [13],[14], economic rationale and industry interest are also predictable in the coming years. The knowledge and experience gained in developing the Thesis are also helpful in developing local SME-scale DC systems, considering the need to achieve renewable energy and efficient energy use targets under the National Climate and Energy Plan 2030[15].

1. ANALYSIS OF TYPICAL ELECTRIC DRIVE SYSTEMS FOR AC INDUSTRIAL ROBOTS

In this chapter, the main properties of industrial robot kinematic systems, motion execution and electrical drive systems are discussed. The author's publications 1 an 2 are related to Chapter 1. For an overview of the intrinsic characteristics and functionality of an industrial robot installation linked to the subsequent analysis of electric drive systems, it is beneficial to examine the classification of robotic equipment. The methodology proposed by the International Robotics Association is considered a comprehensive method for classifying robotic equipment, including manufacturing applications [16]. According to the selected classification procedure, a distinction can be made between several types of equipment eligible as robotic equipment for production purposes. Firstly, it is possible to divide the installations according to their location – stationary and mobile.

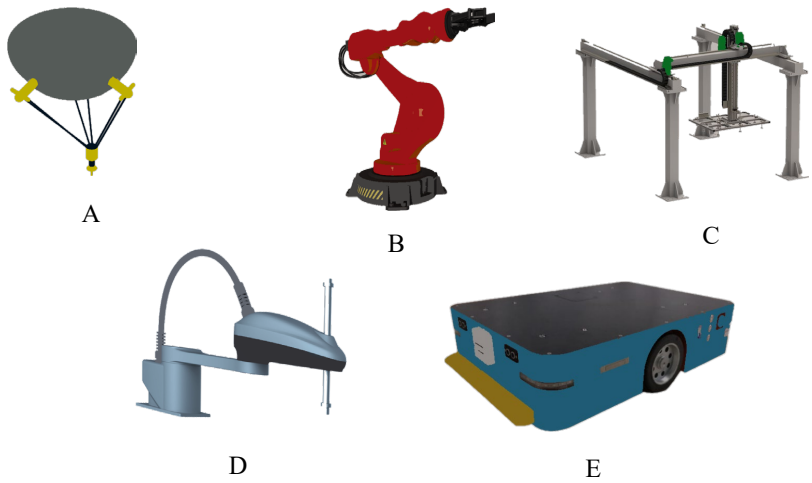

Fig. 1.1. Industrial robot types: A) – Delta; B) – articulated manipulator; C) – Cartesian (linear); D) – SCARA-type; D) – autonomous guided vehicle (AGV).

- The Delta (parallel) robot comprises a base platform incorporating an electric drive and work platforms with a work tool driven by three levers. The specific feature of such a structure is the possibility of reducing the moving parts' weight and obtaining rapid accelerations and precision for the work platform. Typical application directions are packaging, precise assembly and material handling. The market-available mass-produced robot equipment payload is up to 15 kg [16].
- An articulated robot is a machine that consists of at least three rotating joints, and the kinematic system has vast flexibility capabilities that would be somewhat comparable to the range of motion of the human arm from the shoulder onwards. The advantages of such a system are excellent reachability and workspace compared to the robot's size. An articulated robot has been widely used as a typical manipulator in highly automated

manufacturing processes such as automotive, metalworking and electrical equipment manufacturing.

- The Cartesian (linear) robot workspace is a rectangular area in a space that can be described by the coordinates X, Y, and Z adopted in the Cartesian coordinate system, placed perpendicular to each other. Robotic manipulators of this type are widely used in various types of CNC processing machines, lifting and material handling tasks. The device's design allows for relatively simple movement control, but limitations include the inability to reach the working space under the objects.
- The SCARA-type robotic manipulators are comparable to the human arm's operating principle but with more limited movement flexibility, mainly using the ability to bend the arm in the elbow part. The vertical movement of the end effector is carried out only with the last drive built into the manipulator structure, and positioning in a horizontal plane is done with two parallel rotating axes. The drawback of this manipulator is also the ability to perform operations from the top, but the machine is widely used in automated assembly processes, especially in electronics.
- Autonomous guided vehicles (AGV) are also regarded as robotic devices, the control of which can be carried out employing built-in elements (cameras, sensors) and objects integrated into the environment (magnetic strips, dots, signal wires). The AGVs are widely used in automated manufacturing with the introduction of typical packaging elements in the materials supply. As new concepts of flexible production organization evolve, mobile platforms are also seen as a base for installing other production equipment in a customizable environment.

The Thesis provides a focused view of the most popular industrial robot manipulators based on the principle of kinematic structure of the articulated serial manipulator applied in industrial manufacturing. Examples of typical applications are those for ancillary assembly and production tasks in which the robot serves as a platform for installing tools with a significant weight exceeding 100 kilograms.

The role and dynamics of electric drive

The role of electric drive in an industrial robot is to realize time-related positioning demand for individual robot axes. Incremental command of rotational position of each axis is defined following the planned trajectory of the robot end tool, which includes simultaneous calculation of positioning of all axes. It is realized with the help of a robot controller. Figure 1.2 shows a typical industrial robot manipulator and its schematic structure. In this case, the machine is designed as a combination of a series of six rotary joints, with the symbols A1 to A6 indicating the position of the rotary axes.

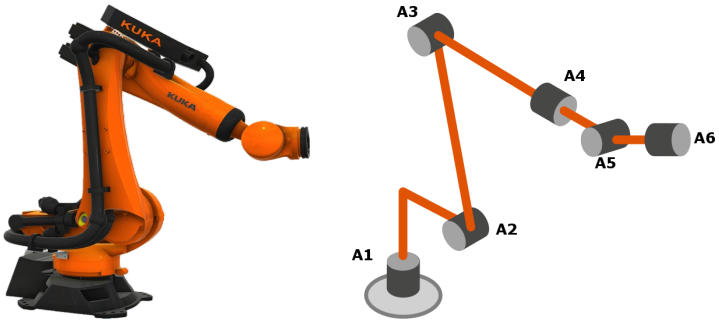

Fig. 1.2. The structure of articulated 6-axis industrial robot manipulator.

An appropriate kinematic model can describe an industrial robot manipulator as a system of series interconnected solid bodies, including moving joint elements [17]. This way, it is possible to analytically investigate possible variations in the positions of individual joints and also the areas or working space available for the end tool of the manipulator.

However, techniques based on applying an appropriate dynamic model are used. Like in the kinematic approach, it is possible to distinguish the direct and inverse dynamics model for the particular robotic manipulator configuration-related dynamics process. The relationship between the individual axis torques of an industrial manipulator and the changes in the positions of the robot manipulator can be described using an inverse dynamics calculation.

Function (1.1) determines the instantaneous values of the required individual axle torque set τ for individual drive nodes to execute the manipulator motion.

$$\tau = f(q, \dot{q}, \ddot{q}, f_{ext}) \tag{1.1}$$

The described manipulator motion is expressed as a system of the set of individual axles of angular positions q, velocities $\dot{q}$, and angular accelerations of $\ddot{q}$. The force component of the external action produced by the robot manipulator is described on each of the axes by a set f_{ext}. As this function describes the dependence of the system input value, which is the torque produced by the drive, on the output parameter set of the manipulator system, this approach is referred to as *the inverse dynamics model*.

The operation of the actual system is described by a *direct dynamic model* (Eq. (1.2)), where the acceleration of each axis $\ddot{q}$ depends on the axis torques τ, angular position q, rotational speed $\dot{q}$ and interaction of external forces f_{ext}.

$$\ddot{q} = f(\tau, q, \dot{q}, f_{ext}) \tag{1.2}$$

For detailed analysis of the inverse dynamics process of the series kinematics-based robot manipulator (Eq. (1.1)), it is described in an expanded form according to Eq. (1.3).

$$\tau = D(q)\ddot{q} + C(q, \dot{q})\dot{q} + f(\dot{q}) + g(q) + e(q) \tag{1.3}$$

Axis torques τ are obtained by the combination of the following effects on the axes of the robot:

$D(q)$ – a matrix, the elements of which depend on the location of current robot axes and the mass of individual parts of the robot describing the induced inertia effect;

$C(q, \dot{q})$ – a matrix with elements describing Coriolis and centrifugal forces;

$f(\dot{q})$ – the vector describing friction events;

$g(q)$ – the vector describing the moments produced by gravity projections on the axes;
$e(q)$ – the vector describing projections of external force action moments on axes.
The main objective of an industrial robot is based on the execution of a real-time continuous work tool positioning task that is translated to position commands of individual axis drives and executed synchronized. Given the need for precise motion, the drive units of industrial robots are most often implemented by electric drives and precision gear drives. Hydraulic and pneumatically controlled joints have also been popular in the early stages of the development of industrial manipulators. Given the trends and affordability of electrical drive technologies from a cost and functionality perspective, electrical drives have become the leading positioning solution in robot technology.

Overview of an architecture of industrial robot controller

According to the robot configuration mentioned earlier, the robot controller structure is designed to provide a synchronized operation of 6-axis drives. Figure 1.3 shows the inner build of the KUKA KRC4 industrial robot controller. From an electrical drive analysis point of view, it is essential to identify three functional units – an AC rectifier that provides DC voltage for two combined inverter units. Inverters provide control of PMSM servo drives grouped by axis mechanical load: 1–3 axes and 4–6 axes, respectively.

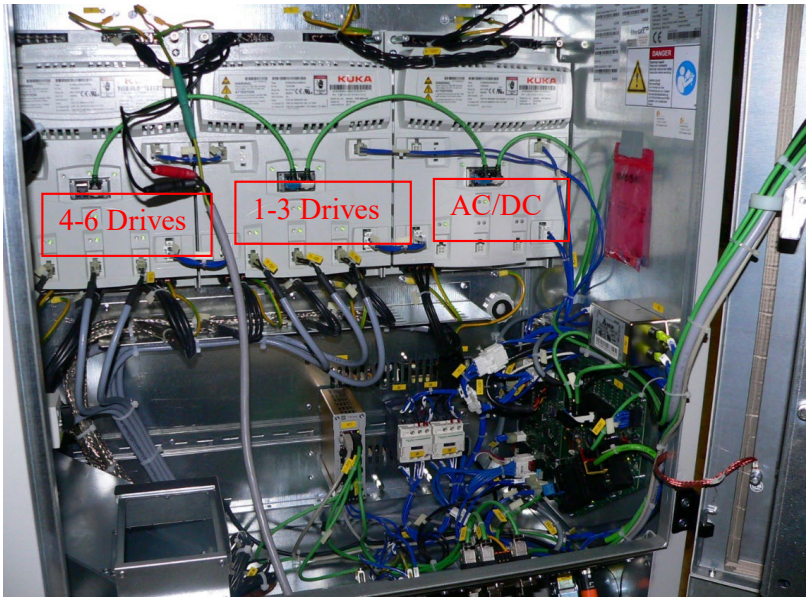

Fig. 1.3. Arrangement of KUKA KRC4 robot controller electrical drives.

Robot manufacturer KUKA provides a robot controller as a modular system and applies manufacturer-specific electrical functional unit designations KPP – KUKA power Pack, and KSP – KUKA Servo pack. For experimental activities related to the Thesis, an industrial robot

with a 210 kg payload capacity was applied, and an AC-type KRC4 controller with the following KPP and KSP parameters was configured according Table 1.1.

Table 1.1

Nominal Data of ElectricalDrive Elements of the KUKA KRC4 Robot Controller

Device	Input parameters	Output parameters
KPP 600-20	3PE AC 400/480 V 20 A 50/60 Hz 14/17 kW	2 PE DC 565/675 V 25 A 14/17 kW
KSP 600-3X40	2 PE DC 565/675 V 25 A	3 PE AC 0-400/480 V 17 A 0–500 Hz 12/14 kW
KSP 600-3X20	2 PE DC 565/675 V 25 A	3 PE AC 0–400/480 V 9 A 0–500 Hz 6/7 kW
Servo drives 1–3	Uph 201 V, Iph 9.5 A	Nn/Nmax 3000/5000 rpm, 4.9 kW
Servo drives 4–6	Uph 152 V, Iph 5.6 A	Nn/Nmax 3000/7200 rpm, 2.3 kW

The figure shows an extended structural diagram of the KRC4 controller, which distinguishes between 24 V voltage level equipment and the equipment connected to the DC bus, presented on a grey background colour.

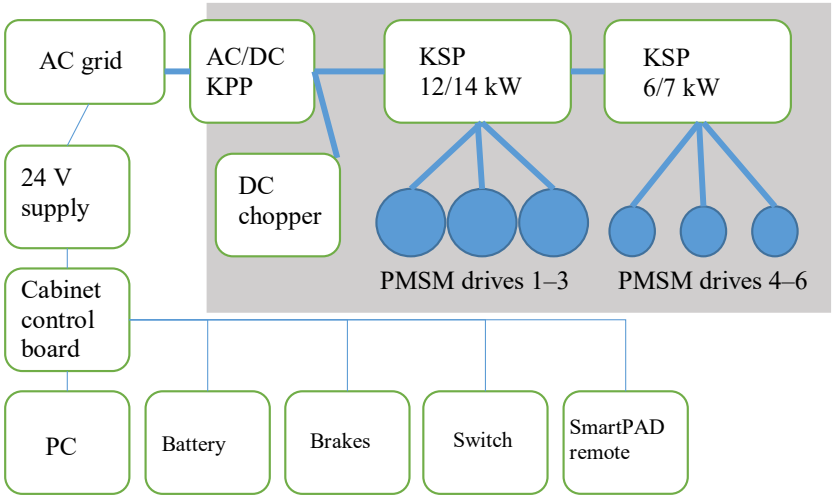

Fig. 1.4. Structure diagram and electric power supply of the KUKA KRC4 controller.

Power consumption or electrical drive recuperation depends on the robot's planned motion program performance [20]. In practice, such data on the power consumed by individual electrical machines or a group of electrical drives during the execution of the program can be obtained by several methods.

- A detailed robot modelling approach, as described in [18] and [19], predict a sequential calculation of the energy flows of an industrial robot, taking into account the power of

individual electrical machines and friction losses. This approach makes it possible to achieve a universal model that is also suitable to address the challenges of motion optimization taking into account energy consumption.

- Practical measurements by connecting current and voltage measurements to the DC bus allow recording of the data obtained, which, employing subsequent processing combined with the measurement of the power consumed by individual inverters, enable a sum of power of the DC bus. Figure 1.5 represents the resulting change in total DC bus power due to a practical measurement of 2 robots.

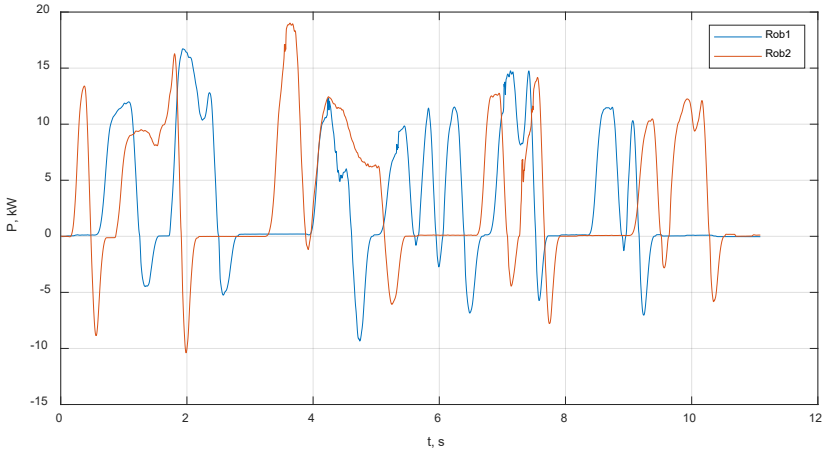

Fig. 1.5. Experimentally obtained DC bus power profiles in two industrial robot operations.

- Alternatively, the recording function of the internal parameters of the robot controller is also mentioned as a method to obtain individual axis power consumption or associated values, such as current and voltage data. This is possible through, e.g., KUKA Trace software feature, which is primarily designed for diagnostics of the robot's internal processes, but the data generated during movement can also be used for further modelling or optimization tasks (Eqs. (1) and (2).

If data are available on the dynamic electric power profile of the 6-axis drive of an industrial robot, an equivalent model of the electrical system can be developed to study the operation of the electric drive and the DC bus. The structure of the model is shown in Fig. 1.6.

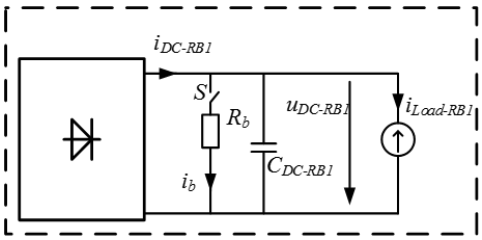

Fig. 1.6. A model of electric system of industrial robot manipulator for AC power supply.

The primary energy source is the AC grid, which is supplied to the DC bus via an uncontrolled rectifier. The value of the rectified voltage at idle operation of the rectifier depends on the grid voltage according to Eq. (1.4), where U_{L-L} is the voltage between the phases in the three-phase system and U_{DCidle} is the value of the rectified voltage at no load.

$$U_{DCidle} = \sqrt{2}U_{L-L} \tag{1.4}$$

Thus, it can be concluded that at the 400 V voltage system standard in Europe, the voltage of the DC stage is 565 V at no load.

Practical analysis of the KRC4 robot controller has made it possible to determine the total combined DC bus capacitance. The value of C_{DC-RB} is 1.3 mF. Similarly, the braking resistor value, R_B , has been determined – 11 Ω. The application of the braking resistor follows from the principle of hysteresis-type control, which measuring the voltage of the DC bus U_{DC} compares to 2 voltage levels U_{RbON} – 685 V and U_{RbOFF} – 665 V. At 685 V DC bus voltage, the energy dissipation within the resistor is initiated until a reduction to 665 V is achieved, and the braking resistor is switched off.

The dynamic power profile of an industrial robot $P_{Load}(t)$ is realized by modelling the equivalent power source according to the equation:

$$I_{Load}(t) = P_{Load}(t)/U_{DC}(t) \tag{1.5}$$

Figure 1.7 shows the implementation of the model structure in the Matlab Simulink modelling environment.

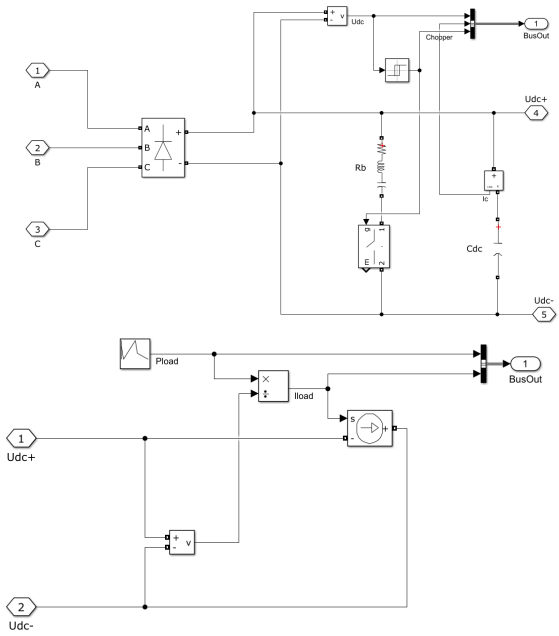

Fig. 1.7. Implementation of AC industrial robot electric model in Matlab/Simulink: rectifier, filter capacitor and brake resistor circuit (above), and equivalent dynamic axis load element (below).

Simulation of the experimentally obtained load profile with the model described above results in the DC voltage variations and braking resistor operation Fig. 1.8.

The established model is valuable for further research on energy efficiency improvement measures. The following chapter explicitly considers modifications to existing AC industrial robot drives by introducing DC network elements.

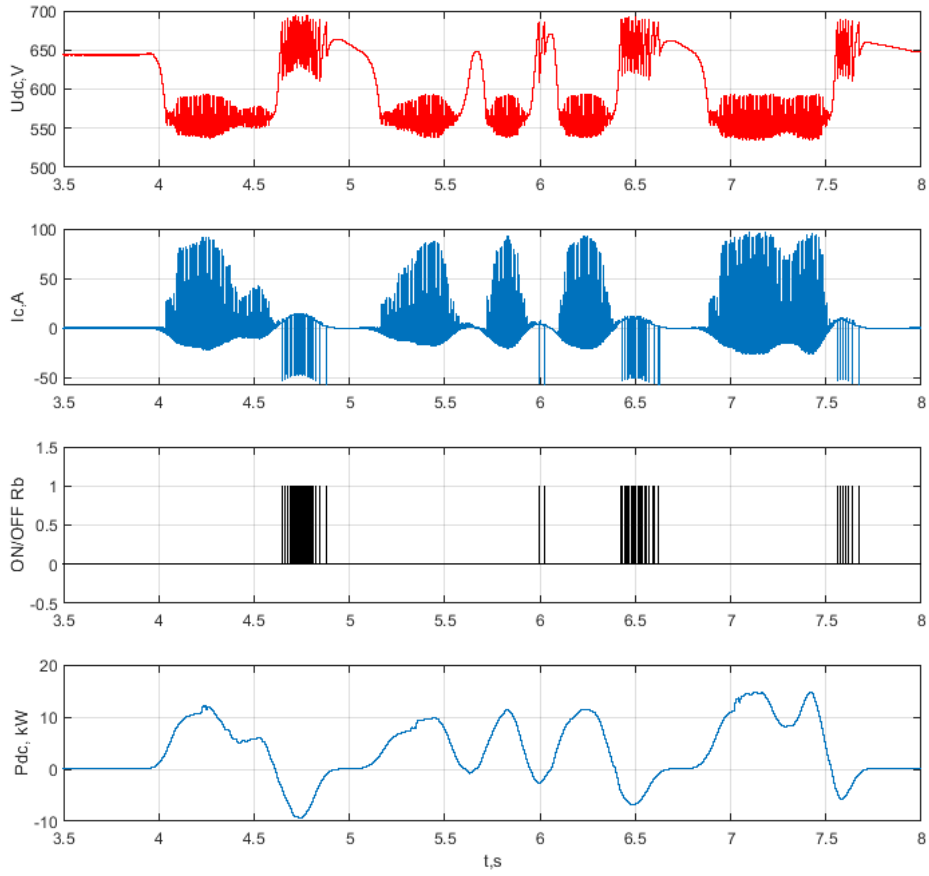

Fig. 1.8. Results of the equivalent electric model of an industrial robot: U_{DC} – DC bus voltage variation; I_C – DC bus capacitor current, braking resistor operating command, and the executed industrial robot program power profile P_{DC}.

2. DEVELOPMENT OF DC-BASED CONVERTERS FOR ENERGY-EFFICIENT MODIFICATION OF AC INDUSTRIAL ROBOTS WITH TRADITIONAL FREQUENCY CONVERTERS

This chapter presents an approach for energy efficiency improvement by modifications of a typical AC electrical supply-based industrial robot. The author's Publications 15–20 represent the findings of this chapter.

By analytical observation of the design of typical AC robot controllers, it can be concluded that braking motions are present depending on the performance of the trajectory execution task. During such motions, recuperated energy is accumulated in the DC capacitor and by the presence of a predefined higher voltage level is dissipated by the braking resistor. Thus, there is a direct potential for improving energy efficiency if the share of dissipated energy in normal working conditions is reduced. Several possible ways of improving energy efficiency from the point of view of optimization of the electrical system are summarized below, but there are also other methods related to optimizing motion trajectories, and software is known [21].

Each of the presented options is increasingly relevant for using DC power transmission in robotic systems:

- Controlled bidirectional rectifier application.

Simply replacing an uncontrolled rectifier with a bidirectional rectifier is significantly more expensive than inserting additional capacitance into the DC bus. Considering related requirements for AC grid power quality and the relatively low individual load power per converter, such a solution should be considered in the context of a significant DC side electrical system dimension and connected load pool.

- Increasing the capacitance of the DC bus.

Such an option requires additional capacitors in each robot controller, which entails additional costs [22] but also has potentially positive aspects in terms of increased system reliability [23]. The optimal choice of capacitor capacity depends on the most significant recovery energy peak generated during the motion trajectory execution task performed. This solution is considered appropriate in cases where there are one or few robot controllers distributed over longer distances in the manufacturing area.

- Interconnection of DC bus of multiple industrial robots.

An alternative approach is the introduction of additional capacitance and its availability through the connection of multiple robots to a shared capacitor module for the efficient use of braking energy. This approach is analysed and discussed in detail along with practical implementation in the following chapter.

- Provision of DC power supply.

As a large-scale solution involving the use of robots and the bidirectional energy exchange potential of industrial drives a single DC microgrid is created with one centralized AC connection.

Interconnection of DC bus of multiple industrial robots

For the short-term accumulation and reuse of braking energy, the capacitance of the DC bus may be utilized if the operating principles of the installation allow for variation in individual DC bus voltage U_{DC_i}. Figure 2.1 depicts the principle for connecting the DC bus of individual drives with a common capacitor module *C*.

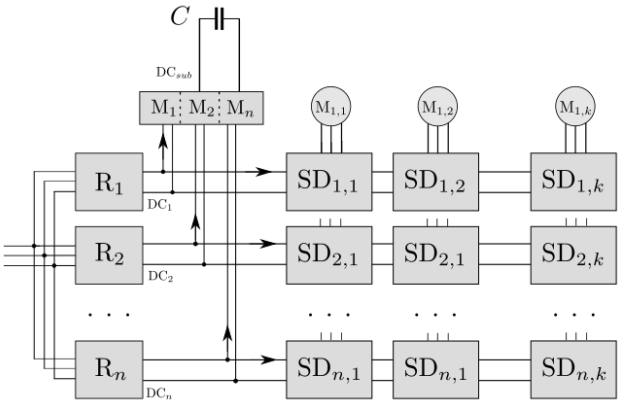

Fig. 2.1. Interconnection of multiple electrical drive inverter *SD* groups with input rectifiers, *R,* with shared DC bus and additional capacitance, *C*, application (the autor's Publication 15).

Each drive system shall retain the existing input rectifier and the structure of the DC bus. Additionally, the interconnection module *M* is introduced, allowing the power flow to be controlled between individual robots and a common capacitor *C* and respective voltage U_C.

Key operating principles for interconnection modules:

- storage and efficient use of recovered energy;
- do not affect the regular operation of the existing drive system configuration providing power from the AC grid.

Within the framework of the Thesis, several versions of the interconnection circuit have been established, which can be divided into asymmetric commutation interconnection (1 version) and symmetric commutation interconnection circuit (2 versions) topology solutions.

Asymmetric interconnection circuit analysis

In order to have practical implementation, an electrical circuit diagram was set up as illustrated in Fig. 2.2.

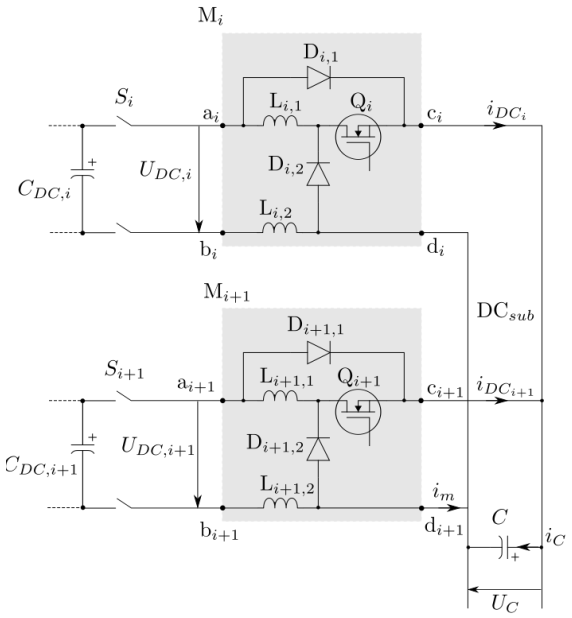

Fig. 2.2. Asymmetric commutation DC interconnection circuit.

In order to ensure the exchange of recovered energy through the external capacitor module, the hysteresis-type control principle is applied, and the capacitor voltage control parameters U_{ON} and U_{OFF} are introduced. The flow of recovered energy to central capacitor *C* occurs by natural commutation and diode *D*. The energy flow and reuse of pre-accumulated energy in each of the robot drives takes place by operating the *Q* semiconductor switch, which is commutated by the following principle (Eq. (2.1)):

$$Q \text{ state} = \begin{Bmatrix} ON \; if \; U_C > U_{ON} \\ OFF \; if \; U_C \leq U_{OFF} \\ previous \; state \text{ otherwise} \end{Bmatrix}. \tag{2.1}$$

The module interconnection instance voltage trigger level U_{ON} of the hysteresis control is higher than the disconnection instance level U_{OFF}, which allows for a more stable operation by introducing a deadband between these values.

$$U_{ON} \geq U_{OFF} \tag{2.2}$$

Practical testing of the presented circuit was carried out (the author's Publication 19) with the interconnection of two industrial robots, resulting in terms of energy consumed over a 1-hour working period Table 2.1.

Table 2.1

Energy Consumption Results for the Asymmetrical Connection of Two Industrial Robots

Robot application	Welding	Handling
Without DC interconnection, kWh	3.66	6.44
With DC interconnection, kWh	3.45	5.11
Difference, %	–5.6	–20.5

Experimentally measured voltage variation and corresponding current during operation are presented in Fig. 2.3.

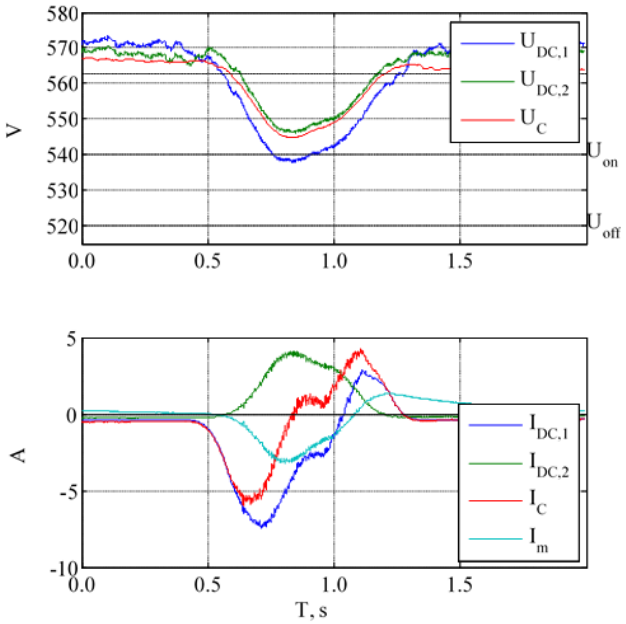

Fig. 2.3. Asymmetric interconnection operating mode at control voltage parameters U_{ON} = 540 V and U_{OFF} = 520 V.

During the experimental test, an *Im* current flow has been observed due to potential equalization effects imposed by directly coupled negative DC bus poles (the author's Publications 17 and 18).

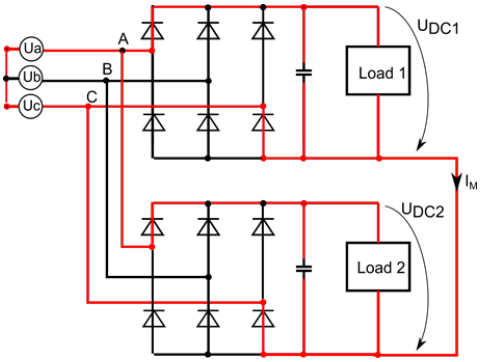

Fig. 2.4. Equalizing current circuit in the case of asymmetric connection.

Such an effect creates a new operation mode for the load of rectifiers. Due to the possibility of modifying existing equipment and developing potential diagnostic errors, it was decided to consider the introduction of symmetric switching modules for future work. It is also important to ensure that discharge of the main capacitor Uc is interrupted at the voltage U_{OFF} before the no-load output voltage U_{DCidle} of the rectifier is reached at 565 V when the 230 V phase voltage system is used.

$$U_{OFF} \geq U_{DCidle} \tag{2.3}$$

The work on creating a new type of interconnection circuit for the task under examination was continued.

Development of symmetric interconnection circuit

Based on the necessary modifications and previous test experience, a new type of DC link interconnection topology (the author's Publication 20) was developed and patented to ensure synchronous switching of both DC circuit poles in the event of interconnection.

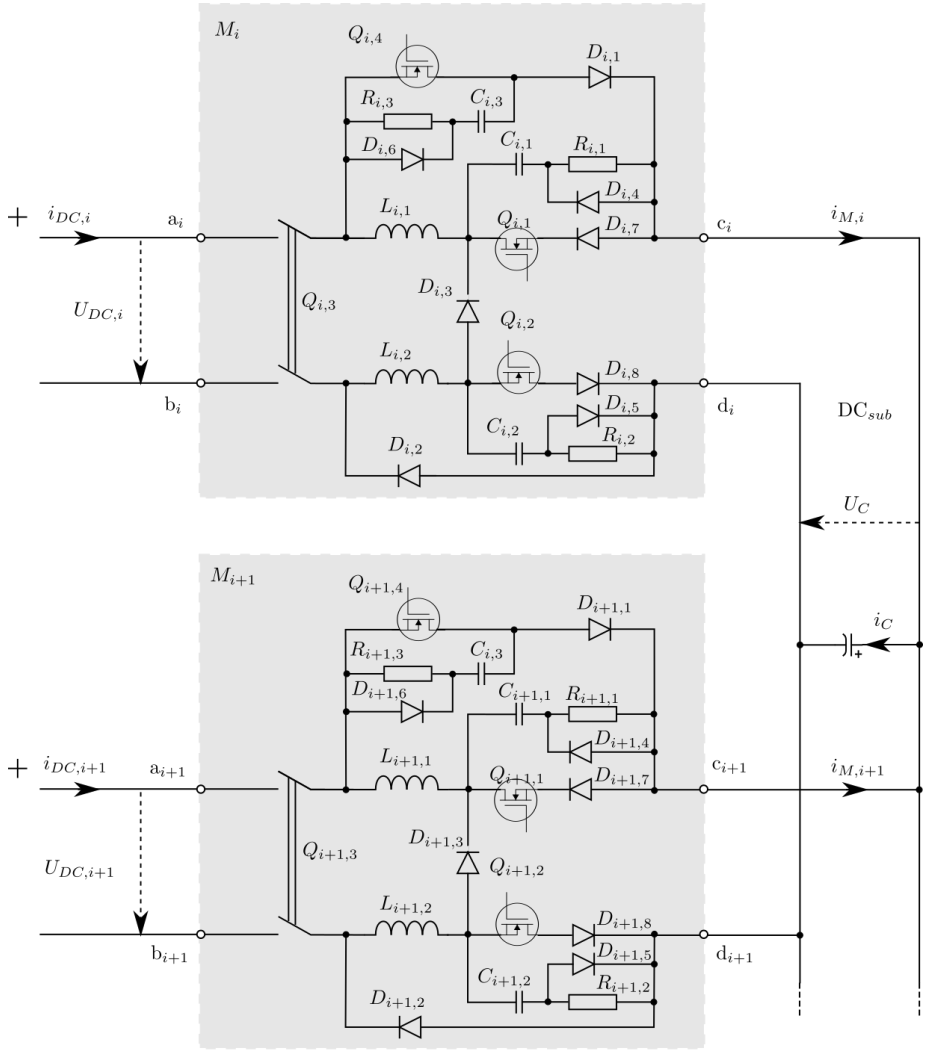

Fig. 2.5. Symmetric commutation DC interconnection circuit.

The main differences are the introduction of an additional semiconductor switch for switching the other pole and the possibility of conducting a controlled pre-charge of the main capacitor from one of the connected DC buses of industrial robots. The interconnection prototype circuit power device module without peripherals is shown in Fig. 2.6.

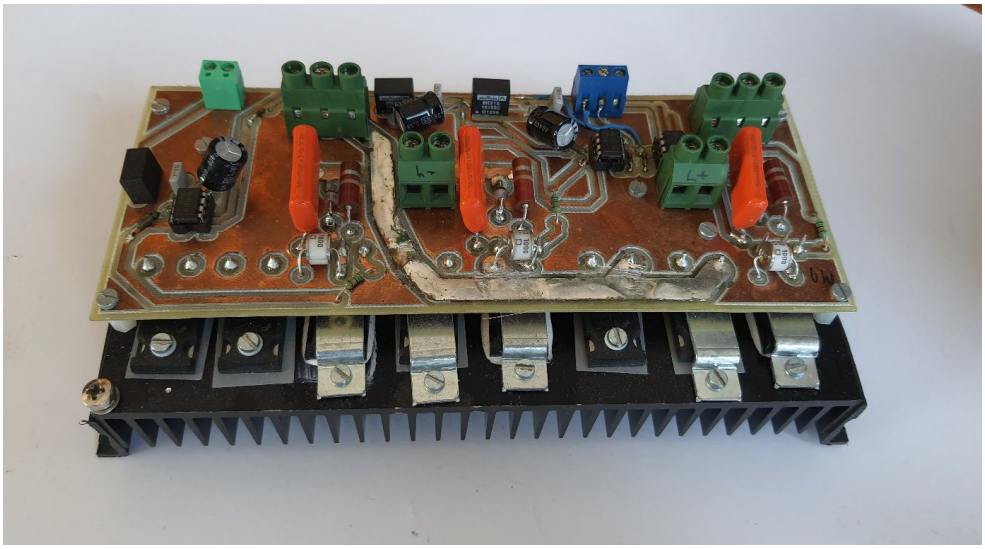

Fig. 2.6. Prototype of symmetric interconnection circuit power switch board.

The installation was subsequently assembled and experimentally tested under industrial conditions in collaboration with Mercedes Benz AG (former Daimler AG), Germany, using industrial robot manipulators KUKA KR210 with additional weight elements 150 kg and 200 kg as reproduced Fig. 2.7.

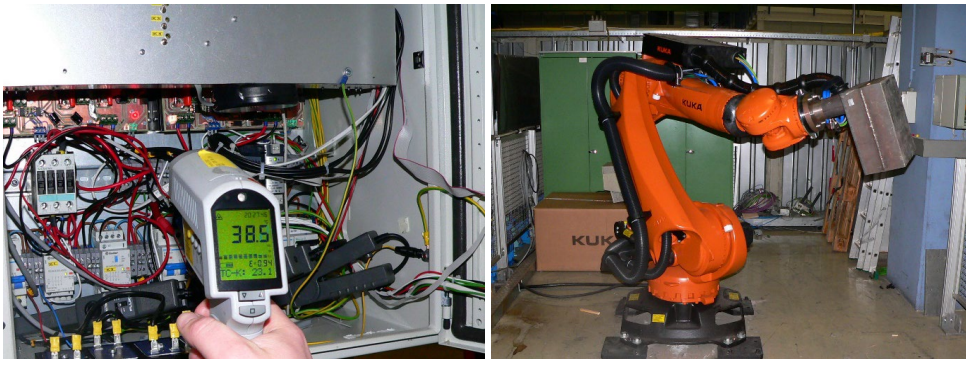

Fig. 2.7. Experimental verification in production area: interconnection module with peripheral devices (left) and one of the interconnected KUKA KR210 industrial robots (right).

During the test, electrical parameter data recording and energy consumption estimation were performed with the equipment shown in Fig. 2.7, FLUKE AC power analyser, and the data logging system.

Fig. 2.8. Application of DC interconnection electric parameter data recording and AC power analyser devices.

A 20-minute operation period analysis was carried out on the power consumed for a 2-industrial robot interconnected system, and the obtained results are presented in Table 2.2.

Table 2.2

Average Power Consumed in the Case of a 2-robot System

Robot application	**Handling – 20 min (no extra weight)**	**Handling – 20 min (with additional weights of 150 and 200 kg)**
Average power without DC interconnection, kW	6.23	8.67
Average power with DC interconnection, kW	4.92	5.11
Difference, %	–21.1	–22.7

The pilot test demonstrates the positive impact of the preferred option on increasing energy efficiency for this robotic application, reaching savings of up to 22.7 % in average energy consumption. It is important to note that, under actual production conditions, the operational tasks of individual robots may vary considerably according to the required motion dynamics, and relatively fast motion and strong recovery modes movement profiles were used in this test to test electrical parameters for the prototype created.

Due to the actual performance of the system, the direct voltage measurements of both individual robots and the shared DC bus, it was possible to develop an equivalent computer model using the modelling tools of Matlab and Simulink, as well as to compare the performance of the model

and the actual measured system (the author's Publication 15). Figure 2.9 compares the results of dynamic variation of the most characteristic parameters in a similar operating mode with the same U_{ON} = 600 V and U_{OFF} = 580 V control parameters.

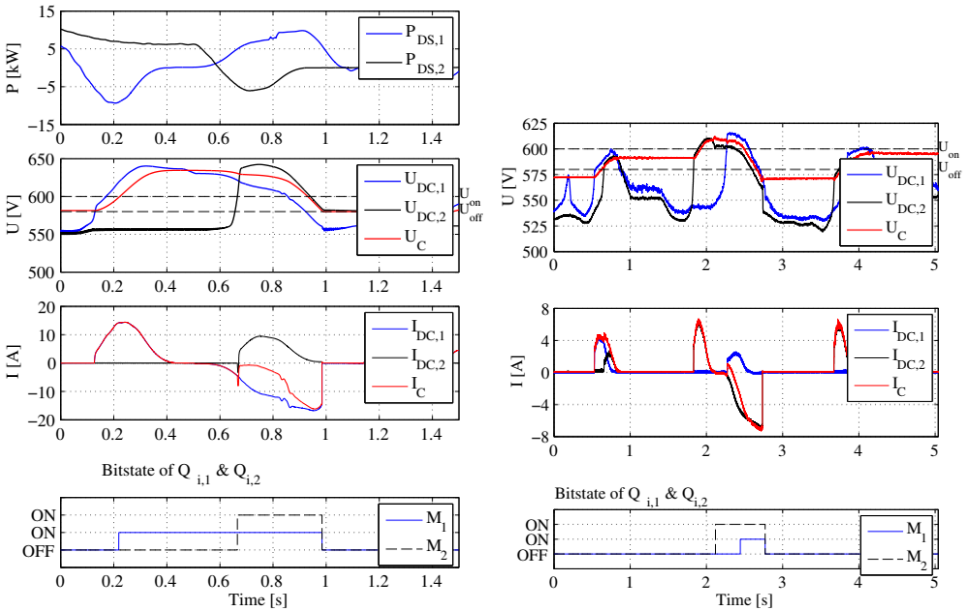

Fig. 2.9. Comparison of interconnection operation examples in a modelled (right) and experimentally measured system (left).

The obtained data allowed further system optimization. As observed, for example, actual U_C voltage reaches a value lower than U_{OFF}, demonstrating the time delay in real system semiconductor switching operation, and has been the subject of more extensive analysis (the author's Publication 16).

Development of a modular system prototype

Given the expected use in an industrial environment, where it would be necessary to organize the energy exchange between individual industrial robots on a similar scale to that achieved from an actual production plant, it is concluded that the typical number of robots placed together is up to five units. This type of electrical equipment would be used to optimize the operation of one production cell by modifying existing robots. Based on the data obtained and the model produced, an analysis was developed to build a system of five robot machines using modelling tools, as well as a practical modification of the design of the prototype taking into account the necessity of a modular system.

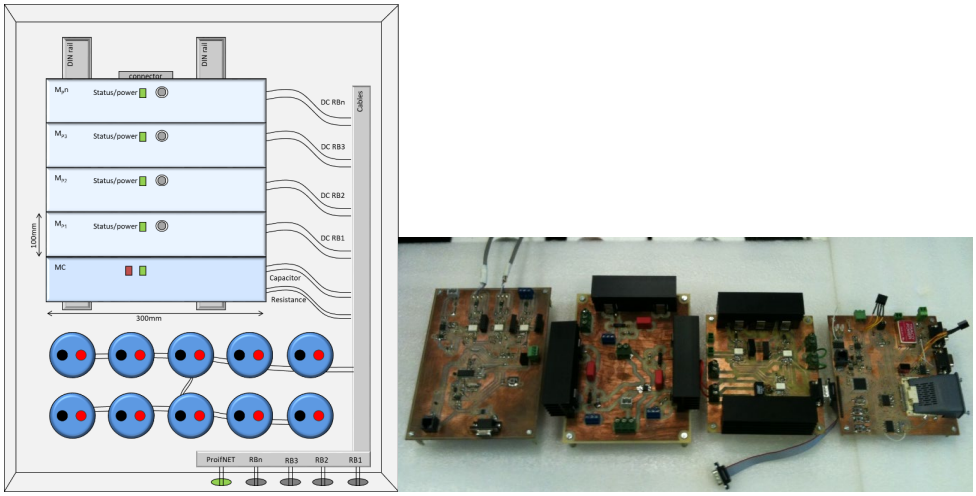

Fig. 2.10. Conceptual sketch of the principle of modular system approach (left) and first prototypes of functional modules (right).

Figure 2.11 shows the realization of the equivalent model of the system in the Simulink environment to determine the operating modes and associated electrical parameter values of the electrical system.

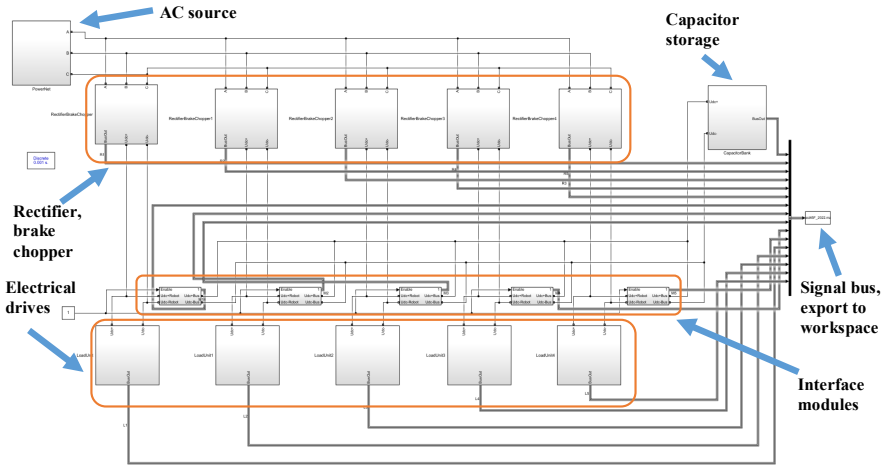

Fig. 2.11. Model structure for five interconnected industrial robot operational analysis.

Modelling results allow to explore interconnection module switching processes and the impact on overall system operation. Figure 2.12 shows part of the data obtained, graphically representing the voltage dynamics of individual DC buses.

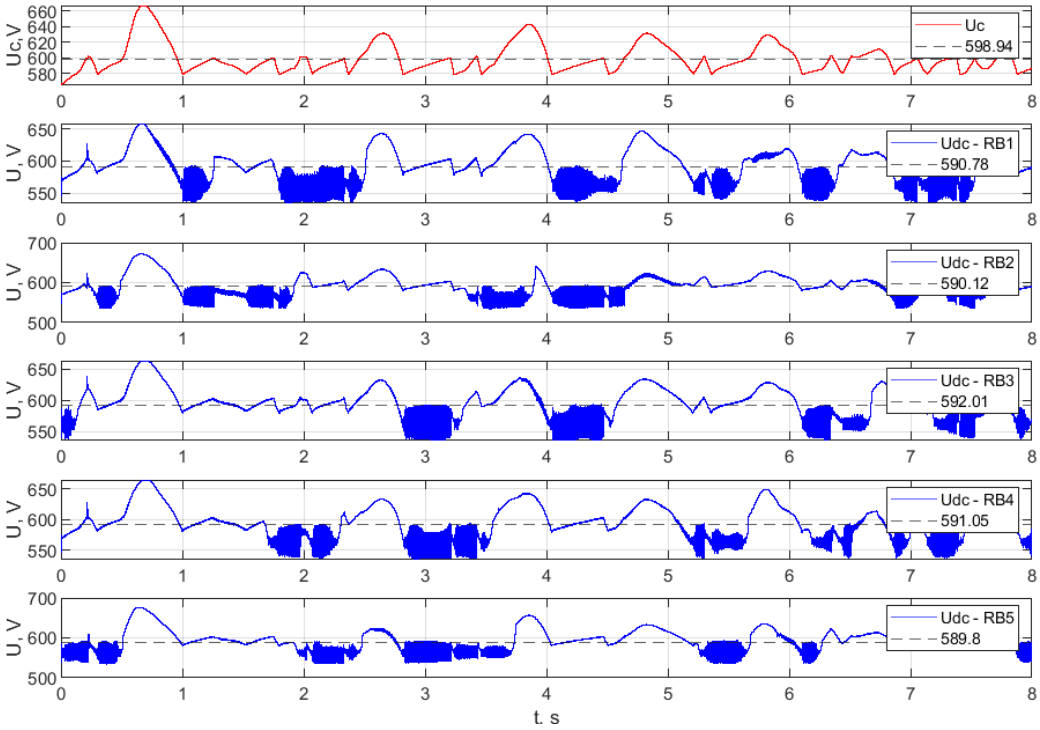

Fig. 2.12. Example of modelling results for the 5-module system – dynamics of individual DC bus voltages.

The choice of transistors and diodes for selected main semiconductor elements was also optimized by studying the appropriate thermal processes, as well as the galvanic insulation of module housings and the ability to combine on single radiators for passive cooling applications.

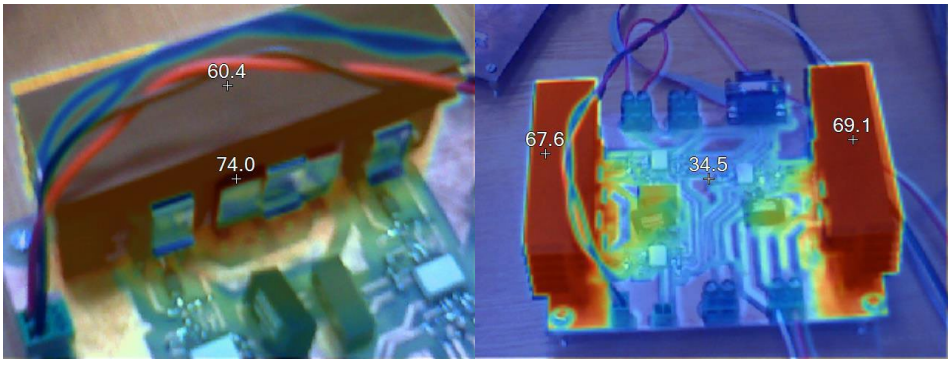

Fig. 2.13. Example of a thermal process identification and testing process with increased power to determine critical temperatures during the design of the equipment.

A version was created in the course of successive development of the solution envisaging the assembly and housing design for the equipment taking into account typical installation

conditions for electrical and automation equipment in cooperation with Daimler AG. Figure 2.14 shows the design of the installation solution and the modules created using 3D CAD software.

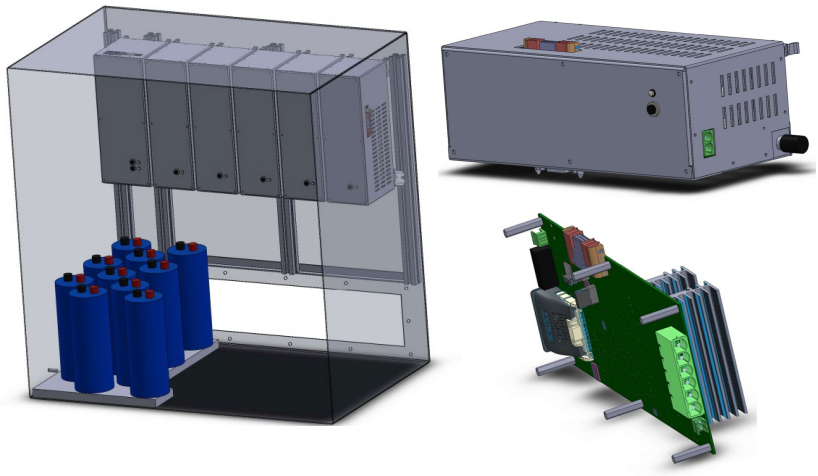

Fig. 2.14. The concept of modular installation assembly and practical implementation of modules in a CAD environment.

A real prototype of the equipment was built (see Fig. 2.15) taking into account the aspects of optimization and modular system described above for industrial applications in the production plant.

Fig. 2.15. A practically implemented modular solution for the DC link interconnection of industrial robots.

3. ANALYSIS OF INDUSTRIAL ROBOT APPLICATION WITHIN LABORATORY SCALE DC MICROGRID

The practical implementation of a DC microgrid for experimental power flow analysis of a few industrial robot applications and possible combinations with energy storage and renewable power infeed has been of interest to Riga Technical university (RTU) Institue of Industrial Electronics and Electrical Technologies. Efforts and related author's findings regarding the implementation of DC testing laboratory are represented in the author's Publications 3, 4, and 8–14.

Interest in physical DC grid implementation as testbed for new converter prototypes and system operation analysis at RTU has aligned with the European Union research project AREUS objectives for the demonstration of market-available DC technologies for industrial DC grid installation and future developments needed. Figure 3.1 represents the top view layout of the RTU AREUS Demo laboratory room at its final setup:

1 – active AC/DC rectifier unit (55 kW);
2 and 3 – universal robot load emulator units (23 kW);
4 – lithium ion battery energy storage system (BESS) 16-22 kW;
5 – supercapacitor storage system (30 kW);
6 and 7 – 600 V DC-Robot prototype and KUKA DC robot controller cabinet with a load of 21 kW;
8 – master PLC controller (cell controller);
9 – solar DC/DC converter (3–4 kW) for 3.3 kW solar panel array;
10 – optional wind energy emulator setup.

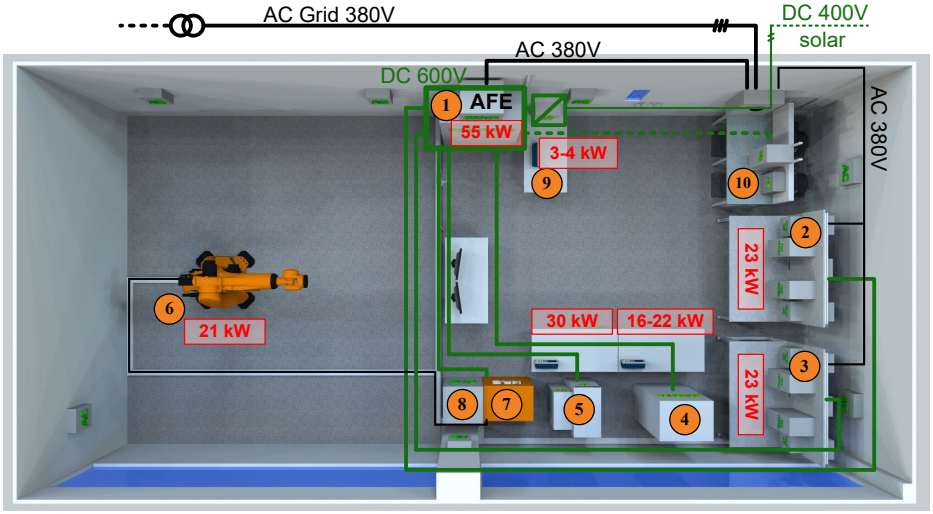

Fig. 3.1. RTU DC microgrid laboratory setup (also referred to as AREUS Laboratory).

The following DC microgrid design aspects and challenges for experimental DC microgrid laboratory implementation have been solved and covered in the Thesis.

- Dynamic DC power flow operation demonstration resembling three industrial robots within limited floor space.
- Implementation of synchronous multipoint power flow measurement solution for experimental data logging and analysis.
- Operational behaviour analysis of central bidirectional AC/DC power interface – also called active front-end converter for DC microgrid supply.
- Cyclic manufacturing process operation analysis and possible optimization measures of electrical equipment.

Development of DC power flow emulator

The small-scale industrial microgrid laboratory environment is foreseen as a physical model of multiple industrial robot installations for manufacturing task execution. Combination of the main task for several dynamic DC load unit implementation along with given constraints of available floor space, investment budget and research areas of IEEI institute allowed to make the decision on the arrangement of an electromechanical system of coupled induction type electrical drives (see Fig. 3.2), combining torque and speed controlled drives for overall system operation objective of controlled DC side power flow.

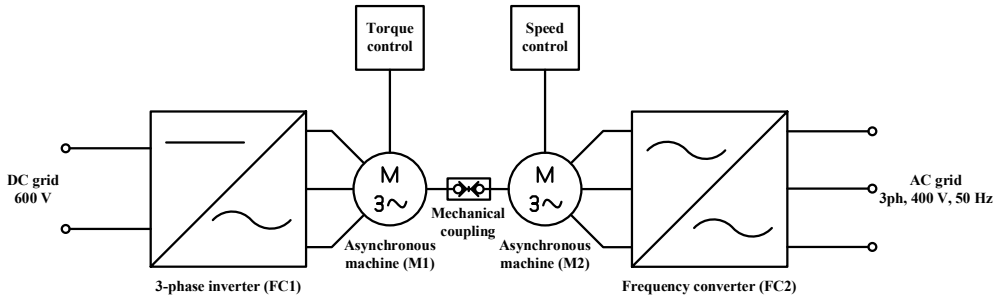

Fig. 3.2. Principal schematic of the bidirectional DC power flow emulator.

Motor drive frequency converter FC2 has an objective of maintaining the stable rotational speed of the coupled system. The other frequency converter, FC1, is operated by an external torque reference provided by the user related to DC power flow demand. Both frequency converters are identical market-available ABB ACS series 22 kW drives, and one of the units is directly supplied by the DC microgrid bypassing input rectifier. The main control principle of DC side power flow control is related to the proportionality of a given torque command, provided mechanical power and respective electrical power consumption or generation as described by Eqs. (3.1)–(3.3).

$$P_{M1} = T_{M1}\omega = \frac{T_{M1} \times n}{9.550} \tag{3.1}$$

P_{M1} is the output mechanical power of electrical machine M1 and the respective mechanical torque T_{M1} by given rotational speed of the linked motor shafts n. If the speed of the linked shafts is kept constant, the desired electrical power flow P_{DC} can be correlated to the necessary torque setpoint. However, the physical system also has losses that can be combined into a single

quantity, ΔP, according to Eq. (3.2) and respective power flows for motoring and generation modes, as represented in Fig. 3.3.

$$\Delta P = \Delta P_{FC1} + \Delta P_{M1,el} + \Delta P_{M1,mech} \tag{3.2}$$

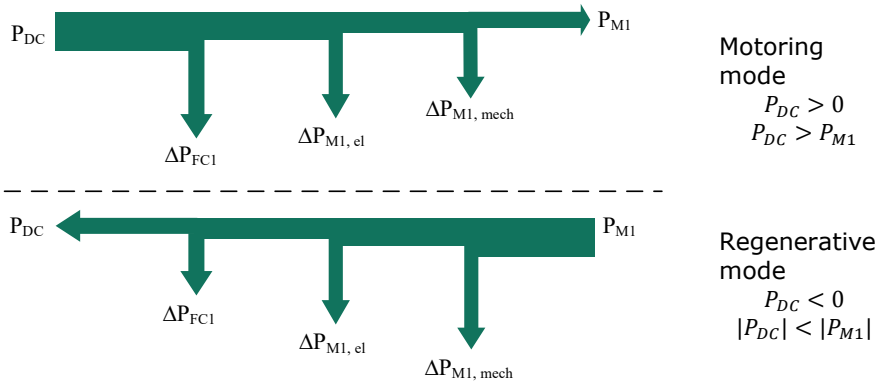

Fig. 3.3. Electrical power flow in motoring (top) and regenerative (bottom) modes.

The exact power balance of DC side connected electrical drive M1 is as in Eq. (3.3).

$$P_{DC} = P_{M1} \pm \Delta P \tag{3.3}$$

A controller has to be developed to dynamically change the torque reference according to the desired DC power flow profile. Since several parameters can vary during operation (speed fluctuations, system losses being dependent on temperature, load conditions, power flow, etc.), a closed-loop controller for calculation of compensated torque reference for the drive FC1 based on the demanded and the measured DC bus power values and the energy losses has to been proposed Fig. 3.4.

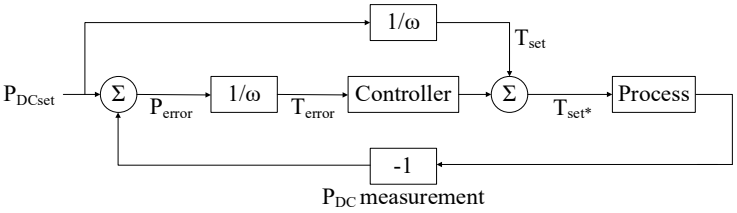

Fig. 3.4. Proposed controller structure for dynamic DC power flow emulation by electrical drive torque variation.

The controller has to compensate only for relatively small deviations from the desired output. In the case of the DC power flow controller feedforward torque reference T_{set} approach based on dominant system behaviour according to Eq. (3.1) is beneficial. The difference between the set and the measured power value is caused by the electromechanical losses present in the system. The task of the controller (Fig. 3.5) is then to modify the torque reference for the compensation of these losses for the final drive arrangement, as represented in Fig. 3.6.

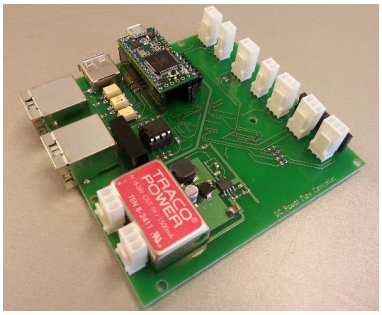
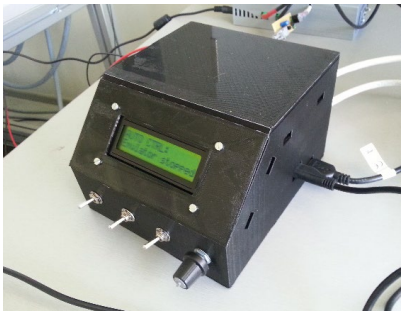

Fig. 3.5. DC power flow emulator controller PCB and enclosure.

Fig. 3.6. DC power flow emulators developed in the RTU AREUS demo laboratory.

The final operating parameters regarding DC power flow physical emulation capabilities are summarized in Table 3.1.

Table 3.1

DC Power Flow Emulator Performance Parameters

DC power ratings	P_{DC} (regenerative)	–18 kW
	P_{DC} (motoring)	+22 kW
Power flow dynamics	dP/dt (regenerative)	–378 kW/s
	dP/dt (motoring)	+448 kW/s

The comprehensive development procedure for the described bidirectional power flow emulator system has been presented in the author's Publication 11. Potential alternatives for

drive control approaches based on funnel controller [24] with respect to a given application have been presented in Publication 14.

Analysis and modelling of an active front-end AC/DC converter

The AC/DC electrical interface converter for bidirectional power exchange between 600 V DC local industrial microgrid system and existing AC infrastructure has been utilized in order to apply power flow conditions similar to those in real production processes.

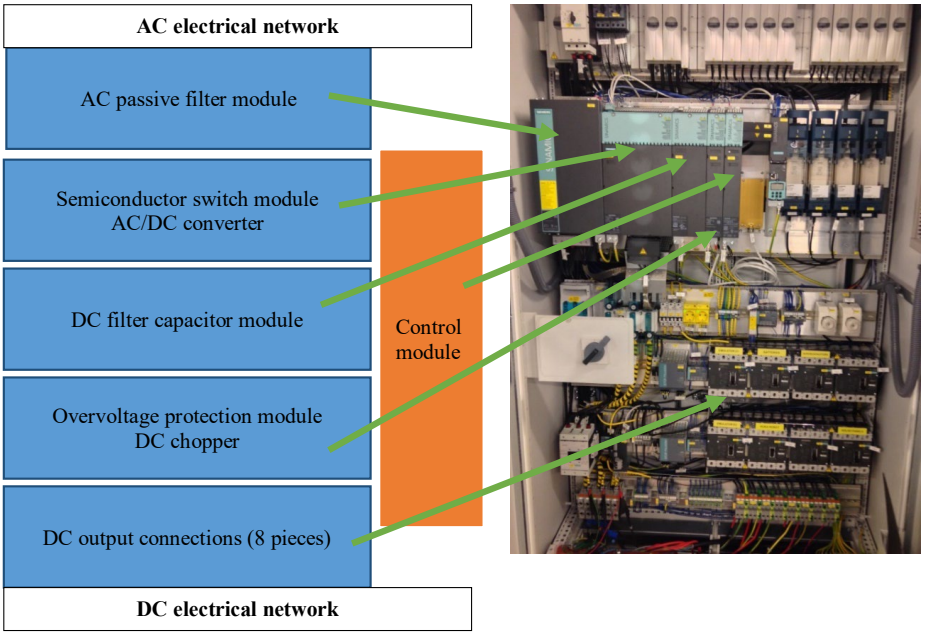

Fig. 3.7. Physical setup of an AC/DC interface converter (right) and a functional block assembly structure (left)

Electrical equipment is based on industrial-grade components selected for specific prototype operation according to planned DC demonstration activities within the AREUS project framework. The significance of a central AC/DC interface converter for DC microgrid requires estimation by measurements of both AC and DC side-related electrical system operating conditions as well as typical characteristics being efficiency, power quality and similar quantities. The idea of a generalized converter operation model extraction based on physical measurements has been applied, since the model-based DC grid design approach has been of interest for future development and practical applications in industry and research environments.

Experimental testing methods

In order to evaluate the performance of AC/DC electrical interface equipment, an electrical system for bidirectional power flow operation has been developed. Electrical testing within the power range of 40 kW for energy consumption and generation with respect to the AC electrical

system has been done. The schematic arrangement using two electrical power flow emulation units has been connected as presented in Fig. 3.8. Electrical power measurement has been done with high-precision power analyser equipment. Two DC-side electrical power flows have been measured with N4L PPA3300 power analysers connected with electrical drive setup for energy flow operation as shown in Fig. 3.9.

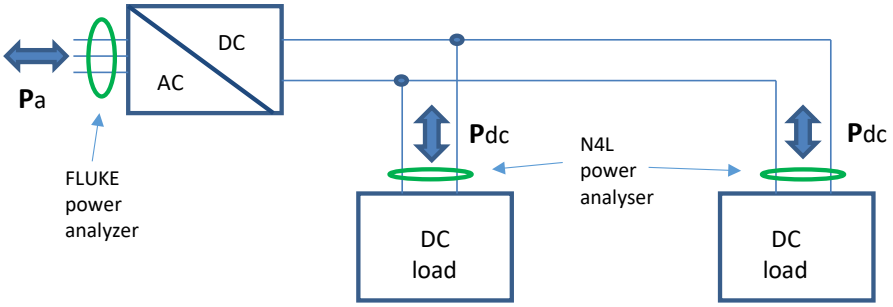

Fig. 3.8. The structure of AC/DC converter operation measurement setup.

Fig. 3.9. FLUKE 434 Series II installed for AC-type electrical measurements (left) and N4L PPA3300 power analyser and DC electrical power flow emulator in the background (right).

The presented testing arrangement has been operated at various load or generated power levels within a range from –36 kW (generating) to 45 kW (loading). The following operational performance indicators have been obtained at various power levels.

Efficiency has been obtained by observing power measurements on both sides of the AC/DC converter and their respective ratio according to power flow. Negative DC power represents operation feeding energy to AC grid, whereas positive energy is drawn from the AC grid. The converter efficiency has been obtained within the range of –36 kW to 45 kW. The efficiency reaches values higher than 0.9 in a broad operating range, exceeding 5 kW for both consumption and regeneration.

Power factor represents the ability of equipment to utilize electrical infrastructure efficiently and consume active power without reactive power component. The ideal case of power factor reaching a value of 1 means that pure active power has been drawn from AC grid. In the case of regeneration to AC grid, the respective ideal power factor value is –1.

The respective efficiency and power factor results related to the DC side power flow are presented in Fig. 3.10.

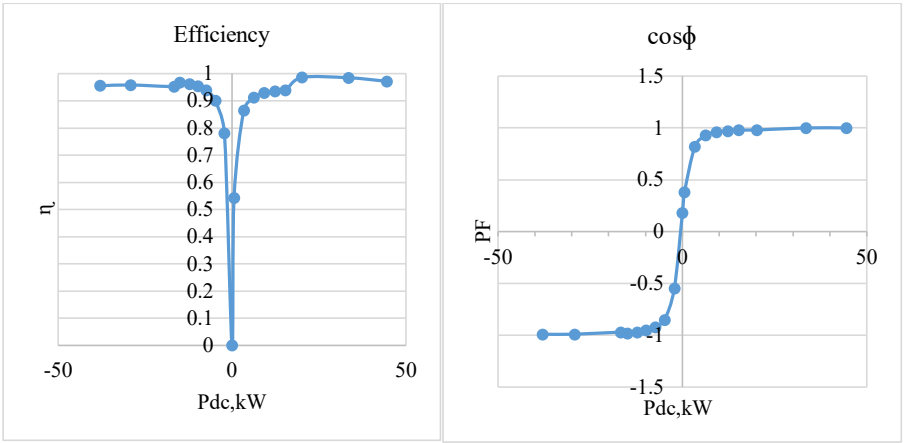

Fig. 3.10. AC/DC converter efficiency and power factor related to DC side power.

Total harmonic distortion factor (THD). The nominal frequency of AC power system is 50 Hz, therefore, the AC waveforms of voltage and current ideally should have only 50 Hz sinusoidal character. In real applications, other harmonics or base frequency multiples are present, adding additional losses and reducing electrical power quality parameters. A parameter known as total harmonic distortion factor (THD) represented in percent allows evaluating the harmonic content of voltage or current. Ideally, the value of THD should be 0 if only the base frequency is present in the analysed waveform. It can be observed that the current waveform quality is significantly reduced at light load conditions, as represented in Fig. 3.11.

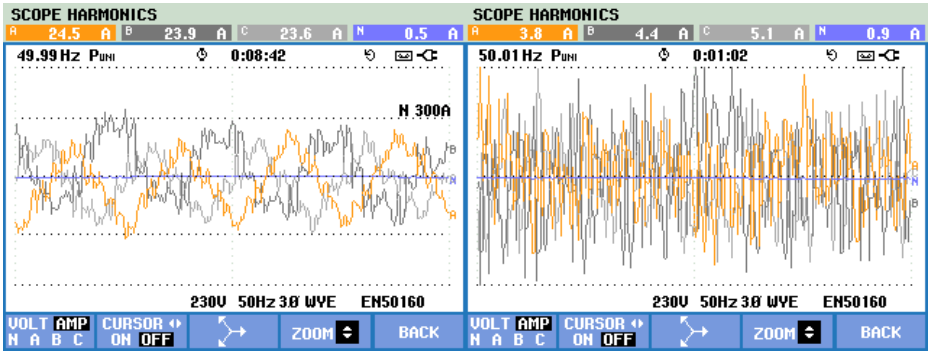

Fig. 3.11. AC phase current waveforms at P_{DC} = 15.3 kW, average current 24 A (left) and P_{DC} = –2.2 kW, average current 4.5A (right).

The results of harmonic analysis and THD coefficient estimation for both waveforms are depicted in Fig. 3.12.

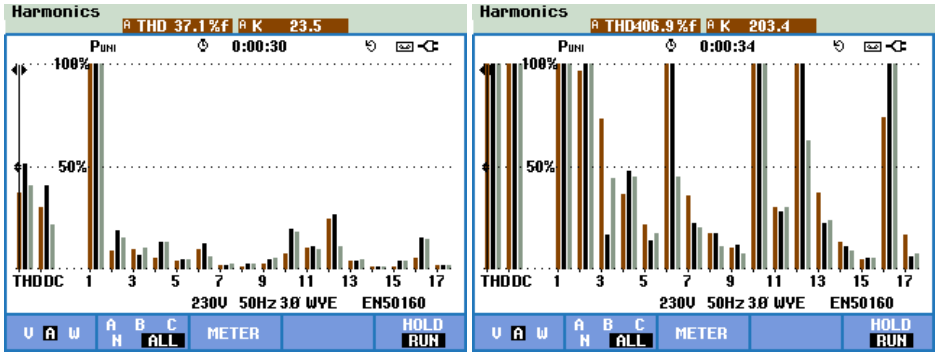

Fig. 3.12. AC phase current harmonic analysis at P_{DC} = 15.3 kW, average current 24 A (left) and P_{DC} = –2.2 kW, average current 4.5 A (right).

The obtained operational behaviour has been measured and represented in Figs. 3.13 and 3.14, where significant variations of AC side current waveforms at light load conditions are represented, whereas voltage distortion is less significant.

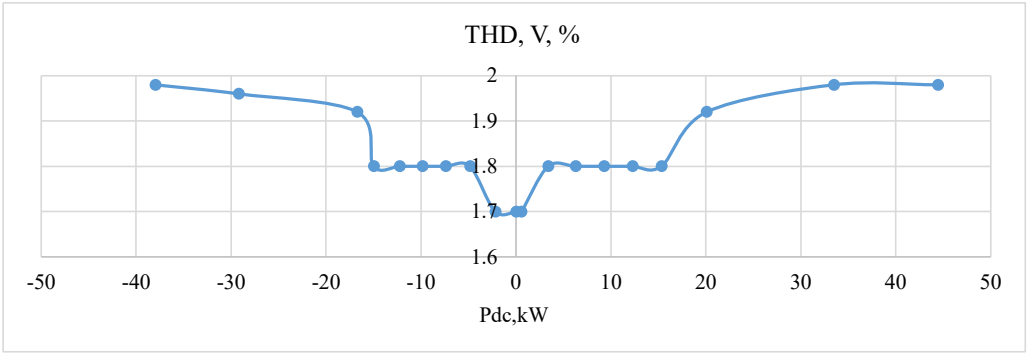

Fig. 3.13. The obtained voltage THD variation referred to DC side power flow operation.

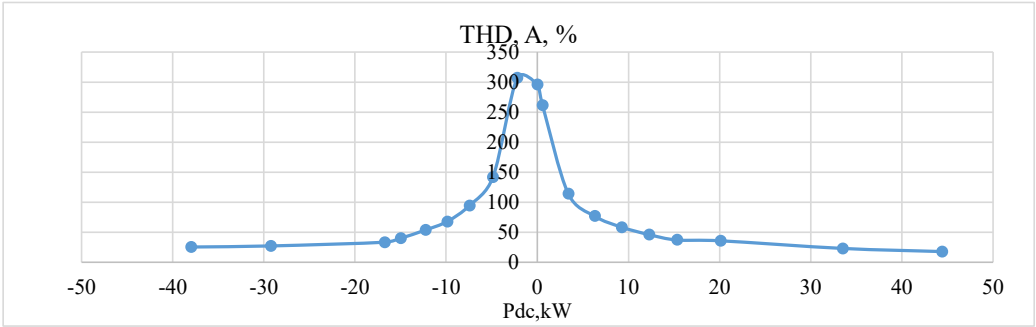

Fig. 3.14. The obtained voltage THD variation referred to DC side power flow operation modelling of AC/DC converter.

DC side measurements

For DC side operation behaviour analysis, AC/DC converter has been operated at various load and recuperation power levels enabled by the DC power flow emulator equipment described

before. Voltage and current waveforms have been obtained through the DataTranslation DAQ acquisition module with a maximum sampling frequency of 44 kHz. The following figures Figure 3.15 represents time and Fig. 3.16 – frequency, which represent the AC/DC converter performance.

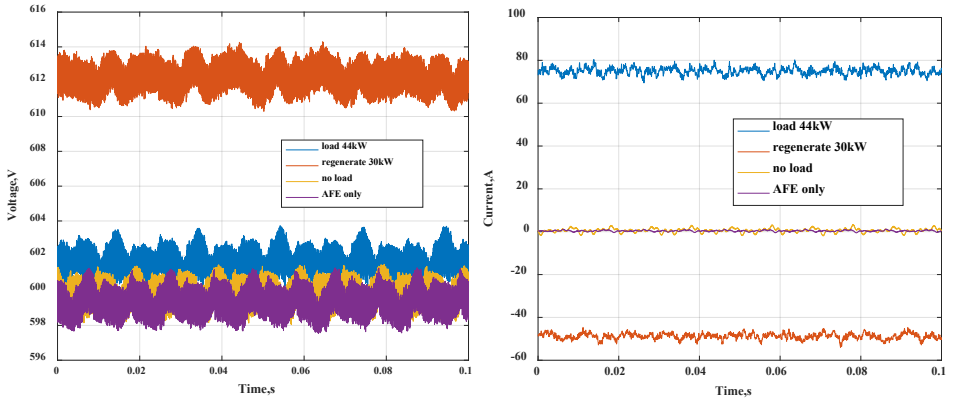

Fig. 3.15. DC link voltage and current waveforms at DC link terminals of AFE converter in time domain.

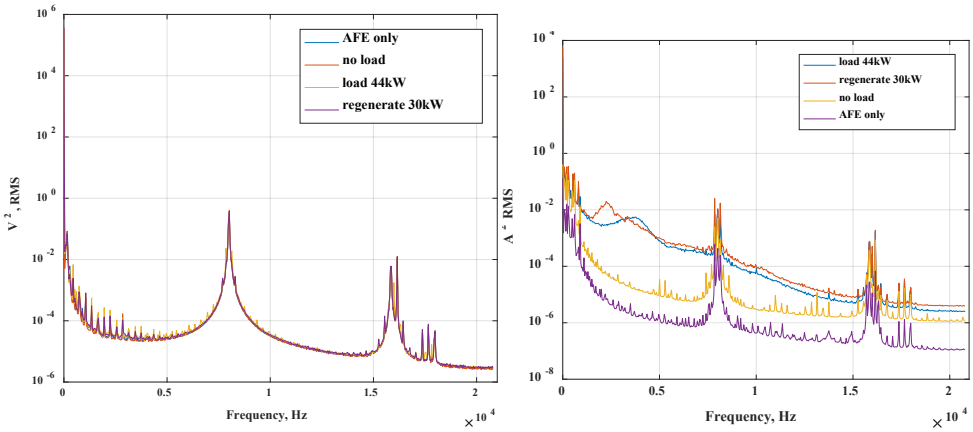

Fig. 3.16. Frequency content analytical results of DC terminal voltage and current at various load states.

The obtained data represent the presence of fundamental 8 kHz AC/DC converter switching frequency and variation of DC side voltage by an increase of 10 V by reversed power flow operation. The spread of the obtained spectrum of current waveform at higher load conditions is observed, and significant multiples of fundamental switching frequency are identified for better design of related measurement equipment and related signal filtering needs. The requirements of DC-related frequency content and related EMC issues is one of the areas being discussed in Publication 8, and while some standards are applicable already, for example, of PV related LVDC systems, many aspects have to be included in future standardisation activities [25], [26].

Development of a simplified model of AC/DC unit.

Based on available data, an approach for the respective AC/DC converter model development has been implemented and described in Publications 9 and 12. Pulsed load testing for voltage dynamic variation on DC bus has been done with a step load variation of 6.5 kW. The simplified dynamic model has been designed according to the structure presented in Fig. 3.17.

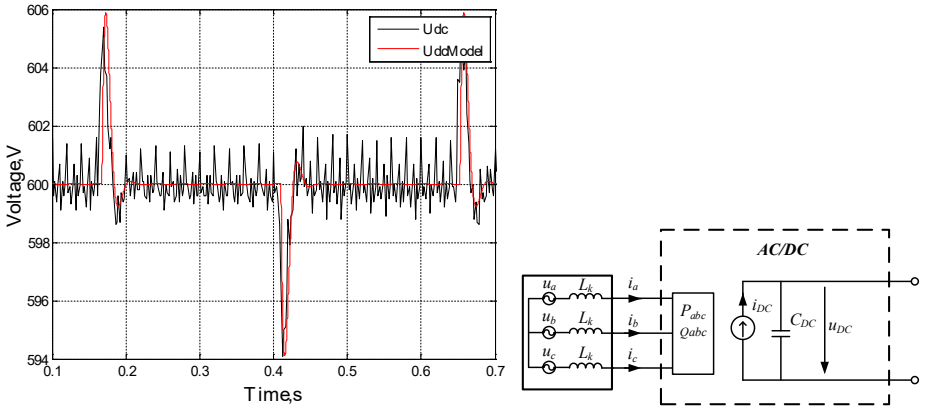

Fig. 3.17. Actual and modelled DC bus voltage dynamics (left) and implemented model structure (right).

The basic principle is the current source control feeding current into a capacitor representing the 4.1 mF output filter capacitor. The reference voltage of the capacitor is set 600 V, representing the microgrid nominal voltage. The charging and discharging of the capacitor have been controlled by the PI-type controller observing output voltage with respect to the reference voltage and respective current source implementation. Other aspects, such as AC and DC side power balance and converter losses, have been based on an approximation of the previously described efficiency and power factor data obtained by measurements.

Application of a synchronized power flow measurement system

In order to perform synchronized power flow measurements for AC and DC-based electrical supply systems, a set of measurement devices has been developed and introduced within the laboratory and industrial DC supply infrastructure. The motivation for applying customized power measurement equipment is related to immediate and time-coordinated data collection needs and future extension for data transfer via industrial communication networks such as Profinet. The ever-expanding relevance of non-sinusoidal, bidirectional, AC and DC-based power flows in real electrical installations demands low-cost distributed power monitoring and measurement solutions. Previous research activities have led to a novel power flow measurement approach utilizing non-even time sampling [27].

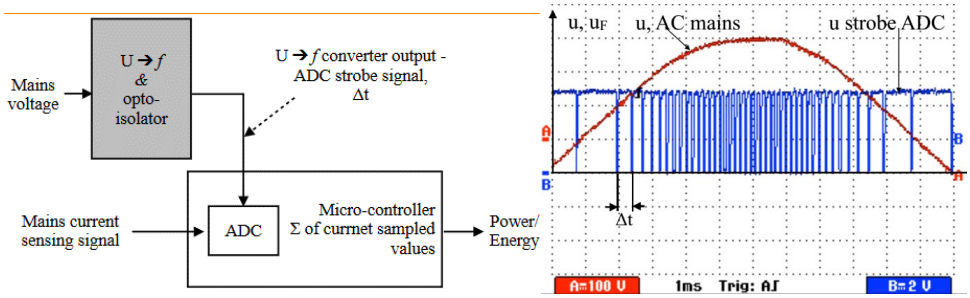

Fig. 3.18. Working principle of a voltage-controlled variable oscillator-based sampling system [27].

The approach is to utilize a variable frequency oscillator for sampling that corresponds to an instantaneous measured voltage *u* by linear function *K,* as in Eq. (3.4):

$$f_{sample} = Ku \tag{3.4}$$

The sampling frequency determines integration time periods *Δt* for energy calculation, as in Eq. (3.5).

$$\Delta t = \frac{1}{f_{sample}} = \frac{1}{Ku} \tag{3.5}$$

Energy calculation within the determined time period *T* is obtained according to the function of Eq. (3.6):

$$\mathrm{W} = \sum_{0}^{T} p\Delta t = \sum_{0}^{T} ui\Delta t \tag{3.6}$$

Since periods *Δt* are related to the variable sampling process in linear relation to voltage, the equation can be rearranged according to Eq. (3.7):

$$\mathrm{W} = \sum_{0}^{T} ui\Delta t = \sum_{0}^{T} \frac{ui}{Ku} = \frac{1}{K}\sum_{0}^{T} i \tag{3.7}$$

Based on the presented principle, a set of measurement devices has been designed for application in industrial microgrids and analysis for individual manufacturing equipment units and respective electrical power flow. Since various types of electrical connection technologies and methods are present in real installation, electrical power flow metering equipment has been adapted for both integrated and external current measurement solutions. Industrial robot electrical power metering units have been implemented as extension cables for existing industrial connectors being used, as shown in Fig. 3.19.

Fig. 3.19. Power flow meter as industrial robot extension cable.

An integrated DC power flow measurement device set has been applied with an internal current measurement sensor. Higher power level measurements and 3-phase arrangement have been achieved by measurement devices with external current measurement clamps, as shown in Fig. 3.20. Additional communication modules for optical data transfer and industrial data protocol standard Profinet are integrated within the same device.

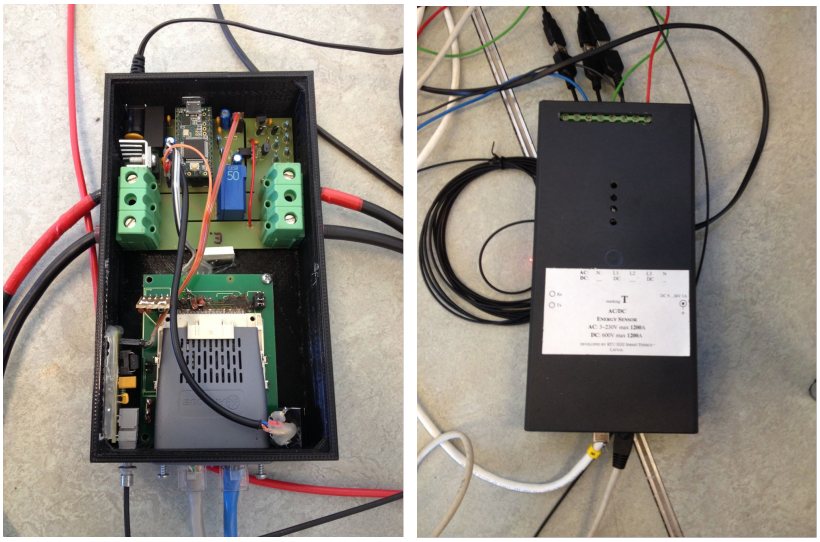

Fig. 3.20. Power meter with integrated current measurement and external current clamps.

In order to achieve time-synchronized and consistent data of distributed power flow measurement installation, optical data communication has been implemented. Figure 3.21 represents a central optical fiber connection for centralized data acquisition.

Fig. 3.21. Optical fiber data transmission and aggregation device.

The synchronized data set is produced by aggregating individual metering unit data with a bidirectional optical communication data network, providing synchronous requests for every power flow meter every 20 ms. Internally, each power meter unit has a sampling frequency of 2.8 kHz and provides an averaged value on request for the previous 20 ms acquisition time period.

Cyclic operation-related parameter analysis

As laboratory scale installation of DC microgrid is physically implemented, respective analysis of system operation and related selection of protection equipment or power supply dimensioning has been of interest. Significant property within industrial manufacturing operations is related to the cyclic repetition of automated processes and respective electrical power consumption dynamics.

Typically, the data with a given sampling frequency f_{sample} for a respective period time frame with length t_n is available from measurements or simulations. An approach for input data analysis based on the sliding analysis window concept along extended operational period data has been applied. The sliding analysis window being shifted along the whole dataset and with variable window width can provide a method for data categorization or time-related distribution analysis as presented in Fig. 3.22.

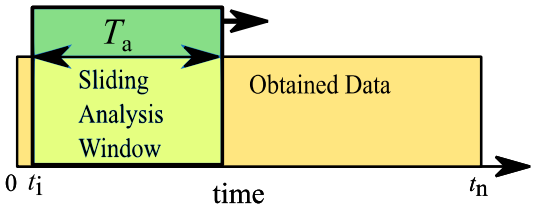

Fig. 3.22. Visualization of sliding analysis window approach application for power data analysis.

The presented idea is applied for dynamic power variation analysis to retrieve an overview of the characteristic behaviour of electrical load maximal instantaneous power requirement and respective combined power demand for a group of loads (the author's Publication 8).

Therefore minimum and maximum sliding window size options can be defined based on Eqs. (3.8) and (3.9).

$$T_{min} = \frac{1}{f_{sample}} \tag{3.8}$$

$$T_{max} = t_n \tag{3.9}$$

The minimum analysis window is defined by an applied sampling frequency of data and the respective distance in time between two adjacent samples. The maximum window available for analysis is limited by the total data sampling time frame t_n. By variation of window size, T_a, the respective number of following samples for evaluation within the analysis window can be defined according to Eq. (3.10).

$$n = \frac{T_a}{f_{sample}}, T_a \in [T_{min}, T_{max}] \tag{3.10}$$

Evaluation of average power P_{avg} within the scope of analysis window being shifted according to the number of samples i is represented by Eq. (3.11).

$$P_{avg}(i, T_a) = \frac{1}{n}\sum_{i}^{i+n} P_i, i \in [1, t_n - n] \tag{3.11}$$

The final analysis result for a particular analysis window width being shifted along initial data is determined according to Eq. (3.12).

$$P(T_a) = \max(P_{avg}(i, T_a)) \tag{3.12}$$

By analysis according to equations, the characteristic behaviour of electrical load instantaneous peak power requirement can be determined, as given in the example.

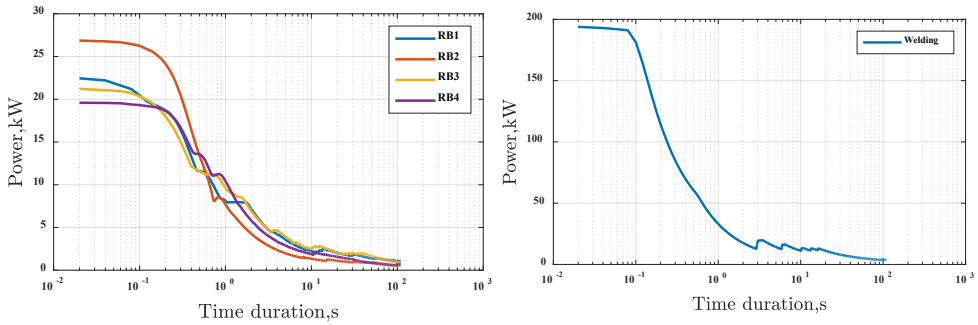

Fig. 3.23. Peak power analysis results of a 4-manipulator set (left) and the welding process (right).

The analytical approach has been further applied for interconnected DC microgrid peak power rating and respective infeed converter power rating selection. The following graphical workflow in Fig. 3.24 represents two approaches based on available information if only individual electrical unit power profiles are available or information about combined system behaviour and time-based coordination is available.

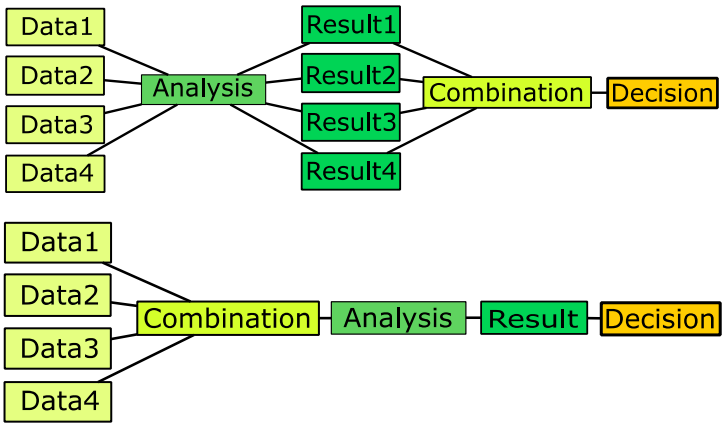

Fig. 3.24. Comparison of the parallel power peak demand analysis approach (top) and the combined approach (bottom).

The obtained results represent a significant variation of achieved peak power demand character, and therefore, the significance of system modelling needs in advance for the electrical system and component dimensioning.

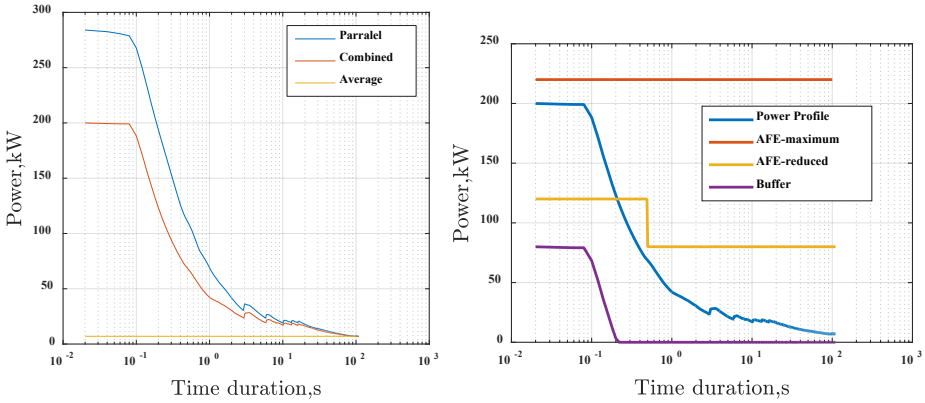

Fig. 3.25. Parallel and combined analysis result for power demand (left) and potential converter dimensioning scheme with dynamic energy buffer application (right).

A similar approach has been applied to analyse industrial robot cyclic current profiles (Publication 10). The interest in individual unit current flow behaviour analysis has been related to the optimal selection of appropriate circuit protection rating as well as the identification of unique patterns for each robot for diagnostic application in future. In combination with semiconductor-based circuit protection developments [28], an adaptive approach for critical parameter adjustment can be considered. Current reference profiles are used as input data set of industrial robot, as represented in Fig. 3.26.

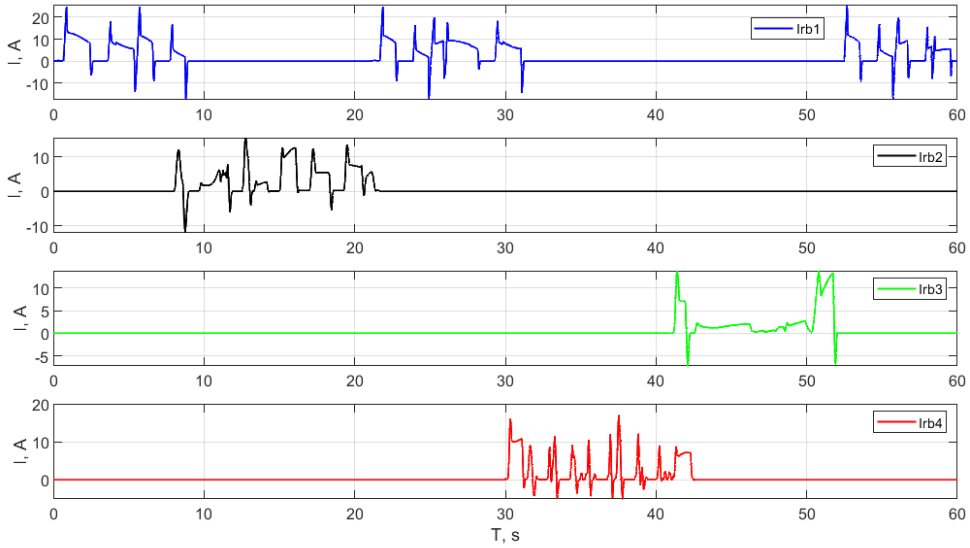

Fig. 3.26. Example of a 60-second repetitive industrial production cycle and consumer electrical load current profiles in the case of four industrial robots assisting for several operations: IRB1 – material handling; IRB2 – to carry a welding gun; IRB3 – to carry a glue dispenser; IRB4 – to carry clinching equipment.

The analysis of peak average values of the current concerning time duration has been represented in and compared to a few typical fuse characteristics available in datasheets for PV and general type loads.

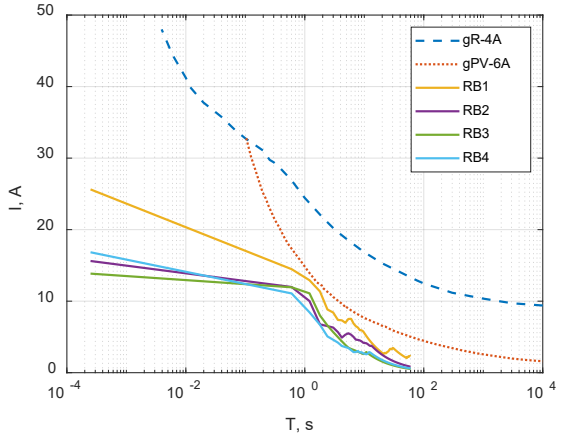

Fig. 3.27. Comparison of the sliding window analysis for highest mean current values and the typical fuse current-time curves of types gR-4A and gPV-6A.

Another approach has been carried out using the sliding window approach for categorization of obtained measurement sample data within categories C of measured values x. In this way the total operation period time span from 0 to final sample t_n has been assigned according to

respective sample measurement values to categories from C_1 to Cn covering the whole measured current profile value range.

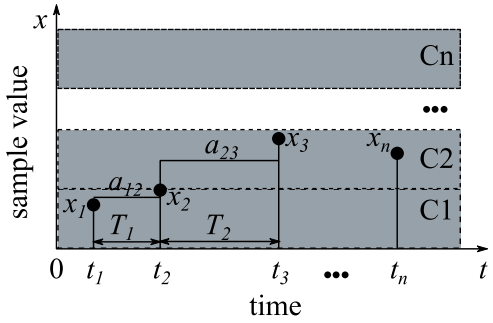

Fig. 3.28. Graphical representation of current sample *x* categorization analysis within classes C.

Such an approach has been considered for future operation online observation and application that would generate patterns for each individual robot operation within a given manufacturing cycle. If cycle time is fixed, then the analysis pattern result obtained by the logged current profile would also represent similarity. Fig. 3.29 provides a graphical representation of load current behaviour.

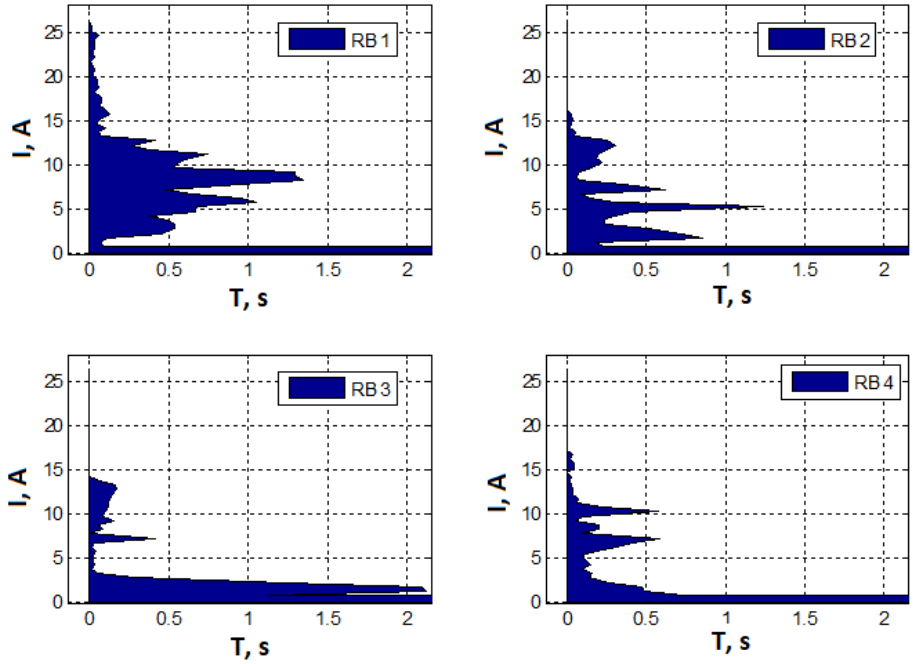

Fig. 3.29. A magnified view of analysis results for time span below 2 seconds.

4. EXPERIMENTAL TESTING OF AN ENERGY EFFICIENT DC MICROGRID IN A LABORATORY AND A ROBOTIC AUTOMOBILE MANUFACTURING INSTALLATION

Implementation of robotic manufacturing DC microgrid for automotive production

For experimental verification of DC microgrid-related equipment and demonstration of available state-of-the-art technologies, a new purpose-built DC microgrid installation has been implemented by Mercedes-Benz AG (previously Daimler AG) company in a factory located at Sindelfingen, Germany.

Joint research and development activities have been pursued together with Riga Technical university within AREUS research project; therefore, the availability of an industrial DC system for operation analysis has been valuable, as represented in the author's Publication 5. Within the implementation of the AREUS project, an installation referred to as the AREUS DC demo cell was designed, commissioned, and used for experimental verification. Since the company Mercedes-Benz AG has know-how and experience in automobile manufacturing and respective automation infrastructure development, a new DC electrical system has been implemented according to the typical approach of continuous automotive production process distributed into separate areas referred to as production cells.

The design and functionality of a particular DC demonstration cell have been based on the following objectives and background motivation aspects, the main of those being:

- to copy a part of the actual manufacturing process and demonstrate a design for the conversion of AC-based electrical supply infrastructure to DC-based electrical supply infrastructure;
- to apply existing technology and automation standards and guidelines implemented by Daimler AG globally in a series of factories;
- to incorporate several technology tools and joining technologies for car body production and carry out respective equipment adaptation for DC-supplied operation;
- to obtain knowledge of market-available DC electrical equipment and supplier base and identify technological solutions to be developed in future.

As a result of defined objectives single existing production cell design dedicated for assembly of several prefabricated metal parts into single part for futher processing has been selected. Primary operations are carried out by a group of four industrial robot manipulators combined with spot welding, rivet punching, and adhesive bonding as applied production technologies. The physical installation has been presented in Fig. 4.1.

Fig. 4.1. DC microgrid realization as an automotive manufacturing cell for experimental analysis (Publication 5).

A DC microgrid cell has been built within a square area of around 10 meters side length and separated by a safety fence. Industrial robot controllers and other electrical technology equipment cabinets have been placed along the border, and the DC electrical supply rail has been implemented as a ring type busbar raised above the safety fence. Figure 4.2 represents a combination of applied equipment and related measurement locations for data collection of power flow analysis by spatially distributed power flow measurement equipment installed by RTU.

System component overview

Key system components of DC microgrid cell are:

- active front-end AC/DC converter unit (AFE) of rated power 450 kW assembled by industrial energy conversion modules;
- a set of four industrial robots KUKA KRC4, 210 kg payload manipulators;
- li-ion battery with interface converter of rated power 30 kW;
- PV infeed DC/DC converter;
- electrolytic capacitor bank, 132 mF;
- technology tools adapted for DC operation (spot welder, rivet punch tool, glue dispenser, rotating conveyor table).

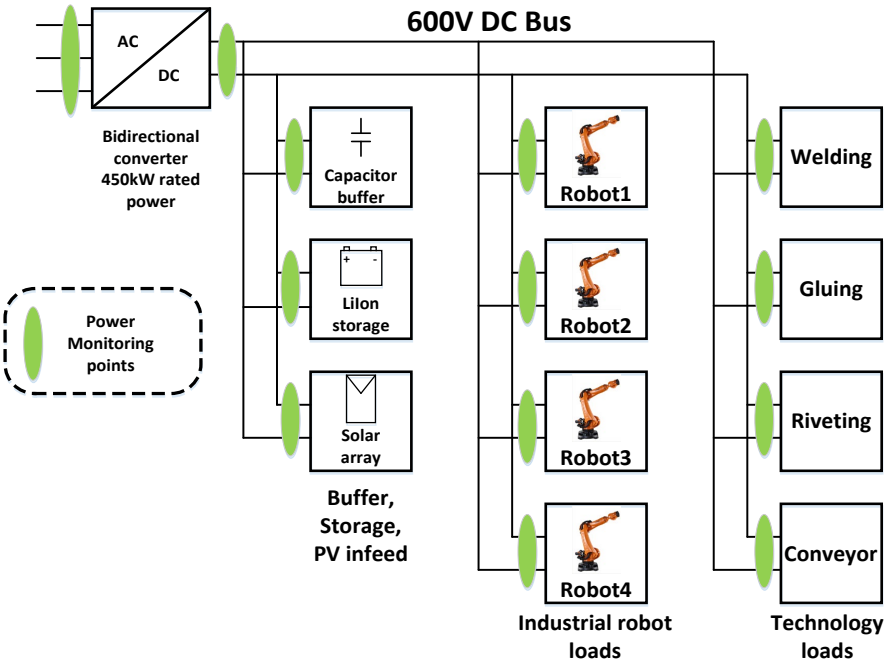

Fig. 4.2. Structure of examined DC microgrid for automotive manufacturing application.

The available setup has been utilized for several experimental tests of power and energy-related performance estimation of industrial application DC microgrid systems.

Individual robot unit test

- Conversion of industrial robot power supply from AC to DC and related energy efficiency variation.

DC microgrid operation test

- Estimation of reused energy potential in industrial application of individual units.
- Dynamic effects of high peak power demand operation.
- Estimation of the power balance of DC-type microgrid system and central interface converter performance.

Analysis of individual robot's operation by converting the control cabinet from AC to DC supply.

In this series of power flow measurements, a physical substitution approach of industrial robot control cabinets of type KUKA KRC4 from conventional AC-based products to DC-based protoype designs has been applied. Since the applied power flow measurement equipment has the capability of both AC and DC type electrical power data acquisition, the same devices are used and designed explicitly for industrial robot cabinet KUKA KRC4 electrical interconnection needs, as described in the previous chapter. Measurements were taken during the production process, and it was observed that the motion type of robots varied due to the

position of individual parts used for assembly. The parts are supplied stacked vertically and pick-up time is increasing, since the following part has to be picked up at lower position than previously. A typical completed production cycle length of 98 seconds for all four industrial robots has been obtained for AC to DC cabinet conversion analysis.

Fig. 4.3 represents a graphical comparison of power flow profiles of industrial robots within the production cell of the combined four industrial robot operations for AC and DC-type electrical supply use cases.

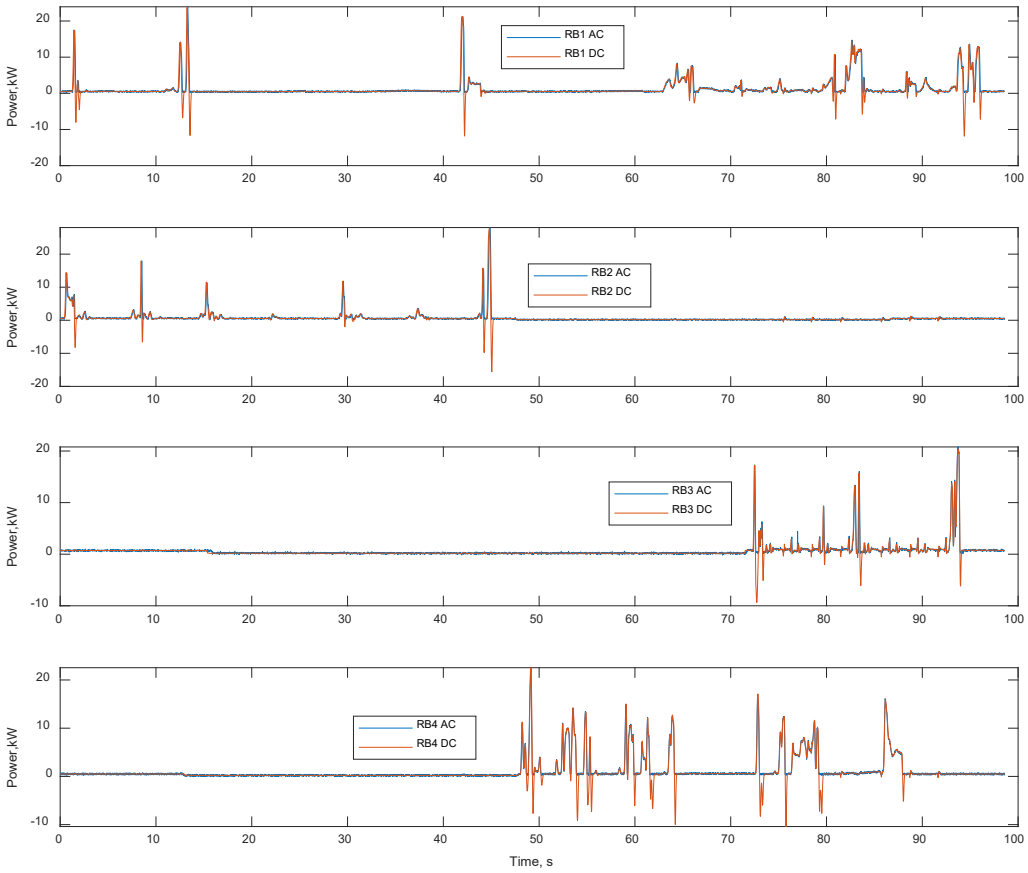

Fig. 4.3. Power flow of a set of four industrial robots for same production cycle, AC and DC based operation.

Calculation of mean power over the production cycle has been done for each industrial robot's control cabinet as well as for combined consumption of all units. The results are summarized in Table 4.1. In all cases, replacing the AC supply-designed control cabinet with a DC-based supply cabinet has reduced average consumed power variation between 5.64 % and 12.55 %. The most significant reduction has been observed of industrial robot picking and placing small metal parts for later processes of joining technologies supported by other industrial robots. All involved industrial robots are equipped with additional tools of weights above 100 kg.

Table 4.1

Result Summary of AC to DC Robot Controller Conversion Test

Robot No.	Related task	Mean power, AC case, kW	Mean power, DC case, kW	Difference (DC case vs AC case), kW	Difference, % of AC case
RB1	Glueing	1.274	1.161	–0.113	–8.87 %
RB2	Riveting	0.693	0.634	–0.059	–8.51 %
RB3	Welding	0.638	0.602	–0.036	–5.64 %
RB4	Part feed	1.211	1.059	–0.152	–12.55 %
Total (4 units)	-	3.818	3.457	–0.361	–9.45 %

Conversion of an AC-based industrial robot application to a DC-based industrial robot application allows utilisation of energy provided by recuperation, and such example of four industrial robots presents a total mean consumed power reduction of 9.45 %. A graphical representation of the total four industrial robot power flow of AC- and DC-based systems is shown in Fig. 4.4.

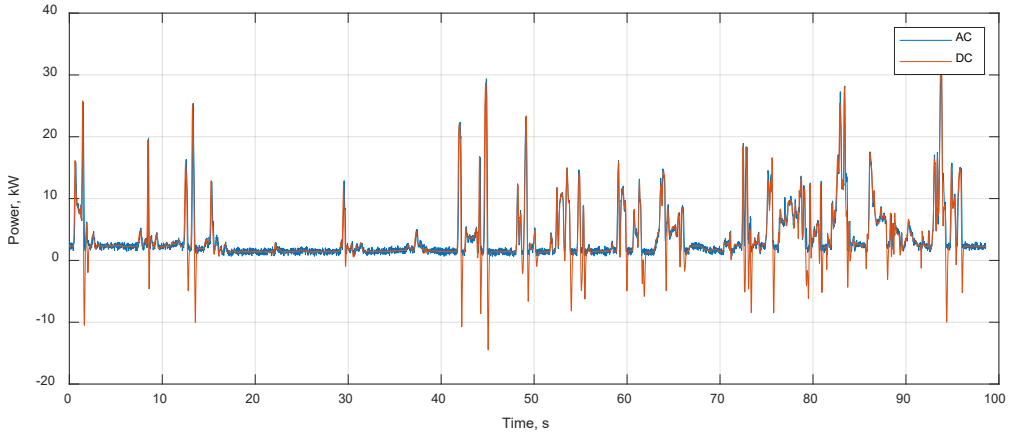

Fig. 4.4. Total power flow of set of four industrial robots, AC and DC based operation.

The performed experimental tests ofreplacing individual market-available AC-designed industrial robot control cabinets with the prototypes for DC-type electrical supply support the hypothesis of energy efficiency improvement related to modification of energy supply system.

Analysis of DC microgrid operation test

The following chapter analyses several aspects of complete DC demostration manufacturing cell operation as a DC microgrid system.

Figure 4.4 represents the obtained power flow results, including thirteen measurement locations within a microgrid. Due to differences in variation and magnitudes of power demand for individual units, the figure shows three groups of devices. All four industrial robot units have similar operational behaviour and are represented in the top axis. Technology tools, li-ion batteries, and PV infeed converter operation have lower power values than 10 kW and are depicted in the middle axis. High power units, being AFE AC/DC converter and spot welding

tool supply are combined in the third axis. The figure represents the operation period in time of 116 seconds, covering one cycle of the continuous process of part assembly involving welding, riveting glueing and related handling of materials. During the test period, power supply from PV panels has also been available and fed into the common DC bus.

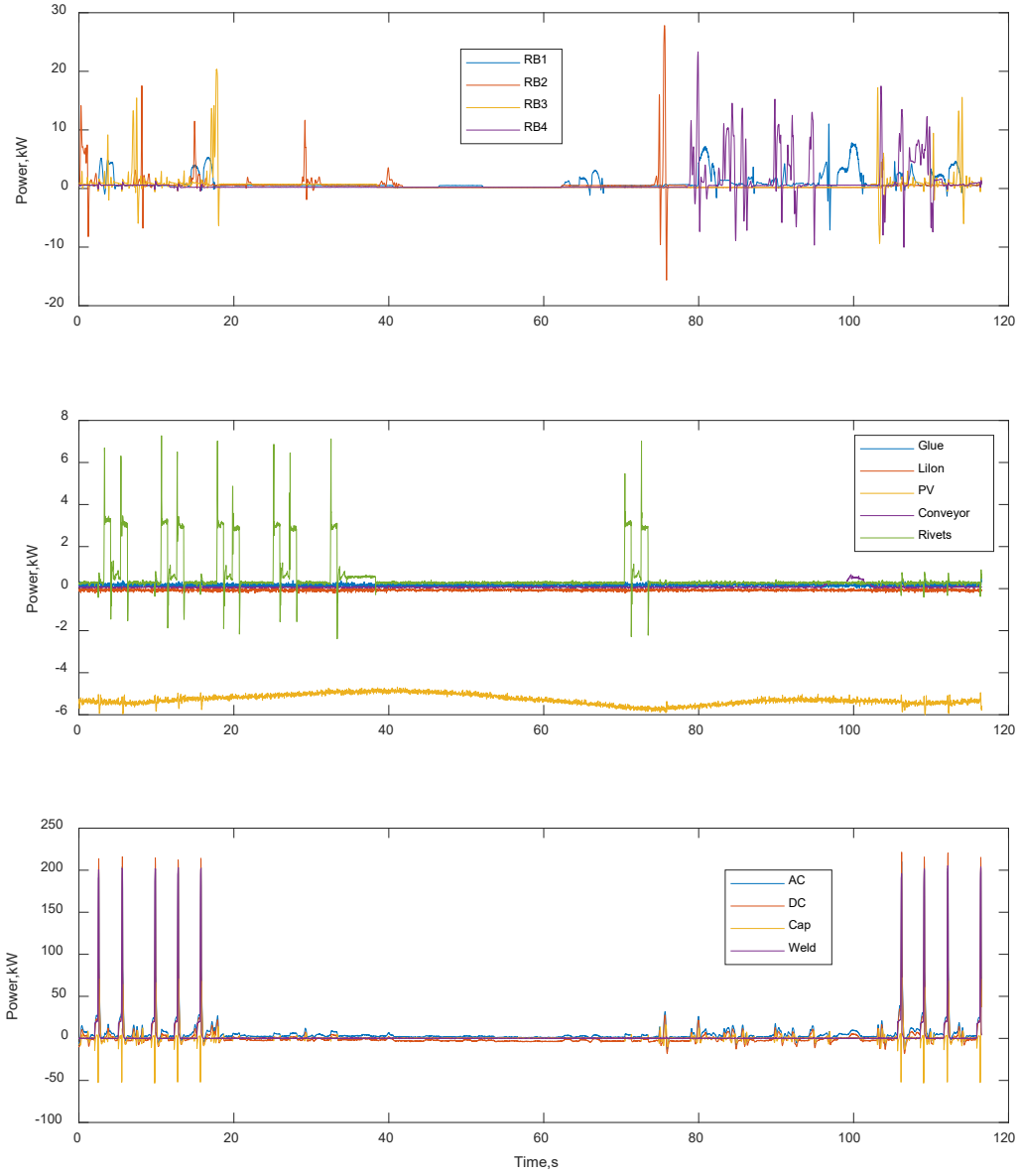

Fig. 4.5. Representation of synchronous power flow measurement results, 13 locations within industrial DC microgrid installation.

Estimation of reused energy potential in industrial application of individual units

One of the particular aspects of interest has been an evaluation of bidirectional energy flow and the relative amount of energy available for reuse due to the advantages of simple energy exchange within DC-type systems in dynamic operation conditions and recuperation events of industrial robots. Eqs. (4.1) and (4.2) represent mean power calculation by separating positive and negative components of power flow P within a certain period of analysis, T.

$$P_{pos} = \frac{\int_0^T P(t)}{T}; P(t) \in [0, \infty) \tag{4.1}$$

$$P_{neg} = \frac{\int_0^T P(t)}{T}; P(t) \in [-\infty, 0) \tag{4.2}$$

Table 4.2 represents the calculation results of bidirectional energy flow for industrial robot units and electrolytic capacitor modules connected to the DC bus of the manufacturing cell.

Table 4.2

Calculation of Mean Positive and Negative Power Flow Values for Individual DC Microgrid Units

DC unit	Related task	P_{pos}, kW	P_{neg}, kW	P_{neg}/P_{pos}, %
RB1	Glueing	1.123	0.044	3.92
RB2	Riveting	0.660	0.040	6.10
RB3	Welding	0.582	0.029	4.95
RB4	Part feed	1.011	0.098	9.71
Total (4 robots)	-	3.376	0.211	6.26
Capacitor bank		1.089	0.677	62.21

The results represent the contribution of industrial robot braking energy reuse cases expressed as negative mean power flow values. The combined operation of four robots led to the average ratio of recuperated power being 6.26 % concerning consumed power. According to motion profiles and manufacturing process needs, individual robot values vary from 3.92 % to 9.71 %. Another DC microgrid element of interest has been a capacitor module installed as an energy buffer element for DC voltage stabilisation. The results represent significant mean power flow values of capacitor operation comparable to single industrial robot units. Accordingly, as the capacitor module has been operated as a dynamic energy storage element, the power flow returned to DC bus has a significantly higher value than industrial robots. The ratio of reused energy with respect to the supplied energy of the capacitor module is 62.21 %. Such results represent the overall efficiency of dynamic operation and related losses of electrolytic capacitors as balancing elements for dynamic operation discussed in the following chapter.

Spot welding power analysis and dynamic effects

Several part-joining manufacturing technologies have been applied within the DC demonstration manufacturing cells. The technology of particular importance has been the aluminium spot welding method performed by a spot welding gun carried by an industrial robot manipulator. The DC-based prototype of the spot welding gun supply and control unit has been

produced by Bosch Rexroth company and designed for operation, replacing the conventional AC welding gun supply unit. The spot welding process presents challenging operation conditions for electrical supply infrastructure due to high power demand of individual spot welding instances of short periods. A complete data set of values at thirteen locations within DC microgrid was obtained through the applied power flow measurement system. The most significant dynamic variation of power flow due to the welding process is represented in the Fig. 4.6. The power flow balance combined of the spot welding tool, both sides of the active frontend AC/DC converter, and the capacitor module power flow are shown.

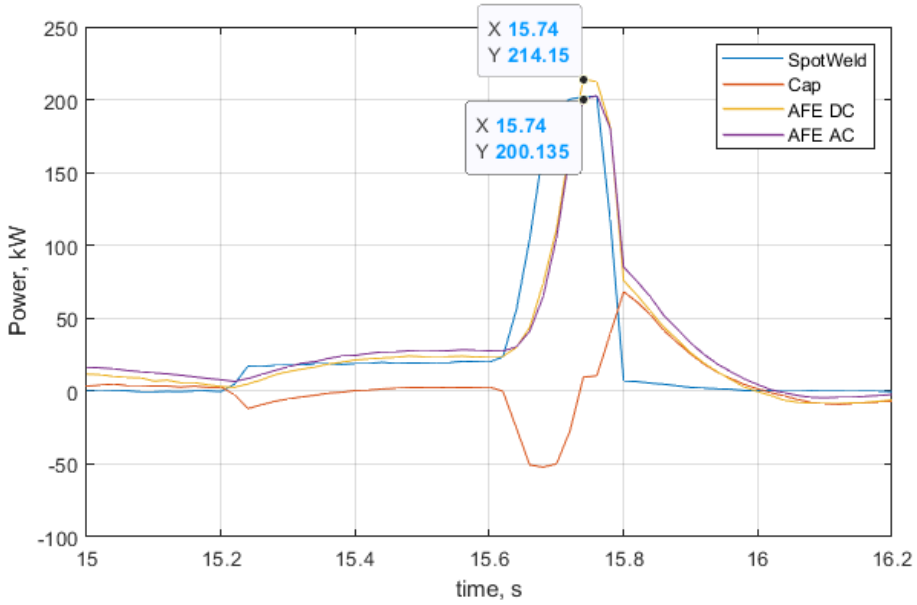

Fig. 4.6. Spot welding instance power of spot welding tool, active front-end AC and DC side and capacitor module.

The single spot welding operation lasts around 0.6 seconds and combines preheating and main welding procedures. The maximum power drawn by the spot welding tool reaches 200 kW. Due to the rapid power demand response of the capacitor module, the power flow is clearly visible. During high power peak rise time the power delivered DC bus capacitor module reaches a 50 kW level. After stabilisation of load power pulse, power supply is provided by the main AC/DC frontend converter. One can observe that the values of the AFE converter DC side exceed those of the AC supply side. The difference can be calculated according to Eq. (4.3), where $P_{AFE\ AC}$ is active fronted AC grid side drawn power and $P_{AFE\ DC}$ is the DC side delivered power flows within a microgrid.

$$P_{AFE\ loss} = P_{AFE\ AC} - P_{AFE\ DC} \tag{4.3}$$

The difference in power flow $P_{AFE\ loss}$ represents the power flow of combined converter power losses including the power used for auxiliary consumption, such as 24 V automation and safety equipment power supply, SCADA system and power commutation equipment control.

Therefore, a more detailed analysis of AFE converter loss power flow combined welding process is presented in Fig. 4.7.

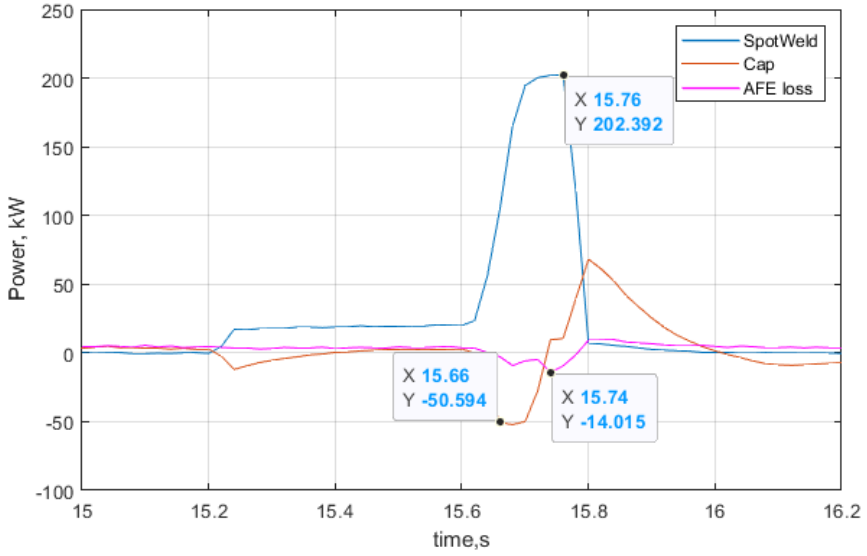

Fig. 4.7. Example of power flow drawn from the capacitor module and reverse pover flow of AC/DC converter internal circuits.

The dynamics of power consumption represent the behaviour that requires power for spot welding tools, which has also been provided from internal devices and circuits within the AC/DC converter cabinet. The AC/DC converter has internal filter capacitors that behave similarly to the main capacitor module and provide power as the main capacitor module power is reduced.

The AFE internal loss power variation with respect to AFE DC side power demand is mapped as shown in Fig. 4.8.

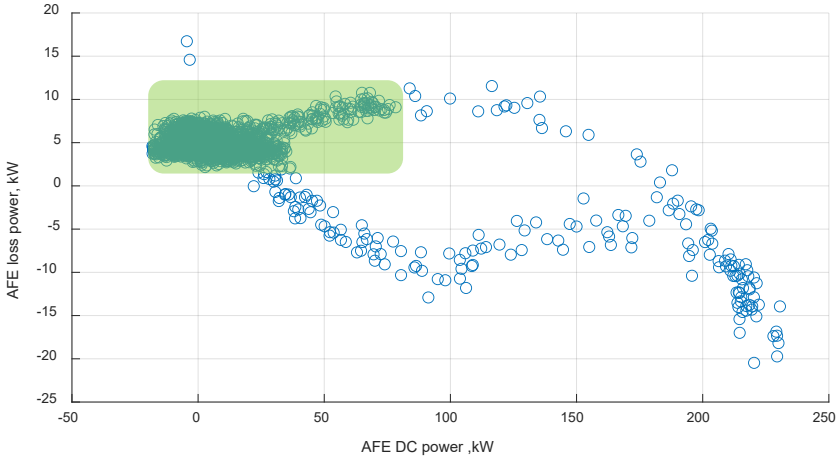

Fig. 4.8 Active front-end converter internal loss power flow vs active front-end converter supplied DC power.

After observing the operating point density in time over the whole manufacturing process, it is visible that internal AC/DC converter loss and auxiliary equipment power demand are aggregated at 0 kW to 10 kW level during stable operation below 75 kW. The sparse operating points outside the green area represent pulsed power effects related to spot welding power demand.

DC side power flow balance evaluation using superposition approach

In order to verify the dynamic performance of the applied multipoint synchronous power flow measurement system and measurement result data, the calculation of power flow balance of 12 location power flows has been done. Adding all 12 power flows connected to DC bus would provide zero sum in idealized case if physical electrical losses were neglected and no measurement error would be present. According to such a superposition approach, the value *SumDC* has been introduced. The results obtained over the time frame are presented in Table 4.3.

Table 4.3

Key Results of DC Bus Power Flow Balance Value *SumDC* Calculation

	Max. value, kW	**Min. value, kW**	**Mean value, kW**
SumDC	44.29	–27.64	0.180

Analysis of the obtained *SumDC* parameter with respect to DC system operation dynamics reveals that increased deviation of DC bus power flow balance calculation has been obtained during peak power demand instances. Figure 4.9 represents the observed balance deviation with respect to welding power peak demand.

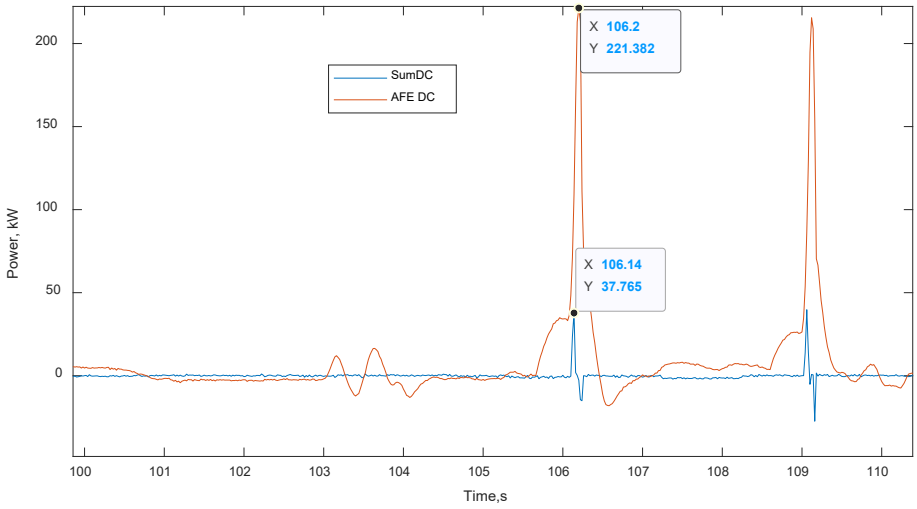

Fig. 4.9. DC bus power flow balance parameter *SumDC* variation during spot welding process compared to AC/DC AFE converter supplied DC power.

The mean value of *SumDC* power flow value over the full time period of DC microgrid observation reaches the value of 180 W. The dynamic variation during steep power flow rate of rise or fall can be explained by potential errors of measurement that could be induced by the dynamic behaviour of applied current measurement equipment based on the Hall effect current clamps.

Power balance of DC manufacturing cell

In order to obtain an overview of mean power flows over continuous manufacturing process and related energy distribution within microgrid system, Fig. 4.10 has been developed.

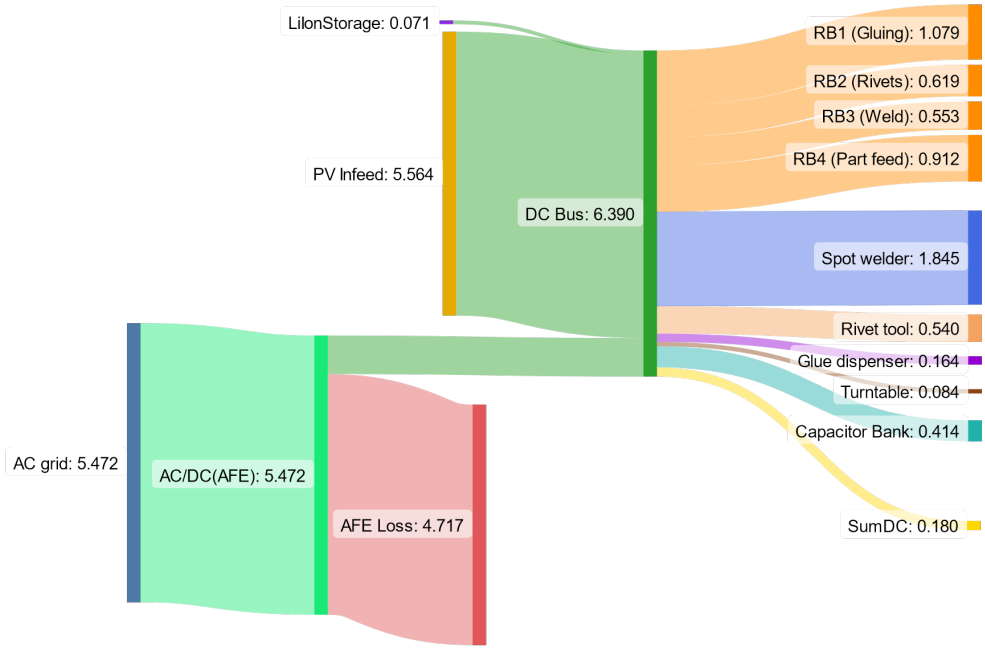

Fig. 4.10. Full DC manufacturing cell mean power distribution based on synchronous 13-point power flow measurement system test data.

- Power sources

The particular configuration of DC microgrid has two major power supply sources, being AC grid and PV panels (PV infeed) of average renewable power flow of 5.64 kW. The connected li-ionbattery module has operated in standby mode with a neglegable contribution.

- Central AC/DC active front-end (AFE) operation

The main AC/DC bidirectional converter operation has been analysed by calculating the internal power demand $P_{AFE\ loss}$ over the operational period. The average value of 4.72 kW may appear large compared to technology-related loads discussed further and within the same scale as solar renewable power delivered. However, this power flow represents several functional needs of the whole DC installation, i.e., 24 V supply of automation and safety equipment and several control and operator panels, electrical cabinet air conditioning and converter losses being the most significant. Considering the ability of selected infeed converter configuration for large industrial DC microgrid system power supply, such auxiliary power demand can also be considered reasonable.

- Industrial robot and technology tool consumption

The group of four industrial robots has similar mean load power values in the range of around 0.5 kW to 1 kW. As discussed before, the power drawn from the DC bus has been reduced by recuperation energy utilization. The most significant technology load has been the spot welding application, reaching around 1.8 kW mean load power, but the requirements imposed for DC

microgrid operation due to high peak power are fundamental for design of electrical installation. Other technology loads have low average power consumption requirements of 0.6 kW or less.

- Capacitor module operation and total balance of DC bus power

Due to dynamic power flow behaviour, the overall performance of the electrolytic capacitor module installed on the DC bus represents a mean power requirement of 0.414 kW. Such value has been obtained according to dynamic operation of around 50 kW discharge and 60 kW charging peak power pulses related to common DC system balancing needs imposed by spot welding application. An average power of 0.414 kW represents combined mean losses due to electrolytic capacitor series resistance character and related conduction losses of modular arrangement of individual cells.

The value of *SumDC* parameter 0.18 kW represents a combination of all DC side power flow measurement equipment errors mainly related to dynamic current detection during steep power change instants. The other component contributing to the overall result of *SumDC* loss power is introduced by the real physical connection of individual devices to the DC busbar system, therefore, physical losses are also included. The extensive cross section of selected copper busbars installed with respect to the average combined DC bus load power being 6.39 kW allows concluding that total expected conduction losses are also within the range of estimated *SumDC* power flow calculation.

Installation of a laboratory scale robotic manufacturing DC

The verification of DC microgrid-based operation for small-scale production tasks involving a few industrial robots has been done by means of a DC microgrid laboratory setup assembled in a single room at the RTU faculty building, as represented before. The author's Publications 6 and 7 are related to this aspect.

Analysis of individual robot energy reuse potential has been done within various scenarios, from a single unit to a combination of three robots. The physical implementation has been achieved by using a DC supply converted KUKA Quantec series 210 kg payload industrial robot prototype and two DC power flow emulators composed of coupled induction electrical machines and respective variable frequency drives with a common control unit. The interface active front-end (AFE) AC/DC converter of 65 kW nominal power has been used as the main power supply. Table 4.4 represents the summary of test configurations performed for DC microgrid analysis. Test scenarios 1 to 3 present an analysis of single robot and emulators performing the tasks based on industrial power consumption obtained in the industrial application at the factory. Tests 4 and 5 are performed as simultaneous operations of several industrial robots within the same production area.

Table 4.4

Test Configurations for DC Microgrid of Industrial Robot Applications

Configuration	DC KUKA robot (Prob)	Drive emulator EM1	Drive emulator EM1
Test 1	Welding		
Test 2		Part feed	
Test 3			Rivet punching
Test 4		Part feed	Rivet punching
Test 5	Welding	Part feed	Rivet punching

Figure 4.11 represents original power demand profiles used for interconnected DC microgrid analysis for small enterprise applications performed in RTU DC laboratory microgrid installation.

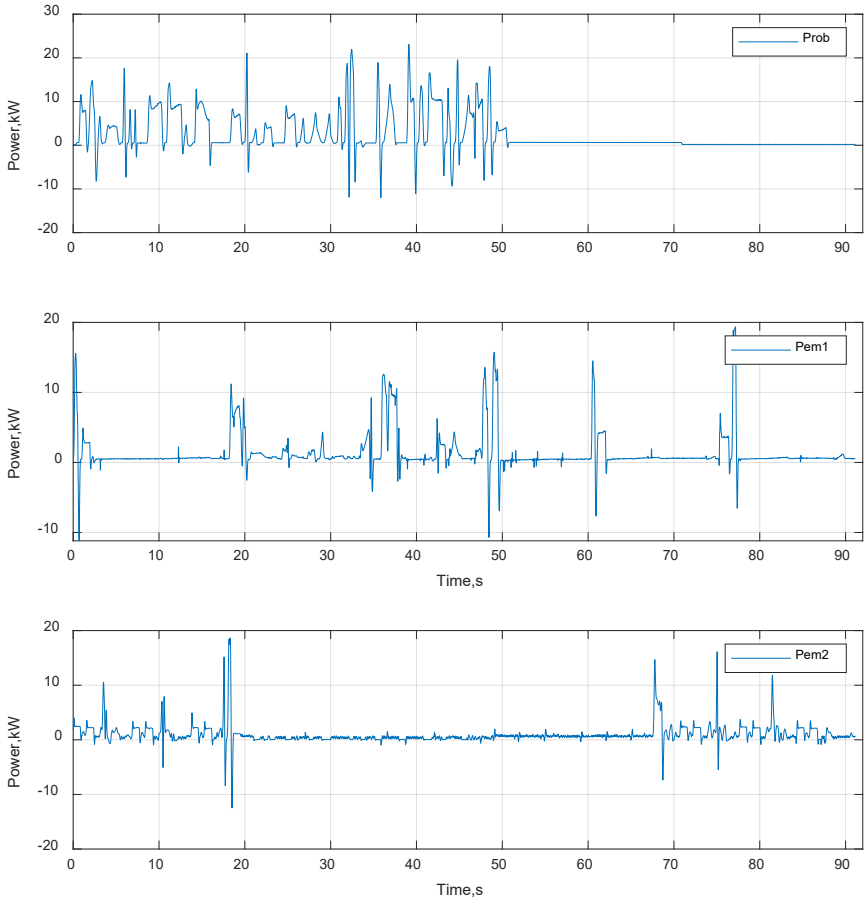

Fig. 4.11. The set of individual industrial robot consumption power profiles: KUKA DC robot *Prob*, and two drive emulators *Pem1* and *Pem2*.

As the complexity of a system is increased, a total combination of three DC microgrid load units representing industrial robots is achieved. A total combination of central AC/DC converter power flow and DC microgrid load profiles is presented in Fig. 4.12.

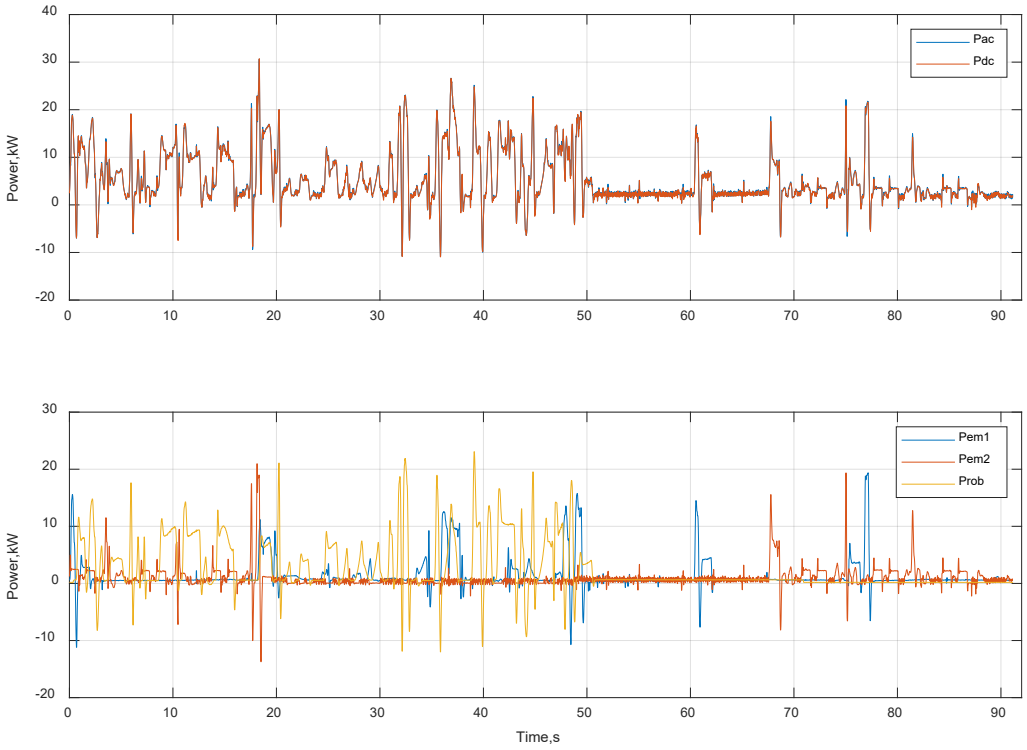

Fig. 4.12. Dynamic power flow of Test5 configuration with respective AC grid (*Pac*) and DC microgrid infeed power (*Pdc*) flows (top axis) and all three industrial robot loads (*Prob, Pem1, Pem2*) combination (bottom axis).

The obtained power flows are analysed by calculating the mean load and recuperated power flow values. Figure 4.13 represents an overview of power flow direction analysis by mean power flow extraction within the manufacturing task time period. *Pafe.AC* and *Pafe.DC* are active front-end AC/DC converter measurements on the AC and DC sides. *Prob, Pem1,* and *Pem2* are individual DC load equipment power flows. As total power consumption needs are increased by expanding the DC microgrid load group, active front-end converter power flows are increased for load and recuperation operation over the manufacturing cycle.

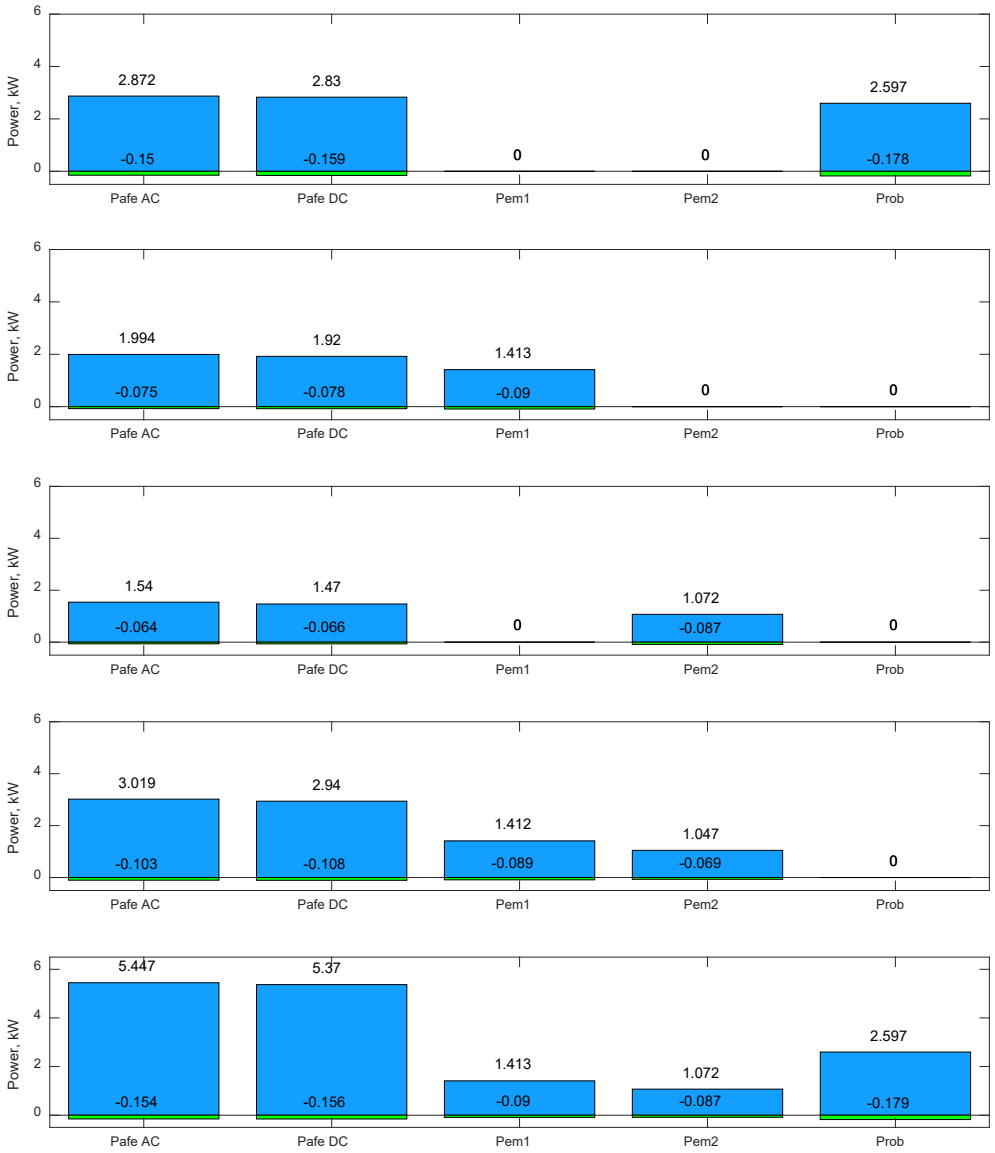

Fig. 4.13. Summary results of five DC microgrid configurations: Test1 (top axis) to Test5 (bottom axis). Mean load power (positive values) and recuperated power (negative values) flow estimation based on experimental measurement results within the 91.14-second manufacturing task.

Figure 4.14 has a similar structure as the previous analysis representation. However, the proportional ratio expressed in % of returned power flow with respect to direct load power flows is visualized. According to Fig. 4.14, it has been observed that the total recuperated energy component is reduced by an expansion of the DC side load unit number with bidirectional power flow capacity. The excess energy generated within the DC bus by robot

braking results in the negative power flow of the front-end converter DC side *Pafe.DC*. In the case of single-unit operations, the interconnected configurations of several robot units represent a reduction of total recuperated power to 2.9 % from 4.07–5.07 %. It can be observed that the energy potential for reuse with the robot (*Prob*) or emulators (*Pem1* and *Pem2*) is higher than that obtained on the AC power grid side or intermediate DC link. It is due to internal consumption being drawn from the DC link for control logic supply at a 24-Volt level as well as losses of bidirectional AC/DC converter feeding energy back into the AC grid.

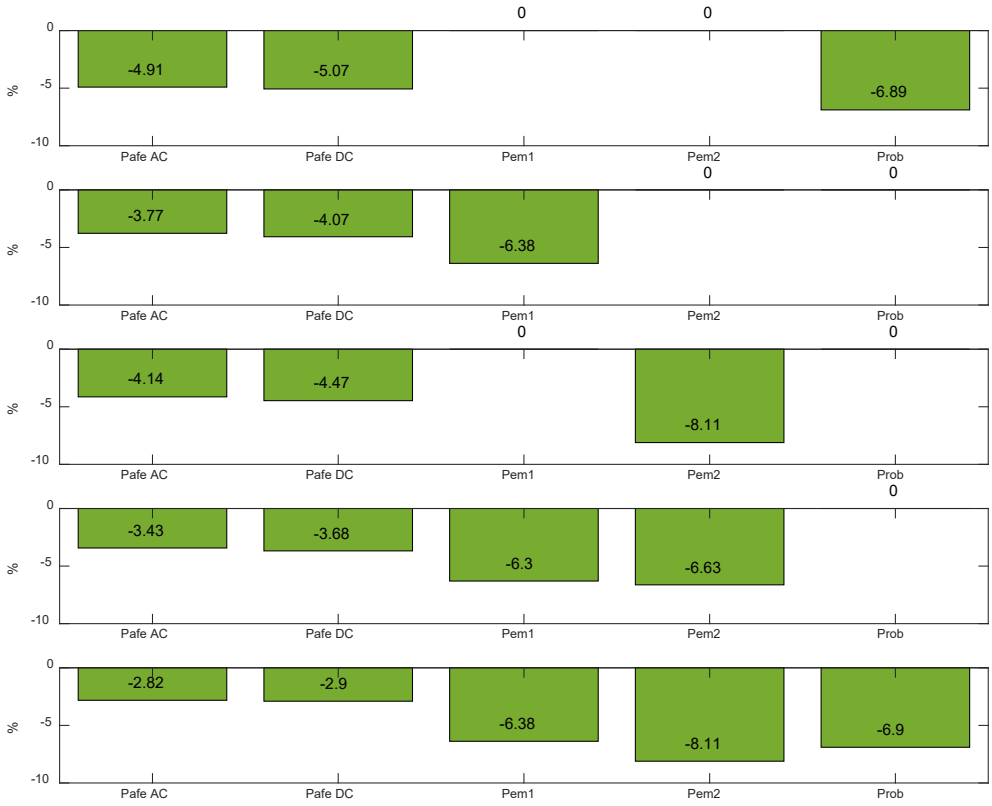

Fig. 4.14. Summary results of five DC microgrid configurations: Test1 (top axis) to Test5 (bottom axis). The obtained ratio in % represents the recuperated power flow compared to the consumed load power flow over the 91.14-second cycle of measured power flows.

Table 4.5 represents an overview of the mean power flow values obtained within the aforementioned experimental test configurations Test1 to Test5. Total power distribution analysis within microgrid installation allows estimation of average power losses within intermediate AC/DC power conversion and DC side distribution processes. Power loss related to active frontend AC/DC conversion losses and converter auxiliary loads is calculated according to Eq. (4.4), where *Pafe.AC* and *Pafe.DC* are converter AC and DC side power flow values.

$$Ploss.afe = Pafe.AC - Pafe.DC \quad (4.4)$$

Power loss *Ploss.DCbus* related to DC electrical connections realized by 16 mm^2 cables and additional 24 V power supply units can be calculated according to Eq. (4.5), where *Pafe.DC* is the power supplied on the DC output of AC/DC converter and *Prob*, *Pem1*, *Pem2* are input connections of robot and drive emulator units.

$$Ploss.DCbus = Pafe.DC - Prob - Pem1 - Pem2 \quad (4.5)$$

Total losses, *Ploss.total*, that are present and not directly related to the operation of individual DC microgrid connected manufacturing tools can be estimated by calculation according to Eq. (4.6).

$$Ploss.total = Ploss.DCbus + Ploss.afe \quad (4.6)$$

Table 4.5

Summary of Average Power Flow and Power Loss of Five Test Cases

		Experimental setup				
Units	**Quantity**	**Test1**	**Test2**	**Test3**	**Test4**	**Test5**
kW	*Pafe.AC*	2.98	1.919	1.476	2.915	5.293
	Pafe.DC	2.90	1.837	1.402	2.83	5.213
	Prob	2.418				2.417
	Pem1		1.323		1.323	1.323
	Pem2			0.985	0.977	0.981
	Ploss.afe	0.080	0.082	0.074	0.085	0.080
	Ploss.DCbus	0.486	0.514	0.417	0.530	0.492
	Ploss.total	0.566	0.596	0.491	0.615	0.572
Relative loss analysis vs *Pafe.AC*						
%	*Ploss.afe*	2.68	4.27	5.01	2.92	1.51
	Ploss.DCbus	16.28	26.78	28.25	18.18	9.29
	Ploss.total	18.96	31.06	33.27	21.10	10.81

The observation of summary results supports the hypothesis of increased energy efficiency by the implementation of an interconnected DC microgrid system for industrial robot-type loads. The AC/DC converter loss level represents a stable average power value of around 80 W. The component of overall DC microgrid loss power is reduced as a number of connected load units expands the system. The setup of two interconnected load units represents a 21.1 % power loss, and the value has reduced to 10.81 % by increasing the number of three interconnected load units.

Influence of industrial robot tool mass on braking energy potential

In order to observe the influence of production tool mass on electrical energy potential available for reuse, experiments with varying load have been done based on the same robot motion trajectory program execution (Publication 6). The specific industrial tool replica (Fig. 4.15) has

been applied with steel plates, allowing incremental changes of total mass at the end of the robot.

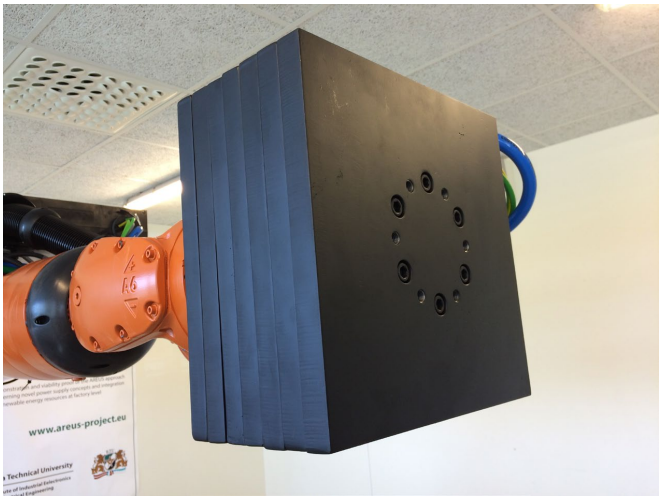

Fig. 4.15. Test tool replica for various tool mass experiments.

Bidirectional power flow measurements have been obtained for the same motion trajectory execution in various tool mass cases, as represented in Fig. 4.16.

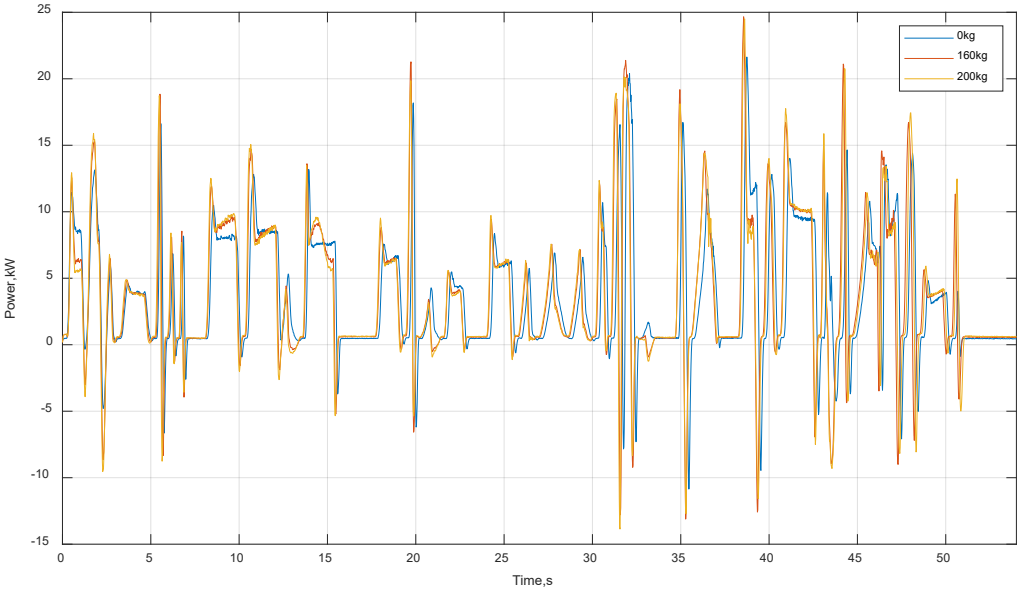

Fig. 4.16. Power flow profiles at various tool mass (0 kg, 160 kg, 200 kg).

Numerical evaluation results support the assumption that the application of braking energy reuse is more relevant for large production tools with significant total mass.

Table 4.6

Average, Consumed and Recuperated Power Flow by Tool Mass Variation

Tool mass, kg	Average total power, kW	Average consumed, kW	Average recuperated, kW	Recuperated vs consumed, %
0	3.612	3.821	0.208	5.45
159.3	3.688	4.031	0.343	8.52
201.3	3.676	4.055	0.378	9.34

According to the observed correlation between the tool mass and energy reuse, potential suitable applications for DC-related electrical system modification or replacement can also be selected. The Thesis has provided an insight into industrial robot applications related to automotive manufacturing processes; however, it can be expanded to other industrial sectors, providing similar parameters of industrial robot tool mass and motion characteristics.

CONCLUSIONS

The initial hypotheses of DC-based energy exchange and supply system relevance for industrial applications involving several industrial robot units and related manufacturing equipment have led to gradual introducing of DC-based electrical systems, starting from standard AC supply industrial robots to industrial DC microgrid installation.

Modification of typical AC supply-based industrial robots by DC shared bus configuration leads to a reduction of average power for the same motion operation and task for more than 20 %, depending on the applied tool payload and dynamics of the motion program.
A new power electronics-based module circuit for power flow control has been successfully developed and patented. An equivalent electrical system model has been developed for further optimization and modular electrical device design, leading to industrial prototypes of a shared DC bus industrial robot system.
A single DC power infeed microgrid demonstration setup of multiple robot systems has been physically implemented on a laboratory scale, and respective experimental measurements and a model of AC/DC infeed converter have been developed.
The operation of a small-scale industrial DC microgrid involving up to three industrial robots demonstrates the potential of reused energy up to 15 %, which is verified by physical experiments in the university laboratory and market available AC/DC conversion equipment. The design for the experiment has enabled new test setups for future emulation experiments and dynamic testing of DC industrial equipment.
Experimental tests of direct AC to DC industrial robot controller architecture substitution for a group of four units and the same manufacturing task reveal a reduction of average power consumption by 9.5 %.
A real-time synchronized data set was experimentally obtained in a large-scale factory-level DC microgrid setup. Detailed analysis of dynamic power flow between individual electrical units and estimation of reused energy has revealed up to 6.5 % energy reuse potential of DC-type industrial robot application of four units.
Overall loss calculation and distribution within the system based on 13 location synchronized power flow measurements have been analysed, and respective future optimization directions have been defined.

Results and experiments support the proposed DC-based electrical system applicability hypothesis for energy efficiency improvement of industrial robot-related industrial manufacturing applications.
Knowledge obtained during the development highlights the importance of further research on DC-type industrial electrical system development methodologies and new design tools supported by experimentally verified models for optimal dimensioning and component selection in real installations, thus enabling new flexible DC microgrid installations for better utilization of advantages expected in future dynamic energy systems.

REFERENCES

[1] IFR – international Federation of Robotics, "World robotics – Industrial Robotics 2023."

[2] IFR International federation of Robotics, "European Union: Industries Invest Heavily in Robotics – International Federation of Robotics." [Online]. Available: https://ifr.org/ifr-press-releases/news/eu-industries-invest-heavily-in-robotics. [Accessed: 28-Sep-2023].

[3] "A European Green Deal." [Online]. Available: https://commission.europa.eu/strategy-and-policy/priorities-2019-2024/european-green-deal_en. [Accessed: 29-Sep-2023].

[4] "The Green Deal Industrial Plan." [Online]. Available: https://commission.europa.eu/strategy-and-policy/priorities-2019-2024/european-green-deal/green-deal-industrial-plan_en. [Accessed: 29-Sep-2023].

[5] R. W. De Doncker, "Power electronic technologies for flexible DC distribution grids," *2014 Int. Power Electron. Conf. IPEC–Hiroshima – ECCE Asia 2014*, pp. 736–743, 2014.

[6] "REPowerEU: affordable, secure and sustainable energy for Europe." [Online]. Available: https://commission.europa.eu/strategy-and-policy/priorities-2019-2024/european-green-deal/repowereu-affordable-secure-and-sustainable-energy-europe_en. [Accessed: 29-Sep-2023].

[7] "Automation and Robotics for EUropean Sustainabile manufacturing | AREUS | Project | Fact sheet | FP7 | CORDIS | European Commission." [Online]. Available: https://cordis.europa.eu/project/id/609391. [Accessed: 29-Sep-2023].

[8] "dc-industrie.zvei.org/en - dc-industrie.zvei.org - Microsite." [Online]. Available: https://dc-industrie.zvei.org/en/. [Accessed: 25-Sep-2023].

[9] "USB-type C to become EU's common charger by end of 2024 | News | European Parliament." [Online]. Available: https://www.europarl.europa.eu/news/en/headlines/society/20220413STO27211/usb-type-c-to-become-eu-s-common-charger-by-end-of-2024. [Accessed: 29-Sep-2023].

[10] "CurrentOS Foundation." [Online]. Available: https://currentos.foundation/. [Accessed: 25-Sep-2023].

[11] "The Second Grid – DC Systems." [Online]. Available: https://www.dc.systems/vision/the-second-grid. [Accessed: 25-Sep-2023].

[12] "Flexible Electrical Networks | Research Campus FEN Aachen." [Online]. Available: https://www.fenaachen.net/. [Accessed: 29-Nov-2021].

[13] "NExT Factory-Efficient Smart Green / Schaltbau." [Online]. Available: https://www.schaltbau.com/en/about-us/portrait/next-factory-efficient-smart-green/. [Accessed: 25-Sep-2023].

[14] "'Factory 56': Mercedes-Benz Cars significantly increases flexibility and efficiency with 'Factory 56'| Mercedes-Benz Group > Innovation > Digitalisation > Industry 4.0." [Online]. Available: https://group.mercedes-benz.com/innovation/production/factory-56.html. [Accessed: 25-Sep-2023].

[15] "National energy and climate plans." [Online]. Available: https://commission.europa.eu/energy-climate-change-environment/implementation-eu-countries/energy-and-climate-governance-and-reporting/national-energy-and-climate-plans_en. [Accessed: 29-Sep-2023].

[16] IFR – international Federation of Robotics, "WR 2021 Industrial Robots – Sources & Methods," 2021.

[17] R. Murray, Z. Li, and S. Sastry, *A mathematical introduction to robotic manipulation*, vol. 29. 1994.

[18] Paryanto, M. Brossog, J. Kohl, J. Merhof, S. Spreng, and J. Franke, “Energy Consumption and Dynamic Behavior Analysis of a Six-axis Industrial Robot in an Assembly System,” *Procedia CIRP*, vol. 23, no. C, pp. 131–136, Jan. 2014.
[19] D. Meike, “Multi-Domain Model for the Evaluation of Large Scale Robotic Applications within Production,” *Riga Tech. Univ. 53rd Int. Sci. Conf. Dedic. to 150th Anniv. 1st Congr. World Eng. Riga Polytech. Inst. / RTU Alumni Dig.*, pp. 113–113, 2012.
[20] A. Rassõlkin, H. Hõimoja, and R. Teemets, “Energy saving possibilities in the industrial robot IRB 1600 control,” in *2011 7th International Conference-Workshop Compatibility and Power Electronics, CPE 2011 – Conference Proceedings*, 2011, pp. 226–229.
[21] D. Meike, “Increasing Energy Efficiency of Robotized Production Systems in Automobile Manufacturing,” 2013.
[22] D. Meike and L. Ribickis, “Recuperated energy savings potential and approaches in industrial robotics,” in *IEEE International Conference on Automation Science and Engineering*, 2011, pp. 299–303.
[23] O. Bormanis, “Increasing Reliability of Robotized Manufacturing Systems,” RTU, Riga, 2022.
[24] C. M. Hackl, A. G. Hofmann, R. W. De Doncker, and R. M. Kennel, “Funnel Control for Speed & Position Control of Electrical Drives: A Survey.”
[25] “Gleichstrom im Niederspannungs-bereich Deutsche Normungs-Roadmap Version 2 VDE | DKE Roadmap.”
[26] ZVEI & consortium DC-INDUSTRIE2, “DC-INDUSTRY_Systemconcept-V2,” DC-INDUSTRIE & ZVEI, 2022.
[27] P. Apse-Apsitis, A. Avotins, and L. Ribickis, “A different approach to electrical energy consumption monitoring,” In: *2014 16th European Conference on Power Electronics and Applications*, 2014, pp. 1–5.
[28] R. Rodrigues, Y. Du, A. Antoniazzi, and P. Cairoli, “A Review of Solid-State Circuit Breakers,” *IEEE Trans. Power Electron.*, vol. 36, no. 1, pp. 364–377, Jan. 2021.

APPENDICES / PUBLICATIONS

Appendix 1

Stupāns, A., Maksimkins, P., **Šenfelds, A**., Ribickis, L. Industrial Robot Energy Consumption Analysis for Gravity-induced Opposing Force Minimization. In: *2022 7th IEEE International Energy Conference (ENERGYCON 2022)*, Latvia, Riga, 9-12 May, 2022. Piscataway: IEEE, 2022, pp.678-682. ISBN 978-1-6654-7983-7. e-ISBN 978-1-6654-7982-0.

DOI:10.1109/ENERGYCON53164.2022.9830240

Industrial robot energy consumption analysis for gravity-induced opposing force minimization

Andrejs Stupāns
Institute of Industrial Electronics and Electrical Engineering
Riga Technical University
Riga, Latvia
andrejs.stupans@rtu.lv

Pāvels Maksimkins
Institute of Industrial Electronics and Electrical Engineering
Riga Technical University
Riga, Latvia
pavels.maksimkins@rtu.lv

Armands Šenfelds
Institute of Industrial Electronics and Electrical Engineering
Riga Technical University
Riga, Latvia
armands.senfelds@rtu.lv

Leonīds Ribickis
Institute of Industrial Electronics and Electrical Engineering
Riga Technical University
Riga, Latvia
leonids.ribickis@rtu.lv

2022 IEEE 7th International Energy Conference (ENERGYCON) | 978-1-6654-7982-0/22/$31.00 ©2022 IEEE | DOI: 10.1109/ENERGYCON53164.2022.9830240

***Abstract*—The paper describes the process of mapping industrial robot energy consumption. It is assumed that using an obtained energy map, an optimal robot workspace area can be found where the robot consumes less energy because opposing force of gravity is reduced. The study focuses on experimental approach rather than computer modelling to decrease complexity and time consumption of energy mapping. The robot's consumed power measurements are taken in its multiple static positions with brakes released. The array of robot positions forms a vertical plane - one slice of the robot's workspace. All the measured power data is combined into the 2D map that shows how much power the robot consumes in different areas of its workspace. Obtained data shows a correlation between energy consumption and robot position in its workspace.**

Keywords — energy consumption, industrial robot, energy mapping, power measurements

I. Introduction

Industrial robots (IR) are being used in various manufacturing applications. These include painting, welding, glueing, riveting, etc. Each robot operates within its programmed algorithm, which consists of dynamic and static parts. Dynamic parts involve moving a spraying gun while painting a surface, moving a nozzle while applying glue to a certain part, etc. While performing those actions every electrical engine works with electromechanical brakes released, so the weight of the robot and its payload is held by IR drives.

An operating IR has to overcome two main forces. One is friction in joints and the second is gravity force acting on the robot's axes, tools, and payloads [1]. All these factors result in additional power consumption of motor drivers. Nevertheless, high payload IRs have a built-in hydraulic counterbalancing system that copes with gravity forces.

It is assumed that it is possible to decrease overall energy consumption if using an IR in its optimal work area where the gravity force impact is minimal. To find energy-efficient areas in a robot's workspace, the methodology is proposed to obtain a practical energy consumption map of an IR instead of simulating one.

This publication was supported by Riga Technical University's Doctoral Grant programme

This work has been supported by the European Social Fund within the Project No 8.2.2.0/20/I/008 «Strengthening of PhD students and academic personnel of Riga Technical University and BA School of Business and Finance in the strategic fields of specialization» of the Specific Objective 8.2.2 «To Strengthen Academic Staff of Higher Education Institutions in Strategic Specialization Areas» of the Operational Programme «Growth and Employment»

Problematics of digital simulation of IR energy consumption lies in the lack of availability of information about the specific IR. Most energy consumption prediction models [2]–[4] require inertial and friction parameters of the robot system that are confidential and cannot be obtained directly. To determine the values of these parameters, parameter identification techniques are used [5]–[7]. It is still a relevant topic in the research field because the precision and complexity of such methods have to be improved.

The study focuses on the experimental approach rather than computer modelling. The proposed method is a practical way of obtaining the energy consumption map that can be used as a starting point for IR energy efficiency optimization. The map consists of measured power consumption values in each segment of an IR workspace. It is crucial to understand that the energy map is obtained for a specific robot with a specific payload (weight, center of mass, etc.), so it is important to keep in mind that the map is unique for each IR application. The map must be obtained individually for every robot. This approach is expected to provide more trustworthy data than computer simulations can do.

It is considered to benefit both already deployed IR systems and systems in their planning stage of development. Energy mapping could be used to choose an optimal IR layout so the payloads it is manipulating are located mostly in the robot's energy-efficient spots. Also, data from an energy map can be considered in trajectory planning algorithms prioritizing motions through energy-efficient areas of IR's workspace.

Based on data presented in [8], the automotive industry is heavily dependent on industrial robots that consume up to 8% of electrical energy. Energy savings impact not only production costs but also leads to CO2 emission reduction.

This paper is structured in six sections. Section II discusses existing methods to optimize the energy consumption of IR systems. Section III describes the experiment on how the energy map was obtained. In section IV results of the experiment are shown. Future challenges and method improvements are presented in section V. Paper concludes with section VI.

II. Methods of Energy Consumption Optimisation

To understand the possibilities of energy consumption optimization it is crucial to know how an IR consumes electrical energy. IR energy consumption can be divided into two components. The first component is IR peripheral consumption - power supply, PC (Kuka KPC), teach pendant (SmartPad), fans for cooling, etc. In this study electrical energy of IRs peripherals is excluded from the measurements because of their unpredictable power consumption that

interferes with the ability to link energy consumption to robot position. The second component is the energy consumed by motor drivers. Drivers control both the servomotors and brakes. In this study, the power of motor drivers is measured.

Electromechanical brakes operate as normally-closed brakes, so electrical energy is used to keep them open during an IR operation. To keep the brakes open on a 6-axis heavy-duty industrial robot approximately 140W is used according to the study [8]. This data is proven to be very close to data measured during the experiment in Section III. When in steady-state, the robot is kept in its position by servomotors, until the moment electromechanical brakes are activated. For Kuka KRC2 and KRC4, the default timeout for brake activation is 20 seconds. In the study [8] it was measured that an IR consumes about 800W being in steady-state with brakes released. Consumption drops to 275W when brakes are activated. That is a difference of about 525W. This is the result of two factors - electromechanical brakes are no longer powered and servomotors are not consuming the energy to keep the IR still.

One of the options to reduce the consumption of electrical energy is to effectively utilize built-in electromechanical brakes, so the gravity-induced payload is carried by the brakes, rather than servomotors [9]. Decreasing the timeout of the brakes and activating brakes when IR is waiting can decrease energy consumption. But it is not a typical approach to maximize the time IR is held by the brakes, because usually, IR programmers tend to minimize the downtime of an IR.

Other methods of electrical energy consumption optimization include IR payload reduction [10], [11]. Reducing IR motion speed and accelerations [12]. Improving trajectory planning algorithms [13]. Reusing kinetic energy by the means of regenerative braking [14]. Most of these methods require costly hardware or proprietary software changes.

It is assumed that energy mapping could help to develop easier and cheaper methods of energy consumption optimization. The energy map of IR is obtained to make it possible to choose the energy-optimal layout design of a robotic working cell, to ensure that IR placed in a given cell operates within the most energy-efficient area of its workspace.

One can implement the proposed methodology in the already installed (deployed) robot system, and also in the planning stage optimizing the layout of the IR cell. Since this methodology is a non-intrusive way to measure IR energy consumption profile, there is no need to modify a control system (both proprietary software and hardware), so not violating any warranty rules is guaranteed.

III. EXPERIMENT

A. Equipment

The power consumption of the Kuka KR210 R2700 Prime robot is examined in this study (Fig. 1). KRC4 controller is a part of the IR system. The IR is not AC-powered, it is connected to the Siemens active frontend unit (AC/DC converter) with 600V output and 55kW power. The robot has been a part of the AREUS project [15]. IR has a 200kg payload attached to its end-effector.

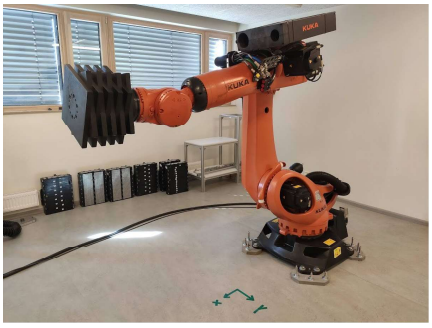

Fig. 1. Kuka KR 210 R2700 Prime used in the experiment.

The electromechanical brakes' timeout of the Kuka robot is set to 10 seconds. Brakes are activated after 10 seconds when the IR stands still. However, it is possible to extend this time periodically performing minor movements that do not affect the position of the IR or the energy consumption. The power measurements are taken during the period when the IR is not moving, and the brakes are still open.

In this scenario, the IR drivers consume energy only in two ways. To keep normally-closed electromechanical brakes open. And to compensate for the gravity force acting on the robot and its payload. The total power of IR is consumed by the driver system and peripherals, such as Kuka PC, smartPad, or fans for cooling. The power consumption of peripherals was experimentally proven to be changing during the experiment. So, the power measurements were taken at both motor drivers' input. The power consumption of the driver mostly consists of power driving the servomotor, power consumed by electromechanical brakes, and driver losses.
A data acquisition device is used to collect and analyse data from the differential scope and the current clamp.

B. Warm-up

Oil viscosity can highly affect IR energy consumption in dynamic motion profile [16] as the temperature of the oil is rising. So, it is important to maintain a stable temperature throughout the experiment. The warm-up procedure thoroughly described in [16] stabilizes oil temperature so it is always the same during measurements and is close to IR real work conditions. In [16] the warm-up process consists of several hours of IR cyclic motion and also short 1-2 minute cycles after each measurement.

This study is focused on taking measurements while the IR is in a static position, so no dynamic motion is present during the measurements. The impact of the oil temperature in this use case is considered neglectable, as long as the temperature is the same during all the measurements.

C. Mapping energy consumption

Only a slice of the full 3D map is obtained in this study. A vertical slice of IR workspace is a 2D plane divided into smaller square segments with dimensions of 30x30cm (Fig. 2). Then the IR is positioned in every segment and its average power consumption is measured. Only one end-effector orientation is considered - parallel with the robot base.

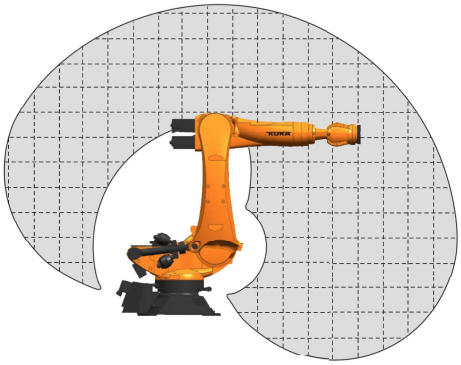

Fig. 2. Example of IR workspace divided into segments for energy mapping

To fill the energy map of an IR, the following approach is used:

1. Position the IR in the centre of an area to be measured
2. Start the power measurement right after the robot stops in the desired position
3. Keep brakes open for 60 seconds, while the robot is still, and then stop the measurements
4. Repeat actions 1-3 three times for a specified robot position
5. Repeat actions 1-4 for each segment on the map

Slightly pressing jogging buttons at the lowest possible speed every 5-10 seconds can keep brakes open for prolonged periods of time. This way the IR is moving, but so slightly that its position does not significantly change, however, the brakes' timeout is restarted.

IV. Results

A. Energy map

The obtained energy map of the Kuka KR210 R2700 industrial robot is divided into segments (Fig. 3). Power consumed by IR in all static positions is written in every segment of the map. Power consumed by the brakes is a constant value of 140W, so it was subtracted from the measurements leaving only IR motor consumption.

Results show that there definitely are robot positions where it operates with its best possible efficiency (green zone) and some positions where electrical energy consumption is relatively high (red zone). The reason for that is the gravity force generating additional payload when the leverage is greater. Authors assume that most of the power is consumed by the motors of the 2nd and 3rd axes, which hold all the other axes. In the near-vertical configuration of the 2nd axis, the power consumption is minimal, because there is less leverage to hold in position.

Also, there are areas in the green zone where the leverage of the 2nd axis is greater, but the power consumed is minimal. It can be explained by the impact of the hydraulic counterbalancing system. It helps the servomotor at the 2nd

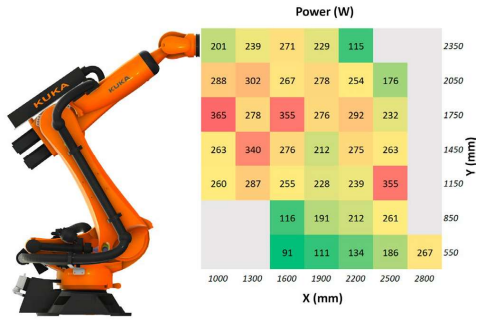

Fig. 3. Energy map of KR 210 R2700 Prime industrial robot

axis to withstand high gravity force in stretched IR configurations. But as the energy map shows, the counterbalancing system does not work when the axis angle is negative (red zone on the left side of the map). Also, the hydraulic counterbalancing system has less impact in highly stretched robot positions (red zone on the right lower corner of the map). The most energy-efficient and the most inefficient robot configurations are highlighted (Fig. 4).

B. Verifying the energy map

To verify the obtained energy map, two IR motions were performed within the map area. Both motions are horizontal linear motions L1 and L2 (Fig. 5). Motions were performed under the same conditions, with the same length, velocity, and acceleration parameters. Average power consumption was measured to be 871W for L1 and 784W for L2.

C. Power consumption in dynamic performance

The trajectory that goes through points P1 – P5 has been programmed (Fig. 6). It consists of linear and circular motions. The points are positioned within the plane of the obtained energy map so that the IRs end-effector goes through both green and red areas of the map. The power consumption of the IR was recorded (Fig. 7). The correlation can be seen between power consumption and robot position in dynamic motion profile, but a lot of other dynamic factors such as velocity or acceleration can have a greater influence on the power consumption and must be taken into consideration in future studies.

Fig. 4. Most efficient and most inefficient robot configurations according to energy map.

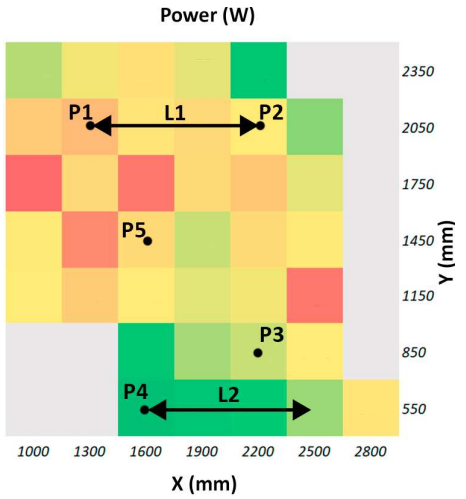

Fig. 5. Motions L1 and L2 performed on the IR to measure energy efficiency in the green and red zone of the obtained map

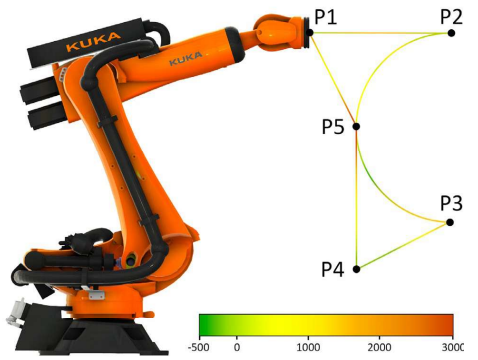

Fig. 6. Programmed trajectory with the power consumption data

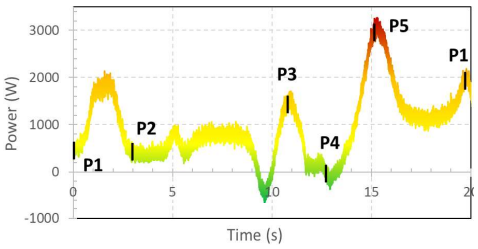

Fig. 7. Power consumption of the IR during the movement through programmed trajectory

V. Future Tasks and Challenges

A. Precise power consumption measurements

One of the possible ways to increase the precision of the power map is to take measurements for each servo drive separately. This way it is possible to perform a deeper analysis of the studied IR system. For example, analyse the impact of the hydraulic counterbalancing system on the energy consumption of the 2nd axis. The work on improving power measurements and making a plug-and-play device to be easily and conveniently used with various robots on-site is in progress.

B. The automatic and universal software approach

For now, the measurements are taken and analysed manually. But the end goal is to develop an automatic or semi-automatic approach to obtain energy consumption maps for industrial robots. The application of this methodology is to provide an IR owner with a fast and non-intrusive way of power mapping and further energy consumption optimization for his specific application of an IR. The process of creating software to automate the process of robot positioning and power measurements has been started.

VI. Conclusion

One slice of a full 3D electrical energy consumption map was created using the proposed methodology. Using the obtained energy consumption map, possible energy consumption optimisation methods have been determined. There definitely are some areas in IRs workspace that are more energy-efficient than the others in terms of compensation of opposing gravity force.

It was concluded that obtaining and analysing an energy map for an IR may result in a more energy-efficient robot operation. Energy mapping helps to practically find the optimal IR layout to increase the time an IR is working in energy-efficient areas of its workspace. In multi-robot configurations it can be ensured that as many IRs as possible are working in their energy-efficient areas, saving energy.

Also, the new trajectory planning algorithms can be studied that could take into consideration the energy map of an IR and prioritize the motions through energy-efficient areas.

Nevertheless, the true effectiveness of the approach is to be determined in future studies.

References

[1] P. Ystgaard, T. B. Gjerstad, T. K. Lien, and P. A. Nyen, “Mapping Energy Consumption for Industrial Robots,” no. January, 2012, doi: 10.1007/978-3-642-29069-5.

[2] A. Liu, H. Liu, B. Yao, W. Xu, and M. Yang, “Energy consumption modeling of industrial robot based on simulated power data and parameter identification,” *Adv. Mech. Eng.*, vol. 10, no. 5, May 2018, doi: 10.1177/1687814018773852.

[3] A. Efimov, M. Gorkavyy, and A. Gorkavyy, “Predicting power consumption of robotic complex based on neuro-fuzzy system,” *Proc. - 2020 Int. Conf. Ind. Eng. Appl. Manuf. ICIEAM 2020*, May 2020, doi: 10.1109/ICIEAM48468.2020.9112066.

[4] J. Yan and M. Zhang, “A transfer-learning based energy consumption modeling method for industrial robots,” *J. Clean. Prod.*, vol. 325, p. 129299, Nov. 2021, doi: 10.1016/J.JCLEPRO.2021.129299.

[5] J. Wu, J. Wang, and Z. You, “An overview of dynamic parameter identification of robots,” *Robot. Comput. Integr. Manuf.*, vol. 26, no. 5, pp. 414–419, Oct. 2010, doi: 10.1016/J.RCIM.2010.03.013.

[6] J. Swevers, W. Verdonck, B. Naumer, S. Pieters, and E. Biber, “An

experimental robot load identification method for industrial application," *Int. J. Rob. Res.*, vol. 21, no. 8, pp. 701–712, 2002, doi: 10.1177/027836402761412449.

[7] A. Janot, P. Olivier Vandanjon, and M. Gautier, "An instrumental variable approach for rigid industrial robots identification," *Control Eng. Pract.*, vol. 25, no. 1, pp. 85–101, Apr. 2014, doi: 10.1016/J.CONENGPRAC.2013.12.009.

[8] D. Meike and L. Ribickis, "Energy efficient use of robotics in the automobile industry," *IEEE 15th Int. Conf. Adv. Robot. New Boundaries Robot. ICAR 2011*, pp. 507–511, 2011, doi: 10.1109/ICAR.2011.6088567.

[9] L. Ribickis and D. Meike, "Analysis of the Energy Efficient Usage Methods of Medium and High Payload Industrial Robots in the Automobile Industry," 2011.

[10] Paryanto, M. Brossog, M. Bornschlegl, and J. Franke, "Reducing the energy consumption of industrial robots in manufacturing systems," *Int. J. Adv. Manuf. Technol.*, vol. 78, no. 5–8, pp. 1315–1328, 2015, doi: 10.1007/s00170-014-6737-z.

[11] M. Gadaleta, G. Berselli, M. Pellicciari, and F. Grassia, "Extensive experimental investigation for the optimization of the energy consumption of a high payload industrial robot with open research dataset," *Robot. Comput. Integr. Manuf.*, vol. 68, p. 102046, Apr. 2021, doi: 10.1016/J.RCIM.2020.102046.

[12] R. R. Garcia, A. C. Bittencourt, and E. Villani, "Relevant factors for the energy consumption of industrial robots," *J. Brazilian Soc. Mech. Sci. Eng.*, vol. 40, no. 9, pp. 1–15, 2018, doi: 10.1007/s40430-018-1376-1.

[13] C. Bryan, M. Grenwalt, and A. Stienecker, "Energy Consumption Reduction in Industrial Robots," *ASEE North Cent. Sect. Conf.*, pp. 1–4, 2010, doi: 10.1007/s00170-014-6737-z.

[14] A. Paugurs, A. Senfelds, and L. Ribickis, "Impact of industrial robot tool mass on regenerative energy," *2017 19th Eur. Conf. Power Electron. Appl. EPE 2017 ECCE Eur.*, vol. 2017-January, Nov. 2017, doi: 10.23919/EPE17ECCEEUROPE.2017.8099185.

[15] A. Senfelds, A. Avotins, L. Ribickis, and P. Apse-Apsitis, "DC microgrid for robotic manufacturing – field demonstration and laboratory experience," *Renew. Energy Power Qual. J.*, vol. 17, pp. 194–197, Jul. 2019, doi: 10.24084/REPQJ17.260.

[16] M. Gadaleta, G. Berselli, M. Pellicciari, and F. Grassia, "Extensive experimental investigation for the optimization of the energy consumption of a high payload industrial robot with open research dataset," *Robot. Comput. Integr. Manuf.*, vol. 68, no. July 2020, p. 102046, 2021, doi: 10.1016/j.rcim.2020.102046.

Appendix 2

Šenfelds, A. Analysis of Motion Modelling Approaches for Industrial Robot Applications. In: *2019 IEEE 7th Workshop on Advances in Information, Electronic and Electrical Engineering (AIEEE 2019): Proceedings*, Latvia, Liepāja, 15-16 November, 2019. Piscataway: IEEE, 2019, pp.145-148. ISBN 978-1-7281-6731-2. e-ISBN 978-1-7281-6730-5.

DOI:10.1109/AIEEE48629.2019.8977112

Analysis of motion modelling approaches for industrial robot applications.

Armands Senfelds
Riga Technical University
Institute of industrial Electronics and Electrical engineering
Riga, Latvia
armands.senfelds@rtu.lv,
http://orcid.org/0000-0003-4039-4270

***Abstract*—This paper address literature research and overview of external controller based motion control and data exchange efforts with industrial robots provided by KUKA. Several existing approaches and applications implemented has been analyzed and common features extracted. Possible application for industrial robot research needs of experimental research disciplines of university laboratory has been presented and research on electrical energy consumption dynamic evaluation discussed in detail.**

Keywords—industrial robot, communication, motion control.

I. INTRODUCTION

Demand for research related tasks utilizing industrial robot manipulators since such equipment has become widespread tool for various tasks in modern society has been growing. Therefore approach for suitable methods and tools to be implemented in research laboratory for future development of new applications of industrial robots by researchers without extensive experience in industrial applications of robots is demanded. This article provide overview of existing control and communication efforts utilized by researchers to current state associated with industrial robot manufacturer KUKA robot manipulators in Section 2. Insight of particular fields of industrial robot use in research activities by university has been provided in Section 3 followed by more detailed discussion of robot application for electrical energy consumption related research.

II. INDUSTRIAL ROBOT MOTION CONTROL AND COMMUNICATION APPROACH OVERVIEW

An initiative to provide Matlab Simulink based programming tool for multi-vendor robotic applications by development of specific Robot Control and Visualization toolbox [1]. Motivated by previous lack of unified robot programming language standards such as Industrial Robot Language (IRL) and Programming Language for Robots (PLR). Demonstration of two robot manufacturer based system with KUKA and Kawasaki. Activities are aimed towards universal tool for control engineering development based on well-established computing such as Matlab.

Approach to develop set of Matlab based functions for simplified programming of KUKA robots has been developed by university of Siena. [2], [3]

User is supplied by high level tool for interfacing with robot controller to develop motion control of low payload and small scale KUKA robots with six axes degree of freedom. KUKA control toolbox has been improved and published as open source tool with around 40 functions for motion control and coordinate calculation, diagnostics and animation. Communication technology is based on KUKA Eth.RSIXML data exchange via TCP/IP connection.

Typical development of industrial robot operational programs is based on offline programming software tools. Evaluation of industrial robot based manufacturing systems in terms of safety and operational aspects can be realized at early stage of robotic system design as well as extract economic data related parameters. Utilization of digital production system design tools in context with future Industry 4.0 initiatives and enhanced functionality for future factories require more vendor independent solutions for offline programming of industrial robots and auxiliary equipment. However many programming tools are closely related to single manufacturer and specific programming language as discussed and presented by [4] and more vendor independent solutions discussed. Summary of leading industrial robot manufacturers and associated programming toolchain has been presented in Table.

TABLE I. OVERVIEW OF MAJOR INDUSTRIAL ROBOT MANUFACTURERS AND RELATED SOFTWARE TOOLS

Robot manufacturer	**Offline programming solution**	**Robot language type**
Kuka Roboter	Kuka Sim Pro	KRL
ABB	RobotStudio	RAPID
Fanuc Robotics	RoboGuide KAREL	KAREL
Universal Robots	RoboDK	URScript

Developments of new industrial robot related hardware and software solutions as for example compute vision and artificial intelligence based decision making systems that has to be integrated by existing industrial robot equipment has motivated research institutions for universal approaches to simplify utilization for wider range of potential robot users apart from industry experts. As one of initiatives RoBO-2L toolbox has been initiated by university of Bochum, Germany. [4] As many other also this toolbox is focused on KUKA industrial robots and utilization of manufacturer provided communication interface known as RSI (Robot Sensor Interface) and UDP/IP data transmission. Developers have initiated link for Matlab based function integration and utilization of Simulink package.

978-1-7281-5709-2/19/$31.00 ©2019 IEEE

Implementation and realization has been demonstrated by [5] based on small payload robot and related software developments. Further developments concerning image recognition and artificial intelligence applications based on Cartesian correction approach for movements has been discussed in [6].

An example of flexible trajectory planning approach based on KUKA robot has been developed by [7] for purpose of composite material automated testing by industrial robot application. The team has implemented flexible robot path calculation and planning enhancing existing off line programming tool presented abilities. Presented application has demonstrated several improvements for automated testing tasks regarding inspection time reduction and synchronization abilities with external scientific measurement equipment for improved positioning precision. Control of industrial robot has been organized externally. Activities in order to utilize universal software solution such as Labview for analysis of industrial robot motion parameters has been described by [8]. Application of CAD models and variety of related parameter availability has been discussed in order to perform analysis for typical industrial robot programming tasks such as collision detection or reachability. Necessary information provided by specific CAD parameters for dynamic motion and kinematic properties is identified.

State of the art automated industrial manufacturing systems are typically based on programmable logic controllers (PLC) and represent approach of fixed programming solutions. However by alteration of products also extensive modifications for production lines arise. Alternative approach for flexible manufacturing approach utilizing KUKA robots with RSI interfaces has been presented by [9] introducing replacement of existing fixed programming approach by flexible programs. Tools such as vision systems for real time adaptive systems has been presented in order to highlight prospective system development.

An open source communication interface for multiple manufacturer KUKA based robotic systems known as OpenShowVar has been presented by [10]. It is based on Java and present cross-platform development covering KR C2 and KR C4 robot controller hardware versions and enable utilization of various external sensor and other equipment. Simplified access to industrial robot operation variables and parameters present ability to develop both open and closed loop type control. Several demonstration case studies has been explained to verify flexibility of proposed communication concept.

Specific communication interface for research activities based on lightweight robots by KUKA has been proposed by [11] known as OpenKC open source controller enabling open source tool for simultaneous control of several robots as well as wide functionality of features and functions of Kuka lightweight robot for external applications.

III. Application Areas for Implementation

Ability for flexible real time capable communication with industrial robots and availability of well-known tools for development of motion control and new peripheral technology integration based on Matlab and Simulink is considered. Therefore significant aspect of successful involvement of students and early career researchers for novel development related to industrial robots is applicability of previous skills and knowledge in engineering system modelling and control development. In Riga Technical University several research directions related to industrial robot application are present. Research of physical motion interaction with human body based on large motion range physical motion simulator as represented in Fig. 1 is utilized.

Fig. 1. Large motion range physical silmulator based on KUKA KR 600 series industrial robot manipulator.

Motion simulation application development require both closed and open loop control system capability and real time communication and execution performance. Communication via RSI communication interface by KUKA utilizing UDP data transfer is used.

For industry like application industrial robot as depicted in Fig. 2 is applied.

Fig. 2. Industrial robot manipulator of 210 g payload class representing basis for typical industrial manufacturing related research tasks.

Such type of industrial robot is applied in many manufacturing and assembly tasks equipped with various application specific tools. Modification for flexible control with external control systems allow for new integration concept verification apart from industry state of the art programming features. Execution of motion programs is typically based on fixed programming structures but introduction of external controller would enable new flexible concepts.

As basis for introduction in industrial robot programming small payload with identical robot control system as large payload KUKA industrial robots, shown in Fig. 3. Such system enhanced with external motion control and sensor interface based on Matlab Simulink for example would allow faster proof of concept of new tasks developed by students as well as novel integration of artificial intelligence based systems.

Fig. 3. KUKA small scale industrial robot manipulator for teaching and programming concept evaluation tasks.

IV. Industrial Robot Motion Type and Related Energy Consumption Evaluation

Industrial robot based manufacturing applications are typically designed for fast execution of manufacturing tasks within fixed time frame as for example in automotive production factories with production process combined by serial execution of separate operations resulting in parts of products. In order to examine energy related performance of industrial robots experimental evaluation of total energy and power has been presented by [12]. Industrial robot tool mass has been realized by gradual increase of additional steel weights. Real installation with additional tool mass has been presented in Fig. 4.

Fig. 4. Industrial robot manipulator equipped for toll mass variation related experiment.

Robot motion has been designed as sequential execution of swing type motions of each axis. Robot kinematic chain is realized by serial connection of six electrical drives and thus also electrical power demand and consumed energy over same operation cycle is available for comparative evaluation. Internal dynamics of spring damper for second axis is not evaluated as separate unit and seen as integral effect for all tool mass variation experiments. Utilized industrial robot has been electrically modified for electrical supply of direct current type at voltage of 600V. Also internal electrical supply structure enable bidirectional electrical power flow that is important feature regarding efficient energy utilization during motions supported by inertial and gravitational forces and has potential for energy production by electrical drives as generators during braking phase of motion trajectory execution.

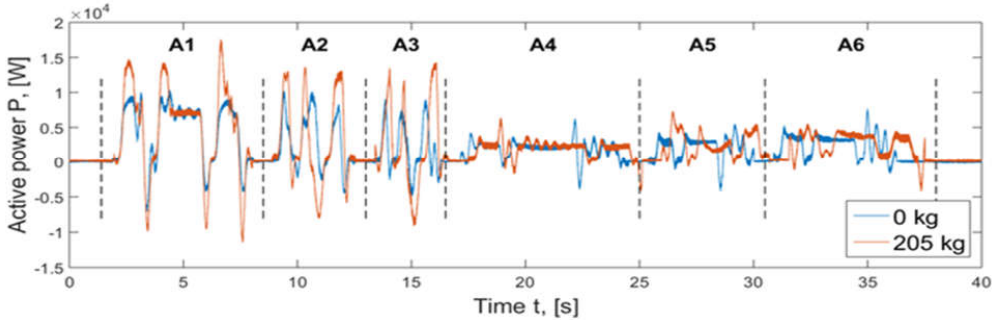

Fig. 5. Illustration of electrial power and attached tool mass performing reference motions of 210 kg industrial robot for each of 6 axis separately.

Detailed visualization for electrical power time variation by execution of same industrial robot program with no load and nearly full payload of additional weight attached to robot flange has been presented in Fig. 5. An interesting observation of tool mass effect on execution time for each axis can be seen clearly representing that first 3 axes are dimensioned for higher dynamic performance than axes four to six which correspond to real power ratings of installed electrical drives within industrial robot manipulator structure. Correlation of tool mass and braking energy reuse potential is also clearly demonstrated by higher negative power flow peak values. Summary of total electrical energy consumption and generation results has been provided by Fig. 6.

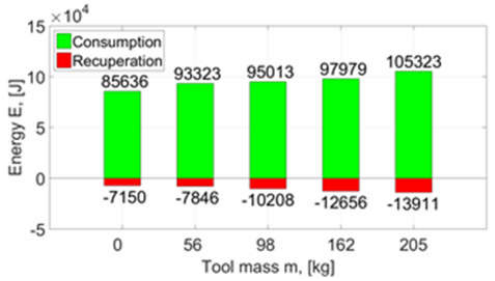

Fig. 6. Total electrical energy consuption and generation ratio by variation of additional tool mass.

It should be noted that real motion trajectories are executed by simultaneous operation of several axis electrical drives in order to reach target motion of end effector. Overall effect of significance of robot tool mass and related has been clearly observed therefore future applications with large tool mass and dynamic trajectory execution present potential for energy reladed optimization.

Next steps in industrial robot electrical energy consumption and related motion analysis would be more detailed separation of electrical power measurements utilized by single drives and flexible motion control at synchronized manner of external control and data acquisition system.

V. Conclusion and Outlook

In future developements for industrial robot related laboratory equipment and industrial robot manipulators particularly ability to have manufacturer provided communicatoin interface such as RobotSensorInterface (RSI) by KUKA is clearly visible by analysis of previous efforts of researcher teams and projects discussed in Section 1. By summary of common features of discussed applications and approaches one can conclude that availability of robot manufacturer provided interface is important for further development of external control and application integration soutions.

In field of physical motion simulation ability of real time external motion controller has been applied but similar performance and features would provide extended functionality also for robot motion related energy and programming concept verification for students within existing laboratories. Application of existing skills of student developed by well-established engineering calculation and simulation software such as Matlab is beneficial if suitable communication and integration solution with industrial robot controller is selected as presented by state of the art projects presented in literature.

References

[1] C. Deatcu, B. Freymann, A. Schmidt, and T. Pawletta, "MATLAB/Simulink Based Rapid Control Prototyping for Multivendor Robot Applications," *SNE Simul. Notes Eur.*, vol. 25, no. 2, pp. 69–78, 2016.

[2] F. Chinello, S. Scheggi, F. Morbidi, and D. Prattichizzo, "KCT: A MATLAB toolbox for motion control of KUKA robot manipulators," in *Proceedings - IEEE International Conference on Robotics and Automation*, 2010, pp. 4603–4608.

[3] F. Chinello, S. Scheggi, F. Morbidi, and D. Prattichizzo, "KUKA2011.

[4] J. Golz, T. Wruetz, D. Eickmann, and R. Biesenbach, "RoBO-2L, a Matlab interface for extended offline programming of KUKA industrial robots," in *2016 11th France-Japan and 9th Europe-Asia Congress on Mechatronics, MECATRONICS 2016 / 17th International Conference on Research and Education in Mechatronics, REM 2016*, 2016, pp. 64–67.

[5] H. L. Elshatarat, M. Baniyounis, and R. Biesenbach, "Design and implementation of a RoBO-2L MATLAB toolbox for a motion control of a robotic manipulator," in *13th International Multi-Conference on Systems, Signals and Devices, SSD 2016*, 2016, pp. 89–95.

[6] H. L. Elshatarat, R. Biesenbach, M. Bani Younus, and T. A. Tutunji, "MATLAB Toolbox implementation and interface for motion control of KUKA KR6-R900-SIXX robotic manipulator," *16th Int. Conf. Res. Educ. Mechatronics, REM 2015 - Proc.*, pp. 12–15, 2016.

[7] C. Mineo, S. G. Pierce, P. I. Nicholson, and I. Cooper, "Robotic path planning for non-destructive testing - A custom MATLAB toolbox approach," *Robot. Comput. Integr. Manuf.*, 2016.

[8] W. Banas, G. Cwikła, K. Foit, A. Gwiazda, Z. Monica, and A. Sekala, "Modelling of industrial robot in LabView Robotics," *IOP Conf. Ser. Mater. Sci. Eng.*, vol. 227, no. 1, p. 012011, Aug. 2017.

[9] L. Rogers and H. J. Vermaak, "Automated adapting component transfer system using real-time robot control within a KUKA RobotSensorInterface environment," in *2017 IEEE AFRICON: Science, Technology and Innovation for Africa, AFRICON 2017*, 2017, pp. 1426–1431.

[10] F. Sanfilippo, L. I. Hatledal, H. Zhang, M. Fago, and K. Y. Pettersen, "Controlling Kuka industrial robots," *IEEE Robot. Autom. Mag.*, vol. 22, no. 4, pp. 96–109, 2015.

[11] M. Schöpfer, F. Schmidt, M. Pardowitz, and H. Ritter, "Open source real-time control software for the Kuka light weight robot," *Proc. World Congr. Intell. Control Autom.*, pp. 444–449, 2010.

[12] A. Paugurs, A. Senfelds, and L. Ribickis, "Impact of industrial robot tool mass on regenerative energy," in *2017 19th European Conference on Power Electronics and Applications (EPE'17 ECCE Europe)*, 2017, p. P.1-P.6.

Appendix 3

P. Apse-Apsitis, K. Vitols, E. Grinfogels, **A. Senfelds** and A. Avotins, "Electricity meter sensitivity and precision measurements and research on influencing factors for the meter measurements," in *IEEE Electromagnetic Compatibility Magazine*, vol. 7, no. 2, pp. 48-52, Second Quarter 2018,

DOI: 10.1109/MEMC.2018.8410661.

Electricity Meter Sensitivity and Precision Measurements and Research on Influencing Factors for the Meter Measurements

Peteris Apse-Apsitis, Kristaps Vitols, Edgars Grinfogels, Armands Senfelds, Ansis Avotins
Institute of Industrial Electronics and Electrical Engineering
Riga Technical University
Riga, Latvia
peteris.apse-apsitis@rtu.lv

Abstract—Methodology, equipment, precision, immunity to electromagnetic emissions and reliable measurement results are important questions for electrical energy measurements. Widely used smart energy meters show good results under laboratory tests and in ordinary applications, but are not very suitable for industrial digital electrical energy supply environment. A different method and inexpensive equipment are used to overcome the above mentioned. The measured power balance between 15 robotized manufacturing cell measurement points (only power losses not measured are the ones in cables) varies in a range of 1,8% (measurement data rate- 20ms), despite the high level of electromagnetic emissions inside and outside of electric cabinets created by power converters.

Keywords— Electromagnetic Compatibility, Smart Meter, Electronic Meter, Interference, Power measurement

I. Introduction

One of the most used measurement devices is electricity meter. It is installed in almost every household and industrial enterprise, and all the electricity expenses are based on its measurements, so it is in everyone's best interests that these devices are as precise and sensitive as possible.

More, in order to increase energy efficiency, measurement device must be connected near each consumer or consumer - generator (smart home or smart robotized production, for example) to spot out inefficient energy consumption. As more electrical energy supply become digital (switch mode supplies) as more robust metering device must be in order to stand multiple wired and wireless electromagnetic influences.

Electricity meter is a measurement device that measures the amount of electrical energy consumed for any electrically powered device, residence or an entire household/enterprise. Every electricity meter needs to meet the IEC protocol standards. For most of the modern households digital electricity meters are used and their input signal is Ethernet frames according to IEC 61850 protocol, as it is communication protocol for digital substations [1][2][3].

In this paper different models of regular electricity meters which are used in regular households and are calibrated and meet the required IEC protocols were used for tests and measurements. Tests are provided in laboratory as well as in industrial applications. Calibration scheme is described in more detail in references [5] and [6].

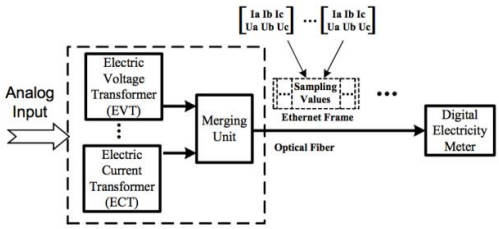

Fig 1. Electrical Energy Measurement in Digital Substations[4].

Suggestions about electrical energy/electrical power metering in digital power supply environment (unidirectional and bidirectional AC/DC, DC/DC, DC/AC converters and inverters) also are discussed.

II. Methodology

A. Electric Power and Electric Energy

Two main methods – C.I.Budeanu method (1927) dealing with non-sinusoidal signal harmonics power and instant power or instant power "p-q" theory (1983) dealing with instant voltage and instant current values (synchronized). Both require complex calculations.

In to microcontroller environment 3rd to 5th order voltage and current delta-sigma modulation and following multiplication and filtering also are widely applied today (*Analog Devices, Inc.* chips, for example).

As we can see – first we measure voltage and current and then calculate power value. Afterwards electrical energy can be obtained by multiplication by time period.

Another method - "non-even sampling method" (proposed earlier by article first author) [7] – where electrical energy are calculated in first and then average electric power are obtained by dividing by time period. Non-even sampling method shows good results in harsh electromagnetic environment in to industrial applications - (1,8% precision over 20ms time period in industrial digital supply environment)

B. Laboratory Tests

Laboratory tests are provided in rooms where low level electromagnetic radiation can be observed.

For all the sensitivity and precision measurements described in this paper, specific devices were used:

- Programmable power supply *PPS400.3*, made by *MTE*.
- Power supply control module *PCS400.3*, made by *MTE*.
- Portable electricity meter testing device *PWS2.3*, made by *MTE*. Testing device equipped with a scanning head *SH2003*.

Before all measurements each electricity meter and measurement device was warmed up for at least half an hour.

Programmable power supply was connected with the electricity meter and with the testing device using 4-wire system in case of a 3-phase meter, and 2-wire system in case of a 1-phase electricity meter. The testing device measured power shown by electricity meter using the scanning head, which fixed meter active powers light emitting diodes blink, also known as an impulse.

Electricity meter sensitivity measurements were made in 3-phase AC power supply voltage values: 253V, 230V and 207V.

Each individual meter measurement was started by applying phase current, which was equal to the minimum current that was shown in the meter's data sheet. For accurate measurements of meter sensitivity, at least two impulses were fixed. As an additional measurement, meter accuracy was determined. If both impulses were received, then measured accuracy was fixed and appropriate phase current was lowered by the step not bigger than 5mA. If impulse was not received in time twice as nominal impulse receiving time:

$$t = \frac{3600}{SK*P}, [s] \qquad (1)$$

then it was considered, that the meter cannot measure passing phase current anymore so the sensitivity limit was determined. In the equation (1) SK is a meter constant and P is the passing power.

Electricity meter precision measurements at different grid voltages were made with meter nominal current (Reference current), in 50Hz frequency, with purely active power. Measurements were made in phase voltage from 250V till 190V with a lowering step of 10V. For precise measurements, testing device was set up for 400 impulse counting mode in case of 3-phase meters and 100 impulse counting mode for 1-phase electricity meters.

Meter precision measurements in various grid frequencies were made in meter nominal current (Reference current), in 230V phase current, with purely active power. Measurements were made in grid frequency ranging from 45Hz to 65Hz with a step of 5Hz. For measurement calculations, a testing device was setup to perform 400 impulse counting for 3-phase meters and 100 impulse counting for 1-phase meters.

Electricity meter precision measurements in various sinusoidal forms were made in 50Hz grid, with voltage fundamental harmonic effective phase value 230V and current fundamental harmonic effective value equal to the meter nominal current given in the data sheet (Reference current). Measurements were made adding third, fifth and seventh harmonic to the main voltage and current signals. Each harmonic was added to each voltage and current signal and to both of them at the same time. For 3-phase meters harmonic percentage composition was set to 20%, but for 1-phase meters harmonic percentage composition was set to 30%. For measurement calculations, a testing device was setup to perform 400 impulse counting for 3-phase meters and 100 impulse counting for 1-phase meters.

For the electricity meter precision measurements in digital (switch mode) power supply working load additional impulse power supplies were used:

- Digital power supply Bestec *EA0061WEA*. The power supply output was set to such active power, so that the power from the network consumer would be approximately 6.3W.
- Digital power supply *S6/S10*. The power supply output was set to such active power, so that the power from the network consumer would be approximately 5W.
- Digital power supply Amigo *AMS3-0502500FV*. The power supply output was set to such active power, so that the power from the network consumer would be approximately 13W.
- Digital power supply *S-150-12*. The power supply output was set to such active power, so that the power from the network consumer would be approximately 100W.
- Digital power supply *VT-20150*. The power supply output was set to such active power, so that the power from the network consumer would be approximately 100W.

For these measurements faculty grid voltage was used. Measurable electricity meter was connected to the grid using 4-wire system in case of 3-phase meter, and 2-wire system in case of 1-phase electricity meter. In the meter output testing device was connected, and in the testing devices output one or more switch mode power supplies were connected. For meter testing one of the switch mode power supplies were connected to each phase. In case of 3-phase meter, one measurement was made, where switch mode power supplies were connected to the first and third phase, but second phase was without any load. The testing device measured power shown by electricity meter using a scanning head, which fixed meter active powers light emitting diodes blink, also known as an impulse. For power supplies with power less than 20W only 4 impulses were used, but for more powerful supplies 20 impulses were uses for each measurement.

III. Laboratory Test Results

The results for electricity meter sensitivity are shown on Figure 2. The minimal current which is detected by the electricity meters varies from as low as 0.008 A till 0.034 A for the electricity meters. Minimal detected currents were measured in different voltages. It is a very low percent from the nominal meter current I_{ref}.

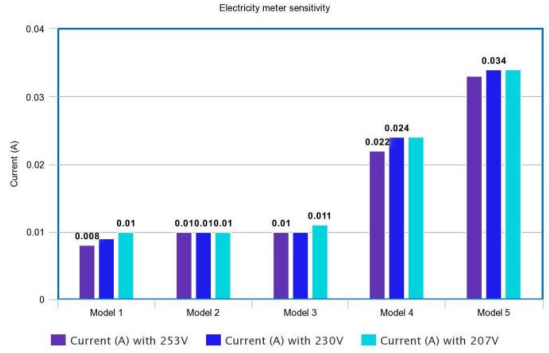

Fig. 2. Electricity meter sensitivity measurement average results for each model.

Electricity meter precision measurement at different grid voltages results are shown in Figure 3.

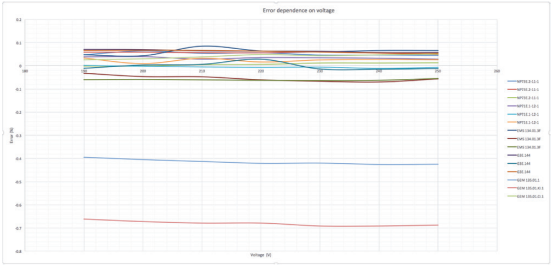

Fig. 3. Electricity meter error dependence on different grid voltage.

The results vary mostly in a range of 0,1 % error for the electricity meter measurements, with two exceptions, where it goes as high as almost 0,7%

For precision measurements in various grid frequencies for the electricity meters the results vary mostly in a range of 0,5 % error for the exact measurement, with few exceptions, where it goes as high as 1,15 % error. The biggest error appears at 65 Hz frequency, and the lowest errors appears in 50 Hz frequency. The results are shown in Figure 4.

In Table 1. the first column shows, which higher harmonic is added to the voltage signal. The second column shows, which higher harmonic is added to the current signal. The third column shows the percentage value of the harmonic added to voltage signal. The forth column shows the percentage value of the added harmonic to current signal. The fifth column shows the measured electricity meter error in %.

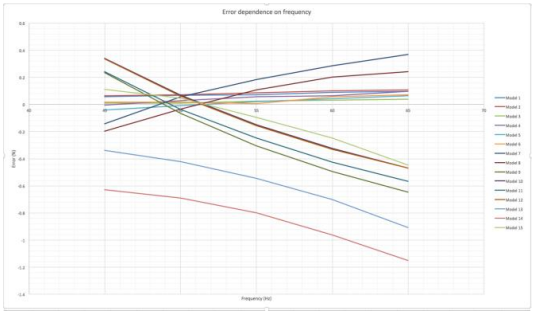

Fig. 4. Electricity meter error dependence on various grid frequencies.

Electricity meter precision measurements in various sinusoidal forms were measured in specific harmonics and order for each meter, with voltage fundamental harmonic effective phase value 230V and current fundamental harmonic effective value equal to the meter nominal current given in the data sheet (Reference current). The results (worst case between several the same model meters) are shown on the Table 1.

Table I. Measurement results, sinosoidal harmonics

Voltage harmonic	Current harmonic	Voltage harmonic value(%)	Current harmonic value(%)	Error (%)
3.	3.	20	20	0,1
-	3.	-	20	0,084
3.	-	20	-	0,095
5.	5.	20	20	0,11
-	5.	-	20	0,092
5.	-	20	-	0,093
7.	7.	20	20	0,113
-	7.	-	20	0,086
7.	-	20	-	0,09
3.	3.	20	20	0,1

As for the measurements in digital (impulse) power supply working load for electricity meters the results are sorted out in tables in Table II. The first column shows information about electricity meter load – DC power supply model, based on simple rectifier with filtering capacitor on AC side, the second column shows each meter's serial number. The second column shows the approximate load power value. The third column shows in which phase the load was connected. The fourth column shows the measured electricity meter measurement error in %. This table shows that for this test the maximum meter error for the specific model could reach more than 3 %.

Table II. Measurement results, rectifier-capacitor load

Load – DC power supply	Load (W)	Connected phase	Error (%)
Bestec	6,3	1.	-3,188
S6/S10	5	2.	-2,922
Amigo	13	3.	-0,555
S-150-12	100	3.	0,125
VT-20150	100	1.	-0,204
S-150-12 and VT-20150	200	3. and 1.	0,027

IV. Industrial Tests

Industrial tests show the uselessness of these energy meters in a dynamic power consumption-recuperation environment. Strong

electromagnetic fields (field generating currents are up to 600 A) influence measurement devices in the similar way like open door electric cabinets cause several model laptop's touch pads "live on their own". At the same time measurement devices and corresponding current transformers must be installed in to the electric cabinets in order to use shorter power cables.

Typically dynamic current changes do not fit into standard defined frame: aluminum spot welding requires power jump from 1-2 KW during stand-by and up to 360KW during welding (Figure 5). Welding time is about 90 milliseconds and it is not known where it occurs over the measurement frame – at the beginning or at the end of the frame.

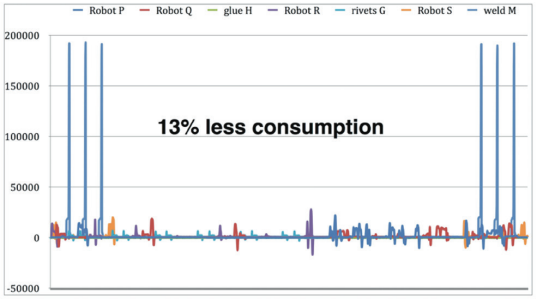

Fig. 5. Industrial production machines and tool power profiles , W.

Non-even sampling method based devices (Figure 6.) are used to synchronically measure multiple machine and tool power profiles in to an AC or DC digital environment. Currently this allow to record robotized manufacturing cell all electric equipment power profiles (consumption and recuperation) by implementation of 15-measurement point setup. Measurement and analysis allow observe and record 13% less energy consumption in to industrial 600 V DC power supply grid.

Fig. 6. Bi-directional AC/DC power / energy flow meter; 20 ms energy sampling rate.

V. Power / Energy Flow Measurement Tools - Discussion

The following must be taken into account in a discussion about electrical power / energy measurements in a digital environment:

- Converters generate emissions and thus influence voltage and current probes and high speed ADC's readings regardless of ADC conversion method (delta-sigma, multi-order delta-sigma or direct SAR conversion).
- Signal filtering/conditioning creates phase shift and filters cut-off frequency influence etc.
- Sensors mainly have a poor dynamic range.
- Blurring of ADC readings up to ±2-4 less significant bits (practical observation) exists due to inducted noise in wires and PCB. Noise typically is very similar to "white" or "rose" noise (definitions from audio engineering), especially if high speed ADC's are used or signal digital processing takes place (Figure 7). It exists regardless of applied shielding method.
- There are no knowns and unknowns in the measurement device processing method implementation. So it is difficult to predict where the attention must be paid more in order to reduce noise and increase precision.

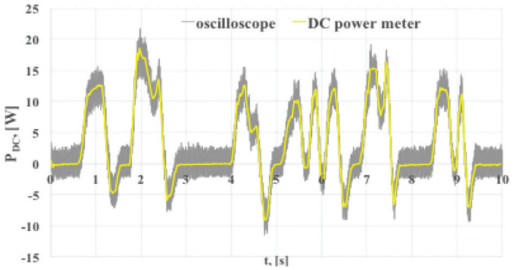

Fig. 7. Noise impact –Oscilloscope v.s. Bi-directional AC/DC power / energy flow meter (20 ms energy sampling rate).

Readings are typically logged or displayed in between of 3…5 seconds rate, however that is not applicable for fast processes. Higher rate leads to lower precision as observed.

Widely used [KWh] units are not applicable for fast processes. Standard SI unit [Ws] must be used.

VI. Conclusion

After various tests and measurements, we can conclude that electricity meter precision is not dependent on the grid quality (higher/lower voltage and frequency). It is also not dependent on the current and voltage load disturbances or interferences. This conclusion is mainly based on the fact that the electricity meter measurement error should be lower than 2%.

A different case is the low power switch mode power supplies, whose consumed current is close to the minimal current for electricity meter sensitivity. In these cases, electricity meters tend to exceed the error limit of 2%. In all the fixed cases it benefits the consumer as the measurements show a lower registered quantity of energy.

When observing or recording micro- or nano-grid energy flow in practice, it is complicated to get precise information about power balance. Noise level, switch mode power supply electromagnetic

emissions and their character change under different processed power, depending on measurement point location. Wiring losses are not constant and sharp power consumption/recuperation change causes additional loses due to wiring inductance and capacitance. Practical observations always show 2-4% imbalance regardless of the precision of the involved measurement devices.

Electromagnetic compatibility always has analog signal character. Applying design principles and techniques from vacuum valve era, well known principles from audio engineering and correct PCB layout design, allows to achieve acceptable results without special measures to reduce noise and the influence of emissions.

However, the "typical and well known" devices do not allow to perform distributed multipoint synchronous measurements. Even multichannel data loggers are not applicable for 5-10-15 meter distances between the measurement points and the logger.

Acknowledgment

Discussed above device development and measurement process was supported by Latvian National Program "Latenergi".

References

1. IEC Technical Committee 38. Specific communication service mapping (SCSM) sampled values over unidirectional multidrop point to point link, 2003.
2. IEC Technical Committee 38. Specific Communication Service Mapping (SCSM) Sampled values over ISO/IEC 8802-3 link, 2003.
3. UCA International Users Group. Implementation Guideline for Digital Interface to Instrument Transformers using IEC 61850-9-2.
4. X. Qing, H. Hongtao, M. Xiaoxing, Z. Jian, D. Meimei, and W. Lei, "Power Output Stability of Digital Power Sources for Calibration of Digital Electricity Meters," pp. 72–73, 2014.
5. HUANG Hongtao, WANG Lei , ZHANG Jiangtao, PAN Xianlin, LU Zuliang. Calibration Method for Digital Energy Meters in Digital Substations. CPEM 2010, pages 261-262, 2010.
6. HUANG Hongtao, WANG Lei , ZHANG Jiangtao, PAN Xianlin, LU Zuliang. Traceability of Digital Electricity Meters. CPEM 2012, pages 234-235, 2012.
7. Apse-Apsitis, P.; Avotins, A.; Ribickis, L., "Bidirectional DC/AC energy flow measurement," in Power Engineering, Energy and Electrical Drives (POWERENG), 2015 IEEE 5th International Conference on , vol., no., pp.465-468, 11-13 May 2015

Biographies

Dr.sc.ing. Peteris Apse-Apsitis *is a Senior Researcher and Associate Professor at the Institute of Industrial Electronics and Electrical engineering, Riga Technical University, Latvia. He defended his Ph.D. thesis in 2013. During his 50 years of practical, scientific research and R&D experience in fields of electronics, power electronics, industrial automatics, ICT, printing & publishing and paper-making, he has listed more than 330 designs and implementations of the devices and projects. He has published more than 30 papers and has three patents.*

Kristaps Vitols *is working towards his Ph.D. at the faculty of Power and Electrical Engineering. Since 2008, he is working at RTU Institute of Industrial Electronics and Electrical Engineering, currently as a researcher. His main fields of interest are related to battery storage systems, electric vehicles, measurement systems and education.*

Edgars Grinfogels *is currently working on Master studies at the faculty of Power and Electrical Engineering, as well as Master studies to obtain an MBA degree. He also has a part-time job at the RTU Institute of Industrial Electronics and Electrical Engineering, currently as an assistant. His main fields of interest are related to converters and power electronics business solutions.*

Armands Senfelds *received the M.Sc at RWTH Aachen University, Germany in 2012. He is currently a Ph.D. student and researcher at Riga Technical University, IEEI. His research interests include design and control of power electronic equipment, electrical drives and electrical mobility.*

Ansis Avotins *is a Ph.D. student at the faculty of Power and Electrical Engineering study program "Computer Control of Electrical Technology". From 2004, he worked as chief Laboratory Manager and researcher at RTU Institute of Industrial Electronics and Electrical Engineering (IEEI). His main field of study and research is energy efficiency solutions in industrial applications. He is a Board member of the Latvian Energy Efficiency Association.* **EMC**

Appendix 4

Šenfelds, A., Avotiņš, A., Apse-Apsītis, P., Grīnfogels, E., Ribickis, L. Investigation on Power Quality Parameters of Industrial 600V DC Microgrid Hardware. In: *2018 20th European Conference on Power Electronics and Applications (EPE'18 ECCE Europe): Proceedings*, Latvia, Rīga, 17-21 September, 2018. Piscataway: IEEE, 2018, pp.1-6.

ISBN 978-1-5386-4145-3.
e-ISBN 978-9-0758-1528-3.

Investigation on Power Quality Parameters of Industrial 600V DC Microgrid Hardware

Armands Senfelds, Ansis Avotins, Peteris Apse-Apsitis, Edgars Grinfogels, Leonids Ribickis
Riga Technical University
12-1 Azenes Street
Riga, Latvia
Phone: +371 26369853, +371 67089300
Email: armands.senfelds@rtu.lv
URL: https://www.rtu.lv

Acknowledgments

This research has been supported within Latvian national research program LATENERGI.

Keywords

«DC power supply», «Active frontend», «Microgrid», «Power Supply»

Abstract

Paper describe physical DC microgrid realization for research and modelling tasks and its alignment with unique DC microgrid installation at automotive factory under real manufacturing conditions. Focus on key component modelling and verification such as bidirectional grid interface AC/DC frontend converter has been presented at real load conditions.

Introduction

Global trends to increase energy efficiency and rise of electricity costs has made an impact also to industrial electricity grids, fostering interest for implementation of renewable energy sources also at industrial factory level, as well as looking for new ways to save energy. Small scale electrical power supply infrastructure with given boundaries due to geographic, economical and other aspects can be observed in forms of grid structures referred as nano and microgrids. Typically separation from main power is related to lack or loss of grid connection or intrinsic nature of system that require supply of electrical energy and preferable type of voltage. In case of industrial manufacturing applications microgrid solutions of DC energy supply enable solutions of energy efficiency increase and storage for sustainable manufacturing. Also applications regarding household and office load supply in buildings has been considered recently. Several studies, like [1], [2], [3], [4] are presenting advantages of DC-grid transmission, as solar panels, fuel cells and Lithium-Ion or supercapacitor energy storage systems are DC-voltage based in their nature, thus it is logical choice to have DC-Grid connection between them, using DC/DC converters, as it would have less conversion stages. As modern industrial factory nowadays use high payload industrial robots, it is possible to re-use their braking energy, which is typically dissipated into braking resistors attached to converters DC-link, by means of storing that energy into capacitor banks or injecting into DC-Grid. Also carbon footprint reduction and product life cycle assessment leads to deeper research also within production process itself.
These initiatives lead to new developments and automated manufacturing infrastructure modifications, including DC microgrid as electrical energy supply concept (see Fig. 1.), with such elements as local PV generation, energy storage and industrial robots and their welding, clinching and gluing tools as

consumers. Furthermore such electrical installation using 600V DC microgrid within automotive manufacturing branch enables to operate such manufacturing cell in islanding mode for certain periods, create new power peak shaving options.

Practical realization of 600V DC-microgrid structure (Fig. 1.a.) is done at Daimler AG factory in Germany as presented in Fig.1.b. System has central AC/DC bidirectional converter (Active Front End) with rated power of 450 kW. Load group is combined of 4 industrial robots and related tools for material joining by spot welding, glue dispensing and punch riveting methods as well as rotating conveyor for part exchange. As auxiliary systems electrolytic capacitor bank of is directly connected to main DC bus as well as LiIon storage and photovoltaic panel array with respective DC/DC power converters. Nevertheless it was a great challenge to create such system, due to lack of electrical component portfolios of typical suppliers with respect to state of the art AC electrical technology, also there is a need for updated and new DC standards for such application. Insight of research activities covering both software and hardware modifications with focus on energy efficient robotic manufacturing has been presented by [2], [5]. If looking more widely real DC-Grid infrastructures enable various practical researches in the field of grid power control and management [6],[7], safety issues [8], and voltage quality issues [9]. If looking into frequency domain like described [10], or measuring [11], [12] it can help to identify equipment faults, thus enabling new approach in the field of equipment and system maintenance. Nevertheless such industrial DC-Grid infrastructure is not widely available, due to high prototype and custom design equipment costs, therefore detailed mathematical models must be created, that are based on real experimental measurements.

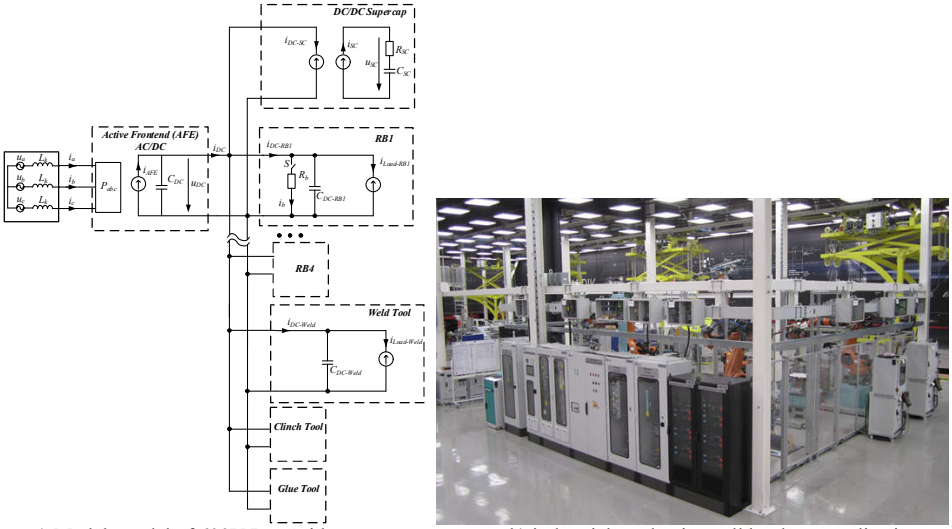

a) Matlab model of 600V DC-Grid structure b) industrial production cell hardware realization

Fig. 1. Structure and realization of 600V DC microgrid for automotive manufacturing application.

For this purpose a special 600V DC-Grid laboratory with real equipment is created in Riga Technical University (see Fig.2.), that uses same architecture, but same time is scalable to the industrial production cell described in Fig.1.

Overview of 600V DC Grid testing infrastructure in Riga Technical University (RTU) laboratory

An experimental laboratory electrically representing a manufacturing work cell is necessary to complete the research objective and demonstration to develop a DC power supply system in which energy could be exchanged, harvested, stored and recovered at a factory level. The main loads in the laboratory have to be several industrial robots, however, due to financial and spatial limits, only one DC powered industrial robot will be implemented. Therefore, a system has been developed which can recreate the dynamic DC bus power flow of an industrial robot. RTU DEMO laboratory layout is shown in Fig.2., where number (1) – Active Front-End AC/DC rectifier unit (55kW), number (2) and (3) universal robot load emulator stands (23kW), able to replicate energy consumption signature of any industrial robot also with combination of robot tools, input is AC, but output is DC (can be switched to AC if necessary), number (4) is prototype Lithium Ion battery energy storage system (BESS) 16-22kW, number (5) is prototype supercapacitor storage system (30kW), number (6) is 600V DC-Robot prototype and DC-Cabinet (7) with load 2kW, number (8) is Master PLC controller (Cell controller), (9) is prototype solar DC/DC converter (3-4kW) for 3.3kW solar panel array, (10) is optional wind energy emulator stand.

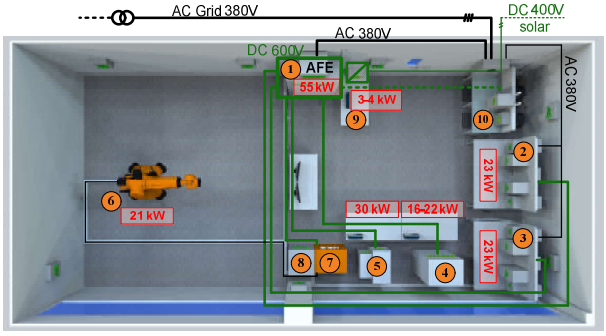

Fig.2. DC-Microgrid layout plan and grid connections at RTU laboratory

Evaluation and modelling of AC/DC interface converter unit.

Regarding DC microgrid structures DC link voltage is often utilized as key parameter for overall system coordination and control. The currents in DC link are directly related to power flows within system. Often by modelling of systems and large scale analysis waveforms of voltage and current are considered to follow idealized DC type quantities. However application central AC/DC grid tied converter or active frontend as important subsystem for DC microgrid supply would require closer analysis regarding actively modulated power electronics and related effects within DC link. Analytical approach discussing DC link behavior related to inverter topologies has been presented by [13]. Rectifier application has been discussed by [14],[15]. The effects of higher harmonics within DC link is also matter of lifetime of capacitor elements as discussed [16].

Evaluation of real AC/DC bidirectional converter operation at laboratory microgrid arrangement has been made possible by dynamic power flow emulation units utilizing coupled electrical machines as presented in Fig.3. and feeding of power back into AC grid. Such arrangement allow to replicate both bidirectional power flow as industrial robots and tools as well as load grid with constant loading conditions.

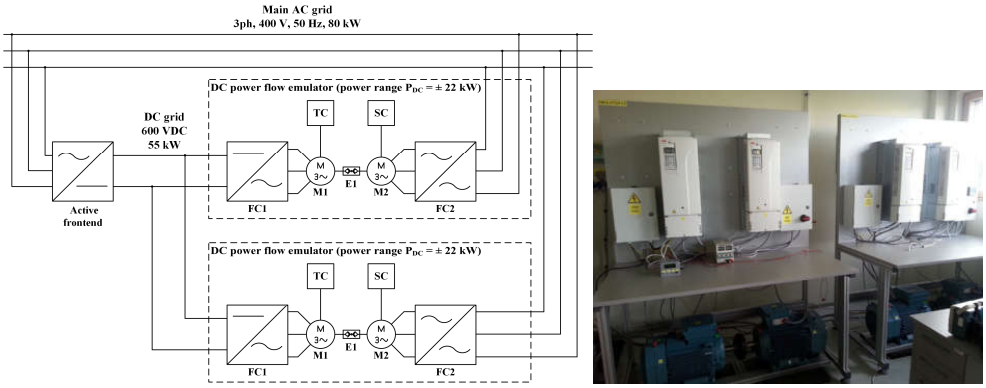

Fig. 3. Principal electric schematic of AC/DC active frontend converter testing with 2 robot load emulator stands.

Initially generalized model of AC/DC frontend converter has been developed and verified against dynamic load changes according to Fig.4 as described in [17] with main focus of converter efficiency estimation and replication as well as behavior on AC grid side during dynamic operation.

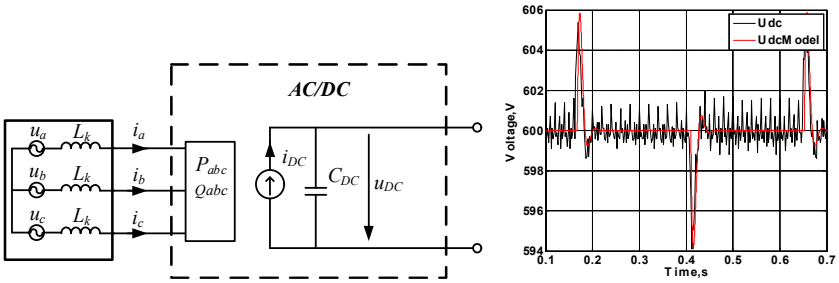

Fig. 4. Generalized model of bidirectional AC/DC converter and simulated DC link voltage behavior of 7 kW load step change.

Higher frequency experimental evaluation for model modification.

As discussed before utilization of actively commutated converters interfaced with microgrid DC link also present effects of higher frequency content within DC power flow. In order to obtain data for electrical system modelling voltage and current data has been obtained with frequency of 41 kHz thus presenting frequency related analysis within range up to 20 kHz. Such frequency range is considered sufficient for electrical mode iteration since it provide insight of fundamental switching frequency of AC/DC converter being 8kHz and its second harmonic. The following pictures represent obtained experimental measurement data of DC link voltage being controlled according to setpoint value of 600V by active frontend converter under several steady load conditions. Four operation conditions have been depicted: simple AC/DC converter operation without DC link (AFE only), operation with load emulators switched on at no load, load of 44kW being consumed from DC microgrid and recuperation of 33kW via active frontend to AC mains. Fig.5 represents voltage and current waveforms at selected conditions at AC/DC converter DC terminals.

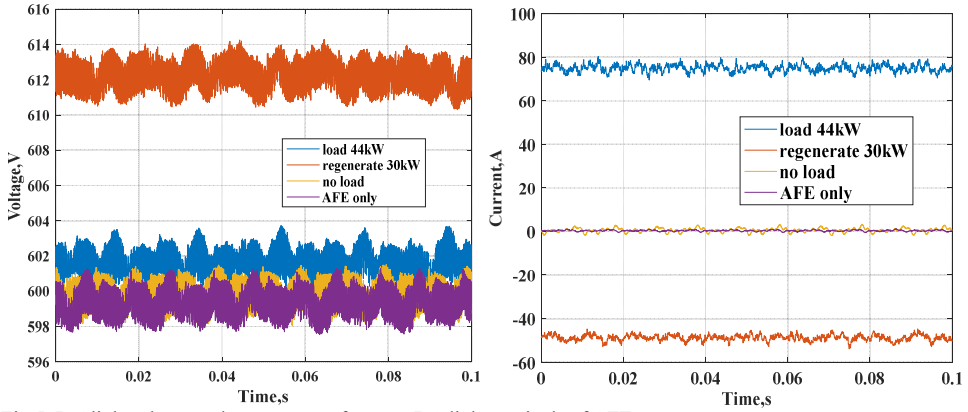

Fig.5. DC link voltage and current waveforms at DC link terminals of AFE converter.

By means of frequency content analysis significant frequencies and relative variation under changing load conditions has been obtained as shown in Fig.6.

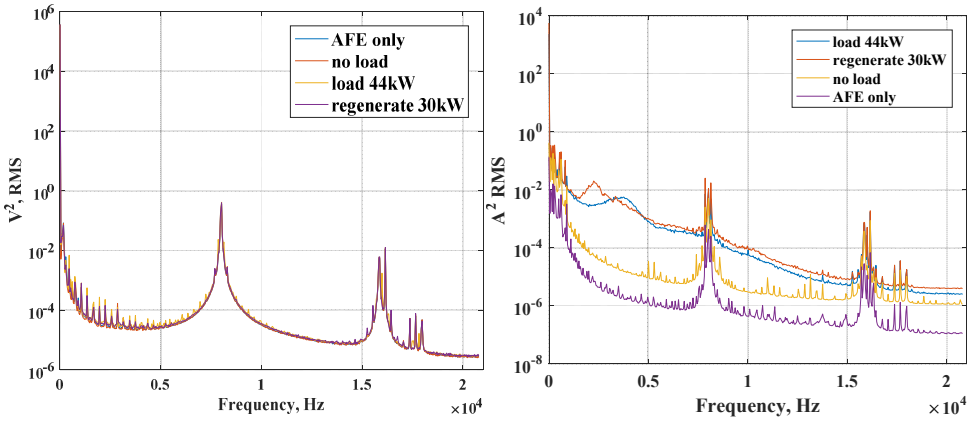

Fig.6. Frequency content analytical results of DC terminal voltage and current at various load states.

Conclusions and future work.

Obtained experimental results of real AC/DC converter operation interfacing DC microgrid and mains with bidirectional power flow capability allow improvement of existing mathematical models. The behavior of higher frequency components at DC link voltage and currents during real load power situations enable detailed design of microgrid electrical subsystems such as dynamic buffering and storage units and their controllers. It has been verified experimentally that voltage harmonic content is less prone to deviate under load conditions as current waveforms when central AC/DC unit is utilized under voltage control approach.

References

[1] R. W. De Doncker, “Power electronic technologies for flexible DC distribution grids,” in *2014 International*

Power Electronics Conference (IPEC-Hiroshima 2014 - ECCE ASIA), 2014, pp. 736–743.

[2] M. Pellicciari, A. Avotins, K. Bengtsson, G. Berselli, N. Bey, B. Lennartson, and D. Meike, "AREUS - Innovative hardware and software for sustainable industrial robotics," in *2015 IEEE International Conference on Automation Science and Engineering (CASE)*, 2015, pp. 1325–1332.

[3] U. Boeke and M. Wendt, "DC power grids for buildings," in *2015 IEEE First International Conference on DC Microgrids (ICDCM)*, 2015, pp. 210–214.

[4] G. Zaleskis and ingars Steiks, "Alternative Energetics DC Microgrid with Hydrogen Energy Storage System," *Sci. J. Riga Tech. Univ. - Electr. Control Commun. Eng.*, vol. 11, no. 0, pp. 21–26, Dec. 2016.

[5] D. Meike, M. Pellicciari, and G. Berselli, "Energy Efficient Use of Multirobot Production Lines in the Automotive Industry : Detailed System Modeling and Optimization," *IEEE Trans. Autom. Sci. Eng.*, vol. 11, no. 3, pp. 798–809, 2014.

[6] P. Sanjeev, N. P. Padhy, and P. Agarwal, "Autonomous Power Control and Management Between Standalone DC Microgrids," *IEEE Trans. Ind. Informatics*, pp. 1–1, 2017.

[7] Y. Li, A. Luo, X. Xiang, Y. Chen, Z. He, Z. Chen, and F. Zhou, "Electromagnetic stirring power supply system with bidirectional energy flow and its control strategy," in *2017 19th European Conference on Power Electronics and Applications (EPE'17 ECCE Europe)*, 2017, p. P.1-P.7.

[8] Z. Liu, A. Shekhar, L. Ramirez-Elizondo, and P. Bauer, "Real time selective detection of experimentally generated DC series arcs," in *2017 19th European Conference on Power Electronics and Applications (EPE'17 ECCE Europe)*, 2017, p. P.1-P.8.

[9] A. Micallef and C. S. Staines, "Voltage rise mitigation and low voltage ride through capabilities for grid-connected low voltage microgrids," *2017 19th Eur. Conf. Power Electron. Appl. (EPE'17 ECCE Eur.*, p. P.1-P.9, 2017.

[10] K. Severson, P. Chaiwatanodom, and R. D. Braatz, "Perspectives on process monitoring of industrial systems," *Annu. Rev. Control*, vol. 42, pp. 190–200, 2016.

[11] S. Sahu, "A Vibration Analysis of a 6 Axis Industrial Robot Using FEA," *Mater. Today Proc.*, vol. 4, no. 4, pp. 2403–2410, 2017.

[12] P. Apse-Apsitis, A. Senfelds, A. Avotins, A. Paugurs, and M. Prieditis, "Power Measurement and Data Logger Device with High-Resolution for Industrial DC-Grid Application," *Sci. J. Riga Tech. Univ. - Electr. Control Commun. Eng.*, vol. 9, no. 1, pp. 36–42, Dec. 2015.

[13] A. Mariscotti, "Analysis of the DC-link current spectrum in voltage source inverters," *IEEE Trans. Circuits Syst. I Fundam. Theory Appl.*, vol. 49, no. 4, pp. 484–491, Apr. 2002.

[14] V. Blahnik and J. Talla, "Study of 3.3 MW voltage-source active rectifier," in *2016 International Conference on Applied Electronics (AE)*, 2016, pp. 27–30.

[15] V. Kus and T. Josefova, "DC link voltage ripple of voltage-source active rectifiers," in *2016 17th International Scientific Conference on Electric Power Engineering (EPE)*, 2016, pp. 1–4.

[16] H. Jedtberg, M. Langwasser, R. Zhu, G. Buticchi, T. Ebel, and M. Liserre, "Impacts of unbalanced grid voltages on lifetime of DC-link capacitors of back-to-back converters in wind turbines with doubly-fed induction generators," in *2017 IEEE Applied Power Electronics Conference and Exposition (APEC)*, 2017, pp. 816–823.

[17] A. Senfelds, O. Bormanis, and A. Paugurs, "Modelling of AC/DC power supply unit for DC microgrid," in *2015 IEEE 3rd Workshop on Advances in Information, Electronic and Electrical Engineering (AIEEE)*, 2015, pp. 1–4.

Appendix 5

Šenfelds, A., Apse-Apsītis, P., Avotiņš, A., Ribickis, L., Hauf, D. Industrial DC Microgrid Analysis with Synchronous Multipoint Power Measurement Solution. In: *2017 19th European Conference on Power Electronics and Applications (EPE '17 ECCE Europe): Proceedings*, Poland, Warsaw, 11-14 September, 2017. Piscataway, NJ: IEEE, 2017, pp.3685-3690. ISBN 978-1-5386-0530-1. e-ISBN 978-90-75815-27-6.

DOI:10.23919/EPE17ECCEEurope.2017.8099322

Industrial DC Microgrid Analysis with Synchronous Multipoint Power Measurement Solution

Armands Senfelds[1], Peteris Apse-Apsitis[1], Ansis Avotins[1], Leonids Ribickis[1], Dominik Hauf[2]
Riga Technical University[1] Daimler AG[2]
Kalku iela 1[1] Mercedes-Benz Werk Sindelfingen[2]
Riga, Latvia[1] Sindelfingen,Germany[2]
Tel.: +371 67089919[1] Tel.: +49 176 309 308 91[2]
E-Mail: Armands.Senfelds@rtu.lv, Peteris.Apse-Apsitis@rtu.lv, Ansis.Avotins@rtu.lv,
Leonids.Ribickis@rtu.lv, Dominik.Hauf@daimler.com
URL: www.rtu.lv[1] ; www.daimler.com[2]

Acknowledgements

This research is supported by Latvian National Research Programme project LATENERGI.

Keywords

« Microgrid », « Industrial application », « DC power supply », « Measurement »

Abstract

Paper is presenting application of synchronized power flow measurement system within 13 locations of DC microgrid installation in production plant with specific measurement equipment system developed for dynamic energy flow analysis. Insight into internal DC bus power exchange behavior and interconnected operation advantages with respect to energy efficiency improvement is provided. Future trends towards DC based manufacturing infrastructure are discussed. Presented results provide insight into electrical energy distribution behavior within DC microgrid system structure operated based of realistic industrial manufacturing tasks. Application of multipoint power measurement system provide real measurement data of various manufacturing technology tool load profiles that serve as important basis for future system modelling and dimensioning tasks.

Introduction

Presented paper is related to DC technology based electrical supply infrastructure integration effort within automotive manufacturing branch and obtained power flow measurement results with dedicated multipoint synchronized measurement equipment. High level European Union policies [1] are demanding investments towards more energy efficient production technologies. Also country specific initiatives such as Energiewende [2] in Germany present concepts toward intelligent DC power distribution in future. Such factors lead to development of highly automated manufacturing infrastructure modifications including DC microgrid as electrical energy supply concept as presented in Fig. 1. Elements of local PV generation, energy storage and consumers as well as ability to operate in islanding mode for certain periods allow to discuss presented electrical installation as microgrid. Green dots represent relevant power flow measurement locations within microgrid structure.

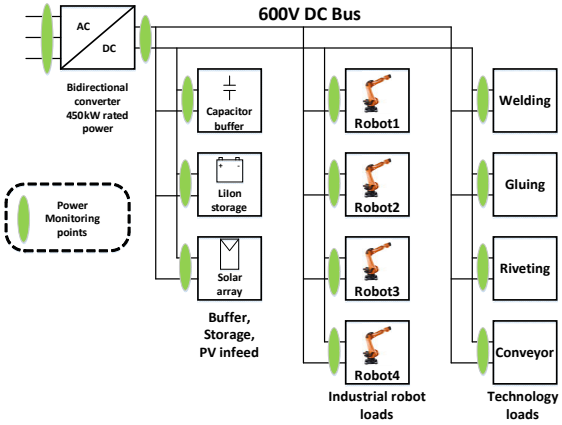

Fig. 1: Structure of examined DC microgrid for automotive manufacturing application.

Development of 600V DC electrical system for integration within existing factory infrastructure arise problems of less developed standard base and electrical component portfolios of typical suppliers with respect to state of the art AC electrical technology. However, future plans covering DC standards have been presented [3]. Insight of research activities covering both software and hardware modifications with focus on energy efficient robotic manufacturing has been presented by [4],[5]. Advantages of DC energy supply systems has recently been identified also in marine applications [6] and buildings [7]. Ideas of verified simulation model development of electrical components as well as parallel development of virtual software analogue of existing manufacturing infrastructure systems also known as digital twin concept has been considered [8]. Such concepts are demanding verified experimental data of power consumption as basis for new modelling and planning software development. Also control strategies of adaptive system operation with respect to energy prices, renewable energy production potential and energy storage options require experimental research. Realization of Fig. 1. presented DC microgrid structure has been built as operating production cell including industrial robot manipulators with related tools and technologies at Daimler AG factory in Germany as presented in Fig.2.

Fig. 2: DC microgrid realization as automotive manufacturing cell for experimental analysis.

System has central AC/DC bidirectional converter with rated power of 450 kW. Load group is combined of 4 industrial robots and related tools for material joining by spot welding, glue dispensing and punch riveting methods as well as rotating conveyor for part exchange. As auxiliary systems electrolytic capacitor bank of is directly connected to main DC bus as well as LiIon storage and photovoltaic panel array with respective DC/DC power converters.

Multipoint power metering system application

Scale of presented system and involved electrical components arise problem for power flow measurement realization. The approximate dimensions of cell are 8 by 8 meters with DC ring bus rail and electrical cabinets located along outer wall. In order to obtain power flow measurement data from 13 distributed measurement points with common sampling time reference power measurement devices combined with optical fiber data transfer system has been created and applied. Power measurement units has been built based on approach presented in [9] utilizing voltage to frequency method for voltage measurement and compensated hall effect sensor current measurement methods. Following Fig. 3 represent power measurement module designed for industrial robot cabinet connection and graph during measurement validation tests.

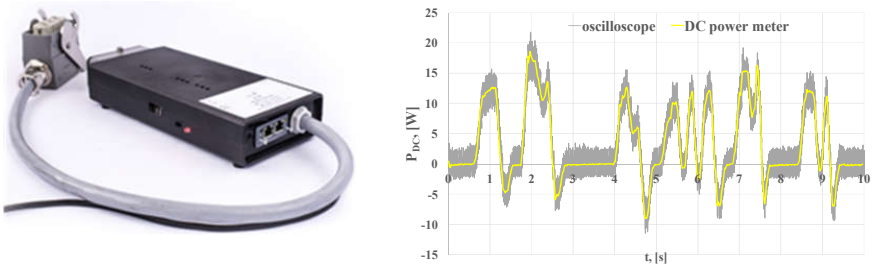

Fig. 3: Power measurement device prototype for DC industrial robot and measurement performance evaluation example against oscilloscope based power measurement.

The basic sampling frequency is 2.8 kHz and averaged values over 20 millisecond periods corresponding to 50Hz AC side power measurement are propagated via optical fiber network for central data logging as text file. The AC side power measurement device prototype is shown in Fig. 4. For installation in existing AC electrical system external current clamps have been preferred with ability to connect without dismantling the high power electrical wiring. All power metering devices have been designed for later integration within industrial automation infrastructure via Profinet communication standard for power monitoring capability. For the current scope of this paper bidirectional optical communication has been utilized enabling synchronized reading of all involved measurement modules to obtain single time base for 12 DC type and one AC type power measurement readings.

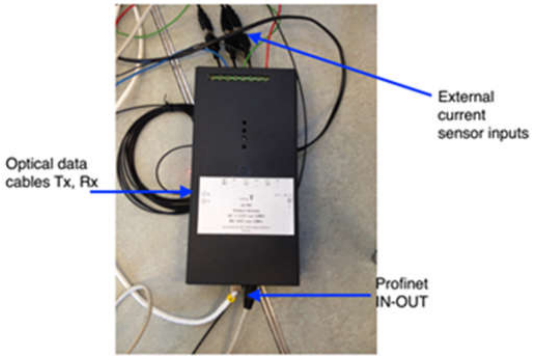

Fig. 4: AC side 3 phase power measurement prototype with external current clamps, bidirectional optical data transfer and Profinet communication module.

Synchronous Multipoint Power Measurement Data example

Based on application of aforementioned measurement setup power flow data has been obtained based on industrial manufacturing application operation of 110 second duration completely supplied via local DC microgrid. Following Fig. 5 represent 13 datasets with common time axis grouped according to similar magnitudes of power flow.

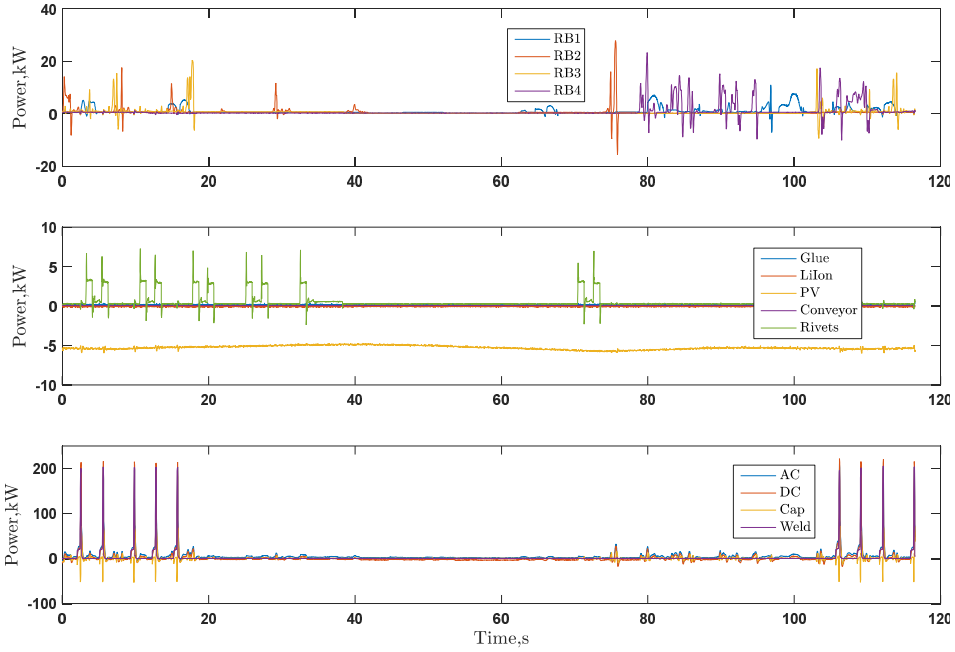

Fig. 5: Obtained synchronous power flow measurement data at 13 microgrid locations: 4 industrial robots (top), tool technologies, PV infeed and LiIon storage (middle), AC, DC, Capacitor buffer and welding (bottom).

Power flow direction is considered positive as consumption from DC bus or AC grid respectively. Alternative way to classify involved microgrid components regarding functional tasks can be addressed as already introduced in Fig. 1.

Industrial DC Microgrid Power Flow Analysis

By observing behavior of consumers it is possible to derive group of elements operating with bidirectional power flow in DC bus. In order to obtain insight about intermediate power flow behavior within DC network following calculation has been performed according to equations (1) and (2) calculating average positive P_{Pos} and negative P_{Neg} power flow within given 116 second operation period T and results have been summarized in Table 1.

$$P_{Pos} = \frac{\int_0^T P(t)}{T}; P(t) \in [0, \infty) \quad (1)$$

$$P_{Neg} = \frac{\int_0^T P(t)}{T}; P(t) \in [-\infty, 0) \quad (2)$$

Table I: The title of the Table I

	DC load group (4 robots, tools, capacitor buffer)	Robot 1	Robot 2	Robot 3	Robot 4	Technology tools (4 units)	Capacitor buffer
P_{pos}, kW	8.01	0.99	0.94	0.68	0.64	3.51	1.25
P_{neg}, kW	1.06	0.012	0.1	0.04	0.04	0.04	0.82
P_{neg}/ P_{pos}, %	13.23	1.21	10.64	5.9	6.25	1	66

Observing analytical results one of advantages of integrating industrial robots within common DC system is verified presenting reused braking energy utilization in range between 1.2% and 10.6% depending on programmed robot motions and tasks. All technology loads have been analyzed as group and also 1% of negative energy flow has been detected that can be explained by significant internal capacitance of welding technology converter. Main electrolytic capacitor bank buffer power flow yield to 66% ratio of supplied average power flow with respect to stored power flow and can be explained by internal losses of assembled unit. Analysis of combination of 4 technology load units, 4 industrial robots and capacitor buffer as common DC load group ratio of reused power flow with respect to fundamental consumptions power flow is 13.2%.
Another aspect of verification of experimental results has been presented in Fig. 6. Assuming that sum of all 11 DC bus end user elements (4 robots, 4 loads, 3 storages, buffer and PV) power flow should be a close match of one infeed power flow value DC respective difference has been calculated as value SumDC. Deviation of average value of SumDC over period is 180W. Higher deviation can be observed during rapid power flow change at welding process. It has to be noted that SumDC represent both internal DC bus conductor rail losses and measurement errors. Obtained value support confidence of experimental measurement dataset of 13 power flow locations. More in-depth analysis of measurement system dynamic response, particularly current sensor behavior at high current rate of rise is foreseen as future activity.

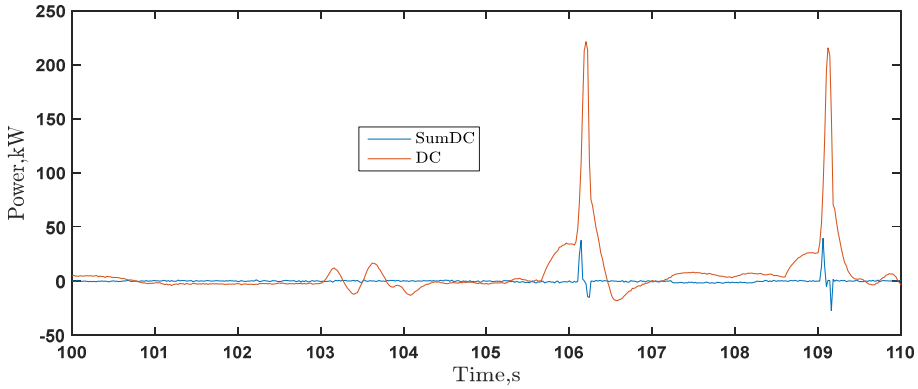

Fig. 6: Comparison of analytical calculation of DC bus component power balance: *SumDC* and measurement of main supply converter DC side power flow: *DC*.

Obtained results allow further analysis of such concepts like power peak shaving since welding process impose dynamic consumption on AC grid side. Also dimensioning of internal storage capacity considering accumulation of renewable energy during weekends or bridging of possible grid outages can be done based on experimental data.

Conclusion

Power flow measurement results covering industrial scale DC microgrid has been obtained in synchronized manner and based on real production equipment operation use case. Such data serve as

important basis for validation of simulation models of both component and system levels. Application of experimentally verified electrical component models regarding dynamic power consumption is considered as one of key advantages for design of energy efficient manufacturing installations. Presented results support expected energy efficiency advantages of interconnecting electrical loads with regenerative energy potential within common DC grid. Further activities are foreseen towards analytical dimensioning of central AC/DC power supply converter regarding planned load group within DC microgrid supply area. Since demand for individual welding tool peak power and production cycle average power present large difference new approaches of intermediate energy storage with dynamic response are scope of further research. Also optimal distribution of capacitance within system is interesting topic and will be analyzed in order to reduce unnecessary energy exchange between loads during operation. All aforementioned topics has been considered during initial design phase of DC infrastructure but more detailed analysis covering all DC microgrid can be pursued with assistance of power flow measurement system introduced in this paper.

References

[1] Directive 2012/27/EU of the European Parliament and of the Council on energy efficiency. [Online]. Available: http://eur-lex.europa.eu/legal-content/EN/TXT/PDF/?uri=CELEX:32012L0027&from=EN. [Accessed: 18-Dec-2016].

[2] De Doncker R. W.: Power electronic technologies for flexible DC distribution grids, 2014 International Power Electronics Conference (IPEC-Hiroshima 2014 - ECCE ASIA), 2014, pp. 736–743.

[3] German Standartization Roadmap, Low Voltage DC Version 1. [Online]. Available: https://www.dke.de/resource/blob/778168/23cb82850b1c37070f3ebc5526770646/german-standardization-roadmap-low-voltage-dc-version-1-data.pdf. [Accessed: 18-Dec-2016].

[4] M. Pellicciari M. Avotins A. Bengtsson K. Berselli G. Bey N Lennartson B. Meike D.: AREUS - Innovative hardware and software for sustainable industrial robotics, 2015 IEEE International Conference on Automation Science and Engineering (CASE), 2015, pp. 1325–1332.

[5] Meike D. Pellicciari M. Berselli G.: Energy Efficient Use of Multirobot Production Lines in the Automotive Industry: Detailed System Modeling and Optimization, IEEE Transactions of Automation Science and Engineering, vol. 11, no. 3, pp. 798–809, 2014.

[6] Hansen J.F. Wendt F.: History and State of the Art in Commercial Electric Ship Propulsion, Integrated Power Systems, and Future Trends, Proc. IEEE, vol. 103, no. 12, pp. 2229–2242, Dec. 2015.

[7] Meckler P. Gerdinand F. Weiss R. Boeke U. Mauder A.: Hybrid switches in protective devices for low-voltage DC grids at commercial used buildings, ICEC 2014; The 27th International Conference on Electrical Contacts; Proceedings of, 2014, pp. 1–6.

[8] Hauf D Lebrecht M. Meike D.: Verfahren zum Betreiben einer Mehrzahl von Robotern einer Produktionsanlage, DE 10 2015 012 111 A1 2016.03.31.

[9] Apse-Apsitis P. Avotins A. Ribickis L.:A different approach to electrical energy consumption monitoring, 2014 16th European Conference on Power Electronics and Applications, 2014, pp. 1–5.

Appendix 6

Paugurs, A., **Šenfelds, A**., Ribickis, L. Impact of Industrial Robot Tool Mass on Regenerative Energy. In: *Proceedings of 19th European Conference on Power Electronics and Applications, EPE'17 ECCE Europe*, Poland, Warsaw, 11-14 September, 2017. Piscataway: IEEE, 2017, pp.1-6. ISBN 978-1-5386-0530-1. e-ISBN 978-90-75815-27-6.

doi:10.23919/EPE17ECCEEurope.2017.8099185

Impact of Industrial Robot Tool Mass on Regenerative Energy

Arturs Paugurs, Armands Senfelds, Leonids Ribickis
RIGA TECHNICAL UNIVERSITY
INSTITUTE OF INDUSTRIAL ELECTRONICS AND ELECTRICAL ENGINEERING
Azenes street 12/1
Riga, Latvia
+371 67089919
ieei@rtu.lv
http://ieei.rtu.lv/

Acknowledgments

This research is supported by Latvian National Research Programme project LATENERGI.

Keywords

«Regenerative power», «Robotics», «Industrial application»

Abstract

Recent research has shown great potential in energy efficiency optimization by harvesting regenerative energy of industrial robots. This paper presents further insight into how dependent regenerative energy is on the mass of the robot tool, as well as how the total regenerative energy is distributed between various robot links.

Introduction

Industrial robotics is one of the key factors for high productivity rates in today's automotive industry, thus having a significant impact on the total electrical energy consumption of the whole factory. An average high payload robot consumes 5.2 MWh annually only during the movement process [1]. Regenerative energy, which occurs due to rapid deceleration of the robot, can sum up to 20% of the abovementioned consumption energy (depending on the robot trajectory and movement parameters). In the state of the art robotic systems the regenerative energy is dissipated on braking resistors [2], which seems to be an outdated method, considering the possibilities of energy storage systems combined with bidirectional power converters, of which both have been researched and improved greatly in the recent years, driving the cost per kWh down and the efficiency up.

Several methods have been discussed and tested on harvesting the regenerative braking energy, thus increasing the overall energy efficiency of robotized production systems. These methods include the use of supercapacitor and battery energy storage systems, implementation of a DC supply microgrid and topology modifications of the robot's power supply unit [3]–[7]. However, not only hardware modifications could lead to improved energy efficiency, various software solutions have also been suggested where the robot movement trajectories and acceleration, deceleration patterns are recalculated as functions of energy consumption. These algorithms demonstrate an improvement in energy efficiency of robotic systems by up to 40% for specific robot cycle programs [8]–[10].

This study presents a better understanding on how the regenerative energy is distributed between robot joints and how dependent is its total amount on the mass of the robot tool.

Experimental Setup

Main components of the particular experimental setup are an industrial robot KUKA KR210, SIEMENS active frontend unit (AC/DC converter, 55 kW, 600 VDC output), DC power measurement device and a specific robot tool with variable mass.

To evaluate the impact of the robot tool mass on the total regenerative energy, a specific robot tool was designed with stackable iron blocks each having approximately 21 kg of mass. The maximum payload of the robot is 210 kg. Five experiments were logged with the following set points in load mass: 0 kg, 56 kg, 98 kg, 162 kg and 205 kg. KR210 has six links by default (A1..A6). Link numeration starts at the base of the robot and ends at the tool fixation plate, thus the variable load is attached to A6. A stack of seven blocks attached to the sixth link of the robot is depicted in Fig. 1, being the fourth set point of 162 kg.

Experimental data is obtained by electrical measurements of KUKA KR210 industrial robot's active infeed power whilst operating a specific robot movement program at maximum velocity. The program is designed to rotate each motor individually close to its angular limitations, a one second pause between each rotation is included for clear data separation at post-processing stage. Such program allows analyzing the impact of each robot link on the overall regenerative energy. Data post-processing was carried out in Matlab R2015a.

Excess energy occurs during rapid deceleration due to large kinetic energy and inertia. At such point the voltage of the conventional AC/AC power supply's DC bus increases and if it surpasses the value of the rectified AC supply voltage, a braking resistor is connected [1]. In this setup the robot's power supply is modified, excluding the built-in rectifier and the braking resistor and leaving the DC bus as the main power infeed point. The DC bus is then supplied externally from a stable 600V DC microgrid, which is generated by the SIEMENS active frontend unit, Fig. 2. In this way the excess, regenerative energy is fed back directly to the supply grid.

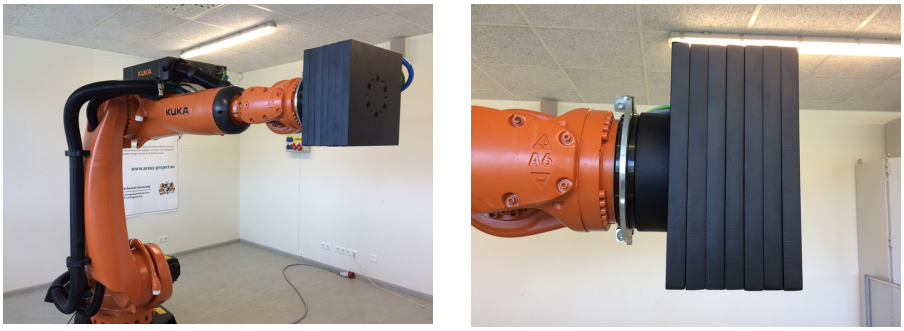

(a) (b)

Fig. 1. Whole industrial robot arm with load (a); variable load (b).

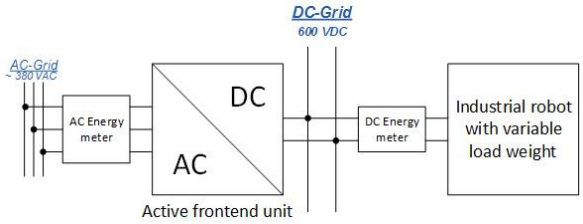

Fig. 2. Principal electrical schematic of the experimental setup.

Power Cycle Measurements

A power measurement of a single full cycle at two different load set points (0 kg and 205 kg) is depicted in Fig. 3. The dashed lines parallel to the Y-axis represent the beginning and the end of each motor's individual movement. For example, at t = 2 s, the largest motor located at the base of the robot (joint A1) starts rotating the robot arm from 0 to +120 angular degrees at maximum velocity. During the motion, only the motor of joint A1 is rotating. The positive power peak represents the maximum power demand due to acceleration, whilst the following negative power peak represents the regenerative power occurring due to rapid deceleration. When the 120 angular degree position is reached, the robot program reverses the motion and rotates the A1 joint from +120 to -120 angular degrees at maximum velocity (t ε [3.7; 6.3] s). Lastly, a third motion from -120 angular degrees to 0 degrees finishes the rotation of joint A1, bringing it to the home position where the motion began. In such manner each following joint (A2, A3, A4, A5 and A6) is individually rotated and its power demand and regeneration is measured and logged.

Comparison of the two power graphs in Fig. 3 shows that the larger mass of the tool significantly increases the consumed and regenerated power peaks of joints A1, A2 and A3, however, the opposite can be said about the regenerative power peaks of the smaller joints A4, A5 and A6, because the larger mass dampens the dynamics of their rotation, increasing the cycle execution time and decreasing the deceleration rate of these joints which leads to lower regenerative power peaks when comparing with the no-load (0 kg) measurement. The larger tool mass also stabilizes the consumption power profile of the smaller links (A4-A6). Motors of joints A1 and A2 have the highest power rating and their dynamics and cycle execution times are therefore less affected by the increase of mass of the tool.

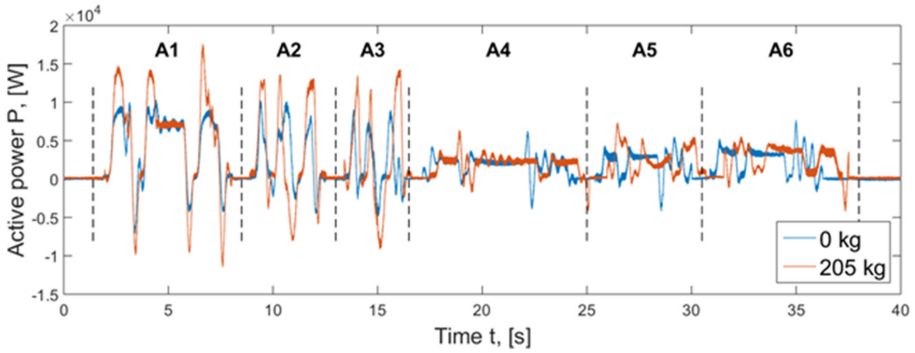

Fig. 3. Comparison of a full cycle power measurement at 0 kg and 205 kg load mass.

Energy Calculation and Analysis

The consumed and regenerated energies are calculated as integrals of measured electrical power graphs throughout the whole cycle (Eq. 1-2). The resulting data are presented in Fig. 4 for all tool mass set points. Intuitively, the total consumed and regenerated energies of the whole cycle increase with the tool mass, however, not with the same proportional coefficient. The rate of change for regenerative energy as a function of tool mass is higher than the rate of change for consumed energy, meaning that the relative regenerative energy (Eq. 3, Fig. 5) increases as well. In other words, the increase of the tool mass causes the regenerative energy to increase with a greater rate than the consumption energy. While the increase of tool mass from no load to 205 kg causes an increase in consumption energy by 23.00%, the regenerative energy increases by 94.60%.

$$E_{consumption} = \int_0^t Pdt; P \in [0;+\infty) \tag{1}$$

$$E_{recuperation} = \int_0^t Pdt; P \in (-\infty;0) \tag{2}$$

$$\varepsilon_{rec} = \frac{E_{recuperation}}{E_{consumption}} * 100\% \tag{3}$$

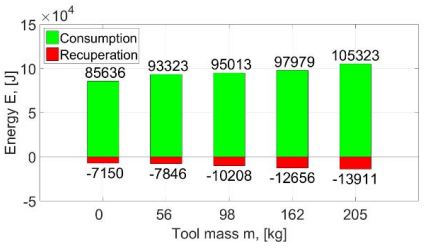

Fig. 4. Consumed and regenerated energy comparison in a single full cycle at different tool masses.

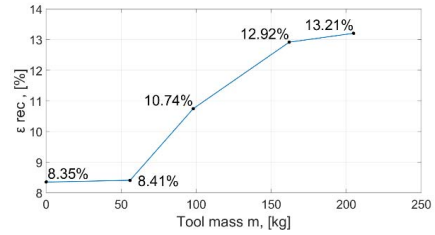

Fig. 5. Percentage of regenerative versus consumed energy as a function of the robot tool mass.

Each robot link's regenerative energy is analyzed by calculating its impact on the full cycle's regenerative energy (Eq. 5). To achieve this, the regenerative energy of each link is calculated separately in each respective time frame when the link is operating (Eq. 4). Time frames are depicted in Fig. 3 with the dashed lines parallel to y-axis.

Fig. 6 depicts the total regenerative energy distribution between each individual link throughout the whole cycle at different tool masses. The first three robot links (A1, A2 and A3) account for 80% to 91% of the full cycle's total regenerative energy, increasing their part proportionally with the tool mass. Vice versa occurs with the smaller, last three robot links (A4, A5 and A6). As the mass of the tool increases, these links account for a linearly decreasing part of the cycle's total regenerative energy – 20% to 9% - which is due to decreasing deceleration rate of links A4, A5 and A6 with increase of the tool mass.

$$E_{recA*} = \int_0^{A*} Pdt; P \in (-\infty;0) \tag{4}$$

$$\varepsilon_{recA*} = \frac{E_{recA*}}{E_{recuperation}} * 100\% \tag{5}$$

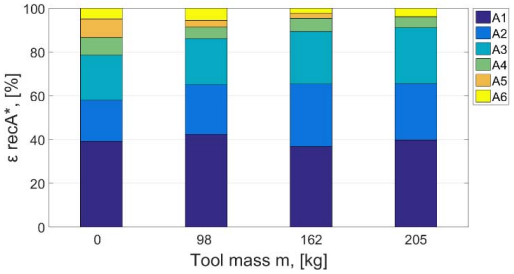

Fig. 6. Regenerative energy distribution between robot links at different robot tool masses.

Economical Aspects

While research and development towards a greener, more energy efficient manufacturing is mandatory, real hardware implementation in large scale manufacturing takes place only when the proposed solution is also economically viable (positive return on investment in a time period which is less than the amortization period of the installed system).

In the case of industrial robotics the calculation of the time period it would take for the return on investment to be positive largely depends on the robot's work cycle (thus, varying the power profile), work intensity (cycles per day), the total number of operating robots in the factory and the investment cost (hardware, installation costs) (Eq. 6).

$$t_{yrs} = \frac{HW_{cost}}{\sum_{k=1}^{k=Rcount} E_{rec(k)} * n_k * \eta_{HW} * e_{electricity}} \tag{6}$$

where:
t_{yrs} – the time period it takes for the investment to return (ROI = 0, in years).
HW_{cost} – the cost of the investment, for example, cost of the active frontend unit.
$E_{rec(k)}$ – the regenerative energy of a particular robot in a single robot cycle (in kWh).
n_k – the number of robot cycles in a year.
η_{HW} – efficiency of the hardware setup necessary for harvesting regenerative energy.
$e_{electricity}$ – the price of electrical energy per kWh.
R_{count} – the number of robots operating in the factory.

To obtain an optimal solution, the investment cost should be divided amongst as many industrial robots as possible. Article [11] addresses a similar issue of power dimensioning an active frontend unit in respect to the power profiles of various industrial robot cycles.

In order to effectively predict the economic aspects of integrating regenerative energy harvesting systems in robotized factories, time-related power profile analysis have to be performed, predicting the energy consumption levels at every given point during the production cycle. Such software planning solutions are proposed in [1].

Conclusion

An industrial robot KUKA KR210 with a modified power supply to enable the re-use of regenerative energy has been studied to better understand the distribution of the regenerative energy between various robot motors. A specific tool with variable masses has been designed to test the impact of the tool mass on the total regenerative energy.

An increase in the mass of the tool increases both the consumption and the regenerative energy, however, the regenerative energy increases with a higher rate in comparison to the consumption energy increase rate. The regenerative energy is 94.6% higher with a 205 kg tool when comparing to a no-load measurement (0 kg tool), whilst the consumption energy increases by 23% when comparing the same load set points.

Regarding the distribution of regenerative energy between various robot links, 80% to 91% of the whole cycle's regenerative energy, is caused by the braking of the first three motors (A1, A2 and A3) due to near-constant deceleration profile and higher motor power ratings. Last thee robot links (A4, A5 and A6) account for the remaining 20% to 9% of the total cycle's regenerative energy. Their impact on the total regenerative energy decreases due to lower deceleration rates caused by the increase of the tool mass.

In order to sufficiently plan the economic aspects of implementing regenerative energy harvesting systems in robotized factories, time-related power profile analysis have to be realized beforehand

for all robotized work cells. The potential economic benefits of such energy harvesting systems are highly dependent on the robot's work cycle, work intensity (cycles per day) and the total number of robots in the factory.

References

[1] D. Meike, "Increasing Energy Efficiency of Robotized Production Systems in Automobile Manufacturing," Riga Technical university, 2013.

[2] D. Meike and L. Ribickis, "Recuperated energy savings potential and approaches in industrial robotics," in *Automation Science and Engineering (CASE), 2011 IEEE Conference on*, 2011, pp. 299–303.

[3] M. Pellicciari, A. Avotins, K. Bengtsson, G. Berselli, N. Bey, B. Lennartson, and D. Meike, "AREUS - Innovative Hardware and Software for Sustainable Industrial Robotics," in *2015 IEEE International Conference on Automation Science and Engineering (CASE)*, 2015, pp. 1325–1332.

[4] K. Vitols, "Design considerations of a battery pack - DC grid interface converter," in *2015 IEEE 5th International Conference on Power Engineering, Energy and Electrical Drives (POWERENG)*, 2015, pp. 476–479.

[5] A. Senfelds, A. Avotins, L. Ribickis, and D. Meike, "Research and Demonstration of New DC Power Supply Concepts for EU Factories of Future at RTU," *Mater. Process. Technol. Riga Tech. Univ. Res.*, vol. 3, pp. 34–37, 2015.

[6] M. Vorobyov, "Research of power electronics converters for supercapacitor storage devices used in industrial systems," in *2015 IEEE 5th International Conference on Power Engineering, Energy and Electrical Drives (POWERENG)*, 2015, pp. 596–599.

[7] A. Senfelds, M. Vorobjovs, D. Meike, and O. Bormanis, "Power smoothing approach within industrial DC microgrid with supercapacitor storage for robotic manufacturing application," in *Automation Science and Engineering (CASE), 2015 IEEE International Conference on*, 2015, pp. 1333–1338.

[8] A. Fenucci, M. Indri, and F. Romanelli, "An off-line robot motion planning approach for the reduction of the energy consumption," in *2016 IEEE 21st International Conference on Emerging Technologies and Factory Automation (ETFA)*, 2016, pp. 1–8.

[9] M. Mahdavian, M. Shariat-Panahi, A. Yousefi-Koma, and A. Ghasemi-Toudeshki, "Optimal trajectory generation for energy consumption minimization and moving obstacle avoidance of a 4DOF robot arm," in *2015 3rd RSI International Conference on Robotics and Mechatronics (ICROM)*, 2015, pp. 353–358.

[10] A. Vergnano, C. Thorstensson, B. Lennartson, P. Falkman, M. Pellicciari, F. Leali, and S. Biller, "Modeling and Optimization of Energy Consumption in Cooperative Multi-Robot Systems," *IEEE Trans. Autom. Sci. Eng.*, vol. 9, no. 2, pp. 423–428, Apr. 2012.

[11] A. Senfelds, O. Bormanis, and A. Paugurs, "Analytical approach for industrial microgrid infeed peak power dimensioning," in *2016 57th International Scientific Conference on Power and Electrical Engineering of Riga Technical University (RTUCON)*, 2016, pp. 1–4.

Appendix 7

Grēbers, R., Gadaleta, M., Paugurs, A., **Šenfelds, A**., Avotiņš, A., Pellicciari, M. Analysis of the Energy Consumption of a Novel DC Power Supplied Industrial Robot. *Procedia Manufacturing*, 2017, Vol.11, pp.311-318. ISSN 2351-9789.

DOI:10.1016/j.promfg.2017.07.111

Available online at www.sciencedirect.com

ScienceDirect

Procedia Manufacturing 11 (2017) 311 – 318

Procedia MANUFACTURING

27th International Conference on Flexible Automation and Intelligent Manufacturing, FAIM2017, 27-30 June 2017, Modena, Italy

Analysis of the energy consumption of a novel DC power supplied industrial robot

Ritvars Grebers[a], Michele Gadaleta[b]*, Arturs Paugurs[a], Armands Senfelds[a], Ansis Avotins[a], Marcello Pellicciari[b]

[a] *Institute of Industrial Electronics and Electrical engineering Riga Technical University*
[b] *Department of Engineering "Enzo Ferrari", University of Modena and Reggio Emilia, Via Vivarelli 10, 41125 Modena Italy*

Abstract

The energy consumption and electrical characteristics of a novel direct current (DC) power supplied industrial robot prototype are compared and analyzed with a state of the art alternating current (AC) supplied industrial robot. An extensive set of experiments shows an important reduction of the total energy consumption for different electrical power profiles measured in various robot trajectories with specific working temperatures. The recuperated energy is also analyzed in the different scenarios. Experimental results show that a DC type robot can be up to 12.5% more energy-efficient than an equivalent AC type robot.

Peer-review under responsibility of the scientific committee of the 27th International Conference on Flexible Automation and Intelligent Manufacturing

Keywords: sustainable manufacturing; AC/DC micro-grids; energy efficient robotics, energy measurements; energy consumption.

1. Introduction

Industry 4.0 leverages digitalization, artificial intelligence and robotics to realize intelligent manufacturing systems and processes. An underestimated drawback of the Industry 4.0 extensive use of industrial robotics and Cyber Physical Production Systems (CPPS) is related with the inevitable drastic rise of the total Energy

* Corresponding author. Tel.: +39-0592056278; fax: +39-0592056129.
E-mail address: michele.gadaleta@unimore.it

Peer-review under responsibility of the scientific committee of the 27th International Conference on Flexible Automation and Intelligent Manufacturing
doi:10.1016/j.promfg.2017.07.111

Consumption (EC), which risks to compromise the overall sustainability of the factories of the future. Then, there is a strong need of engineering methods and technologies able to improve the energy efficiency of industrial robots. To this purpose, the AREUS project [1], a European Commission funded research project, developed a novel generation of energy-efficient direct current (DC) supplied robots to overcome current industrial robots energetic limitations and to leverage the exchange, storage and recovery of energy at factory level. In fact, since industrial robots and mechatronic machinery operate on DC, a rectification power conversion stage is necessary with the state of the art alternating current (AC) supply grid, with a consequent loss of energy. For example, state of the art robots actuators are permanent magnet synchronous motors (PMSM). PMSM are controlled by separate servo inverters that are supplied by a common rectifier using a coupled DC-bus [2]. This means that internally, the system is DC supplied already. By using a DC power grid, the rectification stage at AC mains could be eliminated in many applications, thus saving the energy of the power conversion losses. Furthermore, also renewable energy sources operate in DC, then, the adoption of a DC supplied sub-grid would avoid further conversion stages, with the related costs, energy losses and energy quality problem.

DC systems and DC power grids have been extensively discussed in literature, DC sub-grids improve sustainability and energy efficiency by reducing material usage and weight [3], regenerating and recuperating energy and easing the optimization of trajectories and position accuracy for industrial applications [4]. In fact, one of the DC sub-grids main advantage is the capability to recuperate and regenerate energy efficiently, enabling bidirectional DC power flow, as well described with the motor drive system developed in [5], in which the system replicates the dynamics of industrial robot power flow. Furthermore, a DC grid may harvest and store all the recuperated energy, as demonstrated in [6] by using supercapacitor storage and power smoothing. All of these previous works found in literature confirm the systems energy efficiency improvements achievable with DC sub-grids, ideal to recuperate energy from the actuators with regenerative approaches, while in AC systems such recuperation would be harder and more expensive, often with important losses of the AC network quality [7].

Then, the novel DC supplied robots developed with the AREUS project (www.areus-project.eu) may enable DC industrial smart grids, with full regenerative bidirectional DC power flow and seamless integration of renewable energy sources. This paper presents the energy efficiency experimental assessment of a DC supplied KUKA Quantec KR210 R2700 prime DC supplied prototype robot, and the performance are compared with the ones achievable by the same model AC supplied.

The paper is organized as follows: in section 2 the experimental setup is presented, in section 3 the measurement and data acquisition process are described and in section 4 the experimental results are compared and analyzed.

2. Experimental testing setup

Two industrial 6-axes robots, KUKA Quantec KR210 R2700 prime [8], have been tested in different conditions to measure their energy consumption and trajectories power profile. Both robots are identical, excepting for the power supply system. Each robot weights 1100 kg, has a payload up to 210 kg, and a maximum power rating of 22 kW [8, 9]. In the state of the art AC robot version, a single rectifier creates a common DC-bus from which six inverters draw the energy for the motors (Fig. 1), while in the AREUS project robot prototype the rectifier is removed, allowing the direct connection of the internal DC-bus to a prototype factory DC-grid, (Fig. 2). The DC prototype robot, is supplied by an experimental 600 V DC power grid generated by a 55 kW active frond-end unit (AC/DC converter), developed by Riga Technical University [10].

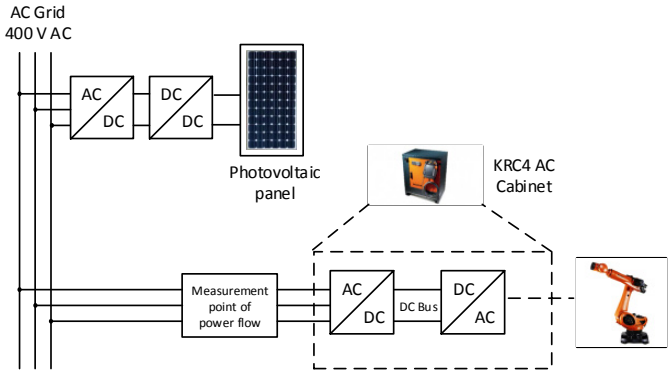

Fig. 1: Example of the state of the art AC supplied industrial robot system

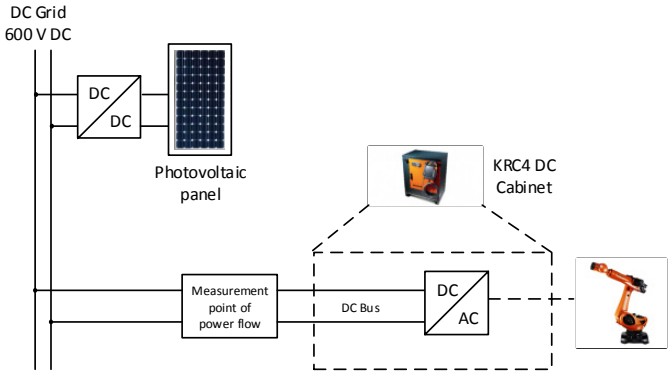

Fig. 2: Example of the DC supplied industrial robot system

3. Methodology

3.1. Measurement setup

During the experiments, the two robots have run the same code, following a trajectory designed to simulate typical motions on a production line. Power consumption curves were logged at different velocities (40%, 60%, 80% and 100% of the maximum velocity) to determine its influence. Furthermore, two different temperature conditions have been considered, called “warm” and “cold”, where the “warm” has a five hours warm-up phase before the measurements in order to emulate the real working conditions and to differentiate the power profiles from different friction losses, while “cold” is the robot working after a brief transient. 80 measurements have been acquired: 5 repetitions for each velocity percentage at both temperature condition.

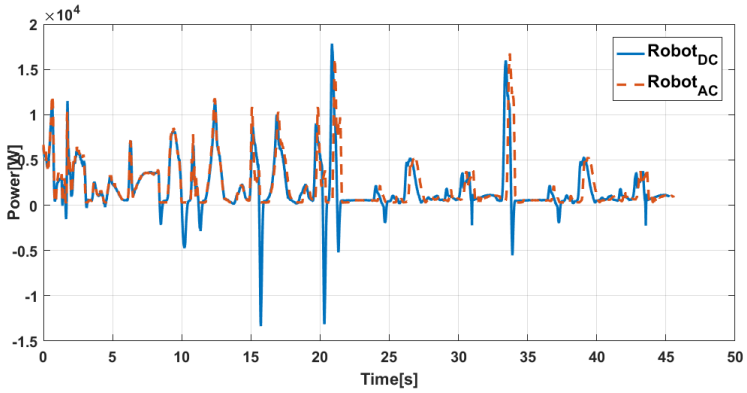

Fig. 3. Test cycle power profiles (W) at 100% execution velocity of the AC (dotted) and DC (line) robots.

3.2. DC/AC energy flow measurement

In both the DC and AC supplied robots, the overall energy consumption can be assessed directly measuring the electrical power flowing into the cabinets. In the AC version, the electrical power can only flow into (positive) the robot cabinet since the energy recuperated during brakes is mainly dissipated into an internal resistor. In the DC version instead, the power can also flow out (negative) from the cabinet to the DC grid allowing for direct measurements of the recuperated braking energy. Such regenerative approaches, extended to the whole cell or plant, may lead to important energy and CO2 emission reduction, as well as contribute to new sustainability assessment methods [11].

In literature are found different approaches to monitor the electrical energy consumption [12]. In this study an AC/DC InLine Bi-direct Energy sensor has been used for data acquisition. This device has been specifically designed to measure instantaneous power values in both consumption and recuperation modes with high accuracy. In previous studies [13], such AC/DC InLine Bi-Direct Energy sensor provided very fast, precise and stable measurements: compared with an expensive calibrated power analyzer (Newtons N4L), the power measurements of over 1kW experienced a deviation under 5%. A single energy sensor module has three current transducers and is capable of measuring a 3-phase 400 V AC grid and a 600 V DC grid [14].

3.3. Data acquisition and analysis

The experimental data have been analyzed, comparing AC cold robot with DC cold robot, AC warm with DC warm, AC cold with AC warm and DC cold with DC warm.

The data analysis has focused on:

- Efficiency of the DC robot in both cold and warm states comparing with the AC robot,
- Energy consumption at different velocities,
- Energy recuperation at different velocities,
- Recuperated energy difference between cold and warm DC robot,
- DC robot energy consumption in both states: cold and warm,
- AC robot energy consumption in both states: cold and warm.

As explained, the AC robot recuperative energy cannot be measured by the Bi-direct energy sensor [15], because such energy is not fed back to the AC grid but internally dissipated in the braking resistors and partly stored in the robot cabinet internal capacitors.

4. Power consumption analysis

4.1. AC/DC robot energy consumption

Analyzing the acquired power profiles of AC and DC robots, some little differences can be noted (e.g. Fig. 3), especially in the power peaks. The cause of such differences can be related with the unavoidable mechanical and electrical construction tolerances between the two robots. The power differences are more accentuated at higher velocity while the curves tend to overlap in the lower ones.

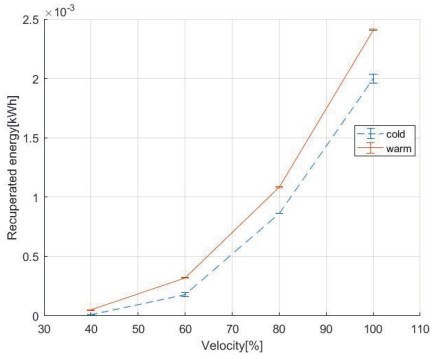

Fig. 4. Recuperated energy of the DC robot at different velocities ("cold" and "warm" state).

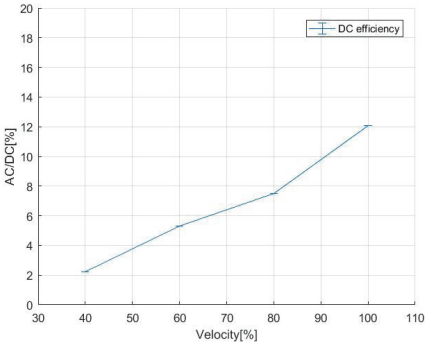

Fig. 5. Energy savings of the DC robot compared to the AC robot ("warm" state).

The energy savings have been evaluated comparing the energy consumption of the AC and DC robot performing the same trajectory at different velocities using (1), the results are presented in Fig. 4.

$$\eta\ [\%] = (1 - \frac{E_{DC}}{E_{AC}}) * 100 \quad \textbf{(1)}$$

In the Fig. 5 it is possible to see that at 40% of velocity the DC robot consumes 2,24% less energy than the AC robot, while at maximum velocity the difference is 12,52%. The increased efficiency in DC robots is due to the capability to recuperate the braking energy, sending it back to the network instead of dissipating. The higher the velocity, the higher the recuperated energy.

4.2. DC robot energy consumption in warm and cold state

An important objective of this study is the evaluation of the DC robot energy consumption by measuring with the Bi-direct energy sensor the energy flow recuperated back to the grid.

Looking at Fig. 4, experimental results show that increasing robot velocity increases the recuperated energy even more if the robot is warm. This effect is reasonably expected due to the reduction of the viscous friction losses in the robot reducers. The most efficient robot execution velocity has been measured around 80% of the full speed. At this speed, DC warm robot is almost 15% more efficient (less consuming) than cold robot. At the maximum velocity, such difference decreases to 12%, as shown in Fig. 6. Efficiency has been calculated using the equation (2). Fig. 4

shows that at 100% velocity warm robot recuperates about 0,002405 kWh per cycle, that is 9% of the total energy consumption, but in case of cold robot it is approximately 7% of the total energy consumption.

$$\eta\,[\%] = (1 - \frac{E_{DC_{cold}}}{E_{DC_{warm}}}) * 100 \tag{2}$$

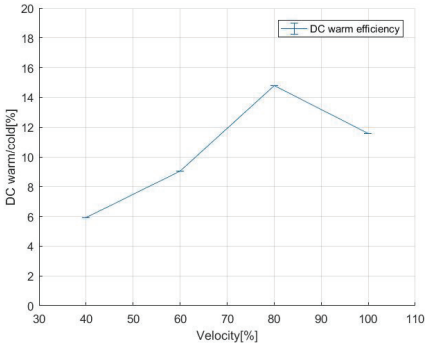

Fig. 6. Energy savings of the DC robot in the warm state compared to the cold state.

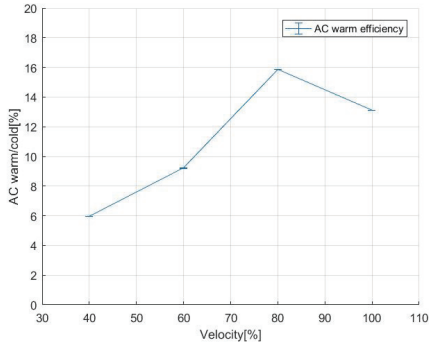

Fig. 7. Energy savings of the AC robot in the warm state compared to the cold state.

4.3. AC robot energy consumption in warm and cold state

As expected, the AC robot energy savings in the warm state (Fig. 7) are very similar to the DC robot ones since the mechanical and electrical systems are ideally identical, excepting for some differences due to inevitable manufacturing tolerances. Warm robot reaches the maximum efficiency at execution velocity of 80% . At this speed warm robot is about 16% more efficient than cold robot, at 100% of execution velocity percentage drops to 13%.

4.4. Measurement relative error analyzes

As it can be seen in figures 4-7, the measurements relative errors are on average under 1%, then the difference between the samples is negligible. Few measurements resulted less accurate, probably for the small scale of the acquired data. The maximum relative error of 8.33% has been obtained in the measurements of the DC robot recuperated energy, at 40% of velocity and in cold state. At the maximum velocity, the relative error is 1.88%. The main cause of such errors can be attributed to the Bi-direct energy flow sensor, which is not suitable to measure precisely low energy levels (less than ~100 watts). In warm state the relative error is smaller, from 3,37% to 0,17% with velocities from 40% to 100%.

Relative error has been calculated with the following method: firstly, it has been calculated an average of the sample measurements (3), such average has been used to calculate the absolute error (4), which is then multiplied by student's t-distribution coefficient (5) to get the systematic error (6). Finally, the systematic error has been divided by the average, obtaining the relative error (7). For indirect measurements equation (8) has been used.

$$x_{vid} = \frac{1}{n}\sum_{i=1}^{n} x_i \quad (3)$$

$x_{vid} - average\ of\ sample\ measurements$

$x_i - sample\ measurement$

$$S_x = \sqrt{\frac{\sum_{i=1}^{n}(x_i - x_{vid})^2}{n(n-1)}} \quad (4)$$

$S_x - Aboslute\ error$

$$t_\beta(n) = 2{,}78$$

$t_\beta(n)$-student's t-distribution coefficient

$$\Delta x_s = s_x t_\beta(n) \quad (6)$$

$x_s - systematic\ error$

$$\varepsilon = \frac{\Delta x}{x_{vid}} * 100\% \quad (7)$$

$\varepsilon - relative\ error$

$$\Delta y = \sqrt{(\Delta y_1)^2 + (\Delta y_2)^2 + \ldots + (\Delta y_3)^2} \quad (8)$$

$y - indirect\ measurements$

5. Conclusions

The energy consumption and regenerative characteristics of a novel DC power supplied KUKA Quantec KR210 R2700 prime prototype industrial robot have been measured and compared with the state of the art AC supplied KUKA Quantec KR210 R2700 prime industrial robot. The tests have been performed with various robot trajectories and different working temperatures. The results confirm that the DC energy supply is more efficient up to 12,52%. As expected, the best results have been achieved in the more demanding application cases whit the robots running at maximum velocity. The DC power supplied robots developed in the AREUS project confirm to be reliable and cost efficient, then can enable a full DC Factory.

Further tests will be performed to better assess the performance gains and cost savings in different applications.

6. Acknowledgements

The research leading to these results has received funding from the European Community's Seventh Framework Programme under grant agreement No. 609391 (AREUS). The authors would like to thank AREUS Project partners DAIMLER AG, KUKA Roboter and SIEMENS AG.

References

[1] M. Pellicciari, A. Avotins, K. Bengtsson, B. Lennartson, G. Berselli, N. Bey, D. Meike, AREUS - Innovative hardware and software for sustainable industrial robotics, IEEE International Conference on Automation Science and Engineering, vol. 2015-October (2015)

[2] C. Hansen, J. Öltjen, D. Meike, and T. Ortmaier, Enhanced approach for energy-efficient trajectory generation of industrial robots, IEEE Int. Conf. Autom. Sci. Eng., pp. 1–7, 2012.

[3] J. Brombach, T. Schröter, A. Lücken, and D. Schulz, Optimized cabin power supply with a / 270 v DC grid on a modern aircraft, 2011 7th Int. Conf. Compat. Power Electron. CPE 2011 - Conf. Proc., pp. 425–428, 2011.

[4] M. Pellicciari, G. Berselli, F. Balugani, and M. Gadaleta, Increasing position accuracy and energy efficiency of servo-actuated mechanisms, IEEE Int. Conf. Autom. Sci. Eng., vol. 2015–Octob, pp. 1339–1344, 2015.

[5] R. A.Paugurs, A.Senfelds, Design of a Motor Drive System for Bidirectional DC Power Flow Control, RTUCON, pp. 7–10, 2015.

[6] A. Senfelds, M. Vorobjovs, D. Meike, and O. Bormanis, Power smoothing approach within industrial DC microgrid with supercapacitor storage for robotic manufacturing application, IEEE Int. Conf. Autom. Sci. Eng., vol. 2015–Octob, pp. 1333–1338, 2015.
[7] D. Meike, A. Senfelds, and L. Ribickis, Power converter for DC bus sharing to increase the energy efficiency in drive systems, IECON 2013 - 39th Annu. Conf. IEEE Ind. Electron. Soc., pp. 7199–7204, 2013.
[8] Kuka Roboter Gmbh, KR QUANTEC prime Spezifikation, 2014.
[9] Kuka Roboter Gmbh, Kr C4 Na ; Kr C4 Ck Na Operating Instructions, p. 227, 2015.
[10] A. Senfelds, O. Bormanis, and A. Paugurs, Modelling of AC / DC Power Supply Unit for DC Microgrid, pp. 5–8, 2015.
[11] T. J. Dijkman, J. M. Rödger and N. Bey, How to assess sustainability in automated manufacturing, 2015 IEEE International Conference on Automation Science and Engineering (CASE), Gothenburg, 2015, pp. 1351-1356.
[12] D. Meike and L. Ribickis, Recuperated energy savings potential and approaches in industrial robotics, IEEE Int. Conf. Autom. Sci. Eng., pp. 299–303, 2011.
[13] P. Apse-Apsitis, A. Avotins, and L. Ribickis, A different approach to electrical energy consumption monitoring, 2014 16th Eur. Conf. Power Electron. Appl., pp. 1–5, 2014.
[14] P. Apse-Apsitis, A. Senfelds, A. Avotins, A. Paugurs, and M. Prieditis, Power Measurement and Data Logger Device with High-Resolution for Industrial DC-Grid Application, Sci. J. Riga Tech. Univ. - Electr. Control Commun. Eng., vol. 9, no. 1, pp. 36–42, 2015.
[15] P. Apse-apsitis, A. Avotins, and L. Ribickis, Bidirectional DC / AC energy flow measurement, vol. 5, pp. 1–4.
[16] D. Meike, A. Senfelds, and L. Ribickis, Power converter for DC bus sharing to increase the energy efficiency in drive systems," IECON Proc. (Industrial Electron. Conf., pp. 7199–7204, 2013.

Appendix 8

Šenfelds, A., Bormanis, O., Paugurs, A. Analytical Approach for Industrial Microgrid Infeed Peak Power Dimensioning. In: 2016 57th International Scientific Conference on Power and Electrical Engineering of Riga Technical University (RTUCON 2016): Proceedings, Latvia, Riga, 13-14 October, 2016. Piscataway, NJ: IEEE, 2016, pp.328-331. ISBN 978-1-5090-3732-2. e-ISBN 978-1-5090-3731-5.

doi:10.1109/RTUCON.2016.7763140

Analytical Approach for Industrial Microgrid Infeed Peak Power Dimensioning.

Armands Senfelds, Oskars Bormanis, Arturs Paugurs
Institute of Industrial Electronics and Electrical Engineering
Riga Technical university
Riga, Latvia

***Abstract* – Method of estimating optimal power supply performance parameters with comparison of two different power measurement data analysis methods is introduced. Application of estimating optimal infeed supply converter performance parameters for industrial DC microgrid with multiple DC supplied industrial manipulators and an spot welding process has been analyzed.**

***Keywords* – Microgrids Industrial engineering Design optimization**

I. Introduction

This paper present insight into approach of existing power profile analysis approach for corresponding dimensioning of main power system interface converter equipment based on production power load data example. Fundamental analytical approach for repetitive power profiles is introduced within Section 2 followed by proposed workflow strategies applying aforementioned analysis in case of several power profile datasets in Section 3. Example application based on real production power profile data has been introduced in Section 4. Obtained analytical results are presented within Section 5.

The switch from conventional AC to DC power supply infrastructure has become an increasingly discussed topic due to several promising benefits increasing overall energy efficiency potential reduction of the amount of raw materials necessary for energy transmission such as copper and insulation materials and minimizing the power conversion stages on the overall system level as discussed by [1],[2],[3],[4]. DC supply grids also enable more energy efficient adaption of renewable energy sources, such as photovoltaic panels, and energy storage elements being batteries since generation of DC voltage is inherent behavior of such technologies [5]. An application of a DC grid based robot work cell has been discussed as example for analytical power profile research within current paper.

Design of a DC microgrid adapted for operation within existing AC type power infrastructure requires central main rectifier converter to generate DC voltage from the AC grid. It is crucial to choose an optimal solution for the rectifier unit by its performance parameters to avoid incorrect power supply dimensioning and thus inefficient exploitation. Industrial power electronic converters are designed according to maximum power requirements of the system, however, with a combination of multiple power supply technologies in a single system, such approach may prove resource wasteful. For example, in a system with multiple DC supplied industrial robots, main rectifier unit is designed to supply the combined maximum power peaks of all robots, even when such occurrence is very unlikely. According to [6],[7] industrial robots spend more time in standby than in movement, therefore, it must be considered when designing the system power supply to avoid over-dimensioning.

It is generally known that when applied with load less than 10-20% of the rated nominal output power converters represent lower efficiency therefore installing a high power main supply unit in a system where the average power significantly below the nominal power of the supply unit power losses are expected due to underutilization of installed equipment. Additionally, this occurs because with increasing the power rating of the supply converter its standby power losses increase as well and make up a larger percentage of the total energy consumption. The proposed analytical methodology can be considered as basis for optimal dimensioning of main supply converters during stage of production plant planning by application of virtual commissioning software as well since energy consumption parameters are planned to be brought into virtual production modelling software tools in near future [5], [8]–[11]. It is to be mentioned that also experimental data of existing process loads can be obtained and considered as basis for analysis in case if extension or modification of existing infrastructure is to be done. Typically energy consumption within production environment is cyclic and repetitive. With access to either measured or simulated energy consumption data assumptions regarding the main supply converter parameters can be made based on defined time cycle according to manufacturing processes.

II. Power Consumption Analysis

Power consumption analysis approach has been presented under assumption that some data about expected production equipment dynamic electrical load variation has been provided by experimental measurements or numeric simulations. The visual representation of analytical data evaluation has been presented in following Fig. 1. The data with given fixed sampling frequency f_{sample} has been obtained for respective time frame length t_{n}. Analysis of input data is based on concept

978-1-5090-3731-5/16/$31.00 ©2016 European Union

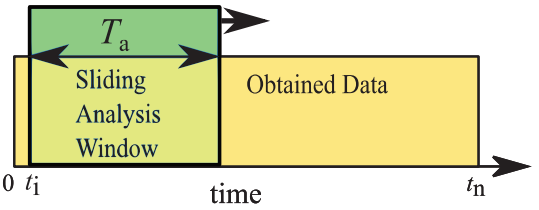

Fig. 1. Visualization of sliding analysis window approach application for power data analysis.

of sliding analysis window being shifted along whole dataset and with variable window width.

Therefore minimum and maximum sliding window size options can be defined based on following equations (1) and (2).

$$1. \qquad T_{\min} = \frac{1}{f_{sample}} \tag{1}$$

$$T_{\max} = t_n \tag{2}$$

The minimum window is defined by applied sampling frequency of data and respective distance between two neighbor values. Maximum window available for analysis is limited by total data sampling time frame. By selecting corresponding time window size T_a to be shifted along data set respective number of samples for instantaneous evaluation within analysis window can be defined according to following equation (3).

$$n = \frac{T_a}{f_{sample}},\ T_a \in [T_{\min}, T_{\max}] \tag{3}$$

Such number of values is selected for evaluation of average power P_{avg} within scope of analysis window being shifted according to number of samples i as represented by following equation (4).

$$P_{avg}(i, T_a) = \frac{1}{n} \cdot \sum_{i}^{i+n} P_i \ ,\ i \in [1, t_n - n] \tag{4}$$

The boundaries of initial position i are maintained taking into account selected analysis window sample number n in order to remain within total time frame of initial data characterized by t_n. The final analysis result for particular analysis window width being shifted along initial data is determined according to equation (5).

$$P(T_a) = \max(P_{avg}(i, T_a)) \ , \tag{5}$$

By analysis according to equations characteristic behavior of electrical load maximal instantaneous power requirement can be determined.

III. Application Strategies of Power Consumption Analysis

In case if several electrical process load data sets are available various routines of application of proposed power analysis approach can be derived. The following section present two potential workflow structure concepts based on same initial power profile data sets but different sequence of performed operations. Such routines may be introduced as post processing activities in higher layers of virtual modelling software applications thus presenting supportive information for decision making on selecting suitable electrical component ensuring local power supply functionality.

A. Parallel analysis structure concept

The visualization of the first concept is presented in Fig. 2. Such approach is based on initial application of power analysis to each available dataset and following combination of obtained analysis results for final decision making procedure. In this case combination of analysis results is performed by maintaining same time reference axis but adding all maximum power demand values for each load within fixed time window.

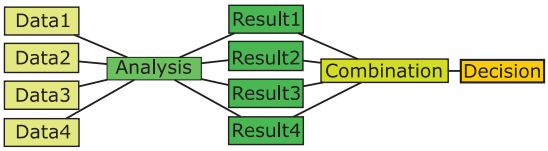

Fig. 2 Visualization of parallel power profile analysis workflow structure.

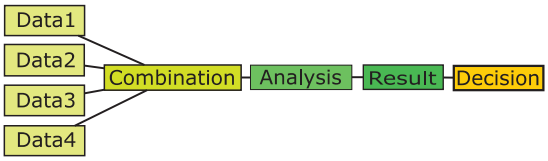

Fig. 3 Visualization of combined power profile analysis workflow structure.

B. Combined analysis structure concept

Another potential workflow structure can be introduced by initial combination of individual power profiles within single time reference maintaining exact location in time and followed analysis procedure applied to such common power profile. Analytical procedure sequence is performed as represented visually in Fig. 3.

IV. Verification on Production Process Power Data

As measure to verify intended analytical procedure set of electrical power consumption data from real production process has been obtained by means of synchronous logging of power consumption during typical manufacturing process cycle. Efforts of data acquisition during development phase of production infrastructure are of rising importance and computer based simulation models as well as functional models of typical production equipment become interesting topic. The following set of electrical loads has been selected for case example in this paper - set of 4 manipulators with

integrated electrical drives and spot welding equipment involved in manufacturing process. Total production cycle for particular process is performed within 110 second time period. Peak power of 4 manipulator devices reach level of 20kW range which is significantly lower compared to welding process electrical load reaching level of 200kW during short pulse wise pattern of 70 ms duration per each welding point instance. The manipulator with index RB4 is combined with welding equipment and during welding process maintain standby position. Other manipulators are also dedicated to production tools which present power loads of low consumption level and are therefore excluded from this analysis since would not present large influence of power analysis results. Combination of 4 manipulator loads and spot welding equipment are presented in following Fig. 4.

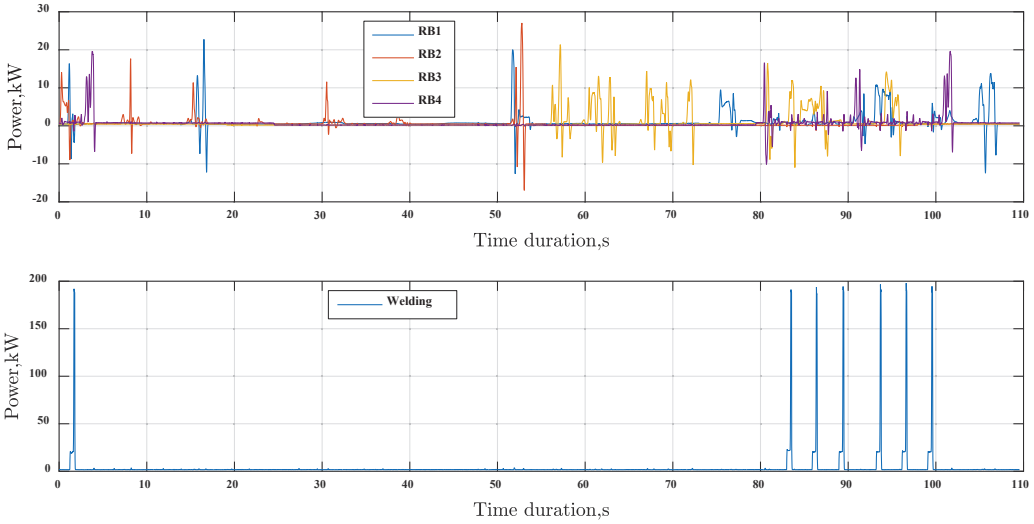

Fig. 4 Example of cyclic production cycle electrical power consumption.

V. Analytical Results

Analytical procedure has been applied on presented power consumption data according to workflows introduced in Section 3. The Fig. 5 present maximum average power analysis results of power profile data of manipulators RB1 to RB4 with highest peak power value presented by RB2 reaching 26 kW.

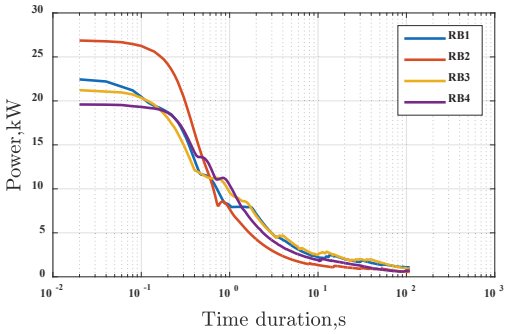

Fig. 5 Power analysis results of 4 manipulator set.

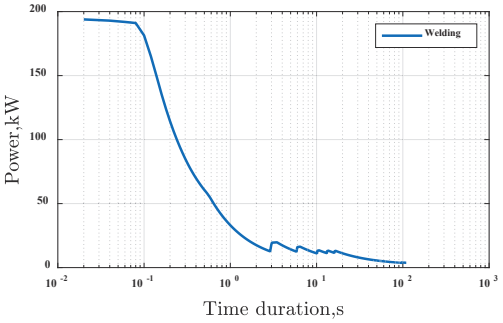

Fig. 6 Power analysis results of welding power profile.

The Fig. 6 represent same analytical procedure results applied to welding load power profile and lead to peak power value of 198 kW. Such data present material for combination of obtained analytical material by summation of peak power of all involved loads during same time window size. Along with parallel analysis structure concept also combined analysis concept structure has been applied by summation of original power profiles based on same time axis leading to total power consumption profile fed into analytical processing. The

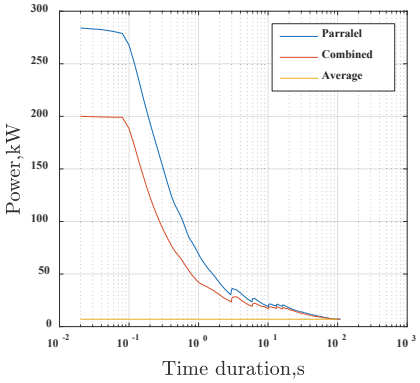

Fig. 7 Comparison of both workflow concept results.

following Fig. 7 present obtained results by both analytical results and average power consumption of 7 kW over long term operation. Difference between parallel and combined analysis present value of 80 kW comparing single values of 280 kW and 200 kW allowing to consider approach of parallel analysis leading to over dimensioning since all short term power peaks are combined. Therefore approach of combined power profile analysis would be favorable since coincidence factor of individual peak power present significant influence on system peak power dimensioning. The obtained analytical data present basis for decision making and operational strategy selection regarding power supply solutions covering whole production process including all electrical load elements and their expected operational behavior. An illustrative example of obtained analytical power curve application for main infeed power converter design is presented in Fig. 8 with respect to active frontend (AFE) being selected for full peak power capability or analytical distribution of power demand requirements between reduced nominal power equipment in combination with energy buffer solution for particular production process.

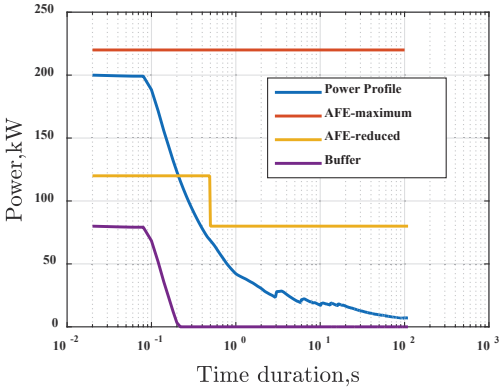

Fig. 8 Example of analytical power demand curve application for infeed dimensioning strategy development.

CONCLUSIONS

This paper introduce concept of peak power and time related analysis applied to set of industrial production process equipment electrical load data set. Analysis can be carried out according to different workflow strategies leading to results and emphasizing necessity of information about peak power coincidence during cycle time. Potential application of analytical results are presented regarding decision making procedure for suitable electrical power supply equipment intended for local production process electrical supply needs.

ACKNOWLEDGEMENTS

This research is supported by Latvian National Research Programme project LATENERGI.

REFERENCES

[1] R. Weiss, “Energy Efficient Low-Voltage DC-Grids for Commercial Buildings,” pp. 154–158, 2015.

[2] P. van Willigenburg, J. Woudstra, P. van Duijsen, B. Groenewald, and H. Stokman, “Second step to full DC-potential: DC grid efficiency for Home Owners Associations,” *2015 Int. Conf. Domest. Use Energy*, pp. 101–108, 2015.

[3] Y. Cao, B. Yang, and J. Zhuang, “Research on a novel DC / DC transformer and its control strategy for DC grid-connected renewable energy,” no. Mmc.

[4] J. Woudstra, P. van Willigenburg, B. Groenewald, H. Stokman, S. De Jonge, and S. Willems, “Direct current distribution grids and the road to its full potential,” *... Commer. Use ...*, pp. 2–7, 2013.

[5] B. Wunder, J. Kaiser, F. Fersterra, L. Ott, Y. Han, and M. März, “Energy Distribution with DC Microgrids in Commercial Buildings with Power Electronics,” pp. 425–430, 2015.

[6] D. Meike and L. Ribickis, “Recuperated energy savings potential and approaches in industrial robotics,” *IEEE Int. Conf. Autom. Sci. Eng.*, pp. 299–303, 2011.

[7] D. Meike, M. Pellicciari, and G. Berselli, “Energy Efficient Use of Multirobot Production Lines in the Automotive Industry: Detailed System Modeling and Optimization,” *Autom. Sci. Eng. IEEE Trans.*, vol. 11, no. 3, pp. 798 – 809, 2013.

[8] R. Neugebauer, F. Pürzel, A. Schreiber, and T. Riedel, “Virtual reality-aided planning for energy-autonomous factories,” *IEEE Int. Conf. Ind. Informatics*, pp. 250–254, 2011.

[9] O. Bormanis, “Development of Energy Consumption Model for Virtual Commissioning Software,” pp. 1–4.

[10] A. Vergnano, C. Thorstensson, B. Lennartson, P. Falkman, M. Pellicciari, C. Yuan, S. Biller, and F. Leali, “Embedding detailed robot energy optimization into high-level scheduling,” *2010 IEEE Int. Conf. Autom. Sci. Eng. CASE 2010*, pp. 386–392, 2010.

[11] A. Vergnano, C. Thorstensson, B. Lennartson, P. Falkman, M. Pellicciari, F. Leali, and S. Biller, “Modeling and optimization of energy consumption in cooperative multi-robot systems,” *Tase*, vol. 9, no. 2, pp. 423–428, 2012.

Armands Senfelds received B.Sc.eng. of Riga Technical University, Latvia and M.Sc of RWTH Aachen University, Germany at 2009 and 2012, respectively at field of Electrical Power engineering. He is a PhD student and researcher at Riga Technical university, Institute of Industrial electronics and Electrical engineering. His research interests include design and control of power electronic equipment, electrical drives and electrical mobility.

Oskars Bormanis received B.Sc.eng. and M.Sc.eng. in electrical engineering from Riga Technical University, Latvia in 2014 and 2015. Since 2011 he is employed by Institute of industrial electronics and electrical engineering of RTU. Main research interests include industrial robots, industrial DC grids. He is a member of IEEE Industry Applications Society.

Arturs Paugurs received B.Sc.eng. and M.Sc.eng of Riga Technical University, Latvia in the field of Electrical Engineering. Practised in Daimler AG, (Sindelfingen, Germany) in a project regarding energy efficiency optimization methods in robotic systems.He is a member of IEEE Industry Applications Society and a member of RTU Student Branch.

Appendix 9

Šenfelds, A., Bormanis, O., Paugurs, A. Modelling of AC/DC Power Supply Unit for DC Microgrid. In: *Advances in Information, Electronic and Electrical Engineering (AIEEE 2015) : Proceedings of the 2015 IEEE 3rd Workshop*, Latvia, Riga, 13-14 November, 2015. Piscataway: IEEE, 2015, pp.81-84. ISBN 978-1-5090-1202-2. e-ISBN 978-1-5090-1201-5.

doi:10.1109/AIEEE.2015.7367294

Modelling of AC/DC Power Supply Unit for DC Microgrid

Armands Senfelds, Oskars Bormanis, Arturs Paugurs
Institute of Industrial Electronics and Electrical Engineering
Riga Technical University
Riga, Latvia

***Abstract*—This paper report about modelling approach based on basic experimental measurements of bidirectional AC/DC converter. Modelling of existing AC/DC power converter has been seen in context with development of DC microgrid supply system where operational efficiency and DC side voltage stability are seen as primary tasks for individual component modelling within interconnected system.**

Keywords—AC-DC power converters Power system modeling Microgrids

I. INTRODUCTION

Alternative power supply concept evaluation of industrial manufacturing infrastructure by converting conventional alternating current (AC) based electrical energy distribution system to direct current (DC) based intelligent distribution systems is background motivation for proposed research paper. Initiative of such research and development activities is new functionality and improvement of energy efficiency for production processes as well as evaluation of technological solutions to be implemented. Physical demonstration facility of highly automated manufacturing based production process with common DC supply converter interface to conventional AC system is developed for innovative technology verification. In order to evaluate technological and economical aspects of new power supply concept it is crucial to develop various operating scenarios and hardware interaction solutions based on detailed analysis by means of numerical simulations and process modelling including technological subsystems. This research paper cover descriptive approach to existing AC/DC converter experimental measurement in order to develop functional model for further interconnected system analysis by means of simulations. Simulation models can be developed by various approaches with respect to desired complexity and specific effect examination. Detailed converter operation oriented simulation of active frontend converter has been presented by[1]. DC electrical supply system oriented modelling of converter dynamics has been presented by [2] and [3]. Detailed modelling considering internal control dynamics has been presented by [4]. Similar concept of energy exchange by conversion from AC to DC and utilization of common DC grid has been presented by[5].

II. EXPERIMENTAL TESTING SETUP

In case of new DC based production equipment supply system key element to conventional AC power grid is AC to DC power converter also known as active frontend unit. Such converter has to be verified and modelled for several aspects to assess future potential and limitations for integration into innovative power supply concept. Available electrical converter setup of 55kW nominal power is selected for detailed testing of several technical parameters and functional behavior analysis. Such equipment enables bidirectional power flow from or to typical AC power system. Important features are bidirectional power flow enabling return of excess energy into power grid which is important for integration of renewable energy resources such as photovoltaic generation. Also control of DC grid voltage is possible by application of active frontend converter. In order to create controlled testing environment for physical measurement of previously introduced AC/DC electrical power supply equipment it is necessary to add electrical load for energy consumption operation or electrical power generation in order to test regenerative energy return into AC grid infrastructure. Practical solution of such task has been realized by means of two electrical drive setup arrangements each presenting ability to consume or produce electrical power up to 22kW peak power. Such testing arrangements are built by means of two electrical motors where one of them is designed to be supplied from 600V DC grid. The designed electrical drive motor-generator setups as presented in Fig. 1 enable energy efficient testing of DC microgrid equipment up to 40kW load levels by utilization of bidirectional rectifiers of drive frequency converters FC2 and at loading drive side thus returning power generated by loading the DC side back to AC grid. Power to be consumed or produced can be varied continuously in a controlled manner enabling good testing conditions for electrical supply infrastructure testing.

III. MODELLING REFERENCE DATA EXTRACTION

In order to develop and verify simulation model of AC/DC active frontend converter it is necessary to gather information about physical behavior of equipment by means of experimental measurements. Several key parameters have been identified and selected for measurements to serve as reference data for modelling. Power conversion efficiency is fundamental parameter for both operating condition analysis as well as strategic decision of technology application in order to improve energy efficiency. Therefore power conversion efficiency is obtained by comparing AC and DC side electrical

978-1-5090-1201-5/15/$31.00 ©2015 IEEE

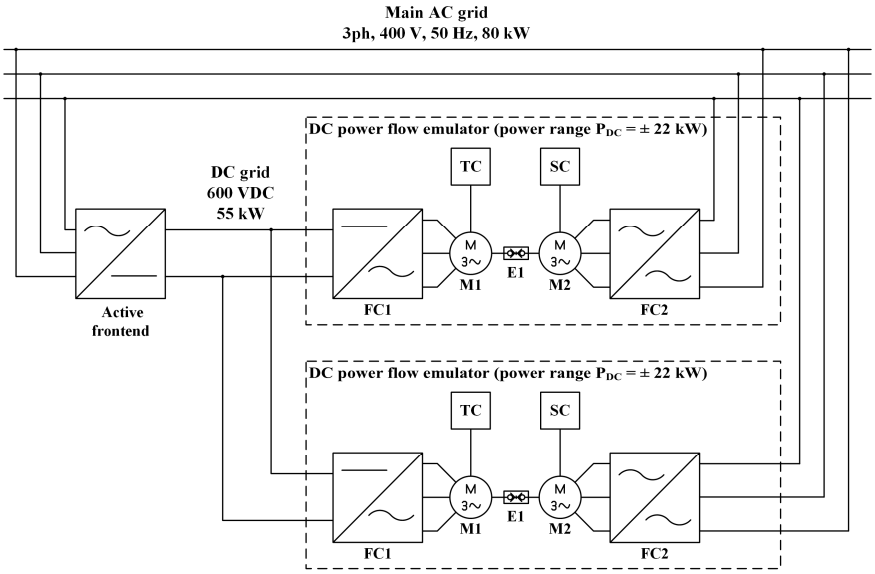

Fig. 1. Electrical infrastructure for AC/DC converter experimental measurements

power quantities. AC power quality is strictly regulated by several standards and grid codes how energy can be consumed or produced for injection into AC grid therefore also factor parameter variation has been obtained by measurements.

IV. Simulation Model Development

Based on obtained physical measurement numerical model has been developed based on Matlab numerical simulation environment as verified against experimental measurement results. Such model enable further DC type system operation analysis and development of optimal operation strategies and hardware application solutions. Simulation model present basic model structure for further development of various power level electrical equipment analysis. Development of hardware verified simulation model provide fundamental framework for system wide system evaluation and decision making for optimal DC electrical infrastructure development for automated manufacturing equipment supply from few devices to scales up to factory level. The structure of AC grid connected AC/DC converter model has been presented in Fig. 2. The power balance is observed based on DC side power flow therefore

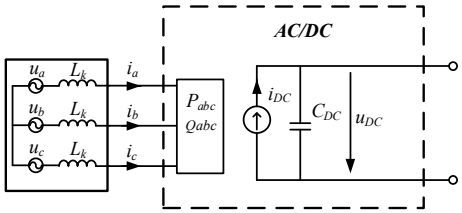

Fig. 2. Model structure of AC/DC converter.

other quantities are referred to DC power flow for operation of lookup method. The AC side grid inductance has been selected to be 1.27 mH corresponding to typical 1 MVA distribution transformer approximation for modelling applications. The AC side load has been composed as symmetrical 3 phase controllable load. The instantaneous values for active power P and reactive power Q can be varied during modelling according to observed power factor. The initial values of AC power P_{ac} and DC power P_{dc} and power factor has been obtained and steady operating points within power ranges from -40 kW to 45 kW. The respective variation of AC power referred to DC power has been presented in Fig. 3 and power factor variation in 0.

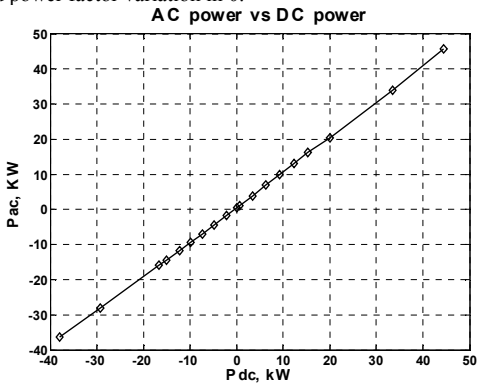

Fig. 3. AC side power with respect to DC side power.

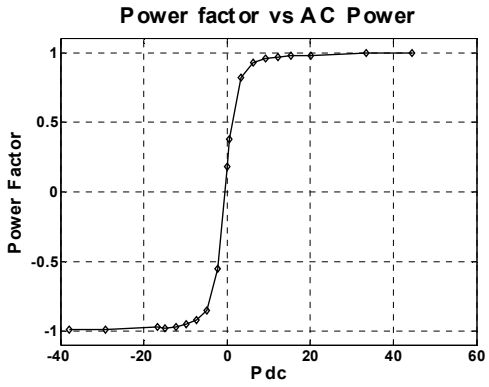

Fig. 4. Power factor with respect to DC side power.

The power losses can be derived by comparison of AC and DC power at same operating point, therefore loss power variation with respect to DC power has been obtained as shown in 0. The reactive power reference value has been derived based on following equations (1) and (2) where *PF* represent measured power factor parameter.

$$\varphi \approx \arccos(PF) \tag{1}$$

$$Q \approx \frac{P_{ac}}{\cos(\varphi)} \cdot \sin(\varphi) \tag{2}$$

The variation of reactive power with respect to DC power variation has been presented in following Fig. 6 as result of aproximation based on aforementioned equations .

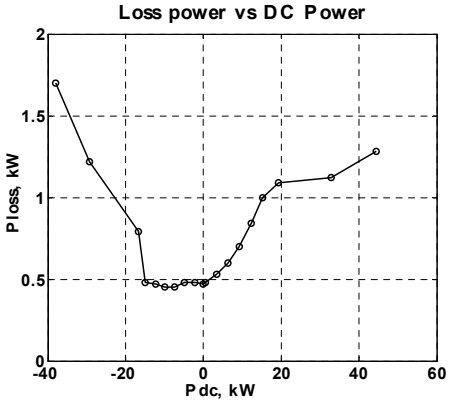

Fig. 5. Loss power with respect to DC power.

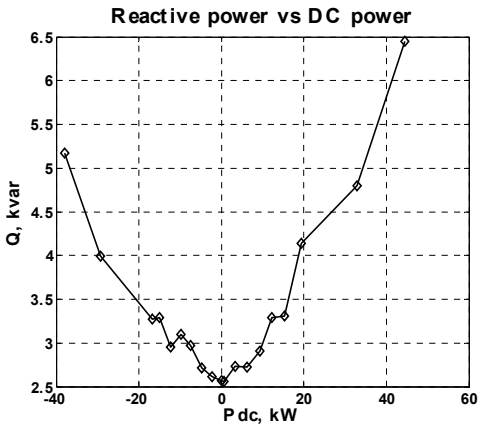

Fig. 6. Reactive power *Q* with respect to DC side power.

V. Model Operation Analysis

In order to develop dynamic variation of DC side voltage under load conditions the controlled current source in combination with capacitor representing 4.1 mF output filter capacitor converter has been assembled. The reference voltage of capacitor is chose to be 600V representing desired microgrid nominal voltage. The charging or discharging of capacitor has been done by ideal current source controlled by PI type controller observing output voltage with respect to reference voltage. The operation of modelled electrical circuit has been compared with real operation of converter under step change of load from 0 to 6.5 kW and vice versa. The respective model DC link voltage with respect to real measurement has been presented in Fig. 7. The AC side power modelling has been verified by power consumption measurement of 2 reference load profiles *Pr1* and *Pr2* representing dynamic electrical drive operation with energy recuperation to AC side therefore utilizing both directions of power conversion as represented in

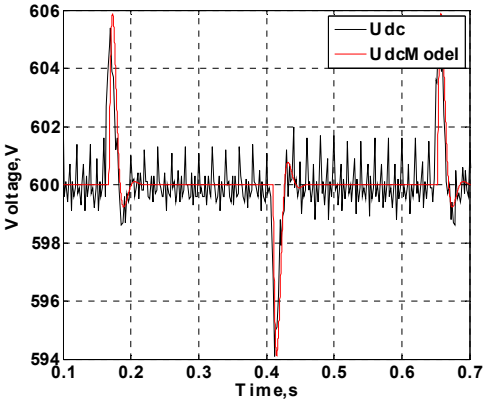

Fig. 7. Simulation model and real system DC voltage variation under step load change.

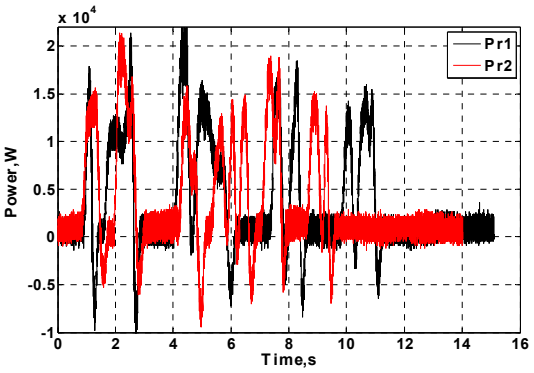

Fig. 8. DC side power profiles for reference measurements.

Fig. 8. The average power consumption per cycle has been obtained by measurement using Fluke power analyzer equipment within operating period of 10 minutes. For same profiles and time period. The numerical values have been presented in TABLE I. The difference in measurement and modelling data represent 7.8% and 6.8% variation for both power profiles applied

TABLE I. MEASUREMENT AND MODELLING DATA

Profile	Average load power, kW		
	Experimental	*Model*	*Difference, %*
Pr 1	***0.204***	***0.19***	***-6.8***
Pr 2	***0.192***	***0.177***	***-7.8***

Since power measurement of AC/DC converter represent total consumption including internal peripheral devices such as cooling cabinet, contactor coil control and other that can vary their specific power demand during longer time operation from cycle to cycle some uncertainty is present. AC side current variation has been presented in Fig. 9 as obtained by simulation and correspond to DC side power dynamics.

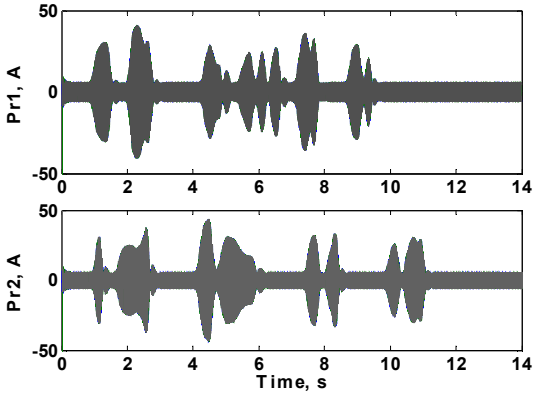

Fig. 9. Modelled AC currents for 2 testing profiles

CONCLUSIONS

Simulation model of AC/DC bidirectional power converter has been developed based on basic experimental data gathered during operation within designed power range. DC side voltage dynamics have been modelled by PI controller adjusted based on practical measurement of DC voltage fluctuation. AC side active and reactive power consumption has been modelled based on obtained variation of power factor within converters operating range and approximation of reactive power referred to active power. Model verification reveal slight deviation over longer operating time period including several cycles of reference load power. Evaluation of AC side power consumption with respect to simulation data reveal deviation which can be explained by internal consumption of AC/DC converter cabinet. Future activities for modification of developed model that would be necessary include analysis of harmonic content of AC side power as well as unbalance of 3 phase system and more detailed distribution of loss power and peripheral device consumption.

ACKNOWLEDGMENT

The research activities have been supported by Latvian National Research program LATENERGI.

REFERENCES

[1] R. Mathew, M. Shah, and P. N. Tekwani, "Design , Modelling and Simulation of Three-Phase Front-End Converter for Unity Power Factor and Reduced Harmonics in Line Current," *Eng. (NUiCONE), 2013 Nirma Univ. Int. Conf.*, pp. 1–6, 2013.

[2] L. Ott, Y. Han, O. Stephani, J. Kaiser, B. Wunder, M. März, and K. Rykov, "Modelling and Measuring Complex Impedances of Power Electronic Converters for Stability Assessment of Low-Voltage DC-Grids," in *DC Microgrids (ICDCM), 2015 IEEE First International Conference on*, 2015, pp. 51–56.

[3] M. Imecs, C. Szabo, and I. I. Incze, "Modelling and simulation of controlled bi-directional power electronic converters in a DC energy distribution line with AC grid- and motor-side active filtering," *2007 Eur. Conf. Power Electron. Appl.*, 2007.

[4] R. F. Coelho, T. B. Lazzarin, and D. C. Martins, "Modelling and control of the single-phase dc-ac PWM converter for grid-connected applications including a loop for average primary current controlling," in *Power Electronics Conference (COBEP), 2011 Brazilian*, 2011, pp. 334–340.

[5] G. Zaleskis and V. Brazis, "The Concept of Simulation of Two Electrical Vehicles with Energy Storage Systems Connected to Common Contact Network," in *13th International Symposium „Topical Problems in the Field of Electrical and Power Engineering" and „Doctoral School of Energy and Geotechnology II*, 2013, pp. 114–117.

Appendix 10

Šenfelds, A. Analysis of Cyclic DC Load Currents for Intelligent Electrical Protection. In: *2015 56th International Scientific Conference on Power and Electrical Engineering of Riga Technical University (RTUCON) : Proceedings*, Latvia, Rīga, 14-14 October, 2015. Riga: Riga Technical University, 2015, pp.165-168. ISBN 978-1-5090-0334-1. e-ISBN 978-1-4673-9752-0.

DOI:10.1109/RTUCON.2015.7343162

Analysis of Cyclic DC Load Currents for Intelligent Electrical Protection.

Armands Senfelds (*Doctoral student, Riga Technical University*).

***Abstract* –Conceptual analysis of repetitive current of DC load is presented for two type of data processing approaches. Offline post-processing type approach as well as online adaptive data analysis method is introduced. Application of introduced analysis in case of repetitive DC current cycle with fixed duration is presented focusing of current-time behavioral investigation. Comparison of obtained analysis data and typical fuse character curve data is presented followed by brief discussion of prospective advantages.**

***Keywords* – Smart grids, Data analysis, electrical safety**

I. Introduction

Increasing interest in DC type electrical power distribution and supply systems lead to broad range of DC applications emerging. Electrical safety and protection measures have been well established within AC systems but applications within smart DC microgrids with various types of energy production, storage and consumption elements as well as multidirectional power flow capability present needs for equivalent electrical system coordination and protection technologies. Comparative overview regarding various DC microgrid operational units and protection technologies has been presented by [1]. Protection measures on various DC voltage levels and applications such as mining [2], shipboard power system [3], residential buildings [4] and data centers [5]. Development of adaptive overcurrent protection device operation has been presented by [6]. Adaptation of semiconductor type switches for DC type electrical applications has been discussed in [4], [5], [7]. Also inductor based current limiting technique has been proposed by [8]. Early concept of adjustable overcurrent protection based on microcontroller is presented by [9]. This paper present DC industrial load of robot manipulators fed by steady 600V voltage with known and repetitive operation cycle time presented in Section 2. Followed by two data analysis concepts of repetitive load current-time profile investigation utilizing post-processing or online adaptive analysis in Section 3 and Section 4 respectively. Discussion on obtained analysis results and prospective application advantages has been presented in Section 5.

II. DC Microgrid Based Cyclic Application Example

As basis for investigation of repetitive electrical load current analysis an application of DC voltage based electrical supply system has been considered. It is assumed that stable DC voltage is supplied to several industrial loads operating on repetitive manufacturing cycle basis. As example data of industrial robot manipulator electrical load has been provided in Fig. 1 leading to equivalent current being drawn from 600V DC electrical supply system. The system has total manufacturing cycle length of 60s and 4 industrial robot operations has been carried out within this cycle – handling of material, handling of spot welding equipment, handling of glue dispenser and handling of clinching equipment. Handling operation provide moving of material between last three joining processes as it can be observed also on common time axis in Fig. 1.

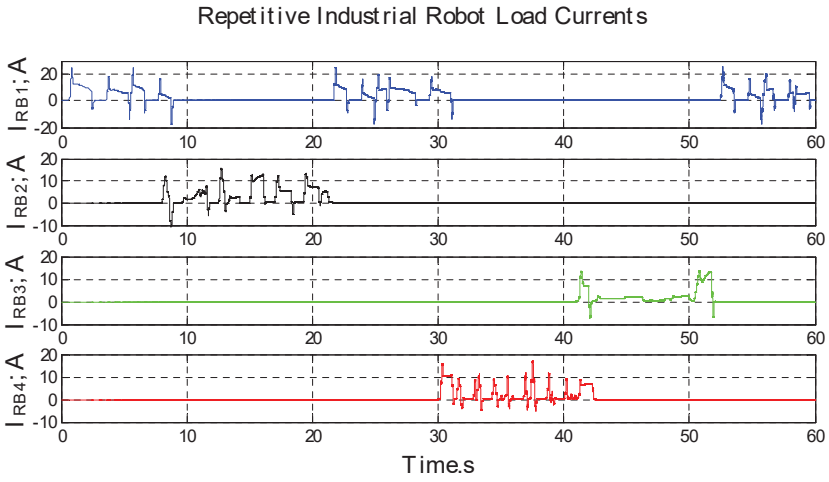

Fig. 1. Example of 60 second repetitive industrial production cycle and consumer electrical load current profiles in case of 4 industrial robots assisting for several operations: I_{RB1} –material handling ; I_{RB2} – carry welding gun; I_{RB3} –carry glue dispenser; I_{RB4} – carry clinching equipment.

978-1-4673-9752-0/15/$31.00 2015 ©European Union

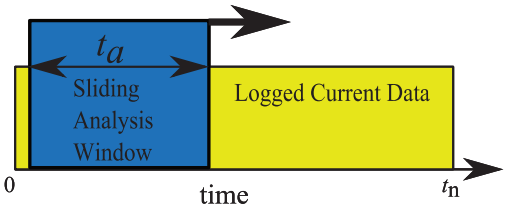

Fig. 2. Graphical representation of sliding window data analysis operation principle.

III. Offline Analysis, Post Processing Method.

A. Analysis approach

One of the methods for detailed analysis of repetitive load current profile would be to record full current cycle and perform data analysis after process has completed. Concept of analysis by sliding data window over full cycle data has been illustrated in Fig. 2. Data of load current of time period t_n has been recorded and stored after process operation. From electrical overcurrent protection perspective analysis of highest average current within various time periods is advantageous. An iterative analysis process by variation of sliding window width t_a from one sample to full cycle has been carried out. Maximum value of mean current value within sliding window for each step has been stored.

B. Obtained result

In case of presented load cycles data analysis of positive current direction has been carried out representing consumption since recuperative operation and negative current flow has lower amplitude and is considered not relevant for overcurrent protection operation. Highest short term current peak value of 25.6A has been observed in case of industrial robot RB1 application for material handling operation with rapid acceleration profile. Industrial robots RB2 to RB4 present similar behavior with peak current values in range from 13.8A to 16.8A since slower movement of production

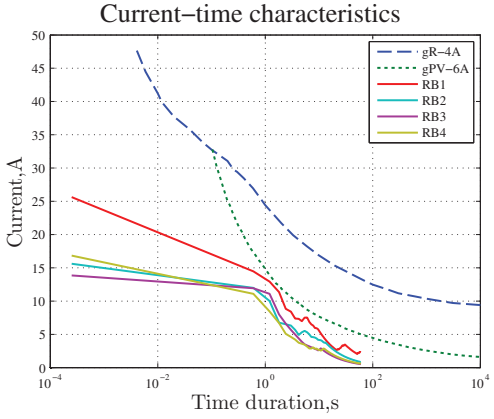

Fig. 3. Comparison of sliding window analysis for highest mean current values and typical fuse current-time curves of types gR-4A and gPV-6A.

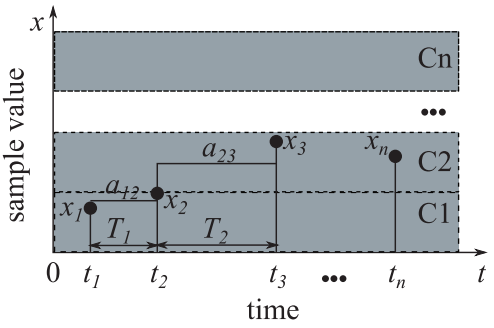

Fig. 4. Graphical representation of online adaptive current sample analysis within classes C.

tools is present. Such analysis present ability to evaluate behavior of observed current profile with respect to real electrical overcurrent protection device character. Typically fuse manufacturers provide device current–time operational characteristic data as graphs. Comparison of obtained sliding window analysis of 4 current profiles I_{RB1} to I_{RB4} and two different type fuse characteristics of gR and gPV current-time character has been presented in Fig. 3.

It can be observed that difference between fuse character and short term current values of analyzed currents is present. Detection of operation within such region below typical fuse ignition curve may not be critical for electrical equipment but may provide information about tendency to reach overcurrent threshold. Ability to adjust short term overcurrent protection for individual devices as well as optimize analysis process for online operation as embedded device reducing necessity for large data logging would be advantageous therefore approach for online analysis is presented in following section.

IV. Online Adaptive Current Analysis Approach.

A. Analysis approach

In order to simplify current profile data analysis and decrease computational effort and memory requirements approach of adaptive data analysis has been presented as in Fig. 4. Discrete samples of current values x have been obtained with respective timestamps t. Average values a for each interval between two samples has been obtained as well as respective period lengths T. Obtained data is intended for following sorting according to classes C covering whole sample value range. For example average value a_{12} belong to class C1 as it fits within this class value range of x. Also respective time period T_1 belonging to this average value is assigned to class C1. Following such routine sample by sample covering whole operation cycle period of length t_n respective time periods T are assigned to classes C1 to Cn.

Such approach enable adaptive behavior and can be realized in following steps:

1) Cycle 1 – obtain current profile maximum value, determine value range x and develop distribution in number of classes Cn with respective value range for each class.

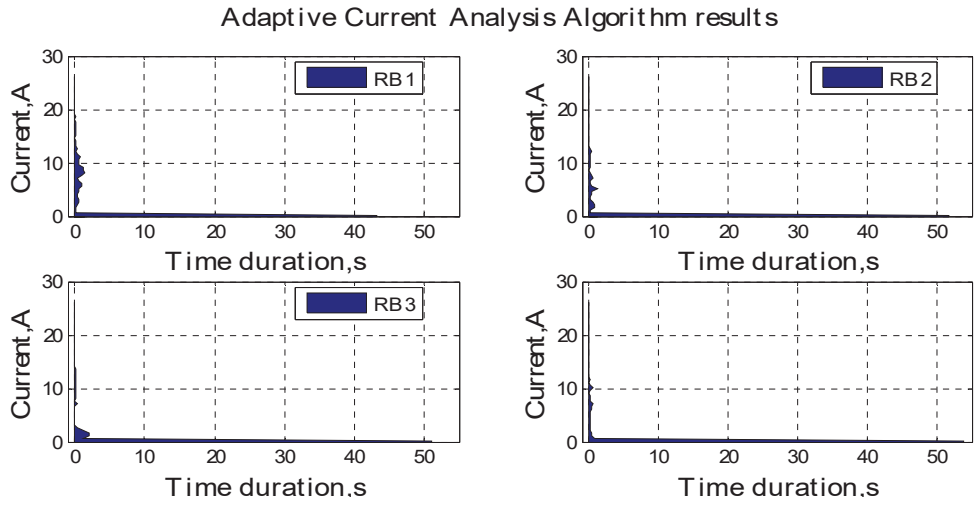

Fig. 5. Adaptive analysis results for full 60 s production cycle load currents.

2) Cycle 2 – perform sample by sample analysis according to defined classes C1 to Cn. Distribute total cycle time t_n into periods T_1 to T_n and assign them to respective classes based on average values a_1 to a_n

B. Obtained results

Results of analysis based on proposed approach applied for load current profiles has been presented in Fig. 5. During first operating cycle it has been obtained that analysis up to 26A value is relevant since highest value arise for current cycle IRB1 having 25.6A peak. Total cycle time distribution into classes has been based on 0.5A wide classes resulting into total of 52 classes covering whole data range. It can be observed that majority of cycle time load current values are

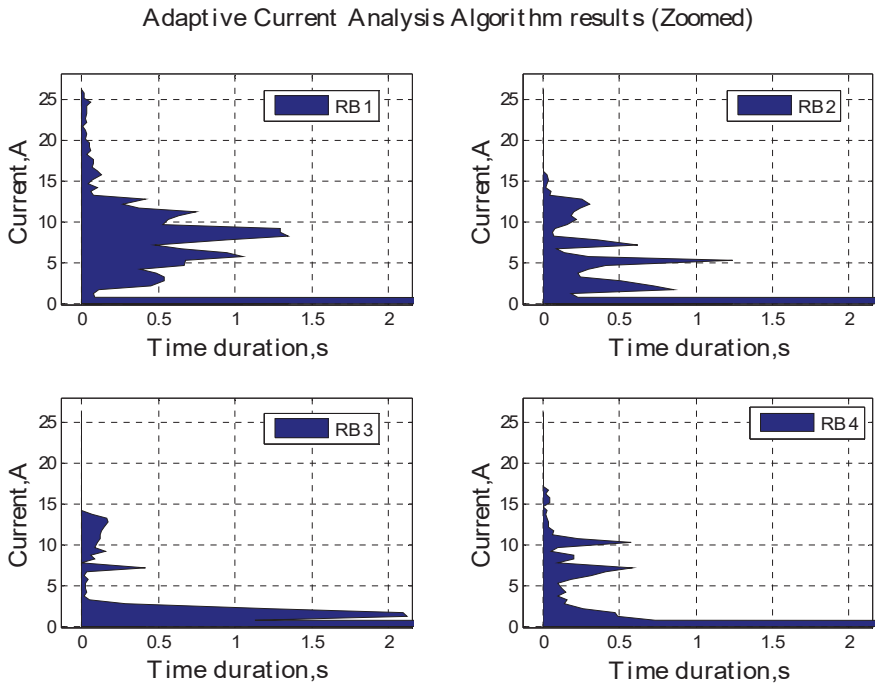

Fig. 6. Magnified view of analysis results for time span below 2 seconds.

placed in classes less than 1A. Magnified view of current distribution of time span below 2 seconds is presented by Fig. 6. Since total plot area in Fig. 5 marked with blue color represent 60 second total cycle it can be observed that only short time periods with high current flowing to the load are present which correspond to initial current waveforms presented in Section 2. Fig. 6 presents analytical results of short term current behavior below 2 second time span. Analysis RB1 correspond to current profile I_{RB1} for handling operation of industrial robot. This load also has the highest current peak value of 25.6A which can be observed as respective width of highest value class above 25A. Following load current analysis of RB2 to RB4 present results for remaining joining processes but current peak values are lower around 15A level. Behavior variation of load type can also be observed in analysis of RB3 for example representing slow motion of industrial robot during glue dispensing with steady load current of about 2A between 43th and 45th second of original production cycle. Respective influence can be also observed in Fig. 6 diagram of RB3 where horizontal peak of about 2 second operational time can be identified corresponding to current value class of 2A. Such analysis provide ability to obtain individual current-time signature profiles for each of presented electrical loads.

V. Conclusions

Comparison of two presented data analysis concepts applied to available data of electrical current corresponding to cyclic load of industrial robot manipulator equipment being operated on repetitive basis may lead to several observations.

By detailed analysis of short term current pulse duration it is observed that some margin is present below typical fuse-time characteristic and real current behavior as presented in highest mean value analysis with variable time window as introduced Section 2. Detection of system operation within this region may be utilized for coordination of larger scale electrical protection equipment on predictive basis.

Adaptive analysis by means of amplitude value classes present ability to obtain individual current-time profile signatures for each of loads by online data processing. Such information may serve as basis for detection of deviations from normal operation on cycle to cycle comparison basis and present ability for process monitoring and coordination.

Practical application possibilities may strongly vary of performance of available measurement device resolution and sampling rate as well as variation of process load under normal operation conditions and are subject to future experimental analysis under real manufacturing equipment. The optimal technical equipment necessary for data analysis and computing is another aspect of potential application feasibility.

Acknowledgment

The research leading to these results has received funding from the European Community's Seventh Framework Programme (FP7/2007-2013) under grant agreement No 609391, project AREUS (Automation and Robotics for European Sustainable Manufacturing).

References

[1] D. M. Bui, S. Chen, C.-H. Wu, K.-Y. Lien, C.-H. Huang, and K.-K. Jen, "Review on protection coordination strategies and development of an effective protection coordination system for DC microgrid," in *Power and Energy Engineering Conference (APPEEC), 2014 IEEE PES Asia-Pacific*, 2014, pp. 1–10.

[2] C. Yuan, M. A. Haj-ahmed, and M. S. Illindala, "Protection Strategies for Medium-Voltage Direct-Current Microgrid at a Remote Area Mine Site," *IEEE Trans. Ind. Appl.*, vol. 51, no. 4, pp. 2846–2853, Jul. 2015.

[3] M. E. Baran, S. Teleke, and S. Bhattacharya, "Overcurrent Protection in DC Zonal Shipboard Power Systems using Solid State Protection Devices," *2007 IEEE Electr. Sh. Technol. Symp.*, pp. 221–224, 2007.

[4] P. Meckler, F. Gerdinand, R. Weiss, U. Boeke, and A. Mauder, "Hybrid switches in protective devices for low-voltage DC grids at commercial used buildings," in *27th International Conference on Electrical Contacts, June 22 – 26, 2014, Dresden, Germany*, 2014, pp. 120–125.

[5] R. Mehl and P. Meckler, "Comparison of advantages and disadvantages of electronic and mechanical Protection systems for higher Voltage DC 400 V," no. October, pp. 236–242, 2013.

[6] A. Tjahjono, "Overcurrent Relay Curve Modeling and Its Application in the Real Industrial Power Systems Using Adaptive Neuro Fuzzy Inference System," pp. 1–6, 2015.

[7] P. Meckler and W. Ho, "Does an electronic circuit breaker need electrical contacts?," *Proc. 50th IEEE Holm Conf. Electr. Contacts 22nd Int. Conf. Electr. Contacts Electr. Contacts, 2004.*, vol. 00, no. C, pp. 480–487, 2004.

[8] P. Arsénio, N. Vilhena, J. Murta-Pina, A. Pronto, and A. Álvarez, "Design Aspects and Test of an Inductive Fault Current Limiter," *Electr. Control Commun. Eng.*, vol. 5, no. 1, pp. 40–45, 2014.

[9] G. Benmouyal, "Design of a digital multi-curve time-overcurrent relay," *IEEE Trans. Power Deliv.*, vol. 6, no. 2, pp. 656–665, Apr. 1991.

Armands Senfelds received B.Sc.eng. of Riga Technical University, Latvia and M.Sc of RWTH Aachen University, Germany at 2009 and 2012, respectively at field of Electrical Power engineering.

He is a PhD student and researcher at Riga Technical university, Institute of Industrial electronics and Electrical engineering.

Research with focus on intelligent industrial DC power distribution systems with renewable energy integration and storage applications is carried out within PhD student activities.

His research interests include design and control of power electronic equipment, electrical drives and electrical mobility.

He is a member of IEEE Power Electronics, Industry Applications, Industrial electronics, Robotics and Automation and Power and Energy Societies.

Appendix 11

Paugurs, A., **Šenfelds, A**. Design of a Motor Drive System for Bidirectional DC Power Flow Control. In: 2015 56th International Scientific Conference on Power and Electrical Engineering of Riga Technical University (RTUCON), Latvia, Riga, 14-14 October, 2015. Riga: 2015, pp.265-268. ISBN 978-1-5090-0334-1. e-ISBN 978-1-4673-9752-0.

DOI:10.1109/RTUCON.2015.7343145

Design of a Motor Drive System for Bidirectional DC Power Flow Control

Arturs Paugurs (*Doctoral student, Riga Technical University*), Armands Senfelds (*Doctoral student, RTU*)

***Abstract* – A motor drive system for the purpose of bidirectional DC power flow control has been developed. A laboratory test bench has been setup to determine the dynamic properties of the system a nd to verify the proposed power flow control principle. Control board prototype has been developed and briefly described. Results of full reference power cycle tests have been summarized.**

***Keywords* – Bidirectional DC power flow, motor drive, power control.**

I. Introduction

The power flow of current industrial robot systems in respect to the power supply grid is unidirectional, since the braking energy is dissipated on braking resistors. Papers [1], [2] introduce methods of saving the robot braking energy by adding external capacitance to the common DC bus of the inverters driving the robot motors. The industrial robot system could also be modified to feed the regenerative energy back to the supply grid. The objective of the paper is to describe the development of a laboratory test bench designed to replicate the power flow of a 20 kW industrial robot system with regenerative properties in respect to the supply grid.

A novel approach of using a single, bidirectional AC-DC converter as the power supply of a DC grid based subsystem can increase the overall energy efficiency by minimizing the conversion stages from the source to each of the loads [3]. Elements of the subsystem include regenerative motor drive systems as loads, batteries and supercapacitors as electrical energy storage elements and renewable energy sources – wind turbines and PV panels. The purpose of the laboratory test bench is to act as the subsystem load. Development and testing of power control algorithms based on increasing energy efficiency of the subsystem can then be carried out.

II. Theoretical Basis

Main components of the proposed solution include two mechanically coupled induction motors each controlled by a separate motor drive (Fig. 1). Motor drive FC2 is set to keep the rotational speed of the linked shafts constant, thus according to (1), the power consumed or produced by motor M1 can be varied by changing the torque reference of FC1.

$$P_{Mech} \approx T_{ref} \cdot \omega \tag{1}$$

The power balance between the DC supply grid and the mechanical output of motor M1 in motoring and generating modes is given in (2) and (3) respectively. $\Delta P_{Inverter}$ and ΔP_{Motor} are the electromechanical losses in motor drive FC1 and motor M1.

$$P_{DCM} = P_{Mech} - \Delta P_{Inverter} - \Delta P_{Motor} \tag{2}$$

$$P_{DCG} = P_{Mech} + \Delta P_{Inverter} + \Delta P_{Motor} \tag{3}$$

Motor and motor drive losses are considered relatively small in respect to the general power flow from or to the DC supply grid, hence the approximation in (4).

$$P_{DC} \approx T_{ref} \cdot \omega \tag{4}$$

The system has been modelled and the theory has been verified in [4]. This paper covers practical setup (Fig. 2) and testing of the laboratory test bench.

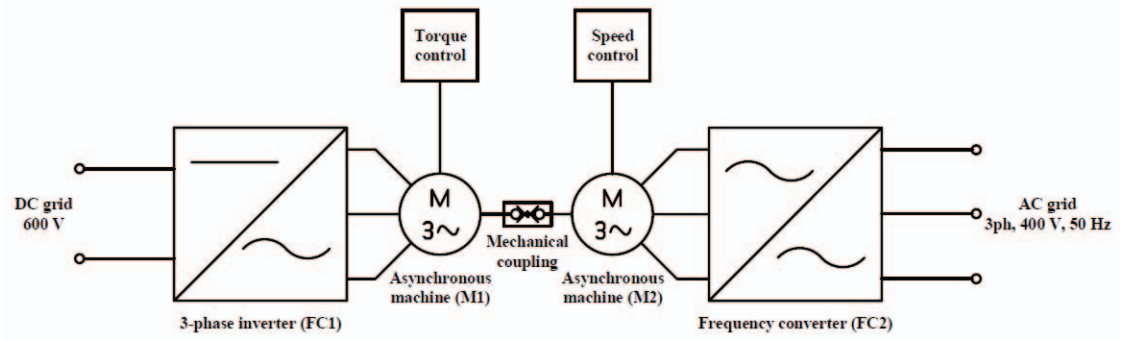

Fig. 1. Principal schematic of the motor drive system designed for the replication of the industrial robot power flow

978-1-4673-9752-0/15/$31.00 2015 ©European Union

III. LABORATORY TEST BENCH

Fig. 2. Laboratory test bench setup of the motor drive system. FC1 and M1 are located on the left side and FC2, M2 on the right side with their respective power supply enclosures.

TABLE I
GENERAL PARAMETERS OF THE MAIN COMPONENTS

Induction machine M1	Power rating	22 kW
	Voltage	400V, 50Hz, 3 phases
	Pole pairs	2
	Nominal torque	143 Nm
	Nominal speed	1465 r/min
Motor drive FC1	Power rating	22 kW
	Voltage	600VDC
	Control algorithm	Direct torque control
	Additional specification	Regenerative to the DC grid

Motor drive FC2 and machine M2 match the parameters summarized in Table I. Both drives are standard AC-AC power converters, however, the active rectifier in drive FC1 is bypassed and the main power is supplied directly to the intermediate DC bus.

IV. SYSTEM DYNAMICS ANALYSIS

The power flow of an industrial robot dynamically varies due to the rapid accelerations and decelerations required for manufacturing processes. The intermediate DC bus power flow of an industrial robot system has been logged (Fig. 3) in a single robot work cycle. The power graph is converted to a torque graph by (4) and used as a reference for the drive FC1 of the motor drive system.

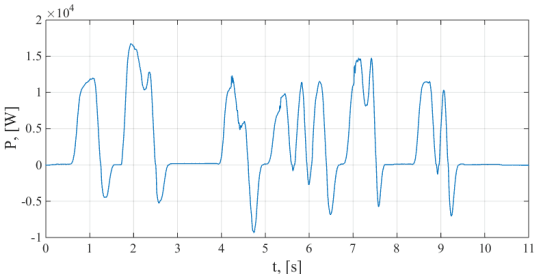

Fig. 3. Intermediate DC bus power flow of an industrial robot system in a single work cycle. The negative power peaks occur when the robot is decelerating.

Derivative of the reference graph (Fig. 4, a) shows the power flow rate of change in the robot system in both acceleration and deceleration phases. The derivative graph peaks are interpreted as the minimum dynamic requirements for the motor drive system to be capable of replicating the reference power graph. The rate of change of the robot power flow peaks at ~160 kW/s when power is consumed from the supply grid and at ~ -186 kW/s whilst deceleration.

Derivative analysis of step response tests with ±15 kW steps in motoring (Fig. 4, b) and regenerative (Fig. 4, c) modes show the rate of change of the input DC power flow in the motor drive system. Results verify that the motor drive system meets the dynamic requirements for the replication of the reference power graph. For example, a 20 kW change in motoring mode in the reference power graph takes 0.126 seconds and 0.06 seconds in the motor drive system.

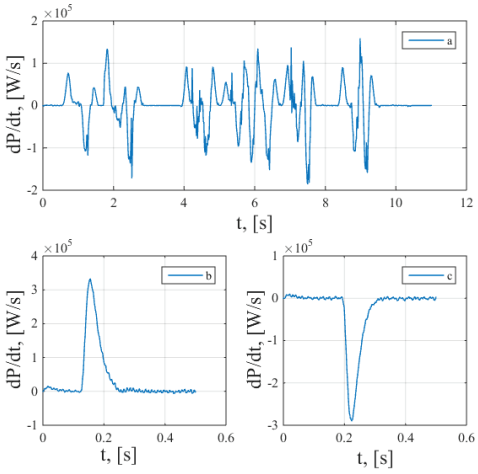

Fig. 4. Power flow rate of change in the robot system (a) and in the motor drive system whilst performing step response tests both in motoring (b) and regenerative (c) modes. The step reference is set to 15 kW.

The DC power flow rate of change in the motor drive system is mainly dependent of the rate of change of the input current, since the DC supply grid voltage is near constant. U_{DC} = 600V -1% / +2% depending on load conditions.

V. DC Power Flow Control Approach

A. Control algorithm

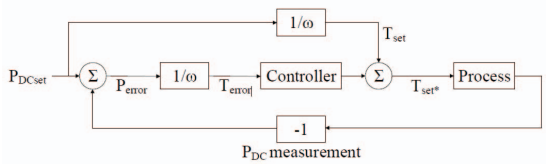

Fig. 5. Block diagram of the base algorithm for bidirectional DC power flow control in the motor drive system.

The base algorithm for DC power flow control is depicted in Fig. 5. Variable T_{set*} sets the momentary torque reference for motor drive FC1. A feedforward link is used, since the general transfer function between input DC power and the torque reference is known (4). Since (4) is an approximation and electromechanical losses, temperature fluctuations and other factors impact the momentary DC power value, a feedback loop is implemented. The momentary DC power value is measured and the controller compensates for any fluctuations from the set P_{DCset} power value.

B. DC power measurement

A novel electrical power measurement approach covered in [5] is used for the feedback loop of the control algorithm. The metering device is connected in series between the DC supply grid and the motor drive FC1 and sends the measured power value to a microcontroller via UART communication protocol.

The DC power measurements have to be sent to the microcontroller with a sampling rate f_s at least twice the Nyquist frequency (5) in order to fully recreate the robot power graph.

$$f_s \geq 2 \cdot f_{Nyquist} \tag{5}$$

To determine the minimum necessary sampling rate, Fourier Transform of Fig. 3 is calculated by (6).

$$Y(f) = \frac{1}{N} \sum_{n=1}^{N} Y(t) e^{-i\frac{2\pi}{n \cdot N \cdot f}} \tag{6}$$

where
Y(f) - the value of the variable transferred to frequency domain,
N – the input time domain graph described by N points, each separated by a constant time step,
Y(t) – momentary value of the graph in time domain,
f – frequency.

The results (Fig. 6) show that the dominant frequencies present in the waveform are in the bandwidth of up to 5 Hz. Based on this conclusion, a sampling rate of 100 Hz is considered sufficient and is chosen for the power measurement feedback loop.

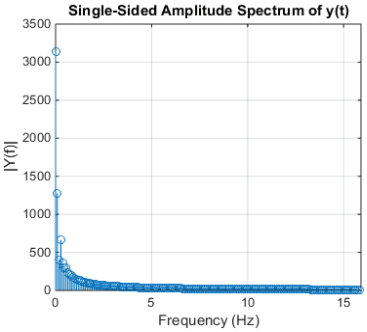

Fig. 6. Fourier Transform of the robot power graph. The general transmitted power is considered to be within the frequency bandwidth of 0 to 5 Hz.

C. Control board prototype

A control board prototype (Fig. 7) has been developed to test the described control approach. The prototype board communicates with both drives (FC1, FC2). As the initial step, a start signal is sent to the motor drive FC2 which has to keep the rotational speed of the shafts constant. The control board detects when constant speed is reached by a signal received from an analog output of FC2, after which drive FC1 is started. Torque reference T_{set*} is calculated by the algorithm in Fig. 5 and sent to FC1 with a sampling rate of 100 Hz.

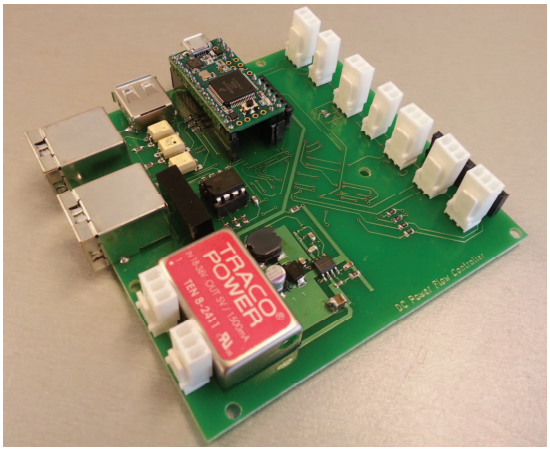

Fig. 7. Control board prototype. RJ45 ports connect with motor drive communication boards, DC wattmeter measurements are sent via USB-A port. Additional space is reserved for an external board for PROFINET communication. Control algorithm is realized using a Teensy 3.1 development board with Cortex-M4 72 MHz microprocessor.

VI. Full Cycle Tests and Analysis

As the first iteration of testing, a proportional regulator was used in the controller block of the algorithm. Critical gain of the P regulator was determined empirically from step response tests. Critical gain is the proportional gain at which the process

variable starts to oscillate with a constant period and amplitude around the set reference value.

Full cycle DC power measurements were logged at various proportional gains varying from zero up to the critical gain. Integral of the absolute error (IAE) (7) is calculated for each logged measurement to determine the impact of the regulator.

$$IAE = \int_0^t |e(t)|dt \tag{7}$$

The IAE criterion of the power measurement in open loop conditions is used as a base parameter by which to determine the effect of the regulator.

A full cycle measurement (Fig. 8) with open loop settings, in other words, with the proportional regulator gain set to zero, verifies the approximation in (4). The measured power flow offset from the set reference graph is relatively small and can be explained by the electromechanical losses present in the system and the self-consumption of the motor drives. Self-consumption of the drive can be measured at zero load conditions, that is, when the torque reference is set to zero.

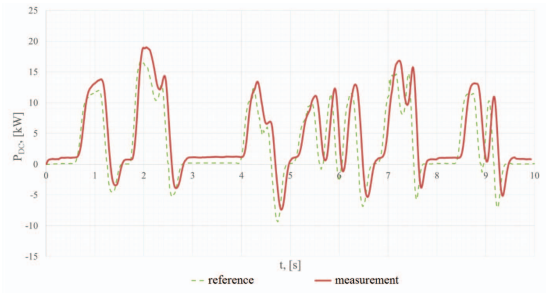

Fig. 8. Comparison of the reference power graph and the measured system response in open loop conditions, in other words, with the controller gains set to zero. Thus the torque reference is calculated only from the feedforward loop by (4).

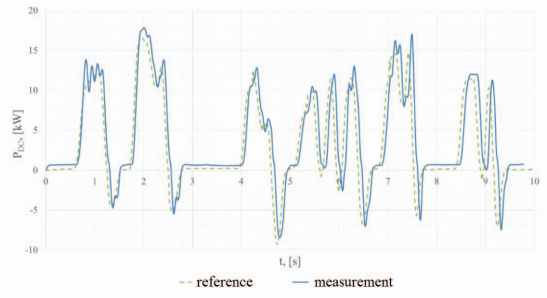

Fig. 9. Comparison of the reference power graph and the measured system response in closed loop conditions with proportional regulator as the controller. Proportional gain set to 80% of the critical gain.

Most improvement by the IAE criterion was achieved with proportional gain set to 80% of the critical gain. The measurement is depicted in Fig. 9. The power graph peaks are more closely replicated in comparison with the full cycle measurement in open loop conditions. IAE criterion was minimized by 24.79% in comparison to the open loop measurement.

VII. CONCLUSIONS

A method of bidirectional DC power flow control by using a motor drive system has been tested in a practical application. System dynamics analysis regarding power flow rate of change and full cycle tests verify that the motor drive system is capable of replicating the dynamic industrial robot power flow. Proportional regulator implementation decreased the IAE criterion by 24.79%.

The motor drive system can be used as a physical simulator for any given DC load / generator power profile within the respective dynamic and power boundaries.

VIII. ACKNOWLEDGEMENTS

Development of this article is co-financed by European Union's Seventh Framework Programme within the project "Automation and Robotics for European Sustainable manufacturing". Grant agreement no. 609391. More information: http://www.areus-project.eu/

REFERENCES

[1] D. Meike, A. Senfelds, and L. Ribickis, "Power Converter for DC Bus Sharing to Increase the Energy Efficiency in Drive Systems," 2013.

[2] I. Rankis, D. Meike, and A. Senfelds, "Utilization of Regeneration Energy in Industrial Robots System," 2013, no. 1, pp. 8–13.

[3] A. Suzdalenko, "Current Sensorless Control of Front-end Bidirectional AC/DC Converter Based on Half-bridge Topology," *Electr. Control Commun. Eng.*, vol. 4, no. 1, pp. 19–25, 2013.

[4] A. Senfelds and A. Paugurs, "Electrical drive DC link power flow control with adaptive approach," 2014, pp. 30–33.

[5] P. Apse-Apsitis, A. Avotins, and L. Ribickis, "A different approach to electrical energy consumption monitoring," 2014, pp. 1–5.

Arturs Paugurs received B.Sc.eng. and M.Sc.eng. degrees in 2014 and 2015 from Riga Technical University, Latvia in the field of Electrical Engineering. Practiced in Daimler AG, (Sindelfingen, Germany) in a project regarding energy efficiency optimization methods in robotic systems.

He is a PhD student and works as a research assistant at Riga Technical University, Institute of Industrial electronics and Electrical engineering.

Current research regards industrial DC power distribution systems, power flow control and energy efficiency optimization methods.

He is a member of IEEE Industry Applications Society.

Armands Senfelds received B.Sc.eng. of Riga Technical University, Latvia and M.Sc of RWTH Aachen University, Germany at 2009 and 2012, respectively at field of Electrical Power engineering.

He is a PhD student and researcher at Riga Technical University, Institute of Industrial electronics and Electrical engineering.

Research with focus on intelligent industrial DC power distribution systems with renewable energy integration and storage applications is carried out within PhD student activities.

His research interests include design and control of power electronic equipment, electrical drives and electrical mobility.

He is a member of IEEE Power Electronics, Industry Applications, Industrial electronics, Robotics and Automation and Power and Energy Societies.

Appendix 12

Šenfelds, A., Vorobjovs, M., Meike, D., Bormanis, O. Power Smoothing Approach within Industrial DC Microgrid with Supercapacitor Storage for Robotic Manufacturing Application. In: 2015 IEEE International Conference on Automation Science and Engineering (CASE 2015) : Automation for a Sustainable Future: Proceedings, Sweden, Gothenburg, 24-28 August, 2015. Piscataway: IEEE, 2015, pp.1333-1338. ISBN 978-1-4673-8184-0. e-ISBN 978-1-4673-8183-3.

DOI:10.1109/CoASE.2015.7294283

2015 IEEE International Conference on
Automation Science and Engineering (CASE)
Aug 24-28, 2015. Gothenburg, Sweden

Power Smoothing Approach within Industrial DC Microgrid with Supercapacitor Storage for Robotic Manufacturing Application.

Armands Senfelds, Maksims Vorobjovs, Davis Meike, Oskars Bormanis

Abstract— **This research paper cover optimization process a converting conventional AC supply system towards DC based industrial power distribution system with supercapacitor storage based power balancing functionality. Electrical power consumption reference data is based on 4 industrial robot manufacturing area with automotive industry specific production processes and respective electrical load examples. Improvement in energy efficiency by interconnection and energy exchange process of production equipment as well as peak loading reduction on supplying AC power grid infrastructure is demonstrated.**

I. Introduction

Improvement of robotic manufacturing applications present in such industries as automotive are subject of high interest due to increasing awareness of emission reduction and efficient utilization of various kind of resources. Also expected price increase for energy resources as well as emerging alternative energy production technologies based on renewable sources present opportunities for development of other type of power distribution infrastructure with improved functionality. Since large number of industrial consumers require DC type electrical power supply, modification of conventional AC based distribution system is matter of interest. Industrial DC microgrid with potential of energy consumption reduction on production area level is presented in this research paper. Robotic manufacturing application electrical infrastructure optimization is based on 4 types of manufacturing processes common in automotive industry – handling, welding, clinching and gluing.

II. Production Process Load Modelling

In order to evaluate electrical power flow within manufacturing equipment supply system reference production sequence has been defined and modelled. Production cycle of 60s period representing robotic manufacturing application of 4 industrial robot operation with related tools has been designed based on typical automotive production tasks. Industrial robot manipulator electrical power estimation is based on previous robot modelling research presented in [1]. Industrial robot model has been verified with 210kg class payload industrial robot which is also applied as suitable manipulator in manufacturing process electrical model being scope of current research. Load power character of production tools is based on generalized approximation of obtained process data within real manufacturing processes. Sequential operation and electrical power profiles are presented in Fig.1.

A. Set of modelled industrial robot manipulator operations

- Robot RB1 – perform handling tasks, part weight 125kg. Three handling movements are performed during reference cycle: placing part in work area (0s to 10s of reference cycle), repositioning of part after welding process (22s to 32s of cycle) and removing part from work area (52s to 60s of cycle).
- Robot RB2 – perform welding task, welding tool weight 180kg. Positioning of welding tool for welding of 5 spots and returning to initial position (8s to 22s of reference cycle).
- Robot RB3 – perform glue dispensing operation with reduced speed, tool mass 50kg. Operation performed between 41s and 52s of reference cycle.
- Robot RB4 – perform rivet clinching operation, tool mass 150kg. Sequence of 5 clinching actions performed between 30s and 42s of cycle.

B. Set of modelled production tool loads

- Welding process – sequence of 5 spot welding actions has been introduced based on averaged power pulse. Power curve of welding process can be generalized in 2 processes - preheating phase duration 0.45s, average power 5kW and welding phase with duration 0.1s average 140kW leading to 15kJ of consumed energy per pulse.
- Clinching process – sequence of 5 clinching actions, each process has duration 0.5s, trapezoidal pulse with peak power of 4.5 kW.
- Glue dispensing – constant power of 100W during dispensing, process duration 8s.

Average total power P_{av} of all presented technologies with total summary power $P_{tot}(t)$ over 60s cycle is 3.78kW.

III. Electrical power distribution System Simulation for Robotic Application

Focus of presented electrical modelling of given production process based on robotic application is to evaluate system

"The research leading to these results has received funding from the European Community's Seventh Framework Programme (FP7/2007-2013) under grant agreement No 609391."

A.Senfelds, M. Vorobjovs and O. Bormanis are with Institute of Industrial Electronics and Electrical Engineering, Riga Technical university, Riga, LV-1020 (e-mail: armands.senfelds@rtu.lv; maksims.vorobjovs@rtu.lv; Oskars.Bormanis_1@rtu.lv)

D. Meike is with Daimler AG, Sindelfingen 71063, Germany (e-mail: davis.meike@daimler.com).

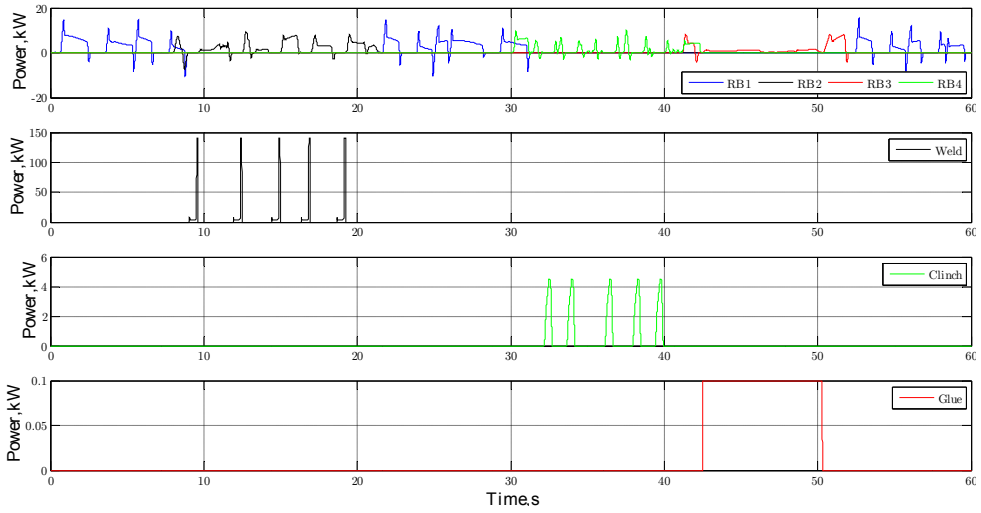

Figure 1. Modelled load power profiles for Industrial robots (RB1 to RB4), welding, clinching and gluing tools within common production cycle of 60s.

behavior and performance within both AC and DC voltage based applications. The task of supplying necessary electrical power for production equipment according to obtained load profiles has to be fulfilled by any of aforementioned approaches to ensure successful production operations. Several energy efficiency improvement measures regarding robotic applications has been presented by [2]. Introduction of DC based system would inherently enable recuperated energy exchange within group of robots that is not possible to implement in existing AC supply system without additional hardware manipulations and electrical DC voltage interconnection equipment [3]. Additionally to direct DC based supply system also integration of energy storage application for power balancing functionality is matter of interest.

A. Overview of energy storage technology options within proposed DC system.

Several energy storage devices options are known to be applied: supercapacitors, flywheels, batteries, fuel cells, are used widely in such applications as electrical vehicles, UPS, storage devices for smart grids. Each of energy storage devices have advantages and disadvantages, which present suitability for particular application. General overview of fundamental parameters of various systems is presented in following Table 1. Typical industrial application is considered to provide average power in range from 1-100kW and have energy capacity of 10kWh as well as functionality to absorb regenerated power. From comparative evaluation based of aforementioned Table 1 suitable solution for such application is supercapacitor. As major benefits of such technology long lifetime as well as fast power exchange are to be mentioned. Technology of supercapacitors also known as double layer capacitors (DLC) are present for about 60 years and fit well in operating range between traditional capacitors and general batteries. Supercapacitors present orders of magnitude higher energy storage capabilities and good cycle stability compared to conventional capacitors. Another two features are the extremely high capacitance values, of the order of many thousand farads, and the possibility of very fast charges and discharges due to extraordinarily low inner resistance which are features not available with conventional batteries. Regarding maintenance

TABLE I. COMPARISON OF VARIOUS ENERGY STORAGE TECHNOLOGY PARAMETERS

	Li-Ion Batteries	**Super Capacitors**	**Flywheels**	**SMES**	**Fuel Cells**
Efficiency[%]	***70-90[5]***	***90-98 (current dependant) [4]***	***90-93[7]***	***95[7]***	***40-55[7]***
Power Range[W]	***1-1.5MW[6]***	***0.7-3MW [4]***	***10kW-800kW [3]***	***10-10MW [7]***	***10kW-2MW [8]***
Energy Range[Wh]	***0.01-150[5]***	***1-1500 [4]***	***300-5kWh [5]***	***1-150kWh***	***Continuous[8]***
Cycle Life	***2000[5]***	***1000000 [4]***	***10000 [7]***	***10000 [4]***	***Continuous[8]***
Charge Time	***hours[6]***	***Milliseconds [4]***	***Seconds [3]***	***Miliseconds [3]***	***Continuous[8]***
Capital Cost [$/kW]	***250[6]***	***150 [5]***	***300 [7]***	***300 [4]***	***1500 [8]***

and lifetime supercapacitors are suitable for operation over a wide temperature range and in diverse environments (hot, cold and moist). The lifetime reaches one million cycles (or ten years of operation) without any degradation, except for the solvent used in the capacitors whose disadvantage is that it deteriorates in 5 or 6 years irrespective of the number of cycles. They are environmentally friendly and easily recycled or neutralized. The efficiency is typically around 90 % and discharge times are in the range of seconds to hours. They can reach a specific power density which is about ten times higher than that of conventional batteries (only very-high-power lithium batteries can reach nearly the same specific power density), but their specific energy density is about ten times lower [9]. Supercapacitors have high capacity, but small nominal voltage values. Usually they are used with power electronics converters. In different applications are use different power electronics converters topologies. As example in electrical or hybrid vehicles are used converters with high power density usually it is dual-active bridge [10] or multilevel converter [11]. In application where efficiency is most important DC converters as buck-boost or similar [12] are preferred.

IV. Conventional AC System Model

As state of the art system conventional 3 phase AC supply grid architecture is considered thus modeling of proposed manufacturing equipment within such infrastructure is necessary. Model has been created according to architecture of Fig. 2.

A. AC Power grid

Typically power is delivered to manufacturing equipment from local 10kV medium voltage distribution grid. Reduction of voltage level to provide regular 3 phase 400V is realized by means of transformer. A typical 10/0.4kV distribution transformer data has been assumed with nominal power rating of 1MVA. Transformer performance under load conditions is characterized by impedance voltage expressed as percentage of nominal voltage during short circuit testing. Typical value for chosen transformer power rating is 4%. In order to create equivalent electrical circuit model considering AC grid transformer series inductance parameter for each phase is calculated according to (1)

$$L_k = (U_n^2 \cdot u_k) / (S_n \cdot \omega), \quad (1)$$

where ω is grid frequency in radians per second leading to 314 rad/s for 50Hz system, U_n represent nominal primary side voltage 10 kV in kV rating, u_k - impedance voltage, S_n – nominal power rating of transformer. Obtained series inductance L_k value applied in model is 1.27mH.

B. Diode bridge rectifier

Conversion of AC voltage to DC type supply for manufacturing equipment supply is usually realized by uncontrolled rectifiers utilizing diodes as semiconductor power devices as cheaper solution compared to controlled rectifiers with active semiconductor devices. Arrangement in 3 phase bridge circuit lead to utilization of 6 diodes per rectifier. In current model diode characteristics were set to be

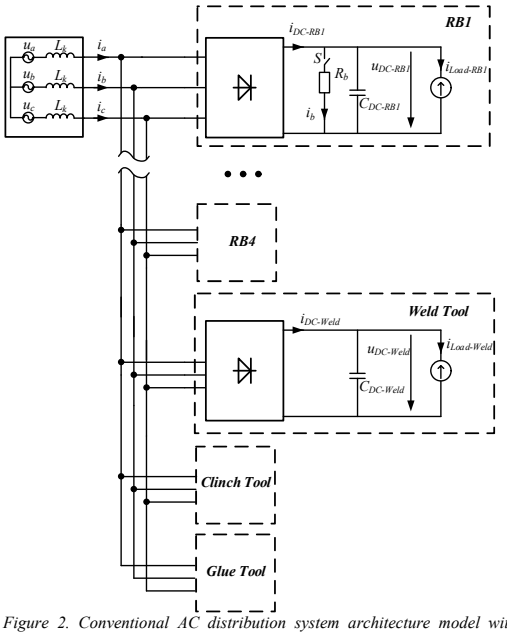

Figure 2. Conventional AC distribution system architecture model with exposed examples of robot (RB) and process load modelling subsystems

0.7V forward voltage drop and 3mΩ on state resistance. Natural rectification of diodes lead to rectified DC voltage level of 565V at no load conditions if 400V AC supply is present and unidirectional power flow from grid to load only.

C. Industrial Robot Electrical Model

Based on obtained load power time variations for reference production cycle each manufacturing equipment device considered is to be modelled as electrical load within electrical power supply system. Electrical model is combined of several subcomponents as presented in Fig 1. For example power flow variation of industrial robot RB1 subsystem is introduced as controlled current source drawing or feeding current $i_{Load\text{-}RB1}(t)$ from or to supply according to given load power time variation $P_{Load\text{-}RB1}(t)$ and instantaneous DC voltage $U_{DC\text{-}RB1}(t)$ according to (2)

$$i_{Load}(t) = P_{Load}(t) / U_{DC}(t), \quad (2)$$

where $P_{Load}(t)$ is respective load profile and $U_{DC}(t)$ instantaneous DC bus voltage for each of load elements being industrial robots RB1 to RB4. The respective DC power drawn from the supply system is obtained according to (3) and cover also the losses within intermediate DC circuit if they may appear

$$P_{DC}(t) = U_{DC}(t) \cdot i_{DC}(t). \quad (3)$$

In case of industrial robot brake chopper unit is applied since voltage can rise above rectified voltage by charging DC filter capacitor C_{DC} of 1.4mF capacitance that is applied in robot DC bus. The switch S is toggled between ON and OFF states according to hysteresis function of DC bus voltage U_{DC}. The upper limit of voltage hysteresis band is 680V when braking

resistor R_b of 11Ω is connected in parallel for discharging until voltage reaches lower threshold value of 660V when discharge process is stopped by opening switch *S*. Since electrical power is being dissipated during reduction of DC voltage respective current i_b in resistor is monitored as well.

D. Process Tool Electrical Model

For production tool electrical modelling same approach has been applied as for industrial robots with modification by removing braking resistor circuit since power flow is unidirectional with respective load current i_{Load} *(t)* always larger than 0 and thus the boosting effect of DC bus voltage is not present. Respective DC bus filter capacitor values are 15mF for welding tool and 1.4mF for both clinching and gluing tool modelling.

V. DC BASED DISTRIBUTION SYSTEM MODEL

Equivalent DC realization of previously introduced AC grid has been simulated according to following structure as presented in Fig.3. Two operational modes of DC system have been observed within this research: *DC System* is referred to power supply by single DC supply converter and *Balanced DC System* when energy storage functionality of supercapacitor is utilized. Balancing power reference for energy storage unit is calculated according to (4)

$$P_{balance}(t) = P_{av} - P_{tot}(t), \tag{4}$$

A. Supercapacitor storage unit

Supercapacitor storage unit with respective simplified interface converter model is created based on power balance in common DC bus and supercapacitor circuit (6)

$$P_{SC}(t) = U_{SC}(t) \cdot i_{SC}(t) = U_{DC}(t) \cdot i_{DC\text{-}SC}(t). \tag{6}$$

As basis for supercapacitor device set of 4 series connected Maxwell supercapacitor modules of 63F and 124V nominal rating each leading to total capacitance C_{SC} of 12.5F and series resistance R_{SC} of 0.1Ω. Supercapacitor current i_{SC} is limited to 260A for both charging and discharging operation. Supercapacitor voltage limitations for fully charged and fully discharged state are chosen to be 500V and 300V.

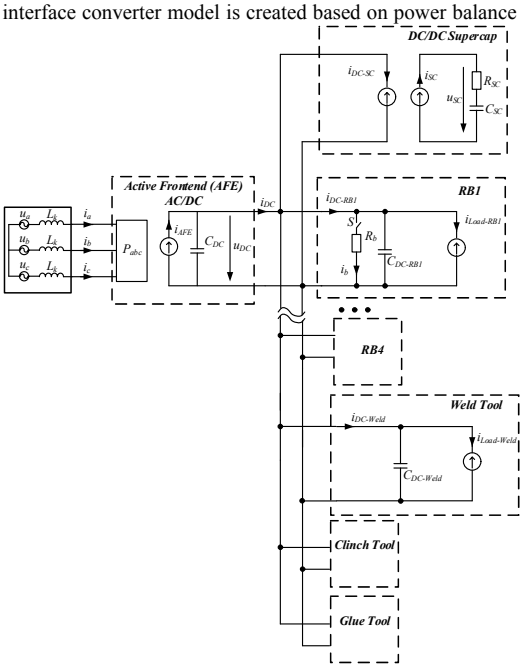

Figure 3. DC based electrical supply system model with AC/DC Active frontend converter (AFE) and DC/DC Supercapaitor storage unit

B. AC/DC Active Frontend model

One of core elements for substitution of AC based distribution system to common DC bus based energy supply is centralized AC/DC conversion stage. Since several individual diode rectifier bridges are eliminated thus reducing necessary installation resources role of central active frontend (AFE) converter is increasing for providing both stable DC voltage supply and meeting AC grid power quality needs. In considered DC system nominal DC voltage is set to be 600V. Implemented AFE model is based on balanced power principle as presented in (5)

$$P_{abc}(t) = U_{DC}(t) \cdot i_{AFE}(t), \tag{5}$$

where $P_{abc}(t)$ controlled symmetrical active power flow on AC grid side and multiplication of $U_{DC}(t)$ and $i_{AFE}(t)$ lead to equivalent power injection in common DC system. In order to maintain stable DC voltage of 600V the voltage controller of PI type has been developed measuring $U_{DC}(t)$ and providing necessary current $i_{AFE}(t)$ to stabilize the voltage over buffer capacitor C_{DC} with capacitance of 4.1mF. Designed controller model has been compared to measured voltage variation during stepwise load power variation between 0kW and 6.5kW with frequency of 2Hz as presented in Fig.4. Obtained controller gain parameters for PI parallel type controller are 1 for proportional gain and 200 for integral gain.

VI. SIMULATION RESULTS

A. Power and efficiency analysis

Table 2 represent results of variation of power and energy

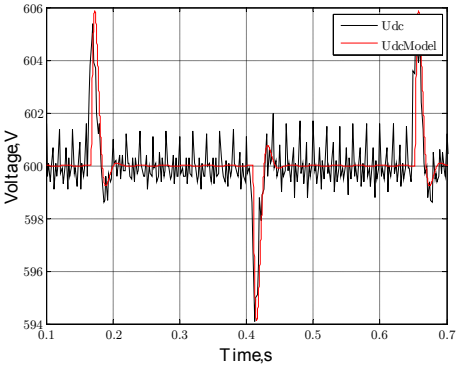

Figure 4. Comparison of available DC voltage measurement Udc and AFE simulation model performance UdcModel under step load variation of 6.5kW.

TABLE II. AVERAGE POWER COMPARISON

	Modelled operating mode		
	AC System	***DC System***	***Balanced DC System***
$P_{TotalAverage}$, kW	3.948	3.787	3.847
$P_{LossBraking}$, kW	0.161	0	0
P_{LossSC}, kW	n/a	n/a	0.061

consumption over one production cycle within 3 modelled systems: *AC system, DC system* and *Balanced DC system*. Quantity of of total average power supplied by rectifiers or central AC/DC converter within production cycle is $P_{TotalAverage}$. Total average loss power of industrial robot braking choppers $P_{LossBraking}$ is obtained from 4 industrial robot models with recuperation capabilities. In case of *Balanced DC system* average loss power of supercapacitor storage unit P_{LossSC} is obtained. Alternative supply system modification from AC to DC supply system present reduction of average consumed power of 4.07% and 2.56% for direct and balanced DC system respectively. Adding supercapacitor storage and considering capacitor losses efficiency improvement is obtained with respect to wasted braking energy in AC system. Operation of 4 involved robot braking resistance due to individual DC voltage boost is presented in Fig.5 typically after acceleration phases.

B. Power balancing performance on AC supply infrastructure

Due to high power load peaks of 140kW present during welding processes strong influence on AC grid is resulting in high current peak values and voltage dip. Fig. 6 and Fig. 7 present phase currents and voltages of AC grid.

1) AC Grid Current effects

In case of *AC system* peak values reach 400A value and current waveform is slightly distorted compared to ideal sinewave. In *DC system* case AFE converter is drawing peak currents of 500A with following oscillation transient due to

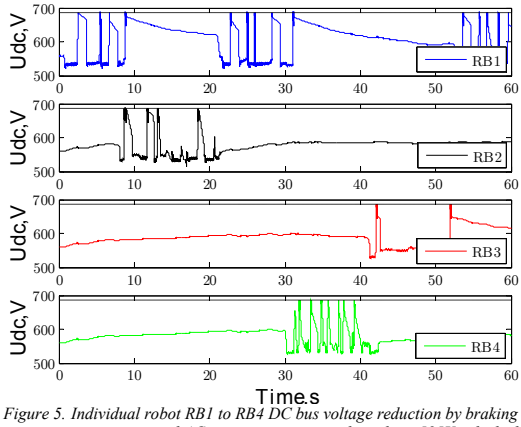

Figure 5. Individual robot RB1 to RB4 DC bus voltage reduction by braking resistance in conventional AC system operation, voltage limit 585V – dashed line.

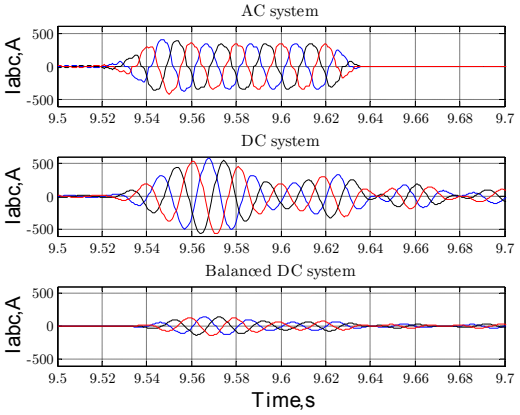

Figure 6. Set of load power time variations according to reference production cycle

voltage controller operation. In case of *Balanced DC system* power demand from AC grid is compensated from spercapacitor storage device thus phase peak currents are reduced significantly to the value of 150A while sinusoidal current waveform is consumed by AFE converter model. Such behavior is advantageous in case if several welding processes may be supplied instantaneously from common AC grid.

2) AC Grid Voltage effects

Similarly also the voltages in Fig. 7 utilizing conventional *AC system* with rectifiers lead to distorted waveforms with voltage dip reaching as low as 290V compared to peak values while no load voltage peak values are 325V. Improved voltage waveform is obtained by AFE converter application but lowest voltage dip of 210V is observed during transient operation for DC voltage control in direct supply *DC system* model. Introduced *Balanced DC system* present best performance in terms of voltage dip reaching smallest value of 315V.

3) Load side DC voltage effects

Fig.8 represent behavior of load side DC voltage during welding process

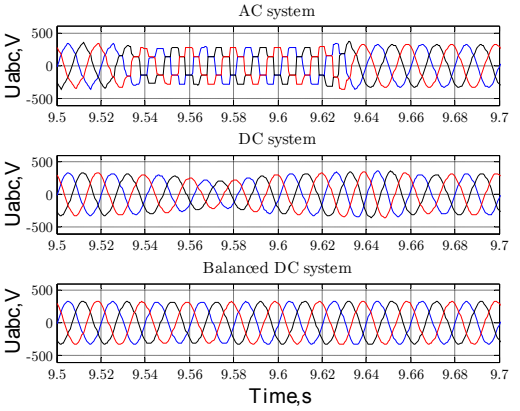

Figure 7. AC supply grid phase voltages of modelled systems: AC System, DC System and Balanced DC System.

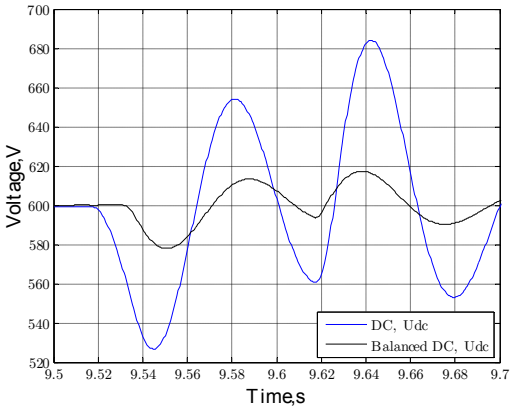

Figure 8. Load side DC voltage behavior during welding process.

Proposed DC supply system is based on approach of common DC bus interconnection for all electrical loads belonging to robotic manufacturing area. As nominal value 600V voltage has been chosen being also reference quantity for active frontend AC/DC converter voltage controller discussed before. Comparison for both operation modes *DC system* and *Balanced DC system* when AFE converter is controlling voltage during welding operation show that application of power balancing lead to reduction of common DC bus voltage fluctuations. Such approach also present alternative to prevent overdesign of AFE input converter and related investment effort. Necessity to provide full welding power capability as well as remaining supply power for other process loads present challenge for AFE converter with respect to thermal cycling effects of semiconductor based elements and related life time of equipment.

VII. Conclusion

This paper present performed analysis of electrical energy consumption reduction by modification of local electrical distribution system towards DC based electrical supply with additional power balancing option. Manufacturing process loads have been based on detailed industrial robot energy consumption models combined with process tool electrical loads typical to automotive production leading to local robotic manufacturing area electrical distribution system model. General model of active frontend type AC/DC converter has been presented and comparison to available measurement data has been done as well as modelling of supercapacitor based energy storage equipment being evaluated as suitable option for industrial application compared to set of alternative energy storage technologies. Introduction of common DC bus supply system present energy efficiency increase possibilities of up to 4.07% compared to conventional AC based local electrical distribution infrastructure and enable complete reduction of recuperated energy losses through braking resistor. Power balancing approach implementation based on supercapacitor storage is presented by simulation and promising results regarding peak loading reduction have been obtained. Such results may serve as basis for further research towards optimal utilization of existing AC grid infrastructure and reduction of overdesign related excessive resource utilization and investment. Based on presented results larger scale modelling is desirable covering major production as well as modification of developed simulation basis towards widely applicable evaluation method for modification or design purposes of future industrial distribution infrastructure.

References

[1] D. Meike, M. Pellicciari, G .Berselli, “Energy Efficient Use of Multirobot Production Lines in the Automotive Industry: Detailed System Modeling and Optimization,” IEEE Transactions on Automation Science and Engineering, vol. 11, Issue: 3, 2014, pp. 798-809.

[2] D.Meike and L.Ribickis,“Energy efficient use of robotics in the automobile industry,” in Proc.IEEE 15th Int. Conf. Advanced Robot., 2011, pp. 507–511

[3] D. Meike, A Senfelds, L Ribickis, “Power converter for DC bus sharing to increase the energy efficiency in drive systems,” in 39th Annual Conference of the IEEE Industrial Electronics Society, IECON 2013, pp. 7199 – 7204.

[4] Maxwell Technologies website, http://www.maxwell.com/, Acessed on 18.03.2015

[5] Digikey website, www.digikey.com, Acessed on 18.03.2015

[6] Abbas A Akhil, Georgianne Huff, Aileen B. Currier ,”SANDIA Report SAND2013 5131 Unlimited Release July 2013 DOE/EPRI 2013 Electricity Storage Handbook in Collaboration with NRECA”,2013,Sandia National Laboratories,USA.

[7] IEC White Paper: Electrical energy storage, http://www.iec.ch/whitepaper/energystorage/?ref=extfooter

[8] D. Connolly, “An investigation into the energy storage technologies available, for the integration of alternative generation techniques”,CPI,2007,52 pp.

[9] von Jouanne, A.; Enjeti, P.N.; Banerjee, B., "Assessment of ride-through alternatives for adjustable-speed drives," IEEE Transactions on Industry Applications, vol.35, no.4, pp.908,916, Jul/Aug 1999

[10] Amjadi, Z.; Williamson, S.S., "Prototype Design and Controller Implementation for a Battery-Ultracapacitor Hybrid Electric Vehicle Energy Storage System," IEEE Transactions on Smart Grid, vol.3, no.1, pp.332-340, March 2012

[11] Tao, H.; Kotsopoulos, A.; Duarte, J.L.; Hendrix, M.A.M., "A Soft-Switched Three-Port Bidirectional Converter for Fuel Cell and Supercapacitor Applications," PESC '05 IEEE 36th Power Electronics Specialists Conference, 2005. ,vol., no., pp.2487-2493, 16-16 June 2005

[12] Rufer, A.; Hotellier, D.; Barrade, P., "A supercapacitor-based energy storage substation for voltage compensation in weak transportation networks," IEEE Transactions on Power Delivery, vol.19, no.2, pp.629-636, April 2004

Appendix 13

Apse-Apsītis, P., **Šenfelds, A.**, Avotiņš, A., Paugurs, A., Priedītis, M. Power Measurement and Data Logger with High-Resolution for Industrial DC-Grid Application. *Power Electronics and Applications (EPE'17 ECCE Europe), 2017 19th European Conference on*, 2015, Vol. 9, pp.36-42. ISSN 2255-9140. e-ISSN 2255-9159.

DOI:10.1515/ecce-2015-0010

DE GRUYTER OPEN

Electrical, Control and Communication Engineering doi: 10.1515/ecce-2015-0010

2015/9

Power Measurement and Data Logger with High-Resolution for Industrial DC-Grid Application

Peteris Apse-Apsitis (*Lead Researcher, Riga Technical University*), Armands Senfelds (*Researcher, Riga Technical University*), Ansis Avotins (*Researcher, Riga Technical University*), Arturs Paugurs (*PhD student, Riga Technical University*), Marcis Prieditis (*PhD student, Riga Technical University*)

***Abstract* – Power and energy measurement and monitoring is a key factor for many industries in terms of energy and cost efficiency evaluation. Due to trends of Smart Grid concept application in industrial environment, including decentralized DC-Grid implementation, for precise evaluation – faster and low-cost measurement equipment is needed. Manufacturing industry widely uses industrial robots that have dynamic load characteristics for which faster measurement equipment is needed.**

This paper gives a brief description of the developed power measurement equipment, its structure and interconnection with industrial Profinet network. Further as a testing method steady state and dynamic loads are selected and analyzed. For testing, specially created industrial DC-Grid testing environment and equipment was used. Testing results show that the selected method and idea is working and is able to measure dynamic loads with high resolution. For other industrial load types there is a discussion going on about the issue of how detailed the resolution is needed in industrial SmartGrids, as energy forecast is a new trend in robotic industry and manufacturing planning.

***Keywords* – Smart Grids; Industrial power systems; Power measurement.**

I. Introduction

Emerging trends towards intensive enhancement of electrical power supply systems for integration of new types of electrical power generation solutions, extensive power and related operating information flow management and intelligent utilization of electrical infrastructure can be summarized as Smart grid. The existing power distribution system is AC based, but with Smart Grid concept, and DC source integration to the AC grid raises the question of DC-Grid implementation feasibility, where some preliminary research shows advantages of DC-Grid implementation [1]. Some studies show that the powering equipment from AC or DC based equivalent power source in home or office application [2]–[4] the DC-Grid is more efficient due to the fact that less conversion stages are used and the improved network quality.

In Smart Grid context electric car or intelligent battery energy storage system [5] can be consumer or producer generally referred as term - prosumer in several articles [6]–[9], by means that regenerative braking energy can be stored and re-used on demand. Integration of such new power sources in Smart Grid creates not only a problem of safety issues such as fast DC circuit breakers [10] and over current protection [11], but also the need for fast and cheap energy flow control instruments for distributed power metering and monitoring applications [12], [13]. The ability to obtain data on instantaneous power consumption or generation is crucial for operation of any higher level system. Since many power consumer devices today can be referred to as smart or advanced electromechanical devices, regardless of their task or operation principles, it could be said that they are based on one or several electro-technological molecules as presented in Fig. 1.

II. Target System Structure

The same is true also for electric smart grids, regardless of their size, where actuators can be seen as power generating units and sensors provide information about power flow. Various enabling technologies are already available on the market, considering methods of data transmission within power system, including embedded power line communication systems, various telecommunication standards and industrial communication protocols. By increasing the share of power measurement equipment units within power systems, in respect to existing setups of nowadays, such parameters as reliability, self-consumption and investment costs have significant role in decision making of major installation of such devices. New developments along with existing AC distribution system approach considering DC power supply in various applications present the demand for adaptation of existing power measurement equipment. The practical application of power meter unit has been done considering industrial DC microgrid as a case study scenario of intelligent power supply system.

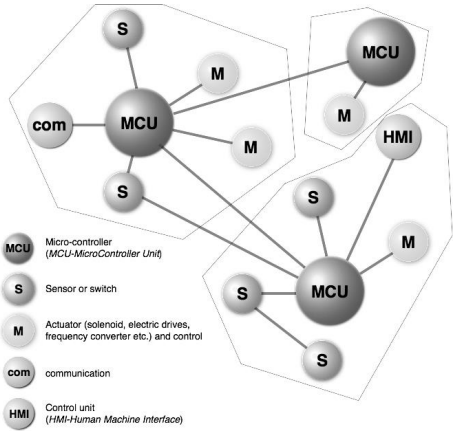

Fig. 1. Visual example of electro-technological molecule structure.

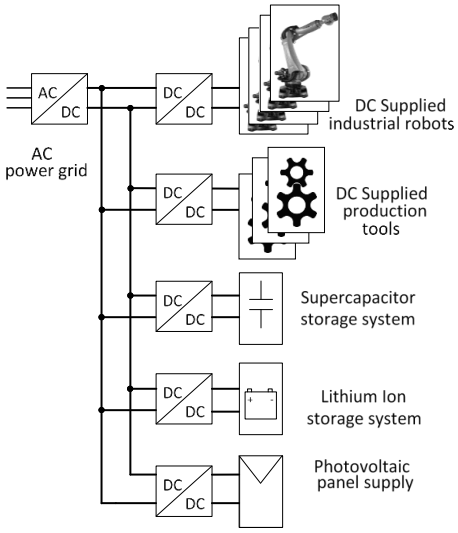

Fig. 2. Example of industrial DC microgrid structure

The concept of such innovative electrical infrastructure has been developed within AREUS project [14] considering 600 V DC voltage based energy distribution, recuperation, storage and exchange operation within manufacturing application. The principal structure of such system is presented in Fig. 2.

A lot of electrical energy consumers or sources operate on DC-Grid. AC/DC or DC/AC converters make it possible to use them also in AC environment. Energy storage devices like super capacitors, batteries, hydrogen cells, etc. allow to store and re-use energy and are designed for DC applications. Such devices are connected to the DC or AC grid via unidirectional or bidirectional energy flow converters. In order to control energy flow this equipment directly points out the necessity to know energy and power values – instantly or in milliseconds, for correct and effective converter and stable power-grid operation. Moreover, simultaneous energy flow monitoring near DC microgrid consumers and energy sources as well as AC grid allow to determine system efficiency and evaluate the weak points of the system from the energy flow point of view. The abovementioned allows making changes in the device workflow in order to increase its efficiency, if possible or necessary. Potential application for intelligent system power flow balancing for manufacturing process is presented in [15].

III. Measurement System Development

Energy measurement device can be seen as a system combined of a set of several subsystems designed for specific tasks. The workflow of energy measurement device can be divided into a sequence of acquisition of electrical quantity, evaluation and information flow within communication infrastructure. In the particular case communication within industrial protocol Profinet was advantageous since application is within automated manufacturing industry case.

A. Suggestions on Electrical Energy Measurement

Typically energy consumption calculations are based on instant power values, especially if consumer generates non-sinusoidal current form. Instant current and voltage value readings (samples) are made and following multiplication is used to calculate instant power, average power or consumed energy [16], [17]. Sampling rate must be at least 4.2 kHz or 42 samples per 1/2T according to standard EN 61000-3-2 [21] and Nyquist frequency.

Active and reactive power measurements and calculations is a continuous dispute between scientists for non linear (or non sinusoidal) waveforms. In general, for power analysis two main approaches exist, where one is Budeanu's definition based on current and voltage value harmonic parameters (1), or Fryze's definition (2) based on voltage and current RMS (Root Mean Square) values, calculating power by active and reactive component values.

$$P = U_0 I_0 + \sum_{n=1}^{\infty} U_n I_n \cos\varphi_n; \quad Q = \sum_{n=1}^{\infty} U_n I_n \sin\varphi_n \tag{1}$$

$$\lambda = \frac{P}{S} = \frac{\frac{1}{T}\int_0^T ui\,dt}{\sqrt{\frac{1}{T}\int_0^T u^2 dt}\sqrt{\frac{1}{T}\int_0^T i^2 dt}} \tag{2}$$

Another method is the averaging of voltage and current values via multi-order delta-sigma modulation and the following multiplication [18]. Thus electrical energy measuring and monitoring device installation near every consumer or generator is very expensive. Several methods are proposed to lower the costs, for example [19], [20], in order to achieve widespread installations of electrical energy measuring/monitoring devices. The main disadvantage is the necessity of separate low power source for measuring IC's power feed and resulting increase in measuring device self-consumption. Moreover, high speed analog-digital converters read grid noise (and generate sampling noise by themselves) and high order filtering must be applied for correct results.

Thus there is a difference between AC and DC energy measurements due to AC and DC environment difference (e.g. power factor existing in AC grid and not existing in DC grid), especially if bi-directional energy flow takes place.

Non-even sampling energy consumption measuring method was proposed to overcome the abovementioned disadvantages. The method allows measuring of bi-directional AC or DC energy flow, design low self power consumption devices and perform measurements down to every 10 ms for DC grids or 20 ms for AC grids or several grids for simultaneous readings.

B. Non-even Sampling Method

According to non-even sampling method [16] the amount of consumed or generated electrical energy during the pre-defined period of time is directly proportional to the sum of current samples over this time multiplied by voltage-frequency

transfer coefficient, if current sampling rate is modulated by applied voltage value (Fig. 3).

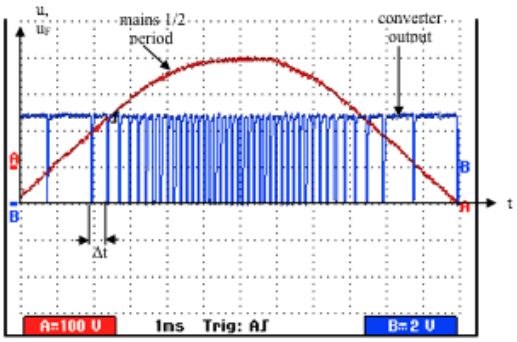

Fig. 3. Example of voltage dependent sampling rate operation.

Converters do not utilize any transformers or voltage dividers and are electrically isolated from micro-controller circuit.

C. Industrial Protocol Selection and Integration

There are various industrial communication protocols and their evaluation [22], [23], but Profinet IO is the leading standard for industrial communication, as it is simple in use and installation, and implementation of PROFIenergy [24] gives benefit in terms of energy monitoring and evaluation. It can be configured to deliver data from one device to another in 1 ms or faster (Isochroous Real Time Profinet IO) [25]. PM (Power Moidule) is connected to Profinet IO via Anybus CompactCom (AnybusCC) module from HMS. This module enables the developer of the embedded system to connect to Profinet IO without advanced knowledge of functionality of Profinet IO.

Data cables in Profinet system are normally made of copper wires. And 100 m cable can be crossed by 1 bit in 0.5 µs. Bridge delay (delay present in switch) depends on conformance type of Profinet IO and its maximum value can be from 3 µs (IRT) to 10 µs (RT). Time of package transmission from the device depends on the length of telegram. If the telegram which consists of 84 bytes is sent (shortest possible Ethernet telegram) then 6.72 µs are necessary. If telegram is 1538 bytes long then the transmission time is 123.04 µs [26]. For example, if data has to cross 4 switch devices and wire connections are 100 m long (Fig. 4) and the shortest Ethernet packet is used then data transmission time can be calculated as shown in (3):

$$4 \cdot (10\ \mu s + 5.0\ \mu s) + 72.6\ \mu s = 132\ \mu s \qquad (3)$$

Time that is needed for data to arrive from AnybusCC to PLC in case of RT Profinet IO configuration, 1 switch, 100 m long connecting wire and telegram size of 1538 bytes should not exceed 0.5 + 10 + 123.04 = 133.54 µs. Another part of circuit that introduces delay is PM data sending to AnybusCC. The fastest and most complex) is the parallel connection to AnybusCC. That would result in approximately 30 ns long delay time [27]. By summing up all possible delay times it can be estimated that total delay of data is shorter than shortest possible bus-cycle time – 250 µs (IRT Profinet IO), which does not present critical influence on system functionality. In one second data from one PM to PLC can be sent 1 s/250 µs = 4000 times, with largest possible delay of 133.54 µs.

IV. Experimental Setup and Measurement Methods

Verification of the developed active power measurement system has been realized within industrial DC microgrid operation with nominal voltage of 600 V (Fig. 5).

The central element of DC microgrid supply is the common AC/DC interface converter (1) of nominal power 55 kW for bidirectional power flow operation with common current sensing technology available in industry, but keeping in mind that it is also possible to use sensorless topologies as described in [28]. The converter performs the task of stable 600 V voltage supply on DC circuit of microgrid. The AC side power flow is controlled for power factor correction and current harmonic reduction by means of applied passive filter unit.

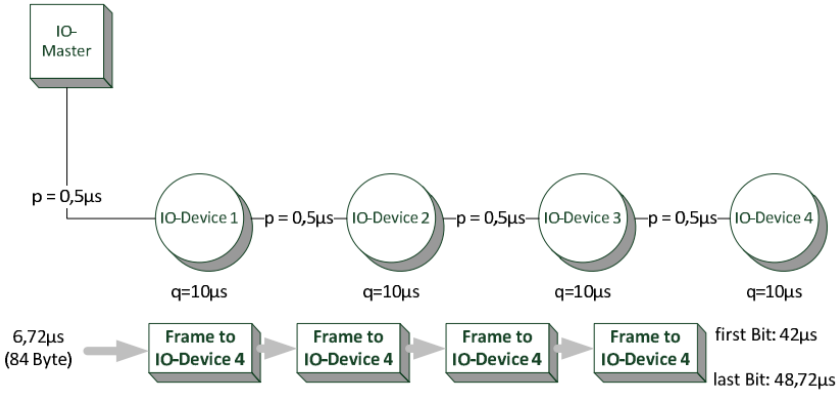

Fig. 4. Calculation of data transmission time.

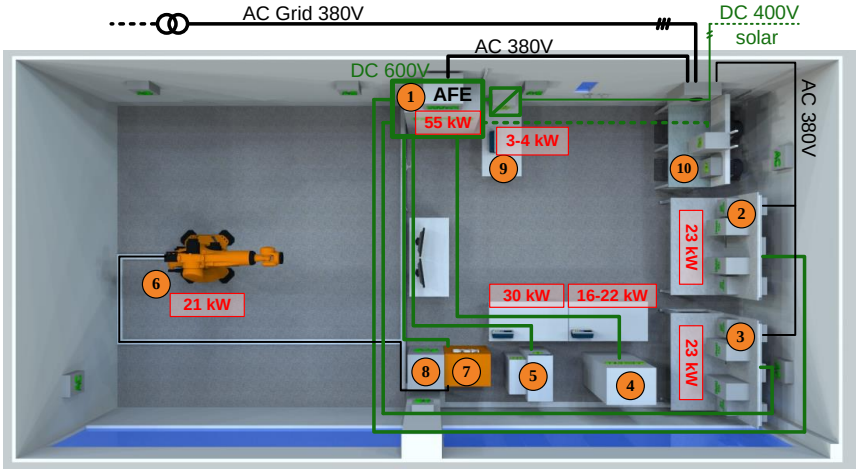

Fig. 5 Experimental verification laboratory hardware testing layout of industrial DC-Grid infrastructure.

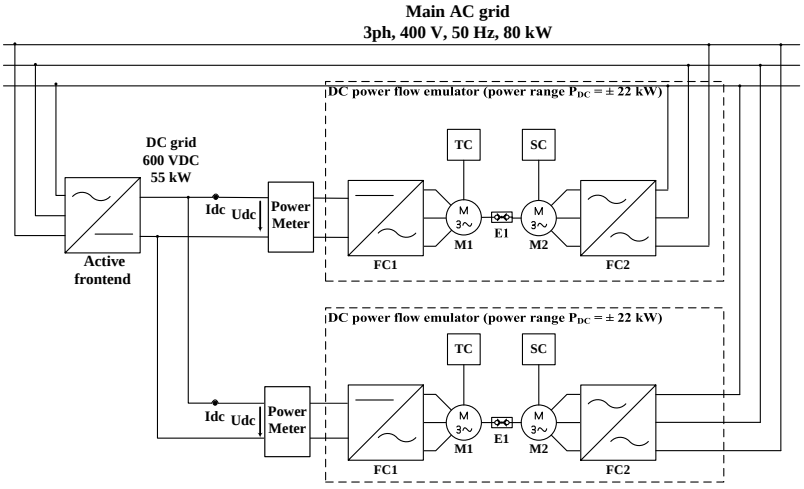

Fig. 6. Structure of DC testing system and measurement points.

The power flow within DC microgrid is enabled by means of drive stand units for power flow emulation (2 and 3). The power range of each of power emulator unit is within 22 kW for both consuming and regenerating energy into common DC microgrid. Such equipment has been designed in order to replicate various power consumption profiles that appear in industrial manufacturing operations taking also possible potential of recuperated energy to be reused within common DC power grid. The operating power profiles applied for dynamic verification of power meter equipment were obtained from industrial robotic manufacturing application. The setup for DC system testing with 2 dynamic power loads is presented in the schematic (Fig. 6).

As shown in Fig. 5, for future testing it is planned also to use other load types, such as solar panel DC/DC converters (9), Lithium-ion battery energy storage system (4), supercapacitor energy storage system (5), and also a 600 V DC powered industrial robot prototype (6) controlled by robot controller (7) and industrial cell Master PLC controller (8), as well as wind generator (PMSG) (10) driven by AC motor can be used as testing object.

For laboratory measurements three tests were created and measured under steady state load, dynamic load (real robot consumption profile), and the comparison with data was obtained through Profinet network.

The developed power measurement hardware testing prototype is shown in Fig. 7 where it has measurement module [12], [13] with two communication outputs, where AnyBus module is devoted to Profinet communication with Programmable Logic Controller and additional optical circuit

is for communication and data transfer to personal computer. The device is powered from 24 V_{DC} voltage, voltage measurements can be done in the range of 200 – 700 V_{DC} and nominal is 600 V_{DC}, current measurements in the range +/−70 A, max measurement resolution is 1ms, but nominal resolution is 20 ms.

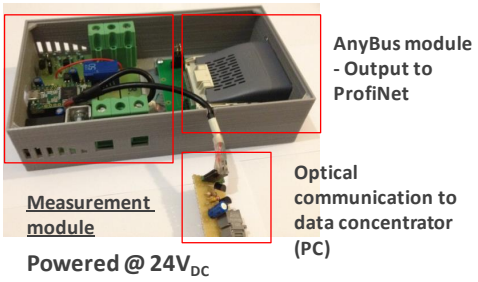

Fig. 7. Developed power measurement hardware testing prototype.

The novel power measurement equipment was compared to the existing laboratory grade Newtons N4L power analyzer with power measurement functionality. In order to verify any existing deviation of the obtained data extracted by means of power measurement prototype with respect to existing and calibrated equipment by manufacturer N4L, model PPA3340 data was collected at steady state operation within power range of 18 kW recuperating to 20 kW consumption, by means of parallel measurements.

In order to evaluate dynamic response of power meter prototype the electrical quantities of voltage and current was obtained by means of oscilloscope along with direct power measurement of measurement device. In this case a motor drive based system (see Fig. 6) was used to test the AREUS DC power meter. The system can dynamically control the DC power flow in both consumption and generation modes within its respected power boundaries of −22 kW to +22 kW.

The power flow control is realized by dynamically changing the torque of an asynchronous machine, whilst keeping its rotational speed constant (4).

$$P_{DC} \approx T \cdot \omega \tag{4}$$

where

P_{DC} power measured at the DC bus of the frequency converter driving the asynchronous machine;

T mechanical torque;

ω rotor angular velocity.

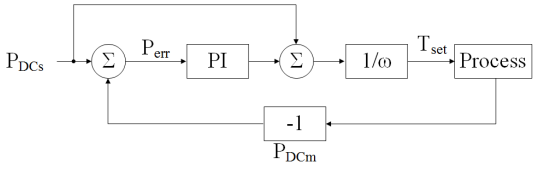

Fig. 8. Block schematic of the motor drive system's power flow control loop.

$$T_{set} = \left(P_{err} \cdot W_{PI} + P_{DCs}\right) \cdot \frac{1}{\omega} \tag{5}$$

where

T_{set} the set torque value;

P_{err} the difference between the set and the measured DC power;

W_{PI} the transfer function of a parallel PI regulator;

P_{DCs} the set power value.

AREUS DC power meter is implemented in the feedback loop of the system's power flow controller (Fig. 8), which enables the inclusion of various regulation methods, thus optimizing the system's performance. The control method used in equation (5) enables 100 % precise recreation of a real industrial robot electrical load (consumption profile), thus giving real-life dynamic testing environment for power measurement device.

PROFINET Data acquisition network structure and functionality of CMs (communications module) has been tested in the line structure of Profinet IO network (Fig. 9).

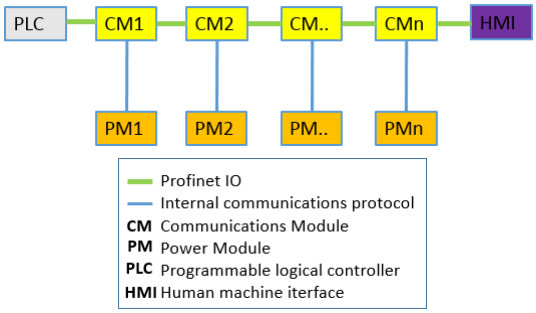

Fig. 9. Line structure of Profinet IO network.

The structure is possible because the Profinet IO 2-Port Plug-In Module (AnybusCC) has a built in switch. For tests, CM in conjunction with PM has been used, which is dedicated to measure power at the nodes of DC busses of industrial robots. As a PLC has been used CPU 1212C from Siemens, IR Profinet IO standard and for visualization of system functionality Siemens TIA portal integrated plotting tool has been used and afterwards data has been extracted and formatted with MS Excel (Fig. 12).

V. Experimental Results and Analysis

The novel DC power meter was connected in series between the AFE 600 VDC output and the motor drive system's DC input and measured the momentary DC power values. Two types of verification experiments were performed. In the first case the dynamic power flow of an industrial robot was emulated with the motor drive system. The DC power meter's averaging time was set to 15 ms. As a comparison, the DC power was measured with Rigol DS1104Z oscilloscope, using PROSyS CP 35 current probe and Tektronix P5200 differential voltage probe. The logged data from both measuring devices are summarized in Fig. 10.

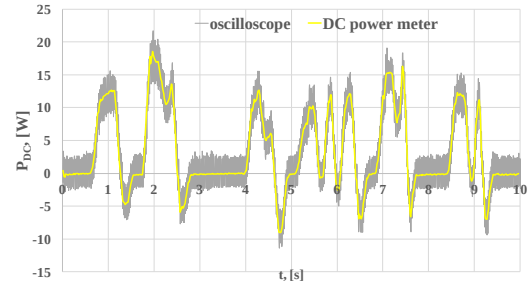

Fig. 10. The first case: dynamic power flow measurements from the novel DC power meter and the Rigol DS1104Z oscilloscope.

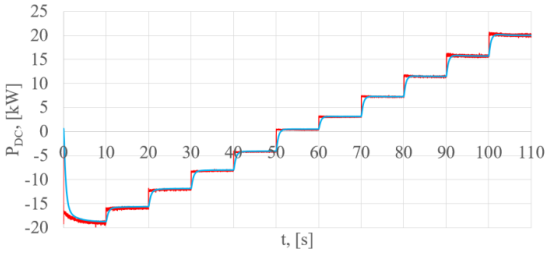

Fig. 11. The second case: constant power steps throughout the motor drive system's power range. Measurements from the novel DC power meter (red line) and the N4L PPA5530 power analyzer (blue line).

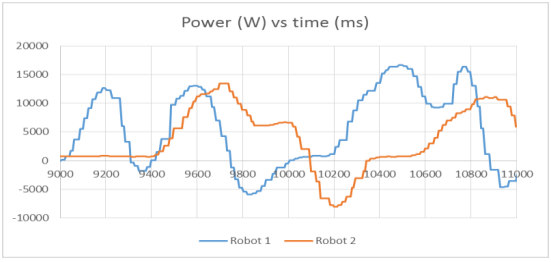

Fig. 12. Instant power consumption of two simultaneously working robots acquired through Profinet.

TABLE I

RELATIVE DEVIATION OF THE NOVEL DC POWER METER IN COMPARISON WITH THE N4L PPA5530 POWER ANALYZER

P_{DC} (DC power meter), [W]	Deviation, [%]
−18974.84	1.44 %
−15920.19	1.32 %
−12037.49	1.32 %
−8169.73	1.97 %
−4203.16	3.06 %
415.60	21.16 %
3061.77	3.22 %
7261.49	0.99 %
11491.05	0.69 %
15798.17	0.86 %
20131.46	0.84 %

In the second case verification tests were performed by applying constant power values throughout the motor drive system's power range (Fig. 11). In this case, the novel DC power meter measurements were compared with data from N4L PPA5530 power analyzer (voltage measurement – internal, current measurement with HF100 current shunt). The PPA5530 was set to DC coupling, 5 Hz filtering. Acquisition window was set to 15 ms.

VI. CONCLUSION

In both steady and dynamic testing cases the developed power measurement equipment shows very fast, precise and stable measurements that are even faster than N4L PPA5530 power analyzer. The measurement deviation in work range is within acceptable range.

Implementation of optical communication interface allows stable real-time measurement data transmission to the personal (PC) computer database, thus eliminating connection problems to PC due to various electromagnetic interference (EMI) radiations, caused by typical industrial equipment.

CM working speed is fast enough to replicate power curves of industrial robots, although PM is not connected directly to AnybusCC by parallel connection, but through one intermediate node and serial connections.

Next measurements should be done in other non-linear load situations and compared against the measurements done with faster and more precisely calibrated equipment. In case Profinet and PLCs are used, there is a discussion about the time resolution for dynamic loads and PLC ability to send the necessary data. At these testing loads, the 20 ms resolution is enough for energy calculation, but more load types should be tested to validate this approach of energy forecast.

Equipment testing within industrial application case is foreseen for determination of optimal functionality followed by price estimation for the prototype modified for typical electronic equipment production process.

ACKNOWLEDGEMENT

This research is supported by Latvian National Research Programme project LATENERGI.

REFERENCES

[1] D. J. Hammerstrom, "AC Versus DC Distribution SystemsDid We Get it Right?" in *Power Engineering Society General Meeting, 2007. IEEE*, pp. 1–5, 24–28 June, 2007. http://dx.doi.org/10.1109/pes.2007.386130

[2] A. Sannino, G. Postiglione, M. H. J. Bollen, "Feasibility of a DC network for commercial facilities," IEEE Trans. Ind. Appl., vol. 39, no. 5, pp. 1499–1507, Sept.–Oct. 2003. http://dx.doi.org/10.1109/TIA.2003.816517

[3] D. Deaconu, A. Chirila, M. Albu, L. Toma, "Studies on a LV DC network," in *2007 European Conf. on Power Electronics and Applicat.*, 2–5 Sept. 2007, pp. 1–7. http://dx.doi.org/10.1109/epe.2007.4417634

[4] K. Techakittiroj, V. Wongpaibool, "Co-existance between AC-Distribution and DC-Distribution: In the View of Appliances," in *2nd Int. Conf. on Comput. and Elect. Eng., 2009*, ICCEE '09., 28–30 Dec. 2009, vol. 1, pp. 421–425. http://dx.doi.org/10.1109/iccee.2009.85

[5] *Tesla Home Battery "Powerwall" system* [Online]. Available: https://www.teslamotors.com/powerwall [Accessed: 27.12.2015].

[6] R. W. De Doncker, "Future DC Grid Technology for more Decentralized Power Production and Renewable Power Supplies," presented at the *IEEE PEDG2012 conference*, 28 June 2012.

[7] S. Grijalva, M. U. Tariq, "Prosumer-based smart grid architecture enables a flat, sustainable electricity industry," in *2011 IEEE PES Innovative Smart Grid Technologies*, ISGT, pp. 1–6, 17–19 Jan. 2011. http://dx.doi.org/10.1109/isgt.2011.5759167

[8] S. Grijalva, M. Costley, N. Ainsworth, "Prosumer-based control architecture for the future electricity grid," in 2011 IEEE Int. Conf. on Control Applications, CCA, pp. 43–48, 28–30 Sept. 2011. http://dx.doi.org/10.1109/cca.2011.6044467

[9] F. Khoucha, M. Benbouzid, Y. Amirat, A. Kheloui, "Integrated energy management of a plug-in electric vehicle in residential distribution systems with renewables," in *2015 IEEE 24th Int. Symp. on Ind. Electron.*, ISIE, pp. 717–722, 3–5 June 2015. http://dx.doi.org/10.1109/isie.2015.7281557

[10] J. Yang, "Protection issue discussion of DC network development: Circuit breaker or fault-tolerant converter," in *Developments in Power Systems Protection, 2012*. DPSP 2012., pp. 1–6, 23–26 April 2012. http://dx.doi.org/10.1049/cp.2012.0085

[11] M. E. Baran, N. R. Mahajan, "Overcurrent Protection on Voltage-Source-Converter-Based Multiterminal DC Distribution Systems," *IEEE Trans. Power Delivery*, vol. 22, no. 1, pp. 406–412, Jan. 2007. http://dx.doi.org/10.1109/TPWRD.2006.877086

[12] P. Apse-Apsitis, A. Avotins, L. Ribickis, "A different approach to electrical energy consumption monitoring," in *2014 16th European Conf. on Power Electron. and Applicat.*, EPE'14-ECCE Europe, pp. 1–5, 26–28 Aug. 2014. http://dx.doi.org/10.1109/epe.2014.6910970

[13] P. Apse-Apsitis, A. Avotins, L. Ribickis, "Bidirectional DC/AC energy flow measurement," in *2015 IEEE 5th Int. Conf. on Power Engineering, Energy and Electrical Drives*, POWERENG, pp. 465–468, 11–13 May 2015. http://dx.doi.org/10.1109/powereng.2015.7266362

[14] M. Pellicciari, A. Avotins, K. Bengtsson, G. Berselli, N. Bey, B. Lennartson, D. Meike, "AREUS — Innovative hardware and software for sustainable industrial robotics," in *2015 IEEE Int. Conference on Automation Science and Engineering*, CASE, pp. 1325–1332, 24–28 Aug. 2015. http://dx.doi.org/10.1109/coase.2015.7294282

[15] A. Senfelds, M. Vorobjovs, D. Meike, O. Bormanis, "Power smoothing approach within industrial DC microgrid with supercapacitor storage for robotic manufacturing application," in *2015 IEEE Int. Conf. on Automation Science and Engineering*, CASE, pp. 1333–1338, 24–28 Aug. 2015. http://dx.doi.org/10.1109/coase.2015.7294283

[16] *Atmel AVR1631: Single Phase Energy Meter using XMEGA A*, Available: http://www.atmel.com/images/doc42039.pdf

[17] P. Apse-Apsitis, A. Avotins, L. Ribickis, "System and Method for Monitoring Real Power Consumption," in International patent application WO 2013/093554 A1, published 27.06.2013

[18] S. T. English, "A Low Cost Watt-Hour Energy Meter Based on the ADE7757," Available: http://www.analog.com/static/imported-files /application_notes/AN-679.pdf

[19] P. Apse-Apsitis, A. Avotins, L. Ribickis, J. Zakis, "Development of Energy Monitoring System for Smart Grid Application," in *3rd IFIP WG 5.5/SOSOLNET Doctoral Conference on Computing, Electrical and Industrial Systems, DoCEIS 2012, Costa de Caparica, Portugal, 2012 Proceedings*, Springer Berlin Heidelberg, New York, ISSN 1868-4238, ISBN 978-3-642-28254-6, pp. 347–354. http://dx.doi.org/10.1007/978-3-642-28255-3_38 b

[20] P. Apse-Apsitis, A. Avotins, L. Ribickis, "Concept of Low-Cost Energy Monitoring System for household Application," in *Proc. ELMAR-2011*, Zadar, Croatia, pp. 149–152, ISBN: 978-953-7044-12-1.

[21] *Harmonic Current Emissions*, Guidelines to the standard EN 61000-3-2, Available: http://www.epsma.org/pdf/PFC20Guide_November202010.pdf

[22] E. Bassi, F. Benzi, L. Lusetti, G. S. Buja, "Communication protocols for electrical drives," in *Proc. of the 1995 IEEE IECON 21st Int. Conf. on Ind. Electron., Control, and Instrumentation*, 6–10 Nov 1995, vol. 1, pp. 706–711. http://dx.doi.org/10.1109/iecon.1995.483494

[23] Siegfried, C.; Constantin, R.; Stancescu, S., "Evaluation of protocol for industrial informatics systems," in *2010 8th Int. Conf. on Commun.*, COMM, 10–12 June 2010, pp. 293–296. http://dx.doi.org/10.1109/iccomm.2010.5509109

[24] PI Whitepaper "The PROFIenergy profile", March 2010, PROFIBUS Nutzerorganisation e.V.(PNO), Available: http://www.profibus.com/download/brochures-white-paper/

[25] P. Ferrari, A. Flammini, D. Marioli, A. Taroni, "Experimental evaluation of PROFINET performance," in *Proc. 2004 IEEE Int. Workshop on Factory Commun. Systems*, 22–24 Sept. 2004, pp. 331–334. http://dx.doi.org/10.1109/wfcs.2004.1377739

[26] H. Bernhard, J. Mottok, "Real-time Behaviour of Ethernet on the Example of PROFINET".

[27] Hardware Design Guide, *Anybus® CompactCom M40*, Doc.Id. HMSI-216-126 Rev. 1.40.

[28] A. Suzdalenko, "Current Sensorless Control of Front-end Bidirectional AC/DC Converter Based on Half-bridge Topology," *Electrical, Control and Communication Engineering*, vol. 4, pp. 19–25, 2013. http://dx.doi.org/10.2478/ecce-2013-0017

Peteris Apse-Apsitis, Dr. sc. ing., is a Lead Researcher with the Institute of Industrial Electronics and Electrical Engineering, Riga Technical University.
His main fields of scientific and research interests are connected with power electronics, robotics and mobile ICT applications.
He is the author of many industrial solutions and applications and patented inventions.
He is a member of IEEE Latvia Association.
Address: Azenes Street 12/1, LV-1048, Riga
E-mail: Peteris.Apse-Apsitis@rtu.lv Phone: +371 67089919

Armands Senfelds is a PhD student and a researcher with the Institute of Industrial Electronics and Electrical Engineering of Riga Technical University. His research interests include design and control of power electronic equipment, electrical drives and electrical mobility.
Address: Azenes Street 12/1-524, Riga, LV-1048, Latvia.
E-mail: armands.senfelds@rtu.lv

Ansis Avotins is a PhD student with the Faculty of Power and Electrical Engineering. His main field of study is autonomous LED lighting systems. Since 2004, he has been a Chief Laboratory Manager of IEEI, RTU. He is a member of IEEE and ACM associations.
Address: Riga, Azenes Street 12/1-507, LV-1048.
E-mail: ansis.avotins@rtu.lv
Phone: +371 67089919

Arturs Paugurs is a PhD student with the Faculty of Power and Electrical Engineering of Riga Technical University. His research interests are industrial DC power distribution systems, power flow control and DC safety applications. Since 2013, he has been a research assistant with IEEI, RTU. He is a member of IEEE Industry Applications Society.
Address: Azenes Street 12/1-524, Riga, LV-1048, Latvia.
E-mail: arturs.paugurs@rtu.lv

Marcis Prieditis is a PhD student with the Faculty of Power and Electrical Engineering of RTU. He is currently a member of research team working on efficiency improvement in industrial robotics.
He is a researcher and lecturer with the Institute of Industrial Electronics and Electrical Engineering of RTU.
He is a member of IEEE Industry Applications Society.
Address: Azenes Street 12/1-524, Riga, LV-1048, Latvia.
E-mail: marcis.prieditis@rtu.lv

Appendix 14

Šenfelds, A., Paugurs, A. Electrical Drive DC Link Power Flow Control with Adaptive Approach. In: *2014 55th International Scientific Conference on Power and Electrical Engineering of Riga Technical University (RTUCON) : Proceedings*, Latvia, Riga, 14-14 October, 2014. Riga: RTU Press, 2014, pp.30-33. ISBN 978-1-4799-7460-3. e-ISBN 978-1-4799-7462-7.

DOI:10.1109/RTUCON.2014.6998195

Electrical Drive DC Link Power Flow Control with Adaptive Approach

Armands Senfelds (*Doctoral student, Riga Technical University*),
Arturs Paugurs (*Master's student, Riga Technical University*)

***Abstract* – An objective to control power flow in intermediate DC link of typical induction drive converter has been introduced and respective drive setup intended for such task. Theoretical considerations and simulation results of control approach utilizing available drive controller capabilities like direct torque control and speed control, as well as introduction of additional adaptive funnel type controller has been presented. Modifications of introduced adaptive control method have been presented and evaluated by simulation. Simulation results support proposed idea of DC link power flow control.**

***Keywords* – Adaptive control, Motor drives, Nonlinear control systems.**

I. Introduction

The presented research paper introduces the objective to provide controlled power flow in electrical drive intermediate power circuit and theoretical considerations on matter in Section 2. Approach of application of adaptive control strategy based on funnel type control in order to omit necessity of detailed system identification effort has been presented in Sections 3 and 4. Obtained simulation results and evaluation has been presented in Sections 5 to 7.

II. Control Objectives of Electrical Drive System

The objective to be obtained is to create controlled power flow in intermediate DC Bus of electrical drive assuming that this power flow could be also supplied via external DC supply system. Drive setup would serve as testing node in larger DC electrical system with controllable power consumption or production replicating load of industrial robot type as considered in [1]. Electrical load time variation would be realized by control system discussed in this paper.

Setup of two coupled electrical machines with their respective inverters and rectifiers is chosen as basis for implementation of control objective as shown in Fig. 1.

It is assumed that measurements of driving converter DC link voltage u_{DC} and current i_{DC} at the input of inverter bridge circuit are available, as well as converters can be controlled by Direct Torque Control (DTC) [2] or speed control (SC) principle with respective inputs T_{ref} and ω_{ref}. Application of DTC driven induction drive has also been discussed in [3].

Power flow in intermediate circuit P_{DC} can be obtained from measurements according to (1)

$$P_{DC} = u_{DC} \cdot i_{DC} . \quad (1)$$

Mechanical power P_{Mech} consumed or produced by driving electrical motor can be estimated according to (2) under assumption that electrical drives are following control reference variables

$$P_{Mech} \approx T_{ref} \cdot \omega_{ref} . \quad (2)$$

If expected power losses are taken into account power balance for driving and generating modes of driving motor can be written as (3) and (4) respectively, where $P_{Inverter}$ and P_{EM} are power losses in inverter and electrical machine

$$P_{Mech} = P_{DC} - P_{Inverter} - P_{EM} , \quad (3)$$

$$P_{Mech} = P_{DC} + P_{Inverter} + P_{EM} . \quad (4)$$

Combining (2) with (3) and (4) and calculating for P_{DC} set of (5) and (6) can be obtained

$$P_{DC} = T_{ref} \cdot \omega_{ref} - P_{Inverter} - P_{EM} , \quad (5)$$

$$P_{DC} = T_{ref} \cdot \omega_{ref} + P_{Inverter} + P_{EM} . \quad (6)$$

Under the assumption that power losses in involved components of inverter and electrical machine are relatively small with respect to main power flow from DC intermediate

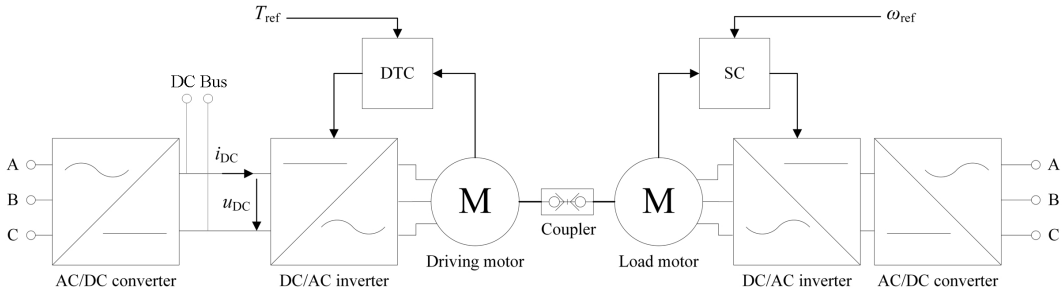

Fig. 1. Setup of two coupled electrical drives based on typical drive converters. Driving motor is available for Direct Torque Control (DTC) and loading motor for speed control (SC). Measurements of driving converter intermediate DC Bus circuit voltage u_{DC} and current i_{DC} are available. Respective control variables T_{ref} and ω_{ref} are fed to typical drive converters.

978-1-4799-7462-7/14/$31.00 ©2014 IEEE

circuit to mechanical system and vice versa it can be rewritten as (7)

$$P_{DC} \approx T_{ref} \cdot \omega_{ref} . \quad (7)$$

Since mechanical system of two coupled electrical machines is subject to inertia of machine rotors and shaft it is considered advantageous to maintain reference rotational speed ω_{ref} at constant level and use variation of torque controller reference T_{ref} in order to control DC intermediate circuit power flow P_{DC}.

III. Adaptive Controller Selection Consideration

The electrical drive includes several variables such as losses $P_{Inverter}$ and P_{EM} for example that would be necessary to estimate or obtain by measurements if model based controller design approach would be implemented. Therefore an application of adaptive control scheme is advantageous. As promising solution for particular application high–gain adaptive controller that would allow to avoiding necessity for system estimation or identification has been chosen. It has been presented in literature as funnel controller and several cases for mechatronic applications [4].

Necessary prerequisites of controlled system for application of funnel control has been indicated such as a system with stable internal dynamics and known sign of high-frequency gain [5]. High frequency gain can be characterized as expected direction of system output time derivative change to applied input action. In case of desired control objective for control of DC intermediate circuit power flow P_{DC} with respect to applied torque reference T_{ref} it can be observed from (7) that increase of T_{ref} would lead to direct increase of power flow so positive high-gain should be used. It is mentioned that funnel controller has been successfully applied to relative degree one or two systems, where relative degree indicates the order of system output derivative that is influenced by input variation. In particular case input action of torque variation has direct impact on change in supplied electrical power flow via DC link.

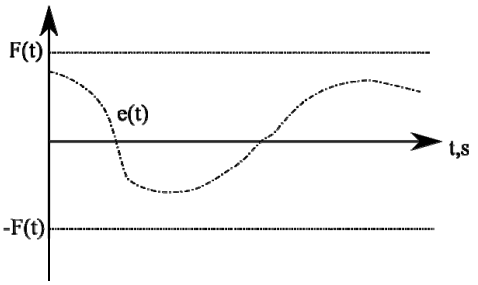

Fig. 2. Example of time evolution of control error $e(t)$ within funnel of symmetrical positive and negative boundaries $F(t)$ and $-F(t)$.

IV. Funnel Controller Operation Principle

The funnel controller utilizes an ability to vary controller proportional gain of amplification according to variation of error $e(t)$ of controlled output variable. Graphical representation of funnel control operation example is shown in Fig. 2. Controller calculate respective input $u(t)$ according to (8)

$$u(t) = e(t) \cdot k(t) , \quad (8)$$

where $k(t)$ is adaptive gain being calculated according to defined funnel boundary $F(t)$ according to (9)

$$k(t) = \frac{1}{F(t) - |e(t)|} . \quad (9)$$

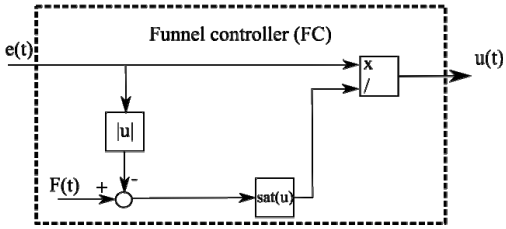

Fig. 3. Structure of funnel controller (FC) with defined boundary $F(t)$ according to control error $e(t)$ and control input $u(t)$ saturation limit.

One can observe that gain $k(t)$ is increased as control error $e(t)$ approaches defined funnel boundary $F(t)$ and can reach infinity in case if the error meets funnel boundary.

In practice control inputs of infinite values are not applicable therefore the method of reduction of controller input saturation has been presented like that in [6]. The idea of saturation control is to limit denominator value of (9) to some minimum value that would lead to maximum limited value of obtained gain $k(t)$.

Since for some control input $u(t)$ to be calculated in funnel controller output, some error $e(t)$ is necessary it has been considered to introduce additional control structure of integral type to maintain control input close to steady state operation.

A. Incorporation of Integral Type Control Structure

As discussed before practical limitations of control input values exist and such character has to be taken into account when designing also integral type control structure. Mechanisms to prevent integral control structure saturation are called anti-windup methods. Good overview has been presented by [7] as well as method has been discussed with respect to adaptive funnel controller [8].

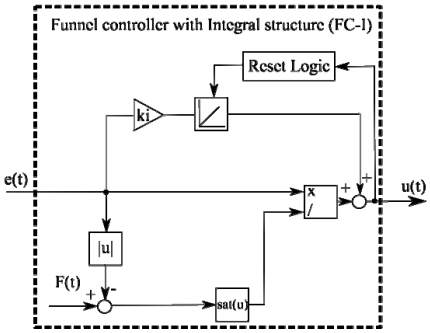

Fig. 4. Funnel controller combined with Integral structure (FC-I), gain ki and anti-windup mechanism based on running integral reset logic.

Integral part is integrating error value multiplied with gain factor *ki*. Running integral is reset if total control input value $u(t)$ is exceeding defined minimum or maximum values. Structure of modified funnel controller with integral structure (FC-I) is shown in Fig. 4.

B. Implementation of Feed-forward structure

In the case if information about actual rotational speed ω by means of encoder or speed controller reference value ω_{ref} is available one could introduce feed-forward mechanism for torque reference calculation based on (2). Torque reference has been calculated and added to form final control input value $u(t)$. Obtained controller structure (FC-I-FF) is represented in Fig. 5.

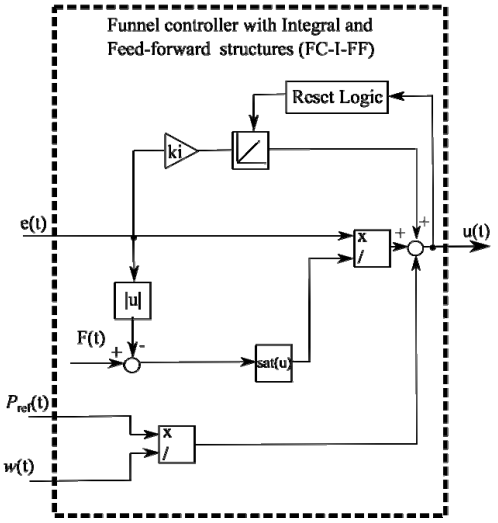

Fig. 5. Funnel controller with Integral and Feed-forward structure implementation (FC-I-FF), where $P_{ref}(t)$ and $w(t)$ represent Feed-forward reference calculation based on (2).

V. Simulation of Electrical Drive System

Simulation model of the presented electrical system has been realized based on Matlab physical modelling software Simscape Powersys toolbox elements. Key parameters of Simscape Induction drive unit have been presented in Table I.

TABLE I

Simscape Induction Drive Parameters

Power supply system	400 V, 50 Hz, 3 phases
Induction motor parameters	22 kW, 2 poles, Moment of inertia 0.13 kg·m^2, Friction 0.005 Nm·s
Speed controller (SC) parameters	Sampling time 0.1ms, $kp = 5$, $ki = 10$
Direct Torque Controller (DTC) parameters	Torque hysteresis bandwidth = 2 Nm, Flux hysteresis bandwidth = 0.02 Wb, Sampling time 20 µs, Max switching frequency 20 kHz
Simulation time step, Solver	$Ts = 20$ µs, ode4

Parameters of developed adaptive control structures have been summarized in following Table II.

TABLE II

FC, FC-I and FC-I-FF Relevant Simulation Parameters

FC boundary	$F(t) = 500$ W
FC gain saturation limit minimum, sat(u)	Min ($F(t)$-$\|e(t)\|$) = 4 W
Integral structure gain	$ki = 0.75$
Reset logic trigger values max/min	$u(t)_{max} = 150$ Nm, $u(t)_{min} = -150$ Nm

Obtained power has been measured utilizing 10 Hz low pass type filter in order to reduce noise of instantaneous current oscillations but observe general power flow.

VI. Simulation Results and Analysis

According to previously described simulation parameters intermediate DC bus power flow was controlled using each of three described control structures – FC, FC-I and FC-I-FF. Results have been presented in the following Fig. 6–8.

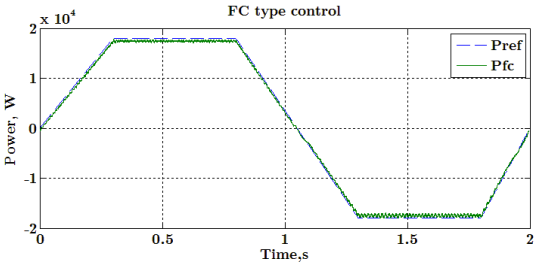

Fig. 6. Obtained simulation result of power flow with FC type control structure.

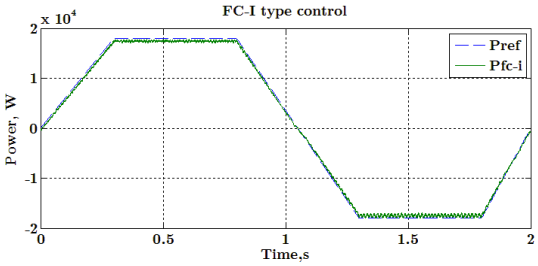

Fig. 7. Obtained simulation result of power flow with FC-I type control structure.

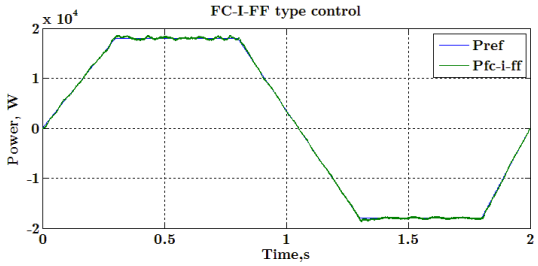

Fig. 8. Obtained simulation result of power flow with FC-I-FF type control structure.

Error time variation of FC-I-FF type controller with respect to funnel width is shown in Fig. 9.

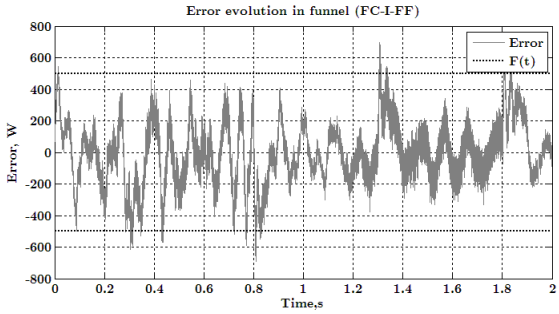

Fig. 9. Error variation with respect to chosen funnel function $F(t)$ in case of FC-I-FF system

Evaluation of each control structure performance has been calculated by ITAE criterion – integral of time absolute error and results summarized in Table III.

TABLE III
INTEGRAL OF TIME ABSOLUTE ERROR (ITAE) VALUES

FC	985.1
FC-I	978.2
FC-I-FF	302.3

As results show and one can also observe by comparing time behavior of all control systems, the best performance has been achieved by FC-I-FF controller structure combining all explained modifications of funnel controller leading to least error with respect to given reference power flow profile. Improvement of obtained controller performance has been observed by adding feed-forward type compensation structure which requires additional information about drive speed. By applying state of the art drive converter such information can be estimated without additional measurement hardware.

VII. CONCLUSIONS

An approach of applying adaptive high-gain based control method of funnel controller for drive converter intermediate DC link power flow control has been verified by simulation. Final application of drive setup as DC load node replicating power consumption or generation according to desired power time variation is to be realized. Simulation results support the idea of intended application and serve as a basis for development of experimental testing hardware setup. Simulation results have been obtained using typical computer model data of electrical motors and converters. In the case of real hardware equipment in laboratory simulation model variables are to be modified to provide closer match of real hardware parameters. Such approach would provide possible simulation model utilization as hardware-in-the-loop application or development of standalone controller unit with set of relevant parameters obtained by demonstrated simulation procedure and following experimental validation.

REFERENCES

[1] Meike, D., Senfelds, A., Ribickis, L., Power converter for DC bus sharing to increase the energy efficiency in drive systems. IECON 2013 – 39th Annual Conference of the IEEE Industrial Electronics Society, 2013

[2] Technical guide No. 1 Direct torque control - the world's most advanced AC drive technology, ABB Drives, 2011

[3] Mazhari, I., Vahedi, A., Masoum, M.A.S., Induction motor load generator system using direct torque control method. AUPEC 2007 Australasian Universities Power Engineering Conference, 2007.

[4] Hackl, C.M., Hofmann, A.G., De Doncker, R.W., Kennel, R.M., Funnel control for speed & position control of electrical drives: A survey. 19th Mediterranean Conference on Control & Automation (MED), 2011

[5] Christoph M., Hackl, Contributions to high-gain adaptive control in mechatronics, PhD Thesis, Technical University of Munich, 2012

[6] Hackl, C.M., Ji, Y., Schroder, D., Nonidentifier based adaptive control with saturated control input compensation, Mediterranean Conference on Control & Automation, 2007. MED '07.

[7] Tarbouriech, S., Turner, M Anti-windup design: an overview of some recent advances and open problems, IET Control Theory & Applications, Volume: 3 , Issue: 1, 2009

[8] Hackl, C.M., PI-funnel control with anti-windup and its application to speed control of electrical drives, IEEE 52nd Annual Conference on Decision and Control (CDC), 2013

Armands Senfelds received B. Sc. eng. of Riga Technical University, Latvia and M. Sc of RWTH Aachen University, Germany at 2009 and 2012, respectively in the field of Electrical Power engineering.

He is a PhD student and researcher at Riga Technical university, Institute of Industrial electronics and Electrical engineering.

Research with focus on intelligent industrial DC power distribution systems with renewable energy integration and storage applications is carried out within PhD student activities.

His research interests include design and control of power electronic equipment, electrical drives and electrical mobility.

He is a member of IEEE Power Electronics, Industry Applications, Industrial electronics, Robotics and Automation and Power and Energy Societies.

Arturs Paugurs received B. Sc. eng. of Riga Technical University, Latvia in the field of Electrical Engineering. Practised in Daimler AG, (Sindelfingen, Germany) in a project regarding energy efficiency optimization methods in robotic systems.

He is a Master's student and a technical specialist at Riga Technical university, Institute of Industrial electronics and Electrical engineering.

Main activities for his Master's thesis include research about industrial DC power distribution systems, simulation of electromechanical systems and three-dimensional modelling.

He is a member of IEEE Industry Applications Society and a member of RTU Student Branch.

Appendix 15

Meike, D., **Šenfelds, A**., Ribickis, L. Power Converter for DC Bus Sharing to Increase the Energy Efficiency in Drive Systems. In: IECON 2013 - 39th Annual Conference of the IEEE Industrial Electronics Society: Proceedings, Austria, Vienna, 10-13 November, 2013. Piscataway, NJ: IEEE, 2013, pp.7197-7202. ISBN 978-1-4799-0225-5. e-ISBN 978-1-4799-0224-8. ISSN 1553-572X.

DOI:10.1109/IECON.2013.6700329

POWER CONVERTER FOR DC BUS SHARING TO INCREASE THE ENERGY EFFICIENCY IN DRIVE SYSTEMS

Davis Meike

Daimler AG
Robotics and Technology Units
(PKL/AST), Germany
davis.meike@daimler.com

Armands Senfelds, Leonids Ribickis

Riga Technical University
Institute of Industrial Electronics and
Electrical Engineering (IEEI), Latvia
armands.senfelds@rtu.lv, leonids.ribickis@rtu.lv

ABSTRACT

It is state of the art for many drive systems like those used in industrial robotics, conveyor systems or diverse numerical control machinery to have a common DC bus power system architecture. Due to regenerative braking, the DC bus voltage increases until a certain limit, which is limited means of a balancing resistor (brake chopper). Systems that require rapid cyclic starts and stops are subject to significant energy waste due to extensive use of the brake chopper.

In this article, a novel power converter for drive systems is proposed that allows the brake chopper to be omitted and enables the exchange of regenerative energy among multiple drive systems within an independent DC subgrid with one centralized energy storage element. The solution does not require identical hardware or exact synchronization between the drive rectifiers, therefore it is applicable to both existing and new production equipment alike. Experimental results in industrial robot drives show savings of up to 20%.

1. INTRODUCTION

Due to complex production requirements, many industrial production applications often require rapid motion control - fast accelerations and reversals are usual. In particular, industrial robots that are typically equipped with several actuators connected in one kinematic chain have a high peak power requirement compared to their average power. It is state of the art for multiple motor drives in one system to be supplied by a single DC power source - an AC rectifier. Despite the fact that existing drive systems today are normally capable of regenerative braking, the recuperated energy is rarely fed back to a network or stored locally due to AC network quality conservation issues or increased costs of the storage systems.

Common DC link applications using a single rectifier and multiple variable frequency drives have been state of the art for many years. Multiple rectifiers and multiple drives that *share* the DC links are typical in some high-power variable frequency drives with nominal power ratings reaching several megawatts in order to equalize the load between IGBT switches. Modular DC bus sharing for functional purposes in a lower power range is available from some manufacturers [1]. Some examples are known from wind power turbines [2] and active power filters [3]. Actual research trends in future power system development present applications of DC transmission and distribution technologies as well like presented in [4]. Commercially available DC distribution system solution for maritime propulsion drives and discussion on potential optimizatoin has been presented [5]. DC based distribution as aircraft application has been discussed [6] as well as comparison on various poweer conversion stages regarding power density of converters. Therefore future integration of industrial production applications based on DC distribution are matter of interest. Analytical research of shared/common DC bus operation can also be found in [7].

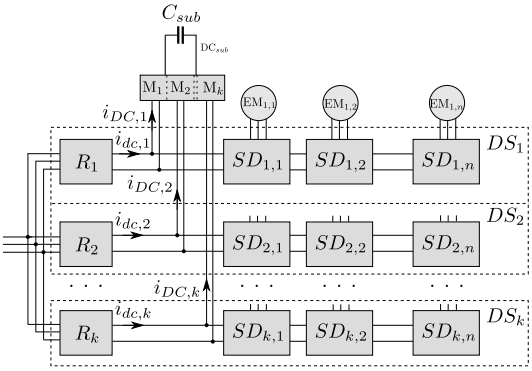

Fig. 1. A shared DC bus configuration with power converters

978-1-4799-0224-8/13/$31.00 ©2013 IEEE

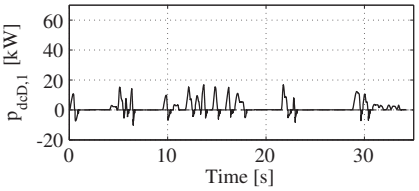

Fig. 2. Consumption of a single robot, $k = 1$

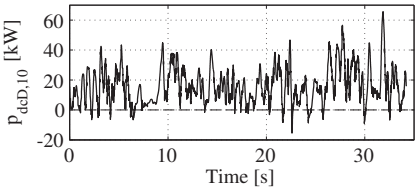

Fig. 3. Consumption of shared robot DC buses, $k = 10$

However, in all these cases, synchronized control of the drive switches is required so that these DC links are equalized. In fact, there is actually one synchronized DC bus that is supplied by more than one parallel rectifier. The previous research by the authors includes an alternative solution for drive sharing in [8] that does not require drive-to-drive synchronization. Using a common-ground power converter, the authors show how any drive system can store its recuperative excess energy in an independent DC subgrid, which can supply the power back when needed. Despite the fact that the solution showed significant energy savings, a common negative-pole connection caused the circular currents between drive systems. In this paper, a power converter uses semiconductor switches in both positive and negative poles of the DC bus to eliminate the side effects. A use case in robotic production with a shared/common DC bus is proposed in [9].

Fig.1 depicts an architecture where DC buses of drive systems are not connected in parallel directly. Instead, power converters are used as the interface between drive systems. Here, k drive systems $DS_1, \ldots, DS_k$ are used where each supplies n servo drives $SD_{i,1}, \ldots, SD_{i,k}$. A servo drive $SD_{i,j}$ supplies an electrical machine $EM_{i,j}$. Each of the DC buses $DC_1, \ldots, DC_k$ are connected to the power converter modules $M_1, \ldots, M_k$. Each module is connected to a subgrid DC_{sub}, so that any module M_i is parallel to any other M_{i+1}. The capacitor C_{sub} determines the size of the energy exchange buffer.

In the following, the Section 2 discusses high-level simulation of power consumption in robotic production. Section 3 describes the proposed power converter unit. Section 4 presents the modeling results of power electronics, but Section 5 provides the experimental validation and viability proof of implementation for industrial robots.

2. HIGH-LEVEL SIMULATION OF INDUSTRIAL ROBOT CONSUMPTION

The simulation was conducted as a reference program using high-payload robot system model as in [10]; the power consumption profiles were compared virtually. A power requirement for the industrial robots connected with shared DC buses is calculated in the form

$$p_{dcD,k}(t) = \sum_{i=1}^{k} (p_{dc,i}(t) - p_{D,i}(t)) \tag{1}$$

where p_{dc} is the power consumption within a DC bus, p_D is the power loss on the brake chopper, and k denotes the number of shared robots. The negative part of the power curve is

$$p^*_{[dcD],k}(t) = \begin{cases} -p_{[dcD],k}(t) & \text{if} \quad p_{[dcD],k}(t) \leq 0, \\ 0 & \text{if} \quad p_{[dcD],k}(t) > 0. \end{cases} \tag{2}$$

The start of the sample robot program has randomly been shifted within in the range $[0 \ldots \frac{\text{duration}}{2}]$. Fig.2 and Fig.3 show the respective power curves for $k = 1$ and $k = 10$. It can be seen that there are fewer negative power peaks than in the case of a single robot. The positive power peaks of the single robot power exceed 17 kW, whereas the maximum peak in the case of ten robots sharing the DC bus is below 65 kW.

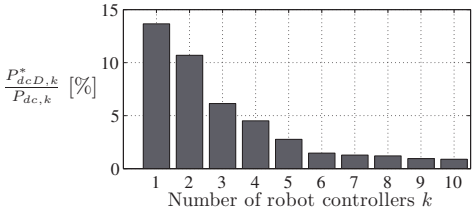

Fig. 4. Energy proportion dissipated on balancing resistors as function of k

The modeling results of varying numbers of shared robot drive systems are shown in Fig.4, where $P^*_{dcD,k}$ is the average dissipated power for k drive systems, but $P_{dc,k}$ is average total consumption of k drive systems. For a single robot, the dissipated average power is $P_D = 276W$, which corresponds to 14.8% of the power requirement within a DC bus (no static losses of the control cabinet considered here). The average dissipated power drops with each additional robot drive system added to

the DC subgrid. With five robots, the dissipated energy of all robot drives is below 3.2% (264 W), but with ten robots it is as low as 1.1% (175 W) of the energy requirement on the DC bus of the respective amount of robots involved..

3. POWER CONVERTER MODULE

In order to enable the flow of electrical power in a controlled manner, an electrical circuit as represented in Fig.5 is proposed. The general structure, the main circuit elements and the application of the subgrid interface module applied are explained in section 4.2. Power flow control considering specific application constraints and the applied technique are discussed in section 3.2. Detailed operation of the proposed circuit is discussed in section 3.3.

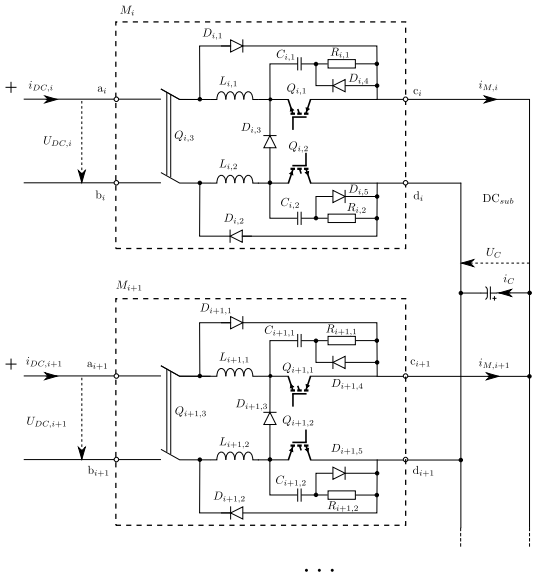

Fig. 5. Electrical circuit of DC subgrid interface module

3.1. Proposed electrical circuit

The electrical circuit enables a bidirectional power flow between individual drive systems DS_i, DS_{i+1} and subgrid DC_{sub}. The module M_i has 4 terminals a_i, b_i, c_i and d_i, where terminals a_i and b_i are connected to the positive and negative poles of a particular DC bus DC_i and terminals c_i and d_i are connected to terminals c_{i+1} and d_{i+1} of the other module respectively. A central capacitor C_{sub} is connected between all terminals $c_{1...k}$ and $d_{1...k}$. The applied circuit allows symmetric disconnection of positive and negative DC connection terminals by means of simultaneous commutation of IGBT semiconductor switches $Q_{i,1}$ and $Q_{i,2}$ avoiding common ground operation as discussed in [8]. Mechanical disconnection of poles for safety reasons is realized by means of contactor $Q_{i,3}$. Inductors $L_{i,1}$ and $L_{i,2}$ are utilized for current damping during coupling of the storage capacitor and drive DC bus.

3.2. Power flow control principles

Since the objective of the proposed system is the storage and utilization of excess electrical energy being generated during recuperation, the system should not influence normal operation when power is taken only from the AC grid. The presence of the recuperation process can be observed since unidirectional rectifiers are applied and energy is stored in smoothing capacitors resulting in a rise of the individual drive DC bus voltages $U_{DC,i}$. The DC bus voltage level corresponding to normal operation from the AC grid can be calculated as

$$U_{dc,idle} = \sqrt{2}U_{rms} \approx 565V. \tag{3}$$

Therefore, a hysteresis type control of storage capacitor voltage U_C is applied in order to utilize excess energy and prevent the discharge of the storage capacitor below (3) to disable direct recharging from the AC grid by rectifier instead of recuperation according to (4), where S_{t+1} represents IGBT switch states of the next simulation time step.

$$S_{t+1} = \begin{cases} 0 & \text{if } U_C \leq U_{off} \text{ and } U_C \leq U_{on}. \\ 1 & \text{if } U_C > U_{off} \text{ and } U_C > U_{on}. \\ S_t & \text{otherwise,} \end{cases} \tag{4}$$

In order to reduce high current peaks arising from the coupling of the storage capacitor and each drive system's DC bus, the voltage difference U_Δ has to be taken into account:

$$U_\Delta = U_C - U_{DC,i}. \tag{5}$$

3.3. Operating modes

During normal operation of the DC subgrid module, contactor $Q_{i,3}$ remains closed and is disconnected in the eventof an unexpected state for safety reasons or maintenance purposes. The charging of the main energy storage unit in DC_{sub} is enabled by natural commutation of diodes $D_{i,1}$ and $D_{i,2}$ when, as a result of the recuperation of DS_i, its voltage $U_{DC,i}$ has increased above the actual subgrid voltage U_C enabling the charging process that results in a positive current $i_{DC,i}$.

The discharging of the subgrid is enabled in a controlled manner through the control of IGBT switches

$Q_{i,1}$ and $Q_{i,2}$. The negative current flow is determined by voltage difference U_Δ according to (5) and inductors $L_{i,1}$ and $L_{i,2}$. When a storage capacitor with the respective voltage U_C has reached a voltage level U_{off} applied for control as in (4), the current $i_{DC,i}$ is interrupted. Since magnetic energy has been stored in $L_{i,1}$ and $L_{i,2}$ during discharge operation, the current freewheeling path is realized by diode $D_{i,3}$ in order to avoid high voltage during turn-off of IGBT elements. The RCD snubber circuit for reduction of overvoltage stress of the IGBT switches has been implemented by combination of elements $R_{i,1}$, $C_{i,1}$ and $D_{i,4}$ regarding snubber of IGBT $Q_{i,1}$ in this particular case as an example. Diodes $D_{i,7}$ and $D_{i,8}$ ensure that no reverse conduction via an alternative charging current path is possible in the case when IGBT switches are enabled.

4. FUNCTIONAL SIMULATION

In order to examine the feasibility of the proposed system, numerical simulation has been applied based on a model of the electrical system implemented by means of a Matlab simulation model. The design approach of the numerical model has been described in section 4.1. The character and origin of the chosen electrical load simulation input data and the results obtained by numerical simulation are evaluated in section 4.2.

4.1. Structure of applied simulation model

The proposed electrical circuit simulation model has been developed according to the functional layout presented in Fig.1; however, reduced to a system with $k = 2$ interconnected drive systems via a shared DC bus. The size of the energy exchange buffer unit C_{sub} has been selected to be 45 mF, representing a real capacitor bank available for the field experiment stage of development. The respective power converter modules M_1, M_2 have been developed according to the electrical circuit depicted in Fig.5. A common power grid of 50 Hz frequency is assumed and implemented as an AC voltage source. Typical brake chopper functionality is modeled: a resistor is triggered if $U_{DC,i} \geq 680V$.

4.2. Simulation results

The performance of the proposed electrical system can be analyzed by examination of electrical quantity time variation. Two industrial robot load profiles were selected as input data. The chosen profiles present a peak load of $18kW$ as well as recuperation with a maximum of $10kW$ generated power within an operation period of 11 seconds. Applied power profile has been obtained by single robot power consumption of industrial robot during handling operation. Over the operation period, both robots result in average power of $7.49kW$.

The expected operation of a control algorithm and the estimated electrical system behavior resulting in $U_{DC,i}$ variation and the respective current flow regarding commutation of the power semiconductors can be observed in Fig.6. The chart at the top of the figure represents the actual power being consumed or generated by each of two drive systems, namely DS_1 and DS_2. The DC bus voltage variation of $U_{DC,1}$, $U_{DC,2}$ and the interconnected U_C part is shown in the second chart down. The third chart down represents the actual current flow from DS_1 and DS_2 to a subgrid as $I_{DC,1}$ and $I_{DC,2}$ as well as a current flow to the storage capacitor I_c. The bottom chart displays the switching states of $Q_{i,1}$ and $Q_{i,2}$ of M_1 and $M2$ respectively. The following processes can be examined:

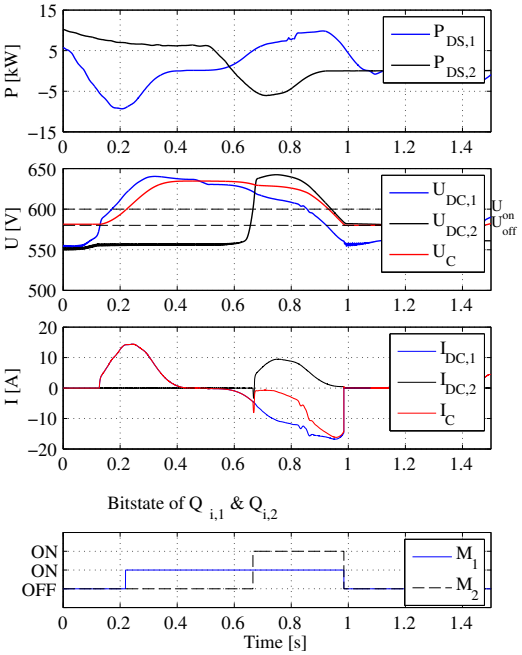

Fig. 6. Simulation of energy exchange between drive systems and asynchronous switching at voltage control levels: 580 V and U_{on} 600 V, allowed voltage difference for coupling $U_\Delta \leq$20V.

- $t = 0 : 21s : DS_1$ has raised the DC subgrid voltage using the recuperation process, the discharge of energy storage of DS_1 is enabled. DS_2 needs power requirement and a discharge of stored energy is not allowed since the voltage difference U_Δ is too large.

- $t = 0 : 65s$: The recuperation process and the voltage increase of DS_2 enable coupling with a shared DC bus. The energy flow from DS_2 to DS_1 via the shared DC bus with a storage capacitor is started.
- $t = 1s$: The shared DC bus voltage U_C reaches a threshold U_{off} and further discharge of the energy storage unit is disabled.

The influence of a control voltage variation on system performance has been observed by a sequence of simulations. The lower control voltage U_{off} has been varied in a range from 560 V to 670 V. A turn-on voltage level U_{on} has been applied 20 V higher than U_{off}.

The reduction in average power achieved per cycle versus the variation of the control threshold is presented in Fig.7. It is obvious that a larger portion of saved energy is present at lower turn off threshold voltage U_{off}; this is a result of better utilization of the energy storage unit leading to a longer discharge process.

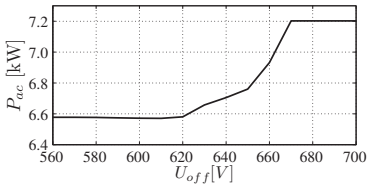

Fig. 7. P_{ac} as a function of U_{off}

5. EXPERIMENTAL VALIDATION

For circuitry and functionality experimental validation, two industrial robots have been selected being utilized in typical production facility: Quantec series with a payload of 210 kg and a KRC4 controller. Both drive systems are connected with modules according to Fig.5. Further configuration parameters include tool load masses 154 kg and 210 kg, the robot application represents sample handling operations programmed with 75% execution velocity. Fig.8 shows the general example of the recuperative energy exchange between both drive systems and a DC subgrid.

General functionality. The measured functionality is shown in Fig.8.The C_{sub} charging is present when the sum of $I_{DC,1}$ and $I_{DC,2}$ is positive. Various processes can be recognized during operation:

- $t = 0.5s$: Recuperation of DS_1.
- $t = 0.6s$: Recuperation of DS_2.
- $t = 1.8s$: Recuperation of DS_2, which causes the U_C increase above U_{on} that triggers to switch-on $Q_{2,1}$ and $Q_{2,2}$ of the module M_2.
- $t = 2.3s$: Supply of DS_2.
- $t = 2.5s$: Recuperation of DS_1, during which $U_{DC,1}$ independently increases above $U_C - U_k$. Here, a direct energy exchange can be observed - DS_2 is supplied from M_1 and C_{sub}.
- $t = 2.8s$: Recuperation of DS_1 is over. DS_1 is supplied by C_{sub} only until U_C falls below U_{off}, when IGBT switches $Q_{i,1}$ and $Q_{i,2}$ of both modules M_1 and M_2 are switched off.
- $t = 3.7s$: recuperation of DS_2 - the process repeats as in the first step.

Therefore, the measurement results comply with the expected control algorithm. A voltage sensor delay may be observed - the $Q_{i,1}$ and $Q_{i,2}$ switching, in fact, is initiated when U_C is well below U_{off}.

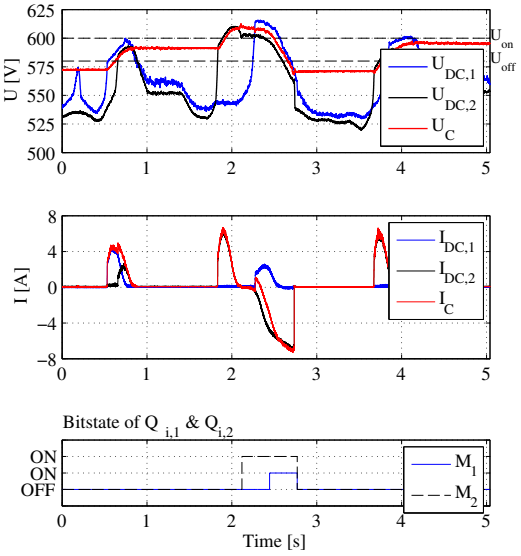

Fig. 8. Measurement of the energy exchange between robot drive systems; $U_{on} = 580V$, $U_{off} = 600V$

Energy consumption measurements. The power requirement on the AC supply side of both coupled industrial robots has been measured over operation period. The results show the energy consumption reduction up to 22.7% in a coupled DC bus configuration over a state-of-the-art systems. Since robot energy consumption is strongly dependent on its tool load, velocity, motor temperature and other parameters, several measurements have been conducted in a sequence, from which some are summarized in Table 1. The average power consumption is significantly higher with a higher tool load; however, the energy savings proportion remain approximately similar. Since only cyclic handling process alike movements

Table 1. Energy consumption measurement results with three-semiconductor switch power modules

Application type	Duration [min]	Velocity [%]	Tool [kg]		Temp. [K]		DC-bus sharing	Avg. power [kW]	Difference [%]
			R1	R2	R1	R2			
Handling	20	100	0	0	333	333	none	6.23	-
Handling	20	100	0	0	331	331	√	4.92	-21.1%
Handling	20	100	154	204	341	341	none	8.67	-
Handling	20	100	154	204	347	347	√	6.70	-22.7%

have been measured, the production standstills in manufacturing process must be considered when estimating the average savings on an annual scale.

6. CONCLUSIONS

This paper presents a new type of power converter for DC bus sharing to increase the energy efficiency of production machines utilizing electrical drives with recuperation possibility. Regenerative energy in machine tools may vary from 10% to 25% of total consumption depending on the application. However, due to expensive energy storage elements or bidirectional rectifiers at AC supply side, it is rarely reused effectively and dissipated at the DC bus braking resistor (i.e. brake chopper).

Simulation results show that the total volume of single, shared electrical energy storage units can be dimensioned much smaller than the sum of multiple separate storages, one each per production machine. The modular power interface system is proposed to enable the exchange and storage of the regenerative braking energy. The functionality of a power module is both simulated and experimentally validated.

The proposed power converter system is applicable to any state-of-the-art drive system with a rectifier, common DC bus and one or more inverters, such as those used in robotics, conveyors and diverse machine tools. The viability is proved using two high-payload industrial robots (KUKA Quantec series KR210 with KRC4 controllers) showing energy savings of over 20%. For implementation, the drive systems do not require any internal synchronization, nor identical components or hardware modifications to be attached to a shared DC subgrid with an energy storage element. Instead, the originial equipment may eventually even be downsized by eliminating or reducing number of utilized the DC bus brake chopper units.

7. REFERENCES

[1] Allen-Bradley, *PowerFlex AC Drives in Common Bus Configurations*, Rockwell Automation, 2011.

[2] Li Meng and Wang Yong, "Research on the parallel technique for the direct-drive wind power converter," in *Electrical Machines and Systems (ICEMS), 2011 International Conference on*, Aug. 2011, pp. 1 – 4.

[3] Prasad N. Enjeti Lucian Asiminoaei, Eddy Aeloiza and Frede Blaabjerg, "Shunt active-power-filter topology based on parallel interleaved inverters," in *IEEE Transactions On Industrial Electronics*, 2008.

[4] Florian Mura and Rik W. De Doncker, "Preparation of a medium-voltage dc grid demonstration project," Tech. Rep., E.ON Energy Research Center, 2011.

[5] T.Myklebust J.F. Hansen, J.O. Lindtjorn and K. Vanska, "Onboard dc grid, the newest design for marine power and propulsion systems," Tech. Rep., ABB Corp., 2013.

[6] A. Lucken D. Schulz J. Brombach, T. Schroter, "Optimized cabin power supply with a +/− 270 v dc grid on a modern aircraft," in *Compatibility and Power Electronics (CPE), 2011 7th International Conference-Workshop*, 2011.

[7] A.H. Wijenayake, T. Gilmore, R. Lukaszewski, D. Anderson, and G. Waltersdorf, "Modeling and analysis of shared/common dc bus operation of ac drives.," in *Industry Applications Conference, 1997. Thirty-Second IAS Annual Meeting, IAS '97., Conference Record of the 1997 IEEE*, Oct. 1997, vol. 1, pp. 599 – 604.

[8] D. Meike and I. Rankis, "New type of power converter for common-ground dc bus sharing to increase the energy efficiency in drive systems," in *Energy Conference and Exhibition (ENERGYCON), 2012 IEEE International*, 2012, pp. 225–230.

[9] Michael Lebrecht and Thomas Schneider, "Robotersystem," patent P817837, Deutsches Patent- und Markenamt, 2010.

[10] Davis Meike, "Multi-domain model for the evaluation of large scale robotic applications within production," in *Proceeding of the 53nd Annual International Scientific Conference of Riga Technical University*, 2012.

Appendix 16

Priedītis, M., Meike, D., **Šenfelds, A**. Micro Controller Unit Process Time Sharing and Digital Filter Analysis in Industrial Energy Exchange System. Power and Electrical Engineering. Vol.31, 2013, pp.106-111. ISSN 14077345

DOI: N/A

Micro Controller Unit Process Time Sharing and Digital Filter Analysis in Industrial Energy Exchange System

Marcis Prieditis[1], Davis Meike[2], Armands Senfelds[3], [1-3] *Riga Technical University*

***Abstract* — this paper provides an evaluation of control principles of power exchange modules used in industrial robotics. There is presented a detailed analysis of MCU computational time sharing between several time-critical functional processes and a digital sensor performance is experimentally validated. Measurements of overall control unit performance drop are done and possible system improvements are proposed.**

***Keywords* – energy efficiency, industrial robots, sensors, digital filters**

I. Introduction

Electrical energy consumption and respective costs are matter of high importance. Different energy saving activities is carried out in many levels of economical and geographical organizations. Target of saving 20% of primary energy by 2020 in comparison to 2007 has been set by EU [1]. Therefore, energy saving actions are considered by industrial energy consumers in EU. Automobile manufacturers in Europe are organizations that try to increase automation levels in their production lines as much as they can, which forces them to spend electrical energy more and more. Single car production chain including various production processes such as welding, handling, gluing, painting lead to a relatively large energy consumption [2]. Local research groups have been analysing energy saving possibilities and have concluded that great energy savings potential can be achieved, if energy recuperation would be introduced at factory level [3].

Energy recuperation system should eliminate braking energy dissipation through braking resistances in a DC bus of an industrial robot and save it in some sort of energy storage device, from which the energy could be acquired back later [4]. The proposed energy recuperation circuit consists of power part and control part.

The main task of power part (PP) is to provide energy transfer's environment that enables regenerative energy transfer to the energy accumulator and back to the robots. The main task of control part (CP) is to enable and control functionality of PP or disable it depending on system states. Different controlling algorithms can be implemented by the help of CP.

Although different topologies and variations of PP and CP are possible, one implementation of each has been practically built and used for experimental tests.

Experimental tests use a capacitor as an energy accumulator. These tests have also been carried out by the use of 2 KUKA industrial robots. Based on real testing environment requirements also CP of energy saving system has been built.

The next sections of this paper will present very general introduction in PP of energy saving system and deeper explanation of CP program architecture and sensor data processing mechanisms.

II. General Description of Power Part of Energy Saving System

Although a future target of this project is to build energy saving system that is able to accommodate any electrical energy consumer device with built in DC bus, this project at its starting phase is focusing on KUKA type industrial robots. Usually KUKA robots consist of a manipulator, typically 6 permanent magnet synchronous servo machines, drive system and a controller [5]. Robots used in a project have a built-in DC bus line which is used to power each inverter [2]. When motors are accelerating they are taking energy from DC bus, when they are braking, the energy is supplied back to the DC bus due to machine recuperation. During the acceleration process a voltage in a DC bus decreases and during the braking process its voltage rises. When it reaches 688 V, a braking resistance is connected in parallel with DC bus in order to dissipate braking energy [4].

The PP of energy saving circuit basically is set of modules that interface each robot in system with energy storage capacitor (Fig. 1). PP mod n stands for n-th PP module. In general more than 2 PP modules can be connected to C.

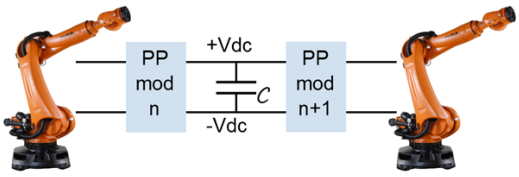

Fig. 1. Energy saving system and PP modules.

The version of PP modules that was used in tests does not enable CP to limit energy flow from robots to C. But the energy flow to the opposite direction can be limited.

Maximal voltage level in C can be greater than 688V, if energy flow to the robots is never enabled. If it is enabled constantly, than voltage level in C should follow voltage level in both DC bus systems [4].

III. Description of Control Part

CP is MCU based system that has voltage sensors on each DC bus (between robot and PP module) and C. It has also the industrial communication based inputs from robot controllers that inform of robot internal states. A HMI interface is also present.

Outputs are electrical signals that are driving IGBTs in PP modules and PROFINET data packets that inform of energy saving system and CP state. 16x2 symbols LCD is an output for user that is operating CP (Fig. 2, 4).

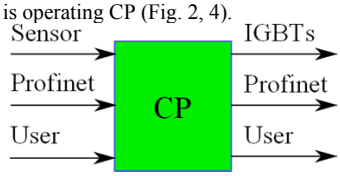

Fig. 2 CP inputs and outputs.

An actual CP that has been used in the tests is built up as a set of 3 modules:

1. Sensor input module (Fig. 3). This module contains 3 optical and 1 all-effect sensors, which enables voltage measurements of 2 DC buses, one capacitor module. It enables also a comparison of two sensor types.
2. A central data processing module (Fig. 4). This module contains MCU PIC24EP512GU810, which executes the main application algorithms. Part of user interface is implemented on it as an LCD and 3 pushbuttons.
3. A communications- and IGBT-control module (Fig. 5). This module has IGBT driver interfacing buffer ICs and device to handle industrial communication from HMS – Anybus Compact Com. This module is meant to work with Profinet IO communications protocol [6]. COM port communication is also possible through this module.
4.

Fig. 3 Sensor input module.

Fig. 4 Central data processing module.

Fig. 5 Communications and IGBT control module.

IV. Processes of Control Part

CP has to implement 4 basic processes:

1. Sensor data processing
2. Communication with robots
3. User interface handling
4. Industrial process control (based on data acquired from previous 3 tasks).

All of the processes have their dedicated interrupt service routines which are executed at different frequencies and with different priorities depending on their influence on the overall algorithm. All of Interrupt Service Routine (ISR) handling mechanisms are the ones which are supported by currently used MCU PIC24EP512GP810 [8].

A. Separate process description

1) Sensor data processing

Due to the fact that CP's algorithm had to be designed for a quite noisy sensor input, digital filtering is present. Fact that a target MCU does not implement DSP capability did not initiate any use of Nyquist criterion for signal sampling and reproduction .[8] Instead was chosen strategy by which the ADC samples sensor inputs as often as possible and then moving average algorithm is used to implement low pass digital filtering.

CP that has been designed for the first tests implements 4 analogue inputs. Three of them are used to measure voltages on DC buses of robots and capacitor module, but fourth one was designed to enable comparison of different kind of sensors that can be connected in parallel with capacitor module's sensor. So that, MCU is configured to sample all 4 analogue inputs in 38 µs.

This time is fast if comparison is done with the time that is needed to apply simple moving average algorithm to 3 sensor inputs - 162µs (Fig. 6). Formula of moving average algorithm is shown here:

$$FV = FV + \frac{(JSV - FV)}{n}, \quad (1)$$

Where FV is a filtered value, JS is a sampled value and n is number that states how many samples have to be averaged.

This type of moving average has some delay which depends on n. But on the other hand, higher n results in a less noisy averaged signal. Experimentally it has been tested that in case when ADC interrupt is called with 5 kHz (which is maximum possible frequency with target MCU and 4 analogue inputs) frequency than n with value of 400 satisfies energy saving process requirements. Of course, optimization should be done to get real value of needed n.

5 kHz makes ADC interrupt the most often interrupt in CP's algorithm, in comparison with rest of the ISRs. But this interrupt has to share MCU resources with other interrupts that are responsible for other processes, which reduces its actual frequency, which also will be calculated later.

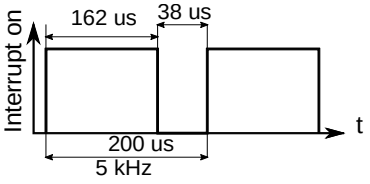

Fig. 6 ADC interrupt length and frequency.

2) Communication with robots

Communication with robots is done by the help of communications module that is able to work in Profinet network. Basically, the communication with robots is reduced to communication with Profinet interfacing module which is done by the help of UART module of MCU [6], [7].

This communication is done by the help of protocol that requires data packet sending and receiving with the minimum size of 19 bytes. Baud-rates can be adjusted to standard baud-rate values. Tests have been done with baud-rate of 19200 bytes per second and proved to satisfy requirements of industrial process. Of course, baud rate optimization can be done [3].

MCU built in DMA modules enables interrupt generation when full message of, for example, 19 bytes is received and not after each single received byte. When a message from communications module is received and interrupt bit has been triggered, a processing of received message starts. Sending and receiving is done by Direct Memory Access (DMA) and Universal Asynchronous Receiver/Transmitter (UART) modules [8].

Tests have shown that a message processing and response generation takes about 150 μs. And it happens with frequency of 33.67 Hz. That is because data sending to communications module, communications module data processing and data receiving takes about 29.7 ms (Fig. 7).

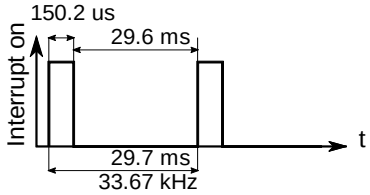

Fig. 7 Length and frequency of communication ISR.

3) User interface handling

User interface handling includes 2 things:

1. Setting and displaying system states;
2. Button press reading.

Both of them are implemented as routines that are called by some interrupt sources.

Setting and displaying system states is done about 2 times per second. Counting and interrupt calling is done by dedicated 16 bit timer. System states and display options are changed by taking into account button presses and dynamically changing data values.

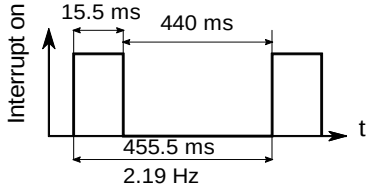

Fig. 8 Length and frequency of ISR which allows setting and displaying system states.

As shown in Fig. 8, an "interrupt on" time is larger than in previous 2 cases. That is mostly because of used FDCC1602N-RNNYBW-16LE display delay requirements after each command that has been sent to it.

Button presses are detected by dedicated interrupt and their values are used by previously described routine.

4) Industrial process control (based on data acquired from previous 3 tasks)

The interrupt of this process is called with frequency of about 3 kHz, because IGBT switches in power part of energy saving circuit does not need to be switched more often to satisfy industrial process requirements. Although process implements main logic of industrial process control algorithm, it is not doing too many calculations, only ready for processing data are compared to each other, new values to variables are given and signals are sent to IGBT and connector driver pins. That is why the MCU time taken by this process does not exceed 12.18 μs (Fig. 9).

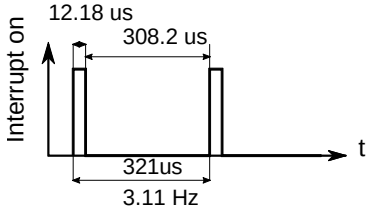

Fig. 9 Length and frequency of industrial process control ISR.

B. Process priority and sequence analysis

Industrial process control algorithm has been given the higher priority than rest of the processes that have been given lower but equal priorities. User interface process is composed of 2 interrupts. And to give user fast response, button responsible interrupt has been given the highest possible interrupt in system.

That means that button press can interrupt any of interrupt service routines that is being executed and industrial process control interrupt can interrupt rest of the system interrupt service routines (except button interrupts).

Rest of interrupt service routines are executed with their frequencies and if one is called during the execution time of the other, than it is executed immediately after previous execution has been finished.

Let's now consider 3 ISRs: Sensor data processing, communication with robots and GUI display and system variable responsible routine. All these routines have the same priority. If sensor data processing ISR is followed by communication ISR, than no delay in sensor data processing sequence is introduced, because communication ISR can be executed at 38 μs gap, which is used for ADC module to physically acquire voltage level at each input and not for sensor input data processing (Fig. 10).

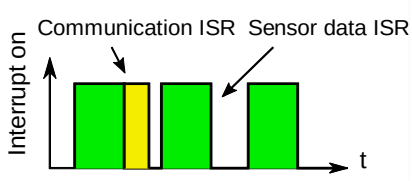

Fig. 10 Time sharing between Communication ISR and Sensor data processing ISR.

When a display-related interrupt is executed, a 38 μs gap in sensor data processing process is too short to fit in it 15.5 ms large ISR. That results in delayed sensor data execution time. Delay can be up to 15.5 ms + 150.2 us = 15.65 ms in case which is shown in Fig. 11.

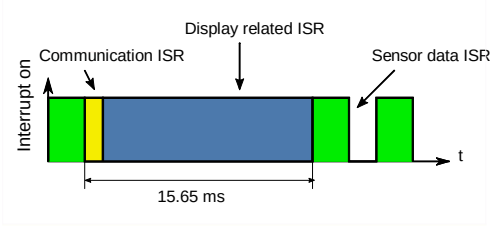

Fig. 11 Delay introduced by display related ISR.

As noted before, a display related ISR appears approximately 2 times in one second. And by taking into account this fact, minimum possible amount of sensor processing ISR executions in one second can be calculated as

$$f_{adc(\min)} = (1-2(T_{Dr}+T_{com}))\times f_{adc(set)} = \\ = (1-2(0.0155+0.000152))\times 5000 = 4.84kHz\text{,} \quad (2)$$

In the previous calculations $f_{adc(min)}$ is a minimum number of processed ADC ISRs per second, T_{com} is a length of communications ISR, T_{Dr} is display related ISR execution time.

$F_{adc(min)}$ is directly related to moving average algorithm. When 400 (practically tested and working value) values are averaged, than frequency that is related to this averaging period ($f_{MA(min)}$) is only

$$f_{MA(\min)} = \frac{f_{adc(\min)}}{MA_{samples}} = \frac{4.84kHz}{400} = 12Hz\text{,} \quad (3)$$

MA – is short form of moving average.

When any of these processes is interrupted by any of the higher priority interrupts than $f_{MA(min)}$ still describes process of averaging well, because it is rounded down value.

IV. Digital Filter Related Process Control Delay

Data that is coming from voltage sensors is basically used to enable the use of regenerated energy or disable it. Current version of CP algorithm enables it when DC bus voltage of central capacitor module is higher than some constant predefined value (HIGHER_LIM) and disables it when voltage in capacitor drops below some constant predefined value (LOWER_LIM).

Delay time between actual voltage signal appearance at sensor input and detection time of it has to be measured in order to describe response time of voltage sensing mechanism.

Theoretical delay was measured by script written in MATLAB that corresponds to the one in real MCU. This script applies step signal to digital filter, with previously described parameters (Fig. 12).

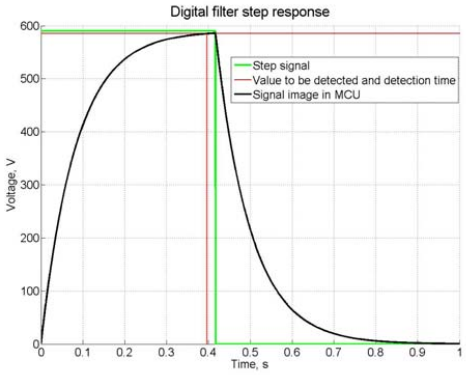

Fig. 12 Step signal applied to sensor input.

In the figure 12 step signal is green one. The length of it is time period that corresponds to digital filter averaging frequency – 12 Hz. It is a bit more than 0.4 seconds.

Black line shows how MCU "understands" step signal input.

Horizontal red line corresponds to some predefined voltage value, which detection delay time has to be measured. Vertical red line just helps to indicate crossing point of predefined voltage with MCU "understood" voltage level at its input.

In the Fig. 12 a predefined voltage level (red horizontal line) is set to 590 V. And output of the simulation shows that it was detected with delay of approximately 0.4 seconds.

In the practical experiments was very important to detect 585 V, which was set as UPPER_LIM. Depending on actual impulse length and amplitude this UPPER_LIM value can be missed or detected by MCU sooner or later. Table which uses impulse length of 0.4 seconds, shows 3 different UPPER_LIM detection delay times at 3 different impulse amplitudes.

TABLE 1.

UPPER_LIM (585 V) DETECTION DELAY TIMES WITH DIFFERENT STEP SIGNAL AMPLITUDES, BUT CONSTANT LENGTH - 0.4 S.

Pulse amplitude (V)	UPPER_LIM detection time (s)
590	0.40
640	0.20
688	0.16

If pulse amplitude would be 585 V, a more than 0.4 seconds of step signal width would be needed to detect this voltage on sensor input. Furthermore, if a pulse with would be shorter, than previously described impulses may not even be detected.

Although delay times are long, and some of pulses can even not be detected, industrial process, can be successfully completed without any losses in energy savings.

The reason why this happens is that a central capacitor works as an energy accumulator where braking energy is being fed in until voltage in it reaches UPPER_LIM. Sensor inputs are scanning just rising voltage in central capacitor unit. And even if UPPER_LIM is detected a bit later, than nothing bad happens – regenerated energy can be used just a bit later.

Long delay times in LOWER_LIM detection may cause some problems in system functionality, because one robot can start to power the other even if it needs energy to itself. Presence of this situation was not measured in practical experiments that have been carried out. But even if it was present, no error messages were generated by robots that were connected to the system. That means that even if this situation was present, than company that has developed these robots have designed their systems to allow energy transfers in this case [7].

V. CONCLUSION

Well functioning multi-process managing architecture has been implemented on PIC24EP512GU810. Analysis and tests has proven that it is adequate to use it for the implementation of supervising algorithm in energy saving system.

Designed program architecture still can be improved by analysing possible effects on lower moving average sample amount. This research may lead to possibility of Nyquist criterion use and lower sensor input sampling frequency that would leave more time to MCU for other tasks or sleeping mode.

Important outcome is fact that amount of saved energy in case of two test robots in system does not change even if sensor delay time is 0.4 seconds. Such a delay time may influence the amount of saved energy in case of more robots, since voltage could change more rapidly in central capacitor. Also smaller capacitance value of central capacitor unit could reduce amount of saved energy when large delay times are present during sensor data processing.

Less noisy sensor input would lead to reduced moving average sample amount. Therefore optimization could be done also in CP electronic design.

REFERENCES

[1] W.E.B.Wesselink, R.Harmsen, *How to triple the impact of energy saving policies in europe*, September 2010

[2] A.Burnham, J.L.Sullivan, M.Wang, *Energy-consumption and carbon emission analysis of vehicle and component manufacturing*, September 2010.

[3] T. Jordan, P. A. Taylor, *Hacktivism and Cyberwars: Rebels with a cause?* London: Routledge, 2004.

[4] R. Hayes, G. Pisano, D. Upton, S. Wheelwright, *Operations, Strategy, and Technology: Pursuing the competitive edge*. Hoboken, NJ Wiley, 2005.

[5] T. J. van Weert, R. K. Munro, Eds., *Informatics and the Digital Society: Social, ethical and cognitive issues: IFIP TC3/WG3.1&3.2 Open Conference on Social, Ethical and Cognitive Issues of Informatics and ICT*, July 22-26, 2002, Dortmund, Germany. Boston: Kluwer Academic, 2003.

[6] K. E. Elliott, C.M. Greene, "*A local adaptive protocol*," Argonne National Laboratory, Argonne, France, Tech. Rep. 916-1010-BB, 1997.

[7] K. Kimura, A. Lipeles, "*Fuzzy controller component*," U. S. Patent 14,860,040, December 14, 1996.

Marcis Prieditis received B.Sc. degree in electrical engineering from Riga Technical University, Riga, Latvia, in 2010. Planning to get M.Sc. in Spring of 2013. Currently is member of research team that puts efforts on efficiency improvement in industrial robotics.

Works at Institute of Industrial Electronics and Electrical Engineering as laboratory assistant.

Address: Kronvalda 1, Riga, LV 1048.

Phone +371 26065753, e-mail: marcis.priedite@rtu.lv

Davis Meike received M.Sc. degree in electrical engineering from Riga Technical University, Riga, Latvia, in 2008 and 2010, respectively.

He is presently a researcher at Daimler AG branch of Automation and Control Engineering, team Robotics and Technology Units, Sindelfingen, Germany.

He is Dr.Sc. student at Riga Technical University and a member of IEEE Robotics and Automation Society. His research interests include robot modelling, intelligent control systems, energy efficient path planning, logical and energetic cooperation of industrial robots, robotized production planning. Address: Kronvalda 1, Riga, LV 1048, e-mail:davis.meike@rtu.lv

Armands Senfelds received B.Sc.eng. of Riga Technical University, Latvia and M.Sc of RWTH Aachen University, Germany at 2009 and 2012, respectively at field of Electrical Power engineering.

He is a PhD student and research assistant at Riga Technical university, Institute of Industrial electronics and Electrical engineering.

He is a member of IEEE Power Electronics, Power and Energy Societies.

His research interests include intelligent design and control of power electronics and electrical drives, future power distribution systems with renewable energy integration and storage as well as electrical vehicles. Address: Kronvalda 1, Riga, LV 1048, e-mail:armands.senfelds@rtu.lv

Mārcis Priedītis, Dāvis Meike, Armands Šenfelds. Mikrokontrolera resursu sadalīšana laikā vairākiem procesiem un digitālā filtra izpēte industriālā enerģijas taupīšanas iekārtā.

Elektroenerģijas taupīšana sāk ieņemt arvien lielāku lomu, kā mājsaimniecības ierīcēs, tā arī industriālās ražošanas ietaisēs. Eiropas plāni 2020. gadam paredz, ka vēlamais enerģijas ietaupījums, sasniegs 20% no enerģijas patēriņa projekcijām 2020. gadā, kas tika izstrādātas 2007. gadā. Līdz ar to par enerģijas taupīšanu sāk domāt arī automobiļu ražotāji. Rakstā ir aprakstīts enerģijas taupīšanas princips, kas rāda, kā uzkrāt industriālo robotu bremzēšanas enerģiju kondensatoros. Uzkrāšanas un uzkrātās enerģijas atdošana tiek vadīta ar speciāla vadības moduļa palīdzību.

Vadības modulis ir bāzēts uz mikrokontrolleri. Tā ieejas signāli ir sprieguma līmeņi uz katra robota līdzstrāvas kopnēm un enerģijas uzkrājējkondensatora. Vadības modulis ir paredzēts darbībai Profinet IO tīklā, kas ļauj tam sazināties ar industriālajiem robotiem, vairāku robotu pārvaldības sistēmu, kā arī arī lietotāju. Darbība Profinet IO tīklā ir galvenokārt paredzēta industriālā procesa svarīgu mainīgo apmaiņai starp vadības moduli, robotiem un lietotāju.

Vadības modulim ir jāvar darbināt 4 paralēli procesi, kam katram ir savs uzdevums un prioritāte sistēmas vadībā. Visbiežāk izpildāmais process ir analogo ieeju skenēšana un noskenēto datu apstrāde. Tā notiek apmēram 4840 reizes sekundē un no tiem ir atkarīgs vai robotiem tiks atļauta reģenerētās enerģijas izmantošana vai nē. Pēc tam ieejas datiem tiek filtrēti ar digitālo filtru, kas ļauj atbrīvoties no trokšņiem. Digitālais filtrs ir viens no vienkāršākajiem zemfrekvenču filtru veidiem, kas izmanto slīdošās vidējās vērtības principu (*moving average*). Slīdošās vidējās vērtības filtra aizkavējums ir 0.4 s. Taču, par spīti tam, industriālā procesā ietaupītās enerģijas daudzums nemainās, jo uzkrājēj kondensatora kapacitāte ir pietiekami liela, kā arī sistēmā darbojošos robotu daudzums ir pietiekami mazs.

Izmantotajā vadības sistēmā, mikrokontrollera procesors ir noslogots gandrīz nepārtraukti, taču iespējams, ka tas varētu tikt atslogots, ja vairāk tiktu izpētīta digitālā filtra kvalitātes maiņa atkarībā no slīdošās vidējās vērtības vidējošanas intervāla.

Марцис Приедитис, Давис Мейке, Армандс Шенфелдс. Распределение ресурсов микроконтроллера для нескольких процессов и исследование дигитального фильтра для энергосберегающей установки.

Сбережение энергии занимает все более значимое место как для домашних, так и индустриальных электротехнических устройств. По планам Европы предполагается, что до 2020 года желаемое сбережение может достигнуть 20% от планированного в 2007 году объема потребления. В связи с этим и производители автомобильных средств начали работы по уменьшению расхода электроэнергии. В статье описан принцип реализации сбережения энергии в конденсаторах при торможении механизмов индустриальных роботов. Управление процессом сбережения осуществляется специальным модулем , который выполнен на базе микроконтроллера. Входные сигналы этого устройства являются характеристиками напряжений на общих шинах отдельных роботов и центрального энергонакапливающего конденсатора. Модуль управления предназначен для связи с индустриальной сетью Профинет 10, что позволяет реализовать связь между отдельными роботами, системой управления группой роботов и пользователем. Модуль управления должен координировать работу 4 параллельных процессов, каждому из которых установлен различный технологический алгоритм и приоритет при осуществлении управления. Наиболее частым процессом, выполняемым управляющим модулем, является сканирование входных сигналов и обработка этих показателей. Это проводится 4840 раз в секунду и от правильного функционирования зависит возможность рекуперации отдельным роботом. Входные данные фильтруются дигитальными фильтрами, что позволяет избавиться от различных помех. Дигитальный фильтр является одним из простейших видов низкочастотных фильтров, который использует принцип скользящего среднего значения. Задержка этого фильтра составляет 0,4 с. Несмотря на такую задержку в процессе работы она не оказывает влияние на параметры процесса рекуперации, что объясняется большой емкость накапливающего конденсатора и малым количеством роботов, подключенных к модулю. В данной системе модуль управления нагружен непрерывно, но возможно, усовершенствуя параметры фильтра, нагрузка модуля могла быть уменьшена.

Appendix 17

Šenfelds, A., Meike, D. Industrial Shared DC Bus Application: Common Ground Current Observation. In: *54th International Scientific Conference of Riga Technical University. Section of Power and Electrical Engineering: Digest Book and Electronic Proceedings*, Latvia, Rīga, 14-14 October, 2013. Riga: RTU Press, 2013, pp.11-13. ISBN 978-9934-10-470-1

DOI: N/A

Industrial Shared DC Bus Application: Common Ground Current Observation

Armands Senfelds (*doctoral student, Riga Technical university*),
Davis Meike (*doctoral student, Riga Technical university*)

***Abstract* – Investigation of shared DC bus system with common ground connection and respective side effect of equalizing current between system units is discussed. Numerical simulation of parallel rectifier system under varying load conditions as well as experimental results of common ground current presence has been shown. Prospective measures for improvement of utilized circuit regarding elimination of common ground current side effect has been presented and discussed.**

***Keywords* – Energy exchange, Industrial power systems, Energy efficiency**

I. Introduction

Topics of efficient utilization of electrical energy in various fields of application resulting in reduced carbon emissions and financial costs are matter of great importance. Industry applications involved in production processes like industrial robots in assembly lines are large group of consumers. Operational behaviour of electrical drives of robots or other computerized numerical control machinery enable process of recuperation since fast acceleration/deceleration phases and reversals are present. Use of regenerated energy is possible if bidirectional power converters are applied and total consumption of multi-robot systems can be reduced [1]. Various existing electrical drive systems present in applications are capable of using regenerative braking of the motors but the recuperative energy is not often utilized in common power network or captured in local energy storage units due to typical utilization of AC/DC rectifiers without bidirectional power flow capability as power supply. Research on energy saving potential by means of extended DC bus capacitance shows positive results [1].

Another possible utilization approach of regenerated energy could be implemented by introduction of parallel operation of individual drive systems interfaced with common energy storage unit [2]. Energy storage technology would enable short term storage according to cyclic behaviour of production process. One of the possible utilization methods could be based on parallel operation of robot supply system with central energy storage device [2]. Investigation of electrical interconnections in such system and mutual influence of processes is topic of this paper being actual for further improvement of the system.

Common DC bus applications utilizing a single rectifier and several variable frequency drives are known in industry application for many years. Several rectifiers and drives sharing the DC buses are known in some high power variable frequency drives facing nominal power ratings of several megawatts and equalization of the load between IGBT semiconductors is needed. Modular DC bus sharing for layout optimization purposes at medium and lower power range applications is presented by few manufacturers [3]. Some applications are present in field of wind power turbines [4] and active power filters [5].

Research of shared/common DC bus operation can also be found in [6]. It is to be noted that complexity of control by synchronization of drive semiconductor switches is increased in order to obtain equalization of DC buses. An application of independent coupling in order to exchange energy of various drive systems based on industrial robot is presented and patented by vehicle manufacturer Daimler AG [7].

Similar system for DC subgrid for energy exchange is proposed in [6], each DC bus is connected through power converter with other DC buses of industrial robots. Regeneration power is fed to the DC bus of parallel robots. Such method is based on smoothing capacitors of all DC buses to be utilized but in case of simultaneously regeneration at different robot drives volume cannot be sufficient for extra energy storage leading to critical state.

II. Shared DC Bus Approach Based Energy Exchange System

Main aspects of DC bus sharing principles are discussed in the following section. General overview of shared DC bus power distribution system is given identifying key elements and functionality. Discussion of expected operation under varying load conditions is presented.

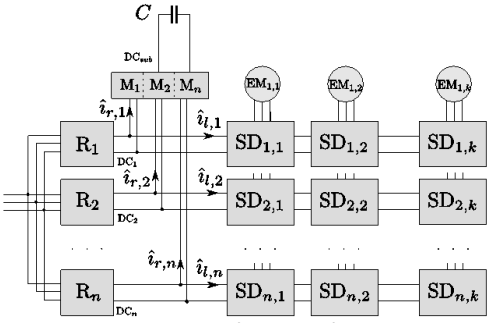

Fig. 1. Block diagram of DC subgrid for energy exchange

The block diagram is shown in Fig. 1. Here, n drive systems are assumed, each having a DC bus DC_n created by application of rectifiers $R_1, \ldots, R_n$ in order to feed several servo drives $SD_1, \ldots, SD_{n,k}$ utilizing electrical machines $EM_{n,1}$, …, $EM_{n,k}$ accordingly. Separate DC buses DCi are interfaced through respective power converter modules $M_1, \ldots, M_n$ to

common DC subgrid DC_{sub}. Single central capacitor C determines the size of the energy storage capacity. Idle state rectified voltage $U_{dc,idle}$ of unloaded DC bus with respect to line voltage U_{rms} assumed to be 400 volts can be calculated as

$$U_{dc,idle} = \frac{3\sqrt{2}}{\pi} U_{rms} \approx 540V \ , \qquad (1)$$

with respective DC bus voltage variation of

$$U_r = \frac{U_{rms}\sqrt{2}}{12\, f\, .R_{dc}.C_{DC,i}} \ , \qquad (2)$$

where $C_{DC,i}$ is the internal capacitance of the DC bus and R_{dc} is the DC bus load and f is the AC power system frequency. By means of Eq. 2., short peak loads of about 25 kW can be expected on DC bus [1] reducing bus voltage to level of 510 V. The upper limitation of U_{DC} is defined by drive hardware applying brake chopper based on energy dissipation by means of braking resistor. Typical brake chopper turn-on voltage levels are varying within the range of 690 to 790 volts.

DC bus sharing principle proposed allows a relatively large voltage variation between connected DC buses without synchronization of individual semiconductor switching instants. Basically a separate DC subgrid is created and energy storage functionality implemented by introduction of additional DC bus.

III. The Proposed Common Ground Circuit

Fig. 2 presents a connection principle of two power transducer modules M_i and M_{i+1}.

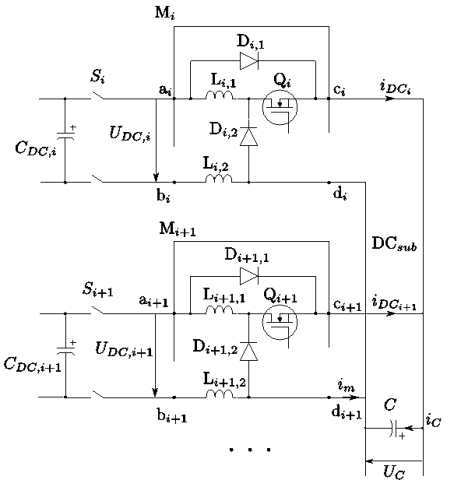

Fig. 2. Electrical circuitry of connections between sub-buses and the central capacitor

Each of the power modules has 4 power terminals a_i, b_i, c_i and d_i. Terminals a_i and b_i (Fig. 2) are to be connected accordingly to the positive and negative terminals of a particular DC bus DC_i. Terminals c_i and d_i of each module are to be connected to the c_{i+1} and d_{i+1} terminals of the other module, here noting that the terminals $d_{1,n}$ are the common ground of all modules $M_{1,n}$ and DC buses $DC_{1,n}$. The important detail is that common ground of explained circuit is not directly connected with AC system earth potential should be noted.

A central capacitor C is connected between all terminals $c_{1,n}$ and $d_{1,n}$ and used as a temporary energy storage device.

The voltage fluctuations of U_{DCi} from the viewpoint of the module M_i can be described as stochastic. Whenever the voltage $U_{DC,i}$ is slightly higher than U_C, the current flows through the power diodes $D_{i,1}$ and D_{i+11} charging the central capacitor C. The switches Q_i and Q_{i+1} are open therefore interrupting the current flow in the opposite direction. Whenever the voltage $U_{DC,i}$ is lower than U_C the diodes $D_{i,1}$ and $D_{i+1,1}$ become reverse biased and the control of current flow from point c_i to a_i is taken over by the switch Q_i. The inductors $L_{i,1}$ and $L_{i,2}$ limit the maximum current rate of rise. The freewheeling diode $D_{i,2}$ has a functionality to eliminate the effects of arc discharge and overvoltage spikes present on the semiconductor switch devices at current chopping by enabling alternative current flow path in order to discharge magnetically stored energy in inductors $L_{i,1}$ and $L_{i,2}$.

IV. Experimental Validation

Many short acceleration/deceleration phases are typically present but not limited to industrial robotics. Therefore, the application tests are done on industrial robot manipulators with permanent magnet synchronous servo motors and their drive systems with three phase full bridge diode rectifiers. High-payload robots *RB*1 and *RB*2 of type KUKA KR200-KRC2 have been selected to execute various applications. Their drive DC buses have been shared according to the power circuit in Fig. 2 using a central capacitor of size C = 45 mF.

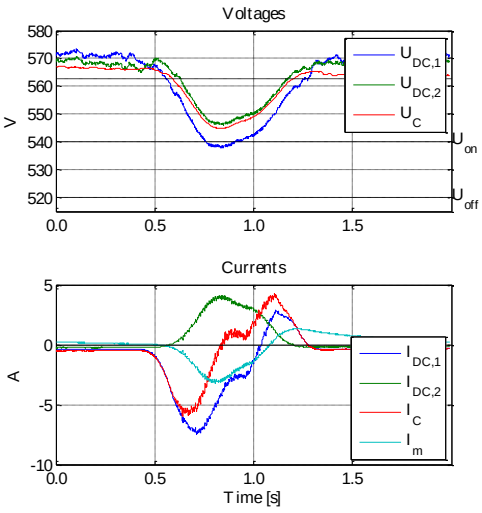

Fig. 3 Working modes with U_{on} = 540V, U_{off} = 520V

Fig. 3 illustrates the case when *off* voltage is low (520 V) and switches Q_i are permanently *on*. Here, the robot *RB*1 is accelerating while *RB*2 is in standstill. *RB*1 causes a temporary voltage drop on its DC bus that is partially

compensated by current flow from DC_{sub} and a preceding voltage drop on U_C. Since the both Q_1 and Q_2 are *on*, the voltage drop on C is passively compensated by $RB2$ with a positive current flow I_{DC2} over the diode $D_{2,1}$.

The effect when a drive system supplies power to a DC bus that does not have a load in its own system, is undesirable therefore closer examination of circular current presence has been done by simulation in following chapter.

V. Circulating Current Examination

Presence of circulating currents involving several converters being utilized in parallel arrangement has been observed in past. Interconverter currents in application of high power converter design by parallel operation of modular units have been discussed in [8]. In case of parallel connection of high and low power converter, circular currents have been invoked, therefore situation with unbalanced loading is considered to be relevant also in current arrangement of shared DC bus application.

A. Simulation approach

In order to examine common ground current effect simulation model has been utilized. Considering proposed electrical interconnection circuit to be in disconnected state simplified circuit can be obtained as represented in Fig. 4.

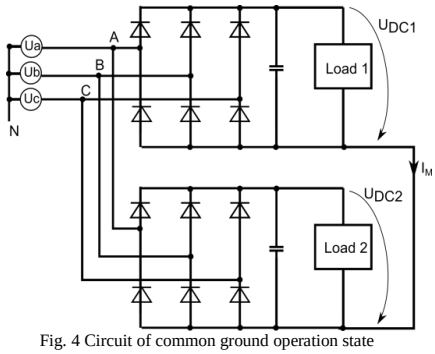

Fig. 4 Circuit of common ground operation state

Parallel operation of two diode rectifier bridges has been foreseen with added smoothing capacitors in DC side. Loading of both rectifiers has been simulated by load units acting as controlled current sources. The reference of current sources is calculated according to equation

$$I_{Load} = \frac{P_{Load}}{560}\ , \qquad (3)$$

where DC bus voltage is assumed to be 560 volts on average. The inductances present in common ground electrical connection are taken into account and assumed to have values of 5 mH each and have series arrangement of two. DC bus smoothing capacitors are chosen to be of 1.4 mF capacitance each. Since interest of applied simulation is behaviour of common ground current several current measurement points are chosen as represented in Fig. 5. Symmetry of DC line currents feeding load would be represented by comparison of currents I_i+ and I_i-. Current I_M in common ground connection is assumed to have positive direction from first rectifier to second.

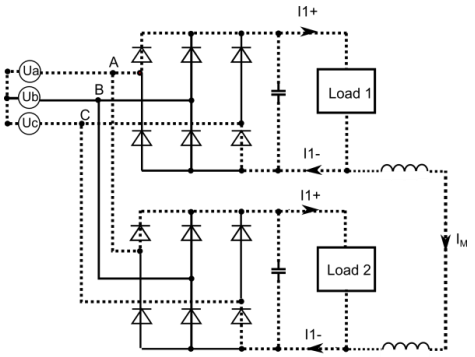

Fig. 5 Common ground current path

Assumed load profiles are generated according to sinusoidal function with cycle frequency of 10Hz. Time variation of load power is set to be 5kW around constant value of 15 or 10kW for first and second rectifier accordingly.

B. Simulation results

Obtained simulation results in steady state are presented in Fig.6.

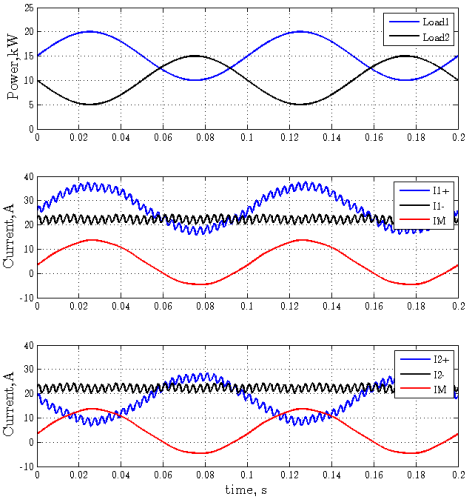

Fig. 6. Common ground current simulation under time varying loading conditions

The upper subfigure represents time variation of aforementioned power of both load units. Second subfigure depicts time variation of currents I_{1+} and I_{1-} as well as common ground current I_M regarding first rectifier circuit. Third subfigure represents currents I_{2+}, I_2 and I_M considering second rectifier.

Estimated RMS value of common ground current is 8A resulting in stable current flow from first rectifier interfaced with larger load to second one being less loaded. It is obvious that current asymmetry is present in unbalanced loading conditions for both observed DC buses. Currents in negative terminals flowing towards AC grid are equalized by common ground connection current flow. Direction of equalization

current depends on load power ratio being positive if first DC bus has greater load than second one. Presence of 5th harmonic is noticeable in load current originating from rectifier terminals but damping is present in common ground connection and can be explained by application of inductances. Conclusion that unsymmetrical current flow through positive and negative DC bus terminals under various loading conditions is present can be made resulting in unequal utilization of individual power semiconductor devices.

VI. Consideration of Common Ground Circuit Modification

Considering presence of common ground equalization current and its influence on shared DC bus system operation by utilizing single rectifier in case if load of other rectifier is applied is not optimal as discussed in Chapter 4. Modification of the proposed common ground topology based on shared DC bus approach has been considered. Symmetrical disconnection of both DC bus terminals by utilization of two semiconductor switch elements would enable electrical disconnection both positive and negative DC bus connections. Charging process would be enabled by utilization and natural commutation of diodes placed antiparallel to decoupling semiconductor devices. Additional controllable semiconductor element is considered to disable charging process if it would be necessary for full control of energy exchange. Proposed modifications are subject to be verified experimentally. Prospective electrical circuit topology example utilizing IGBT type transistors as semiconductor switching devices has been shown in Fig. 7.

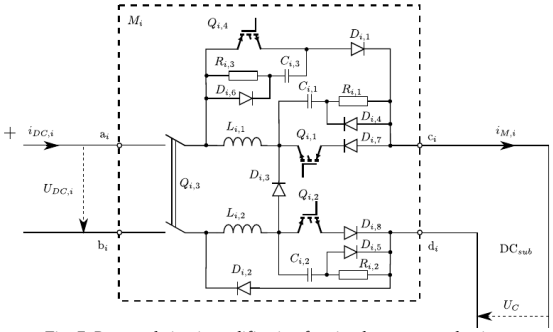

Fig. 7. Proposed circuit modification for circular current reduction

VII. Conclusions

Shared DC Bus application with regenerative energy storage and exchange possibility has been examined experimentally utilizing common ground electrical connection. Interconverter equalizing common ground current has been observed in experimental setup and investigated by numerical modelling method under various load conditions. Modification of electrical DC Bus interconnection equipment by alternative circuit topology has been proposed in order to obtain initial energy efficient operation and mitigate presence of observed common ground current issues.

References

[1] D. Meike and L. Ribickis, Recuperated energy savings potential and approaches in industrial robotics, IEEE 15th Int. Conf. on Automation Science and Engineering, 2011, pp. 299–303.

[2] D. Meike, I. Rankis "New Type of Power Converter for Common-Ground DC Bus Sharing to Increase the Energy Efficiency in Drive Systems" 2nd IEEE ENERGYCON Conference and Exhibition, 2012

[3] Allen-Bradley, PowerFlex AC Drives in Common Bus Configurations, Rockwell Automation Publication, 2011.

[4] Li Meng and Wang Yong, Research on the parallel technique for the direct-drive wind power converter, Electrical Machines and Systems (ICEMS), 2011 International Conference, Aug. 2011, pp. 1 – 4.

[5] Prasad N. Enjeti Lucian Asiminoaei, Eddy Aeloiza and Frede Blaabjerg, Shunt active-power-filter topology based on parallel interleaved inverters, IEEE Transactions On Industrial Electronics, 2008.

[6] A.H. Wijenayake, T. Gilmore, R. Lukaszewski, D. Anderson, G. Waltersdorf, Modeling and analysis of shared/common DC bus operation of ac drives, Industry Applications Conference, Thirty-Second IAS Annual Meeting, IAS '97., Conference Record of the 1997 IEEE, Oct. 1997, vol. 1, pp. 599 – 604.

[7] Michael Lebrecht and Thomas Schneider, Robotersystem, patent P817837, Deutsches Patent- und Markenamt, 2010.

[8] D. O. Neacsu, B.S. Borowy, W. F. Bonnice "Limiting Interconverter Zero-Sequence Currents Within 3-Phase Multiconverter Power Systems - Review and Ultimate Solution" The 27th Annual Conference of the IEEE Industrial Electronics Society IECON, 2001

Armands Senfelds received B.Sc.eng. of Riga Technical University, Latvia and M.Sc of RWTH Aachen University, Germany at 2009 and 2012, respectively at field of Electrical Power engineering.

He is a PhD student and research assistant at Riga Technical university, Institute of Industrial electronics and Electrical engineering.

He is a member of IEEE Power Electronics, Power and Energy Societies.

His research interests include intelligent design and control of power electronics and electrical drives, future power distribution systems with renewable energy integration and storage as well as electrical vehicles.

Davis Meike received M.Sc. degree in electrical engineering from Riga Technical University, Riga, Latvia, in 2008 and 2010, respectively.

He is presently a researcher at Daimler AG branch of Automation and Control Engineering, team Robotics and Technology Units, Sindelfingen, Germany.

He is Dr.Sc. student at Riga Technical University and a member of IEEE Robotics and Automation Society. His research interests include robot modelling, intelligent control systems, energy efficient path planning, logical and energetic cooperation of industrial robots, robotized production planning.

Appendix 18

Šenfelds, A., Raņķis, I. Common Node Circular Current Examination in Shared DC Bus Power System. In: *13th International Symposium "Topical Problems in the Field of Electrical and Power Engineering. Doctoral School of Energy and Geotechnology II"*, Estonia, Pärnu, 14-19 January, 2013. Pärnu: Elektriajam, 2013, pp.85-88. ISBN 978-9985-69-054-3

DOI: N/A

Common node circular current examination in shared DC Bus power system

Armands Senfelds, Ivars Rankis
Riga Technical University, Institute of Industrial Electronics and Electrical Engineering
Armands.Senfelds@rtu.lv, Ivars.Rankis@rtu.lv

***Abstract*— in this paper interconnection of two diode rectifier units is considered in context of potential DC bus interconnection situation as an example of distributed power system based on DC link coupling. Specific circular current flow in case of single pole coupling of separate DC Buses is examined resulting in fixed connection at common node. Influence of unbalanced loading of involved DC bus parts has been explained and results obtained by means of numerical simulations.**

I. Introduction

Nowadays electrical power engineering problems regarding energy saving are very actual. Large group if energy consumers in industry applications are industrial robots in assembly lines. Electrical drives of robots often have bidirectional power converters enabling use of regenerated energy in order to reduce total consumption in multi-robot systems [1]. One of the possible utilization methods could be based on parallel operation of robot supply system with central energy storage device [2] Investigation of electrical interconnections in such system and mutual influence of processes is topic of this paper being actual for further improvement of the system.

II. Assumed Distributed Power System

Various configurations are possible regarding distributed power system architecture. An informative survey considering and comparing both DC and AC systems is presented in [3].

In current paper an electrical power system under consideration is assumed to have a single conventional AC power connection to utility grid. The loads implemented in system are assumed to be fed by means of DC current and both at same voltage level. The possible improvement of system by integration of energy storage element into DC part is proposed. Optional DC connection representing renewable power source being able to charge energy storage unit is foreseen as well. The general overview of described system can be seen in Fig. 1

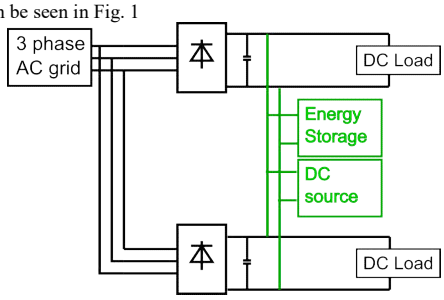

Fig. 1. General overview of electrical system representing conventional power system in black and optional connections for element integration in DC network in green

In order to conduct examination of interaction between separate parts of system more precise choice of functional elements has been defined. The operational state of system is defined as well.

A. AC/DC Conversion

In aforementioned system several possible methods of rectification could be assumed also enabling bidirectional power flow and thus recuperation back into AC grid.

In existing systems often unidirectional uncontrolled diode bridge rectifiers are present due to low cost of such units therefore it is assumed that both loads are normally fed by this type of power converters.

B. Interconnection of DC Line

In current electrical circuit under discussion the connection of DC lines between energy storage unit and individual load DC buses has been considered to be disconnected by single pole circuit disconnection switch placed in both positive terminals. Such approach is chosen in order to examine possible operation when only one semiconductor switching device could be necessary thus offering some economic advantages by saving number of components.

C. Common node

By introduction of single pole disconnection devices in positive DC bus lines no control of negative terminal is possible. Therefore all negative lines of both DC load units as well as negative terminal of energy storage unit remain connected under all circumstances. The electrical potential of all negative terminals is equalized by such common node connection. An important remark to be mentioned is that no middle point is available in DC bus by means of capacitive voltage divider. Therefore DC system is decoupled from AC system neutral and earth lines.

D. Operational State of DC Bus System

The situation when optional power flow from alternative DC electrical source is not present is considered. The state when energy storage unit has been discharged to level when it is decoupled from DC bus is chosen as well.

Therefore system remains in AC grid operation by parallel connection of both diode rectifiers each connected to DC load unit. An important variation compared to initial system considered is the introduced interconnection of both DC load unit negative terminals at the common node.

Considerations on operation in case of shared DC bus by direct coupling of both DC terminals has been proposed and examined by [4].

The resulting electrical circuit after application of aforementioned assumptions has been shown in Fig. 2.

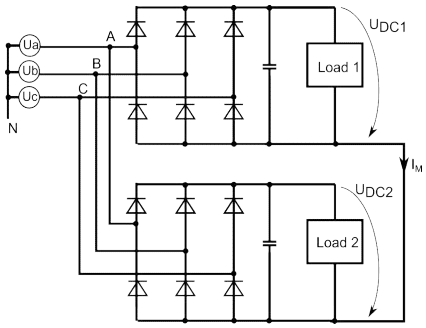

Fig. 2. Electrical circuit of discussed system in operation state after applied assumptions.

III. Parallel Operation of Rectifiers

In circuit under discussion parallel operation of two rectifiers is present. Both rectifiers are fed from AC grid with respective 3 phase voltages being U_{AN}, U_{BN} and U_{CN} against neutral point N. Voltage drop over diodes is assumed to be negligible. The positive terminals of DC Bus are always connected to the most positive phase voltage resulting in voltage U_{DC+} respectively to neutral point N according to (1)

$$U_{DC+} = \max(U_{AN}, U_{BN}, U_{CN}) . \quad (1)$$

The negative terminals of DC Bus are always connected to the most negative phase voltage resulting in voltage U_{DC-} respectively to neutral point N according to (2)

$$U_{DC-} = \min(U_{AN}, U_{BN}, U_{CN}) . \quad (2)$$

The rectified voltage U_{DC} at the rectifier bridge circuit output can be calculated as (3)

$$U_{DC} = U_{DC+} - U_{DC-} . \quad (3)$$

Voltage in the 3 phase diode bridge rectifier output is pulsating with six pulses per period of AC voltage. The peak voltage U_{DCPeak} at the output is calculated according to AC average phase voltage U_{ACRMS} by (4)

$$U_{DCPeak} = U_{ACRMS} \cdot \sqrt{2} \cdot \sqrt{3} . \quad (4)$$

By introduction of DC Bus smoothing capacitance voltage fluctuation over load is reduced. In case when maximum AC voltage between phases is lower than that on smoothing capacitor C being charged to voltage U_{DCPeak} load is supplied by energy being stored in capacitor. Power supply to the load is periodically changed being whether AC grid or smoothing capacitor C. In circuit being discussed in this paper load is assumed to be active and represented by resistance R_{Load}. The voltage reduction rate dU_C/dt on the capacitor during discharge can be calculated as (5).

$$\frac{dU_C}{dt} = \frac{U_{DCPeak} \cdot C}{R_{Load}} . \quad (5)$$

The variation of load resistance results in changes of voltage reduction rate. In circuit under discussion two loads are connected each to individual rectifier and smoothing capacitor. Therefore differences both in both parallel DC Bus voltages are expected under different load conditions.

IV. Electrical Parameters of the System

In system being discussed in this paper an AC grid with 50 hertz fundamental frequency is assumed to be the power source. The phase rms voltage U_{ACRMS} is chosen to be 230 volts resulting in peak voltage U_{DCPeak} at DC Bus being 563 volts. The load resistances R_{Load} are chosen to meet certain active power levels being dissipated as thermal losses in each of parallel loads. The average load voltage is assumed to be 560 volts. Therefore choice of load resistance R_{Load} for given power level P_{Load} is done according to (6)

$$R_{Load} = \frac{560^2}{P_{Load}} . \quad (6)$$

V. Simulation Model of The System

In order to examine parallel operation of rectifier units with separate loads connected at common node numerical simulation by means of Matlab Simulink software was carried out.

For power electronic device simulation specific toolbox called SimPowerSystems was applied. For diode rectifier circuit simulation Universal Bridge element was chosen and parameterized to meet diode rectifier requirements. The forward voltage drop Vf of each diode was set to be 0,7 volts and on state resistance to Ron be 0,001 ohm.

AC power system was modeled as three sinusoidal voltage sources Ua, Ub and Uc with peak voltage being 325 volts with 50 hertz frequency and 120 degree phase shift between voltages.

Each DC Bus smoothing capacitor was set to have capacitance value of 1650 microfarads. Initial voltage of capacitors was also set to be peak of DC bus voltage, 560 volts respectively.

Solver of type ode3 was applied for numerical calculation and continuous type simulation was chosen in Powergui simulation configurator parameter window.

VI. Circulating Current Examination

Presence of circulating currents involving several converters being utilized in parallel arrangement has been observed in past.

Inter converter currents in application of high power converter design by parallel operation of modular units has been discussed in [5]. In case of parallel connection of high and low power converter, circular currents have been invoked therefore situation with unbalanced loading is the matter of interest also in current paper.

Parallel operation of rectifiers and inverters in high power wind generator application also present examination of circular currents as described in [6].

VII. Simulation Results

In order to introduce unbalanced load of both rectifier units different values of load resistances were chosen.

First load unit was set to consume around 15 kilowatts of electrical energy corresponding to equivalent resistance R_{Load1} being 20.9 ohms. Load of second unit was chosen to represent lower consumption compared to first unit at 5 kilowatts leading to equivalent resistance R_{Load2} being 62,7 ohms according to (6).

Variation of DC Bus voltage was obtained as shown in following Fig. 3.

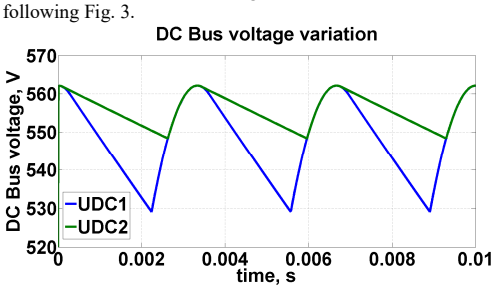

Fig. 3. Obtained DC Bus voltage variation results by numerical simulation. Blue line represents rectified output voltage connected to first load unit of 15 kW. Green line represents rectified output voltage connected to second load unit of 5kW.

In Fig. 3 one can observe voltage pulsation with period 3,33 milliseconds corresponding to 300 hertz frequency, being 6 times higher than fundamental 50 hertz frequency of AC power supply. Charging states of DC smoothing capacitors can be identified by overlapping of both voltage curves since they are connected to the same AC voltage through respective conducting diodes. States when load is supplied by discharge of DC Bus smoothing capacitors can be observed by linear regions of voltage reduction. Differences in discharge voltage slopes are the result of various loads where load with higher consumption leads to faster discharge of capacitor.

Under such operation also current flow through common node connection has been observed as shown in Fig. 4

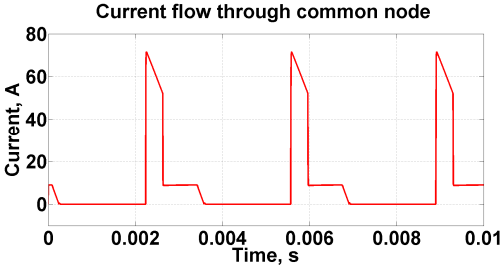

Fig. 4. Red line represents current IM flow through common node connection obtained by simulation. Positive direction is considered to be from the first load unit to second one.

Periodic current pulsation has been observed flowing through common node connection from first unit being loaded with 15 kilowatts to second unit loaded with 5 kilowatts. Repetition interval of current pulses is the same as charging of DC Bus capacitors. Peak value of 71,5 amperes has been detected as charging of capacitor in most loaded unit is started by AC supply voltage and high current pulse is present until both DC Bus capacitor voltages share the same value. The calculated rms value of current in presented operation leads to result of 19 amperes.

With intention to estimate complete circulating current path focus on electrical circuit state in time span from 2.2 to 3.6 milliseconds of simulation.

Current flow in phases A and C in common AC power grid connection and individual rectifier phase connections are shown in following Fig. 5. and Fig. 6.

Respective notation is applied in order to distinguish individual current values:

- IA – total phase A current flowing from AC grid to both rectifiers
- IA1 - phase A current flowing from AC grid to first rectifier
- IA2 - phase A current flowing from AC grid to second rectifier
- IC – total phase C current flowing from AC grid to both rectifiers
- IC1 - phase C current flowing from AC grid to first rectifier
- IC2 - phase C current flowing from AC grid to second rectifier

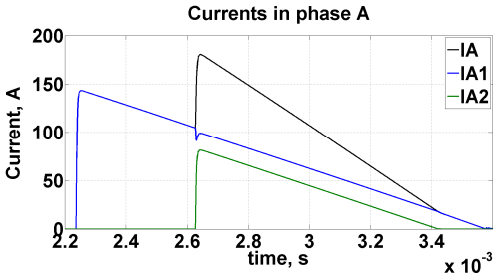

Fig. 5. Total phase A grid current in black, phase A current in first and second unit in blue and green respectively.

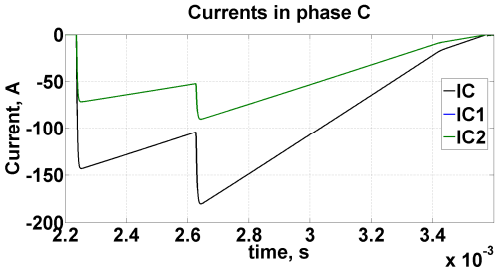

Fig. 6. Total phase C grid current in black, phase A current in first and second unit in blue and green respectively.

In simulation time period starting around 2.22 milliseconds first rectifier is connected to AC voltage between phases A and C where phase A has the positive voltage and phase C has negative one. Charging of first unit smoothing capacitor is started as well as supply of first unit load from AC grid. The whole grid current is flowing into circuit through first rectifier phase A leg upper diode. The current flowing back to Ac mains grid is distributed equally between both rectifier phase C leg negative diodes and thus causing current flow through common node connection.

E.g. at time instance 2.4 milliseconds incoming current value in phase A is approx. 140 amperes and reverse current is shared equally between both rectifiers of approx. 70 amperes resulting in overlapping of both curves IC1 and IC2 in Fig. 6. Schematic view of current path in discussed state is shown in Fig. 7.

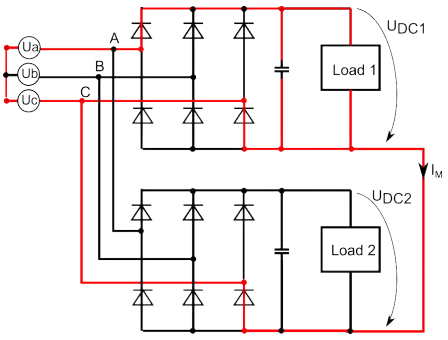

Fig. 7. Grid supply current path in simulation time period 2.4 to 2.62 milliseconds

After time instance 2.62 milliseconds both rectifier smoothing capacitors are charged as well as both loads are supplied by AC grid current. Difference in incoming phase A currents IA1 and IA2 is caused by unbalanced load condition. Again equal sharing of reverse current into AC grid through phase C leg lower diodes is present and equalization of current is caused by current flow through common node connection. E.g. at time instance 2.63 milliseconds respective IA1 and IA2 current values are approx. 100 and 80 amperes. Reverse flowing currents Ic1 and IC2 have same value of approx. 90 amperes. Such situation is possible by equalizing current flow through common node of approx. 10 amperes as one can observe in Fig. 4. Schematic view of current path in discussed state is shown in Fig. 8.

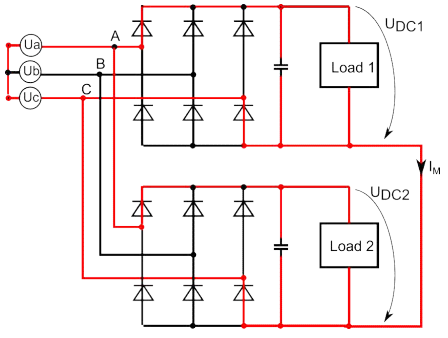

Fig. 8. Grid supply current path in simulation time period 2.62 to 3.6 milliseconds

VIII. Unbalanced Load Influence on Circular Current

In order to estimate unbalanced load influence on circular current presence set of simulations was carried out by varying second load unit power from 1 kilowatt to 15 kilowatt obtaining set of situations with load power ratio P_2 against P_1 from 0,067 to 1 respectively. Value of first unit load power remains constant being 15 kilowatts. Obtained circular current rms values against load power ratio are shown in Fig. 9.

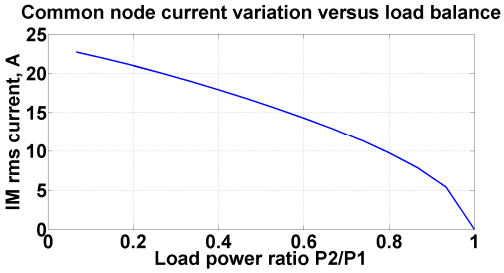

Fig 9. Calculated rms value of common node current IM against load power distribution ratio P2/P1.

According to simulation results one can observe that current flow through common node connection is reduced by equalization of single loads of units connected in parallel to the same AC grid. Unbalanced loading tend to equalize reverse flowing current through lower diodes of rectifier bridge circuit.

IX. Conclusion

This paper examines increased circulating phenomena present in diode rectifiers operating in parallel from same AC grid connection and common node connection on the DC Bus side. Circulating current involving both rectifiers appear under unbalanced load conditions.

In case of single pole disconnection of shared DC Bus system unequal discharge of separate DC link capacitors has to be taken into account.

Circular current flow affect lower diodes of less utilized DC Bus rectifier bridge circuit. Such additional current flow may be a matter of reduced lifetime and increased thermal stress.

Possible solution in order to eliminate or reduce observed pulsating current effect would be increase of common node electrical interconnection impedance or application of dual pole DC bus disconnection device.

References

[1] D. Meike, L. Ribickis "Recuperated energy savings potential and approaches in industrial robotics" *IEEE Conference on Automation Science and Engineering (CASE)*, pp. 299-303, 2011

[2] D. Meike, I. Rankis "New Type of Power Converter for Commmon-Ground DC Bus Sharing to Increase the Energy Efficiency in Drive Systems" 2nd *IEEE ENERGYCON Conference and Exhibition*, 2012

[3] C. D. Xu, K. W. E. Cheng "A Survey of Distributed Power System - AC versus DC Distributed Power System" *4th International Conference on Power Electronics Systems and Applications (PESA), 2011*, pp. 1-12, June 8-10, 2011

[4] A. H. Wijenayake, T. Gilmore, R. Lukaszewski, D. Andersno, G. Waltersdorf "Modeling and Analysis of Shared/Common DC Bus Operation of AC Drives" *32 IEEI Industry Application Society Annual Meeting*, pp. 599-604, 1997

[5] D. O. Neacsu, B.S. Borowy, W. F. Bonnice "Limiting Interconverter Zero-Sequence Currents Within 3-Phase Multiconverter Power Systems - Review and Ultimate Solution" *The 27th Annual Conference of the IEEE Industrial Electronics Society IECON, 2001*

[6] L. Meng, W. Yong "Research on the Parallel Technique for the Direct-drive Wind Power Converter " *International Conference on Electrical Machines ans Systems (ICEMS), pp.1-4, 201*

Appendix 19

Raņķis, I., Meike, D., **Šenfelds, A**. Utilization of Regeneration Energy in Industrial Robots System. *Enerģētika un elektrotehnika*. Nr.31, 2013, 95.-100.lpp. ISSN 14077345.

DOI: N/A

Utilization of Regeneration Energy in Industrial Robots System

Ivars Rankis[1], Davis Meike[2], Armands Senfelds[3], [1-3]*Riga Technical University*

Abstract. **This paper is devoted to the investigation of shared DC Bus systems with common storage capacitor operating on utilization of regeneration energy of electrical drives of industrial robots. The system is elaborated for the connection of the central energy storage capacitor with DC Buses of several robot systems. Simulation of operation of such system has been made with the target to obtain some specific indicators of efficiency of the system at different number of shared DC Buses. Dimensioning of system's parameters as well as some conclusions about necessary principle of control are presented. The results of experimental investigation are presented with the evident operational efficiency of the proposed system.**

Keywords: **robots, supply, capacitor, motors, charge, regeneration, transistor, coil**

I. Introduction

Industrial applications today often require rapid motion control where many fast acceleration/deceleration phases and reversals are presented. Such behavior is typical for industrial robotics and other computerized numerical control machinery [1]. Many existing drive systems today are capable of using regenerative braking of the motors.

However, the recuperative energy is rarely fed back to a network or stored in full extent locally due to AC-DC rectifiers fed supply of frequency converters or increased costs of the storage systems. Previous research shows impressive energy savings potencial using an increased capacitive energy buffer on a drive's DC bus [1].

Common DC link applications using a single rectifier and multiple variable frequency drives have been state of the art for many years. Multiple rectifiers and multiple drives that share the DC links are available from some manufacturers [2]. Some examples are known from wind power turbines [3] and active power filters [4].

Analytical research of shared/common DC bus operation can also be found in [5]. However, in all these cases, synchronized control of the drive switches is required so that these DC links are equalized. In fact, there is actually one synchronized DC bus that is supplied by more than one parallel rectifier. This paper proposes a solution for a recuperative energy exchange approach between drive systems that are controlled independently. The energy is stored in an independent DC subgrid, to which any drive system can ***transfer*** its recuperative excess energy and ***take it back again*** when needed.

An application case in industrial robotics with a shared/common DC bus has been patented recently by the vehicle manufacturer Daimler AG [6].

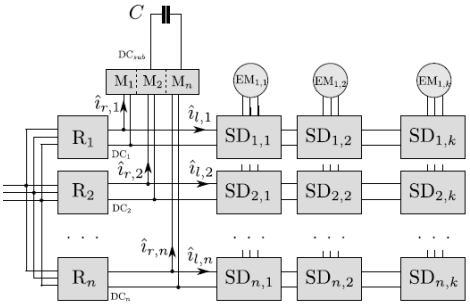

Fig.1. Block diagram of DC subgrid for energy exchange.

Another system for robots' DC subgrid for energy exchange is proposed in [5], where each DC Bus is connected through power converter with adjacent DC Buses of robots. Therefore at regeneration extra power is submitted to the DC Bus of adjacent robots. Such solution utilizes in full extent the capacitors of all DC Buses but the problems may arise when a simulatenous regeneration takes part in different robot drives (then regenerate energy should not be accumulated in capacitors because of lack of their necessary volumes).

II. Energy Exchange within Shared Dc Bus

In the following section, the advantages and main aspects of DC bus sharing principle accepted are discussed. The block diagram is shown in Fig. 1. Here, *n* drive systems are represented, where each has a DC bus $DC_1 \ldots DC_n$ supplying servo drives $SD_{1,\ k}$, $SD_{n,k}$ with frequency converters which control the electrical machines $EM_{i,j}$. Each bus DC_i is connected through power converter modules $M_{1\ldots n}$ to a subgrid DC_{sub}. The central capacitor *C* determines the size of the buffer. The rectified voltage in the idle circuit of DC bus has a fixed value of

$$U_{dc;idle}=1.35U_{rms}\approx\ 540V \qquad (1)$$

with a DC-bus voltage ripple of

$$U_r=\frac{U_{rms}\sqrt{2}}{12\,f\,.R_{dc}.C_{DC,i}}\quad , \qquad (2)$$

where $C_{DC,i}$ is the internal capacitance of the DC bus and R_{dc} is the DC bus load. According to (2), short peak loads of about 25kW measured on DC bus [1] can push a voltage as low as

510V. The upper bound of U_{DC} is limited by drive hardware using a brake chopper operating on dissipation resistor. For various drive systems typically the brake chopper is set anywhere within the range of 690 to 790V.

The proposed DC bus sharing principle allows a relatively large voltage difference between connected DC buses and does not require synchronization of the involved drives. In fact, an independent [n + 1]th DC bus as a DC subgrid is created to be used as an energy exchange buffer.

The electrical charge transmitted to the central capacitor C from n drive systems within the time t_t can be calculated assuming that shape of the average current transmitted from each drive system i is triangular with magnitude $\hat{i}_{r;i}$ and duration $t_{r;i}S_{r;i}$ (see Fig. 2), where $t_{r;i}$ and $S_{r;i}$ are respectively the average duty cycle and duty ratio of all recuperation phases respectively. The duty ratio can be expressed as $S_{r,i}=t_{r,i}/T_i$, where T_i is the process cycle for operation of robot number i.

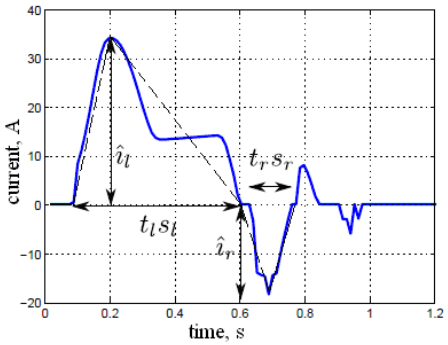

Fig.2. Presentation of current shape at DC input of robot drives.

For energy calculations, the internal capacitance of each DC bus is assumed negligible and that it does not influence the process efficiency. Then the total charge of recuperation is

$$\Delta Q_r = 0.5 t_t \sum_{i=1}^{n} \hat{i}_{r,i} \hat{S}_{r,i} \quad . \qquad (3)$$

As the average voltage U_C over the evaluation interval t_t is constant, the recuperated energy transferred to C equals the energy received. The motor consumption is the sum of the energy from the AC network and the DC subgrid DC_{sub}. The charge consumed by a motor load can also be calculated, assuming that the load current has a triangular shape with a magnitude $\hat{i}_{l;i}$ and duration $t_{l;i}S_{l;i}$, where $t_{l;i}$ and $S_{l;i}$ are the average duty cycle and duty ratio of all load supply phases respectively. Then, the total charge consumed by all n drive systems is

$$\Delta Q_l = 0.5 t_t \sum_{i=1}^{n} \hat{i}_{l,i} . S_{l,i} \quad . \qquad (4)$$

Typically, $S_{l;i} > S_{r;i}$ and $\hat{i}_{l;i} > \hat{i}_{r;i}$ for each of the examined examples in robot controller drive systems. Depending on the application, cycles t_r and t_l as well as magnitudes of currents may differ. The savings can be estimated in terms of the recuperated charge compared to the consumed charge because the positive (consumed) mechanical power does not depend on the existence of energy-saving device:

$$E_f = \frac{\Delta Q_r}{\Delta Q_l} = \sum_{i=1}^{n} \frac{\hat{i}_{r,i} . S_{r,i}}{\hat{i}_{l,i} . S_{l,i}} \quad . \qquad (5)$$

By adopting different relations $\hat{\boldsymbol{i}}_{r;i}/\hat{\boldsymbol{i}}_{l;i}$ and $S_{r;i}/S_{l;i}$ it is possible to find the savings from the diagram presented in Fig. 3. A smaller duty relation $S_{r;i}/S_{l;i}$ usually results in a smaller recuperation/load current relation $\hat{\boldsymbol{i}}_{r;i}/\hat{\boldsymbol{i}}_{l;i}$ and thus, smaller possible savings. However, even at light loads, the energy to be stored may reach 10% of the consumed energy. If the application is more dynamic the proportion of the recuperated current compared to the supply current is higher, and there is a higher duty ratio proportion in both operation cases, the charge to store rises too. For instance, at a duty ratio relationship of 0.5 the duration of the recuperation interval is half of the charging duration and a current magnitude relationship of 0.7 (magnitude of recuperated current is 70% of that of load), it is possible to save as much as 35% of the energy required for the particular movement phase.

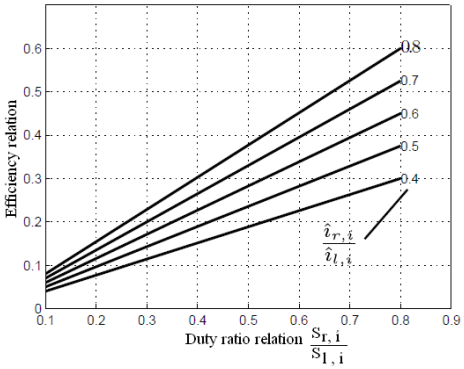

Fig. 3. Estimation of energy savings as a function of the duty ratio and recuperation and loading current magnitude relation.

III. The Proposed Circuit

Fig. 4 shows a connection principle of two power transducer modules M_i and M_{i+1}.

Each of the power modules has 4 power terminals a_i, b_i, c_i and d_i. Terminals a_i and b_i (Fig.4) are to be connected accordingly to the positive and negative terminals of a particular DC bus DC_i. Terminals c_i and d_i of each module are to be connected to the c_{i+1} and d_{i+1} terminals of the other module, noting here that the terminals $d_{1:::n}$ are the common ground of all modules $M_{1:::n}$ and DC buses $DC_{1:::n}$. Note that this is not an earth ground of AC supply system.

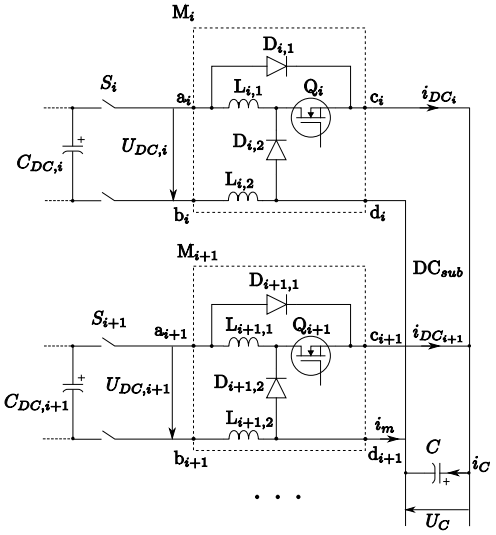

Fig.4. Electrical scheme of connections between sub-buses and the central capacitor.

A central capacitor C is connected between all terminals $c_{1:::n}$ and $d_{1:::n}$ and used as a temporary energy storage device.

The voltage fluctuations of U_{DCi} from the viewpoint of the module M_i can be described as stochastic. Whenever the voltage $U_{DC;i}$ is slightly higher than U_C, the current flows through the power diode $D_{i;1}$ charging the central capacitor C. Switch Q_i blocks the current flow in the opposite direction. Whenever the voltage $U_{DC;i}$ drops below U_C the diode $D_{i;1}$ is reverse biased and the control of current flow from point c_i to a_i is taken over by the switch Q_i. The inductance $L_{i;1}$ and $L_{i,2}$ limit the maximum current stresses. The diode $D_{i;2}$ has a function to eliminate the effects of arc discharge and overvoltage spikes.

In difference from electrical scheme presented in [7] there are 2 coils in each module. Such solution is accepted for supression of circulating currents in common ground wires between supply rectifiers' anode groups diodes (thyristors). By the way the accepted solution allows increase the reliability of switches operation.

IV. Component Dimensioning

The total charging current if all the modules are recuperating must be noted:

$$i_C = i_{DC;1} + i_{DC;2} + : : : + i_{DC;n} \qquad (6)$$

that has to be lower than the maximum charging current of the buffer capacitor

$$i_C \le C\left(\frac{du}{dt}\right)_{\max} \quad . \qquad (7)$$

The capacitor bank is dimensioned accordingly. If the recuperation current is assumed to have a triangular shape with a decreasing slope, i.e., the current is described as $\hat{i}_{r;i}(1\text{-}t/t_{r;i})$ noting that any selected time frame $t \ll t_{r;i}$, then the capacitor voltage change is

$$u_C = \frac{ng}{C}\int \hat{i}_{r,i}\left(1-\frac{t}{t_{r,i}}\right)dt \quad , \qquad (8)$$

which leads to

$$u_C = t_{r,i}\frac{ng\hat{i}_{r,i}}{2C} + U_{dc,idle} \quad , \qquad (9)$$

where g is a coefficient of coincidence of recuperation processes for n drive systems, but $U_{dc;idle}$ is as in Eq.(1). If $n = 1$ then $g = 1$, as n increases, g decreases. Approximately based on experience it can be assumed that

$$g = 1/\sqrt[3]{n^2} \quad . \qquad (10)$$

Taking such a value into account, the maximum permitted value of capacitor voltage $U_{C;max}$ can be reached if capacitance C is

$$C = \frac{\sqrt[3]{n^2}\,\hat{i}_{r,i}.t_{r,i}}{2\left(U_{C,\max} - U_{C,idle}\right)} \quad . \qquad (11)$$

For instance, $\hat{i}_{r;i}$ = 20A, $t_{r;i}$ = 0.3s , $U_{C;max}$ = 670V, $U_{C;idle}$ = 560V, then

- for $n = 4 \rightarrow C = 43.3$ mF,
- for $n = 3 \rightarrow C = 39.3$ mF,
- for $n = 2 \rightarrow C = 34.3$ mF,
- for $n = 1 \rightarrow C = 27.3$ mF.

V. Control Strategy

There are three different operational modes of the device as summarized in Table 1.

Table 1. Various working modes

	Energy flow	$D_{i,1}$ bias	Q_i bias	Q_i state	Voltages
1	From DC_i to DC_{sub}	forward	reverse	any	$U_{DC_i} > U_C$
2	From DC_{sub} to DC_i	reverse	forward	ON	$U_{DC_i} < U_C \ge U_{ref}$
3	None	reverse	forward	OFF	$U_{DC_i} \le U_C \le U_{ref}$

1. The energy is flowing from any module M_i to the subgrid DC_{sub} and is controlled passively.

2. The energy flow from DC_{sub} is controlled with switch Q_i and the current is limited by L_i. Here, a variable U_{ref} is introduced - a minimum voltage that has to be sustained on the DC subgrid. The state of Q_i is *fully on* if U_C is higher than U_{ref} and *fully off* if it falls below U_{ref} . Setting U_{ref} to above $U_{dc;idle}$ means that C never discharges below the voltage of idle DC bus. The charging, as mentioned, is possible only if $U_{DC;i} > U_C$. Thus, it is assured that only the recuperative excess energy is being exchanged in DC_{sub}.

3. An idle state is possible when no energy is being exchanged. This is the case when U_C drops below U_{ref} . All the switches Qi equally depend on UC, thus in normal operation their states are changed simultaneously. (For functional and safety purposes, any of the modules may also be disconnected separately. This, as well as the initial charging of C, however, is not discussed here). In practice, the reference voltage $Uref$ is implemented with a hysteresis and is set in the range

$$U_{ref} = \left[U_{off}; U_{on}\right] \quad . \qquad (12)$$

VI. Experimental Validation

Many short acceleration/deceleration phases are typically present but not limited to industrial robotics. Therefore, the application tests are made on industrial robot manipulators with permanent-magnet synchronous servo motors and their drive systems with three-phase full-bridge diode-rectifiers. High-payload robots *RB*1 and *RB*2 of type KUKA KR200-KRC2 have been selected to execute various applications. Their drive DC links have been shared according to the power circuit in Fig. 4 using a central capacitor of size $C = 45$mF.

Various U_{ref} modes have been tested. Figs. 5 and 6 show the crucial difference between low and high U_{off}. Positive current represents the energy flow towards *DCsub*. Fig. 5 illustrates the case when *off* voltage is low (520 V) and switches Q_i are permanently *on*. Here, the robot *RB*1 is accelerating while *RB*2 is in standstill. *RB*1 causes a temporary voltage drop on its DC bus that is partly compensated by current flow from DC_{sub} and a preceding voltage drop on U_C. Since the both Q_1 and Q_2 are *on*, the voltage drop on *C* is passively compensated by *RB*2 with a positive current flow I_{DC2} over the diode $D_{2;1}$.

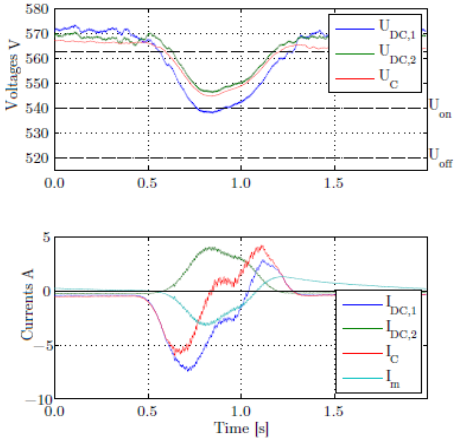

Fig. 5. Working modes with $U_{on} = 540$V, $U_{off} = 520$V.

The effect when a drive system supplies power to a DC link that does not have a load in its own system, is undesirable and can cause certain control errors. To eliminate this effect the criterion

$$U_{off} > U_{dc;idle} \qquad (13)$$

must be satisfied. The operating mode of U_{ref} =[560; 600] is shown in Fig. 6. Various processes are to be recognized here:

_ $t = 0{:}2$s recuperation of *RB*1,
_ $t = 0{:}8$s power requirement of *RB*1,
_ $t = 1{:}5$s recuperation of *RB*1,
_ $t = 1{:}7$s recuperation of *RB*2,
_ $t = 2{:}6$s power requirement of *RB*2,
_ $t = 2{:}8$s recuperation of *RB*2,
_ $t = 4{:}3$s recuperation of *RB*1.

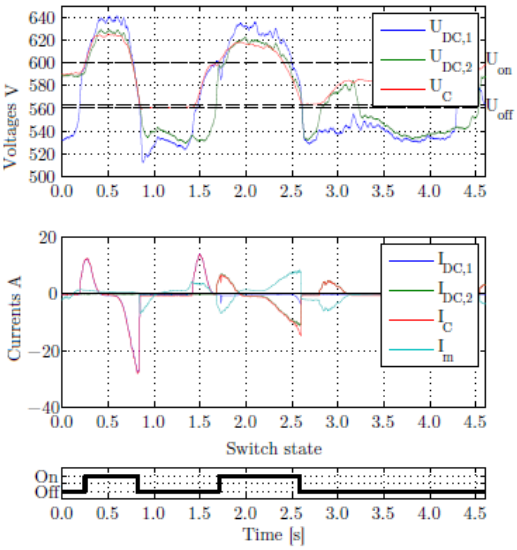

Fig. 6. Working modes with $U_{on} = 600$V, $U_{off} = 560$V.

The current flow of the positive terminal is cut whenever $U_C < U_{off}$. Since at experiments the negative terminals were directly connected, an equalizing circular current I_m is present at the negative terminal and

$$I_{m;i+1} > 0; \text{ if } U_{DCi+1} > U_{DCi}\,. \qquad (14)$$

Value of *Im* at common negative wire depends on the difference of resistances of the lower half-bridge of drive rectifiers. In the experiments, a minimum circular current $I_{m;min}$ has been determined when *RB*1 is in idle mode but *RB*2 is in operation.

Energy consumption of industrial robots highly depends on many parameters such as load, application type, acceleration profiles, etc. [7]. The estimated savings of the DC bus sharing approximately equal the otherwise wasted energy at the brake chopper. Since movements of all robot manipulators are not synchronized, consumption also depends on how much the supply-requirement and regenerative phases overlay as described by coincidence factor $\boldsymbol{g}$ in (10).

Table 2. Energy measurements of robotic applications

Application type	DC bus sharing	Consumption [kWh]	Difference [%]
Welding	none	3.66	-
Welding	√	3.45	-5.6%
Handling	none	6.44	-
Handling	√	5.11	-20.6%

Table 2 summarizes the energy requirement for 1 hour operation of two KUKA KR200-KRC2 robots with a load of approximately 30 kg running two types of programs, in each case with and without DC bus sharing. During the whole measurement, none of the DC links reached the brake chopper threshold voltage. The reference voltage was set to *Uref* = [560; 600]. Previous experiments have shown the energy-saving

potential of using capacitive energy buffers per industrial robot drive system [1]; the proposed DC bus sharing enables the same potential to be reached using just one buffer within a DC subgrid.

For more estmations a computer simulation of robot system operating with common energy storage capacitor and individual bus of robot connection through the scheme of intermediate module according to Fig.4 has been made. Five robot supply rectifiers with common for them AC network have been applied operating with different frequency f_1=0.5 Hz for robot N1; f_2=0.7 Hz for N2; f_3=0.6Hz for N3; f_4=1Hz for N4 and f_5=0.6Hz for robot N5. Respectively duty ratios of loading with averaged current 28 A for each robot were 0.278; 0.305; 0.278; 0.333; 0.278. Averaged meaning of regenerated current was 20 A for each of robots. Simulation process lasts for time interval of 20 s operation in two different situations – without the central capacitor of 45 mF and with central capacitor applying connection modules switches of which have been operated at U_{off}=540 V and U_{on}=550 V.

In table 3 the results of simulation are summarized for operation of all 5 robots and for operation in 3 another cases when each later robot was not activated, i.e. for 4, 3 and 2 robots operation cases.

TABLE 3
VOLUMES OF CONSUMED FROM SUPPLY ENERGY (kJ)

case	Rob.1	Rob.2	Rob.3	Rob.4	Rob.5
without	89.33	99.0	89.2	107.2	89.2
with C	56.9	55.0	66.0	66.4	66.1
With C	59.34	58.5	54.74	73.37	
With C	63.38	60.12	61.17		
With C	69.26	64.5			

As it can be seen without energy storage system total consumption of energy by 5 robots is 473.93 kJ; consumed energy with storage device is 310.4 kJ, i.e. 34.5% of energy is saved. Calculated by (5) saving amount is 30.3%.

In case of operation of 4 robots saving level is 36%; for 3 robot case saving level is 33.5%; for 2 robot case – saving level is 29%. Calculations show very close results.

VII. Prospective Scheme of Converter Module

Presented previous scheme anticipates common connection of DC busses through non-insulating modules to the central storage capacitor. Such solution has certain drawback of introducing extra electrical alignment contours. Better way should be in connection of individual busses with storage central capacitor through their modules with insulating transformers (Fig.7). Primary winding of transformer has to be connected with individual bus through switching converter SC1, but secondary – to the central capacitor through switching converter SC2 of the module. Therefore at regeneration at the bus its converter SC1 will be activated at 180^0 conductivity of its switches but SC2 operates as a rectifier through its diodes. At loading of the bus its module converter SC2 is activated at 180^0 conductivity of its switches but SC1 works as BOOST element with reduced duty ratio of its switches providing reverse flow of power from the storage capacitor to the loaded bus [8].

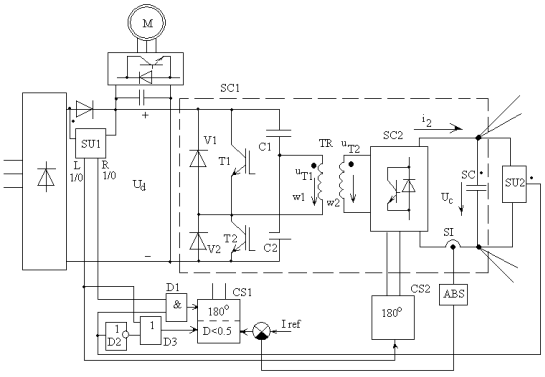

Fig.7. Scheme of the bidirectional power flow module with insulating transformer between DC bus and storage capacitor.

Control of the system can be provided using measurement diode in DC bus circuit with digital sensor SU1 (Fig.7). When regeneration takes place the diode is reverse biased and output R of the sensor is at its high logical level activating through D1 converter SC1 operate with 180^0 conductivity. Output L is at its zero level and switches of converter CS2 are stopped. Transfer of regenerated energy to the storage capacitor takes place. When motors unit of the DC bus is activated through measurement diode current is passing and digital signal exist on SU1 output L; this signal activates converter SC2 on 180^o conductivity of its switches and provides decreasing of duty ratio for switches of SC1, with control of process with current limitation.

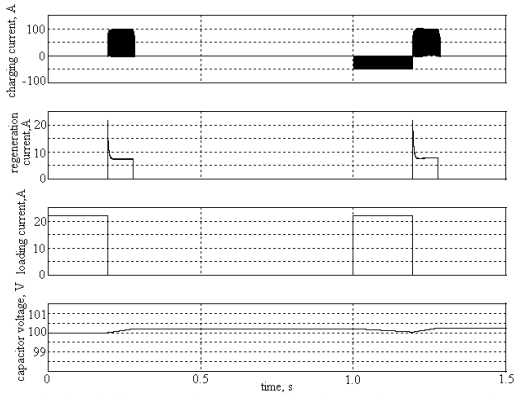

Fig.8. Simulated diagrams of currents and voltage of storage capacitor of 100μF.

Fig.8 presents the diagrams of currents and storage capacitor voltage obtained in way of computer simulation experiments. In very first loading cycle voltage of capacitor is at its lowest

threshold level and output of the sensor SU2 is at zero level disallow discharging of the capacitor.

CONCLUSIONS

1. Regeneration energy of several robot system can be efficiently utilized using one central storage capacitor of sufficient high its capacity.
2. For proper operation of the system each robot's DC bus has to be connected with the storage capacitor through bidirectional power flow converter module.
3. The converter module can be realized with electrically non-insulated connections with other converters as well as with insulated by transformers circuits.
4. The experimental results with industrial robots show energy savings of up to 20% for each system.
5. Computer simulation of robot system with number of involved robots up to 5 shows that it does not depend on the number of robots an operating saving effect can reach up to 30%.
6. Further work includes DC subgrid extension with optional super-capacitor based storage system and electrically mutually insulated DC buses of robots.

REFERENCES

[1] D. Meike, L. Ribickis, *Recuperated energy savings potential and approaches in industrial robotics, IEEE 15th Int. Conf. on Automation Science and Engineering,* 2011, pp. 299–303.
[2] Allen-Bradley, *PowerFlex AC Drives in Common Bus Configurations, Rockwell Automation,* 2011.
[3] L. Meng, W. Yong, *Research on the parallel technique for the direct-drive wind power converter, Electrical Machines and Systems (ICEMS),* 2011 International Conference, 2011, pp. 1 – 4.
[4] P. N. Enjeti Lucian Asiminoaei, E. Aeloiza, F. Blaabjerg, *Shunt active-power-filter topology based on parallel interleaved inverters, IEEE Transactions On Industrial Electronics,* 2008.
[5] A.H. Wijenayake, T. Gilmore, R. Lukaszewski, D. Anderson, G. Waltersdorf, *Modeling and analysis of shared/common dc bus operation of ac drives, Industry Applications Conference, Thirty-Second IAS Annual Meeting, IAS '97., Conference Record of the 1997 IEEE,* Oct. 1997, vol. 1, pp. 599 – 604.
[6] M. Lebrecht, T. Schneider, *Robotersystem, patent P817837, Deutsches Patent- und Markenamt,* 2010.
[7] D. Meike, I. Rankis, *New Type of Power Converter for Common-Ground DC Bus Sharing to Increase the Energy Efficiency in Drive Systems. 2nd IEEE ENERGYCON, Advance in Energy Conversion Symp.,* 2012, pp.263-268
[8] I. Rankis, J. Zakis, *Investigation of Supercapacitor Bidirectional Power Flow System, Pow. And El. Engin.,*vol..30, Riga:RTU, 2012, pp.35-40

Ivars Rankis, professor, Hab.Dr.sc.eng. He graduated from Riga Polytechnic institute in 1960 as an engineer electromechanician. He defended his first degree of Dr.sc. (candidate of technical sciences) in 1970. Defended his second degree Hab.Dr.sc.eng. in 1992 at Riga Technical university. From 1958-1966 he worked as an engineer at Riga Electrical machine building company. From 1966 he started studies as a doctoral student, but from 1970 – as a lecturer of different subjects in electrical engineering at Riga Technical University. Research interests are connected with Power electronics and Industrial automation. Now he is a professor at the department of Industrial electronics and electrical technologies of Riga Technical University. Riga Technical University, Institute of Industrial Electronics and Electrical Engineering

Address: Kronvalda 1, LV1048,Riga. Phone +371 67 089 917, rankis@eef.rtu.lv

Dāvis Meike, M.sc.eng., doctoral student. He graduated Riga Technical university in 2009 . Address: Kronvalda 1, LV1048,Riga. Phone +371 67 089 917

Armands Senfelds, M.sc.eng., doctoral student. He graduated Riga Technical university in 2010. Address: Kronvalda 1, LV1048,Riga. Phone +371 67 089 917, armands.senfelds@rtu.lv

Ivars Raņķis, Dāvis Meike, Armands Šenfelds. Reģenerācijas enerģijas utilizācija industriālo robotu sistēmā
Publikācijā aplūkoti robotu grupas piedziņu elektromotoru reģenerācijas enerģijas utilizācijas iespējas, izmantojot kopēju lielas kapacitātes enerģijas uzkrāšanas kondensatoru. Piedāvāts tehniskais risinājums ar individuālo robotu līdzstrāvas kopņu tiešu sasaisti caur pusvadītāju divvirziena jaudas plūsmas moduli ar centrālo enerģijas uzkrāšanas kondensatoru . Aprēķināta šī kondensatora nepieciešamā kapacitāte atkarībā no robotu skaita sistēmā. Sistēma aprobēta ekspluatācijas apstākļos un iegūti labi enerģijas taupīšanas rezultāti, kas gan atkarīgi no robota veiktās tehnoloģiskās operācijas, bet ietaupījums var sasniegt pat 30% no enerģijas, kas nepieciešama darbā bez uzkrāšanas ietaises. Ieviešot zināmus tuvinājumus, teorētiski aprēķināta iespējamā elektroenerģijas ekonomija robotu grupai atkarībā no robota darba un reģenerācijas intervalu laiku relatīvās attiecības periodiskajā darba procesā un darba un reģenerācijas strāvu amplitūdu attiecības. Parādīts, ka, samazinoties šīm attiecībām, enerģētiskā efektivitāte pieaug un ekonomija var sasniegt būtiskus lielumus. Teorētiskie aprēķini labi sasaka\nojas ar praktiskos eksperimentos iegūtajiem. Parādīts, ka ļoti būtisks moments ir saistīts ar pareizu sistēmas darbības vadību, kura reducēta uz kondenstaora sprieguma vērtību izmaiņu diapazona ierobežošanu. Izveidotā sistēma tomēr nav pilnīga, jo tiešā līdzstrāvas kopņu sasaiste rada strāvas nevēlamas cirkulācijas kontūrus, kurus jāierobežo ar speciāliem reaktīvajiem elementiem. Lai novērstu šo trūkumu, tiek likts priekšā veidot ar transformatoru izolētu sasaisti ar centrālo kondensatoru, kurā iespējams izmantot superkondensatoru ar daudz zemāku spriegumu nekā robota līdzsprieguma sistēmai. Izveidota shēma, kurā transformators no abām pusēm atdalīts no robota kopnēm un kondensatora ar diviem tranzistoru invertoriem, kuri var darboties divos virzienos, nodrošinot enerģijas plūsmu gan robota motoru reģenerācijas laikā - no kopnēm uz kondensatoru, gan robota slogošanas laikā - otrādi.

Иварс Ранкис, Давис Мейке, Армандс Шенфелдс. Утилизация регенерированной энергии в системе промышленных роботов
В публикации рассмотрены возможности утилизации энергии в ходе регенеративного торможения группы электроприводов роботов, используя конденсаторы большой емкости для накопления энергии. Предложено техническое решение, в котором индивидуальные шины постоянного тока каждого робота непосредственно через полупроводниковый модуль двунаправленного потока мощности напрямую соединены с центральным энергонакапливающим конденсатором. Рассчитана необходимая емкость этого конденсатора в зависимости от числа роботов, подключенных к конденсатору. Система апробирована в условиях эксплуатации и достигнуты хорошие результаты по экономии электроэнергии, которые все же зависят от технологического цикла, выполняемого роботом, но возможно достичь до 30% экономии от энергии, потребляемой без энергосберегающего устройства. Введением некоторых упрощений получены теоретические выражения для расчета возможной экономии энергии для группы роботов в зависимости от отношения длительностей интервала активной работы робота и интервала регенерации в периодическом режиме работы, а также отношения амплитуд токов нагрузки и регенерации. Показано, что при уменьшении этих отношений энергетическая эффективность возрастает и экономия может быть существенной. Теоретические расчеты хорошо согласовываются с экспериментально полученными. Показано, что очень существенным является принятый закон управления, который в данной системе редуцирован к ограничению диапазона изменения напряжения энерго накапливающего конденсатора. Все-таки разработанная система не является полноценной, поскольку принято непосредственное соединение шин постоянного тока отдельных роботов и при этом возникают контуры для циркуляционных токов, которые необходимо ограничить реактивными элементами. Предложен новый вариант реализации системы с изолирующим трансформатором между отдельными роботами и центральным конденсатором, в качестве которого может быть исползован суперконденсатор с пониженным по отношению к шинам роботов напряжением. Разработана схема, в которой обе стороны трансформатора подключены через индивидуальные инверторы, способные работать в двух направлениях.

Appendix 20

Lebrecht, M., Meike, D., Rankis, I., **Senfelds, A**. Produktionsanordnung mit wenigstens zwei Antriebssystemen.

German Patent DE 10 2013 010 462 A1, Patent publication date 27.03.2014

DOI: N/A

(19) Deutsches Patent- und Markenamt

(10) **DE 10 2013 010 462 A1** 2014.03.27

(12) # Offenlegungsschrift

(21) Aktenzeichen: **10 2013 010 462.9**
(22) Anmeldetag: **24.06.2013**
(43) Offenlegungstag: **27.03.2014**

(51) Int Cl.: ***H02M 3/158*** (2006.01)

(71) Anmelder:
Daimler AG, 70327, Stuttgart, DE

(72) Erfinder:
Lebrecht, Michael, Dipl.-Ing. (BA), 74321, Bietigheim-Bissingen, DE; Meike, Davis, M.Sc. ing., 71034, Böblingen, DE; Rankis, Ivars, Prof. Dr., Riga - Latvia, LV; Sensfelds, Armands, Riga - Latvia, LV

Mit Einverständnis des Anmelders offengelegte Anmeldung gemäß § 31 Abs. 2 Ziffer 1 PatG

Die folgenden Angaben sind den vom Anmelder eingereichten Unterlagen entnommen

(54) Bezeichnung: **Produktionsanordnung mit wenigstens zwei Antriebssystemen**

(57) Zusammenfassung: Die Erfindung betrifft eine Produktionsanordnung (FTA) mit wenigstens zwei Antriebssystemen (FT1, FT2), welche jeweils zumindest eine elektrische Maschine umfassen, die über jeweilige bidirektionale elektrische Leistungswandler (GS1, GS2) mit einem gemeinsamen, eine Plusleitung und eine Minusleitung umfassenden Gleichspannungsnetz (GV) elektrisch gekoppelt sind, wobei jeder der bidirektionalen Leistungswandler (GS1, GS2) zumindest für eine der Leitungen ein Halbleiter-Schaltelement (Q1.1, Q2.1) und eine Induktivität (L1.1, L2.1) aufweist, wobei wenigstens einer der bidirektionalen Leistungswandler (GS1, GS2) auch in der anderen Leitung ein Halbleiter-Schaltelement (Q1.2, Q2.2) und eine Induktivität (L1.2, L2.2) aufweist.

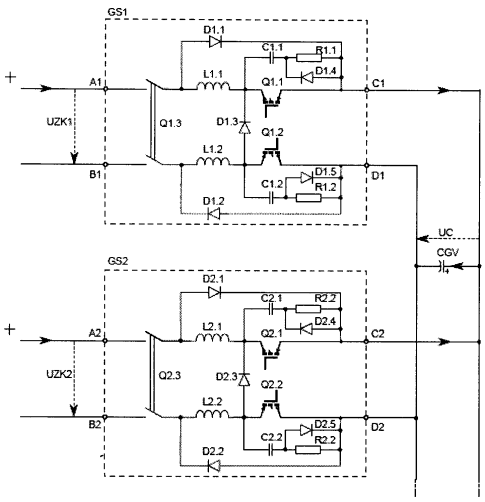

Beschreibung

[0001] Die Erfindung betrifft eine Produktionsanordnung mit wenigstens zwei Antriebssystemen der im Oberbegriff des Patentanspruchs 1 angegebenen Art.

[0002] Eine gattungsgemäße Produktionsanordnung ist aus der DE 10 2011 122 427 A1 bekannt. Die dort gezeigte Produktionsanordnung umfasst wenigstens zwei Antriebsysteme, welche jeweils zumindest eine elektrische Maschine umfassen, die über jeweilige bidirektionale elektrische Leistungswandler mit einem gemeinsamen, eine Plusleitung und eine Minusleitung umfassenden Gleichspannungsnetz elektrisch gekoppelt sind, wobei jeder der bidirektionalen Leistungswandler zumindest für eine der Leitungen ein Halbleiter-Schaltelement und eine Induktivität aufweist.

[0003] Es ist die Aufgabe der vorliegenden Erfindung, eine Produktionsanordnung der eingangs genannten Art bereitzustellen, mittels welcher ein verbesserter Energieaustausch zwischen den elektrischen Maschinen der Antriebssysteme der Produktionsanordnung ermöglicht wird.

[0004] Diese Aufgabe wird durch eine Produktionsanordnung mit den Merkmalen des Patentanspruchs 1 gelöst. Vorteilhafte Ausgestaltungen mit zweckmäßigen und nicht-trivialen Weiterbildungen der Erfindung sind in den abhängigen Ansprüchen angegeben.

[0005] Um einen verbesserten Energieaustausch zwischen den elektrischen Maschinen der unterschiedlichen Antriebssystemen der Produktionsanordnung zu ermöglichen, ist es bei der erfindungsgemäßen Produktionsanordnung vorgesehen, dass wenigstens einer der bidirektionalen Leistungswandler auch in der anderen Leitung ein Halbleiter-Schaltelement und eine Induktivität aufweist. Durch die erfindungsgemäße Lösung ist es gegenüber der aus der DE 10 2011 122 427 A1 bekannten Produktionsanordnung möglich, jeweilige Zwischenkreise der unterschiedlichen Antriebssysteme problemlos voneinander zu trennen, da kein gemeinsamer Minuspol mehr für die jeweiligen Antriebssysteme notwendig ist. Mit anderen Worten ist durch die erfindungsgemäße Lösung eine schnelle, allpolige Entkopplung möglich, wodurch sogenannte circular currents zwischen einem ausgeschalteten Antriebssystem und einem noch aktivierten Antriebssystem in der Produktionsanordnung effektiv vermieden wird.

[0006] In vorteilhafter Ausgestaltung der Erfindung ist es vorgesehen, dass zumindest der eine bidirektionale elektrische Leistungswandler, welcher auch in der anderen Leitung ein Halbleiter-Schaltelement aufweist, zusätzlich in dieser anderen Leitung eine Induktivität umfasst. Dadurch kann auf besonders einfache und effektive Weise eine Spannungswandlung in beiden Leitungen erfolgen, so dass beispielsweise bei einer wechselseitigen Spannungswandlung die jeweiligen Bauteile innerhalb der Plus- bzw. Minusleitung entlastet werden.

[0007] Eine weitere vorteilhafte Ausführungsform der Erfindung sieht vor, dass zumindest einer der bidirektionalen elektrischen Leistungswandler in wenigsten einer der Leitungen eine elektrische Dämpferschaltung umfasst, welche parallel zu dem Halbleiter-Schaltelement und der Induktivität angeordnet ist. Beispielsweise können in den jeweiligen Leitungen entsprechende Schalter vorgesehen sein, um abwechselnd eine entsprechende Spannungswandlung vornehmen zu können. Die Dämpferschaltung ist dazu ausgebildet, dabei auftretende Schaltungsenergien der jeweiligen Schalter aufzunehmen, so dass Spannungsspitzen und im Extremfall eine Zerstörung des entsprechenden Schalter, beispielsweise durch unerwünschte Lichtbögen, vermieden werden können.

[0008] Gemäß einer weiteren vorteilhaften Ausführungsform der Erfindung ist es vorgesehen, dass jeder der bidirektionalen elektrischen Leistungswandler zumindest in einer der Leitungen eine Diode umfasst. Durch die Diode wird ein Stromfluss in eine erste vorgegebene Richtung durch den bidirektionalen elektrischen Leistungswandler und durch Betätigung der besagten Schalter, ein entsprechender Stromfluss in eine zweite Richtung ermöglicht.

[0009] Schließlich ist es in weiterer vorteilhafter Ausgestaltung der Erfindung vorgesehen, dass zumindest einer der bidirektionalen elektrischen Leistungswandler einen elektromechanischen Schalter umfasst, mittels welchem die entsprechende elektrische Maschine von dem Gleichspannungsnetz entkoppelbar ist. Dadurch kann auf besonders einfache und sichere Weise die entsprechende elektrische Maschine bzw. das gesamte, zur elektrischen Maschine gehörende Antriebssystem von dem Gleichspannungsnetz entkoppelt und somit deaktiviert werden.

[0010] Weitere Vorteile, Merkmale und Einzelheiten der Erfindung ergeben sich aus der nachfolgenden Beschreibung eines bevorzugten Ausführungsbeispiels sowie anhand der Zeichnung. Die vorstehend in der Beschreibung genannten Merkmale und Merkmalskombinationen sowie die nachfolgend in der Figurenbeschreibung genannten und/oder in den Figuren alleine gezeigten Merkmale und Merkmalskombinationen sind nicht nur in der jeweils angegebenen Kombination, sondern auch in anderen Kombinationen oder in Alleinstellung verwendbar, ohne den Rahmen der Erfindung zu verlassen.

[0011] Die Zeichnung zeigt in:

[0012] **Fig.** 1 eine schematische Darstellung eines als Roboter ausgebildeten Antriebssystems, welches eine Mehrzahl von elektrischen Maschinen aufweist;

[0013] **Fig.** 2 eine schematische Darstellung einer Produktionsanordnung mit einer Mehrzahl von Antriebssystemen gemäß **Fig.** 1, wobei die Antriebssysteme über jeweilige bidirektionale elektrische Leistungswandler gemeinsam mit einem zur Energieversorgung dienenden Gleichspannungsnetz elektrisch gekoppelt sind;

[0014] **Fig.** 3 eine schematische Darstellung von einem der bidirektionalen elektrischen Leistungswandler; und in

[0015] **Fig.** 4 eine schematische Darstellung zweier miteinander gekoppelter Antriebssysteme, wobei lediglich die jeweils zugehörigen bidirektionalen elektrischen Leistungswandler dargestellt sind.

[0016] **Fig.** 1 zeigt schematisch ein als Roboter ausgebildetes Antriebssystem FT1. In **Fig.** 2 sind eine Mehrzahl derartiger Antriebssysteme FT1 bis FTn gezeigt. Derartige Antriebssysteme FT1 bis FTn können beispielsweise auch als Werkzeugmaschinen, als Fördereinrichtungen oder dergleichen ausgebildet sein.

[0017] Um teilweise sehr große Massen sehr dynamisch zu beschleunigen und abzubremsen, ist eine große elektrische Leistung notwendig, welche sich in großen Motorströmen widerspiegelt. Elektrische Antriebsmaschinen M1 bis Mm derartiger Antriebssysteme FT1 bis FTn können durch jeweils einen intelligenten Wechselrichter WR1 bis WRm angesteuert werden, der Drehzahl, Drehmoment und Drehrichtung vorgibt.

[0018] **Fig.** 1 zeigt einen schematischen Aufbau einer typischen Architektur eines derartigen Antriebssystems FT1, welches einen als Gleichspannungszwischenkreis ausgebildeten Zwischenkreis ZK1 aufweist, welcher einen Gleichrichter GR und einen oder mehrere Wechselrichter WR1 bis WRm umfasst. Der Gleichrichter GR versorgt somit über den Zwischenkreis ZK1 die verschiedenen Wechselrichter WR1 bis WRm mit Energie für die Bewegung der jeweiligen Antriebsmaschinen M1 bis Mm. Dazu ist er mit einem elektrischen Energieversorgungsnetz EV gekoppelt, welches als Wechselstromnetz ausgebildet ist. Jede einzelne Antriebsmaschine M1 bis Mm hat einen vorgelagerten Wechselrichter WR1 bis WRm, der die Ansteuerung für die jeweilige Antriebsmaschine M1 bis Mm übernimmt.

[0019] Die Antriebsmaschinen M1 bis Mm sind ebenfalls dazu ausgebildet, eine Bewegung des Antriebssystems FT1 bzw. der von der jeweiligen Antriebsmaschine M1 bis Mm angetriebenen Teile des Antriebssystems FT1 abzubremsen. In diesem Fall arbeiten die einzelnen Antriebsmaschinen M1 bis Mm nicht mehr in einem Motorbetrieb, in welchem sie zum Antrieb des Antriebssystems FT1 bzw. von den jeweils zu bewegenden Teilen arbeiten, sondern in einem Generatorbetrieb, und wandeln Bewegungsenergie in elektrische Energie um, im Folgenden als regenerative Energie bezeichnet. Diese wird wieder dem Zwischenkreis ZK1 hinzugefügt.

[0020] Wird eine Antriebsmaschine M1 bis Mm beschleunigt und eine andere zur gleichen Zeit abgebremst, hat dies den positiven Effekt, dass keine zusätzliche Energie aus dem elektrischen Energieversorgungsnetz EV entnommen werden muss, sondern die Energie zum Beschleunigen aus der regenerativen Energie einer anderen Antriebsmaschine M1 bis Mm verwendet werden kann. Somit fallen auch weniger Energiekosten für einen Betreiber des Antriebssystems FT1 an.

[0021] Werden von den elektrischen Antriebsmaschinen M1 bis Mm, die sich auf einem Zwischenkreis ZK1 befinden, gleichzeitig mehr Antriebsmaschinen M1 bis Mm abgebremst als beschleunigt, so kann ein Überangebot an Energie im Zwischenkreis ZK1 entstehen. Diese überschüssige Energie wird bei derartigen Antriebssystemen üblicherweise über einen Bremswiderstand BW in Wärmeenergie umgewandelt und steht somit für einen weiteren Antrieb des Antriebssystems FT1 nicht mehr zu Verfügung.

[0022] Eine energetische Kopplung mehrerer Zwischenkreise ZK1 bis ZKn ermöglicht diesen oben beschriebenen Energieaustausch nicht nur in einem einzigen Antriebssystem FT1, sondern eine Ausweitung auf mehrere Antriebssysteme FT1 bis FTn einer Produktionsanordnung FTA. Auf diese Weise kann der Energieverbrauch der Produktionsanordnung FTA mit mehreren Antriebssystemen FT1 bis FTn gesenkt werden. Eine derartige Produktionsanordnung FTA mit einer Mehrzahl von Antriebssystemen FT1 bis FTn ist in **Fig.** 2 näher dargestellt.

[0023] Um den Austausch der Energie zwischen verschiedenen Zwischenkreisen ZK1 bis ZKn der unterschiedlichen Anstriebssysteme FT1 bis FTn zu ermöglichen, ist eine kontrollierte energetische Kopplung mithilfe von bidirektionalen Leistungswandlern GS1 bis GSn erforderlich. Ein derartiger Leistungswandler GS1 ist in **Fig.** 3 dargestellt. Diese Leistungswandler GS1 bis GSn und die elektrische Kopplung der Zwischenkreise ZK1 bis ZKn über diese Leistungswandler GS1 bis GSn, welche in **Fig.** 4 anhand eines Beispiels mit zwei gekoppelten Zwischenkreisen ZK1, ZK2 näher dargestellt ist, ermöglichen es, rekuperierte, regenerative Energie unter den Zwischenkreise ZK1 bis ZKn antriebssystemübergreifend zu verteilen und bereitzustellen.

[0024] Nachfolgend wird die Funktionsweise des in **Fig.** 3 gezeigten Leistungswandlers GS1 exemplarisch für alle Leistungswandler GS1 bis GSn erläutert. Die Zwischenkreiskopplung der Zwischenkreise ZK1 bis ZKn der Produktionsanordnung FTA erfolgt mittels der bidirektionalen elektrischen Leistungswandler GS1 bis GSn, welche auch als Gleichspannungswandler, DC-DC-Spannungswandler oder als DC-DC-Wandler bezeichnet werden. Jeder Zwischenkreis ZK1 bis ZKn weist jeweils einen derartigen Leistungswandler GS1 bis GSn auf. Die Zwischenkreise ZK1 bis ZKn sind über ihre Leistungswandler GS1 bis GSn über ein gemeinsames Gleichspannungsnetz GV miteinander elektrisch gekoppelt. Die Gleichrichter GR1 bis GRn, welche in **Fig.** 2 nicht dargestellt sind, sind in den jeweiligen Antriebssystemen FT1 bis FTn weiterhin vorhanden. Das Gleichspannungsnetz GV dient hauptsächlich zum Austausch der regenerativen Energie zwischen den Antriebssystemen FT1 bis FTn. Dieses Gleichspannungsnetz GV kann zusätzlich, ohne Nebenwirkungen zwischen den einzelnen Gleichrichter GS1 bis GSn hervorzurufen, über einen zentralen Gleichrichter mit dem Energieversorgungsnetz EV oder mit einer Gleichstrom-Energiequelle verbunden sein.

[0025] Der in **Fig.** 3 dargestellte Leistungswandler GS1 weist einen ersten, einen zweiten, einen dritten und einen vierten Anschluss A1, B1, C1, D1 auf. Ein Eingangsschalter Q1.3 trennt die Anschlüsse A1 und B1 von der hier nicht gezeigten Leistungselektronik des Antriebssystems FT1. Nachfolgend wird ein Zustand beschrieben, in dem der Eingangsschalter Q1.3 geschlossen ist.

[0026] Der erste Anschluss A1 ist mit dem dritten Anschluss C1 über eine erste Leistungsdiode D1.1 in Durchlassrichtung verbunden. Der zweite Anschluss B1 ist mit dem vierten Anschluss D1 über eine zweite Leistungsdiode D1.2 in Sperrrichtung verbunden. Wird beim Bremsen Energie in den Zwischenkreis des Leistungswandlers GS1 zurückgespeist, steigt die Spannung über eine Ruhespannung Uref. Uref ergibt sich aus dem Effektivwert Uph des sinusformigen Niederspannungsnetzes von Dreiphasensystemen. Die gleichgerichtete Ruhespannung im Zwischenkreis hat ein festes Verhältnis zum Effektivwert:

$U_{ref} = U_{ph}\sqrt{2}$.

[0027] Ist eine Klemmenspannung UZK1 zwischen dem ersten und zweiten Anschluss A1, B1 des ersten Leistungswandlers GS1 nun größer als eine Netzspannung Uc des Gleichspannungsnetzes GV, wie in **Fig.** 4 dargestellt, dann fließt der Strom vom ersten Anschluss A1 zum dritten Anschluss C1 über die erste Leistungsdiode D1.1 in das Gleichspannungsnetz GV und vom vierten Anschluss D1 zum zweiten Anschluss B1 über die zweite Leistungsdiode D1.2.

[0028] Ist im ersten Zwischenkreis ZK1 ein Energiebedarf nötig und ist die Netzspannung Uc größer als die Klemmenspannung UZK1, wird der Stromfluss vom dritten Anschluss C1 zum ersten Anschluss A1 über einen Schalter Q1.1 gesteuert und der Stromfluss vom vierten Anschluss D1 zum zweiten Anschluss B1 über einen Schalter Q1.2 gesteuert. Abwechselnd wird der Strom in der Spulen L1.1 und L1.2 aufgeladen. Der Schalter Q1.1 wird in Abhängigkeit von der aktuellen Klemmenspannung UZK1 und der aktuellen Spannung Uc im Gleichspannungsnetz GV gesteuert.

[0029] Des Weiteren weist der Leistungswandler GS1 eine dritte Leistungsdiode D1.3 auf. Die Schalter Q1.1 und Q1.2 sind beispielsweise Bipolar-Transistoren mit einer isolierten Gate-Elektrode (IGBT), die den Strom nur eine Richtung fließen lassen, aber in entgegengesetzter Richtung arbeiten sie in Sperrrichtung, ähnlich wie eine Diode. Die Leistungsdiode D1.3 verringert den Lichtbogeneffekt, der beim Schalten vom Gleichstrom entsteht. Die Diode D1.4, der Kondensator C1.1 und der Widerstand R1.1 funktionieren wie ein Dämpferschema, welches die Schaltungsenergie vom Schalter Q1.1 aufnimmt. Identische Funktionalität haben die Elemente C1.2, D1.5 und R1.2 für den Schalter Q1.2.

[0030] Die Schaltungsausbildung der anderen Leistungswandler GS2 bis GSn ist analog. So weist, wie in **Fig.** 4 dargestellt, auch der zweite Leistungswandler GS2 entsprechend die vier Anschlüsse A2, B2, C2, D2 sowie die Dioden D2.1 bis D2.5, die Schalter Q2.1 bis Q2.3, die Spulen L2.1, L2.2, die Kondensatoren C2.1, C2.2 und die Widerstände R2.1 und R2.2 auf.

[0031] Der erste Zwischenkreis ZK1 des ersten Antriebssystems FT1 wird mit dem Plus- und Minuspol an den ersten und zweiten Anschluss A1, B1 des ersten Leistungswandlers GS1 angeschlossen und entsprechend geschlossen. Dies gilt analog auch für den zweiten Zwischenkreis ZK2 des zweiten Antriebssystems FT2, welches an die ersten und zweiten Anschlüsse A2, B2 des zweiten Leistungswandlers GS2 angeschlossen wird, an welchen die Klemmenspannung UZK2 des zweiten Zwischenkreises ZK2 anliegt, wie in **Fig.** 4 dargestellt. Analog gilt dies für die weiteren Zwischenkreise ZK3 bis ZKn aller weiteren Antriebssysteme FT3 bis FTn Leistungswandler GS3 bis GSn der Produktionsanordnung FTA. Für jeden angeschlossenen Zwischenkreis ZK1 bis ZKn ist somit also ein eigener Leistungswandler GS1 bis GSn erforderlich.

[0032] Der erste Leistungswandler GS1 ist mit seinem dritten und vierten Anschluss C1, D1 parallel zu dem dritten und vierten Anschluss C2, D2 des zweiten Leistungswandlers GS2 geschaltet, d. h. sie sind über das Gleichspannungsnetz GV parallel ge-

schaltet. Auch dies gilt analog für alle weiteren Leistungswandler GS3 bis GSn der Produktionsanordnung FTA, wie in **Fig.** 2 dargestellt, wodurch an allen Kontakten zum Gleichspannungsnetz GV die Netzspannung Uc anliegt.

[0033] Ein zentraler gemeinsamer Speicherkondensator CGV, mit welchem alle Zwischenkreise ZK1 bis ZKn über ihre Leistungswandler GS1 bis GSn gekoppelt sind, ist erforderlich, um die regenerative Energie aller Antriebssysteme FT1 bis FTn kurzzeitig zu speichern. Solange die Zwischenkreisspannung eines Antriebssystems FT1 bis FTn größer als die Netzspannung Uc im Gleichspannungsnetz GV ist, fließt der Strom über die Leistungsdioden D1.1 und D1.2 des entsprechenden Moduls. Somit wird die Energie zum gemeinsamen Gleichspannungsnetz GV übertragen. Sobald die Zwischenkreisspannung eines Antriebssystems FT1 bis FTn kleiner als die Netzspannung Uc wird, wirkt die jeweilige Leistungsdioden D1.1 und D1.2 in Sperrrichtung und die Steuerung des Stromflusses übernehmen die jeweiligen Schalter Q1.1 und Q1.2.

[0034] Nachfolgend werden vier unterschiedliche Betriebszustände des Leistungswandlers GS1 beschrieben.

1. Betriebszustand

[0035] Energie wird vom Zwischenkreis ZK1 des Antriebssystems FT1 zum gemeinsamen Gleichspannungsnetz GV übertragen. Der Strom fließt von A1 zu C1 und vom D1 zu B1 über die Leistungsdioden D1.1 und D1.2.

1.1. Voraussetzungen:

1.1.1. Die Zwischenkreisspannung UZK1 des Antriebssystems FT1 muss höher als die Spannung Uc des Gleichspannungsnetzes GV sein um einen Stromfluss zu ermöglichen.

1.2. Zustand des Leistungswandlers GS1:

1.2.1. Der Schalter Q1.1 ist aus und befindet sich dauerhaft in Sperrrichtung.
1.2.2. Die Leistungsdioden D1.1 und D1.2 befinden sich in Durchlassrichtung.
1.2.3. Der Schalter Q1.3 ist an.

2. Betriebszustand

[0036] Die Energie wird vom gemeinsamen Gleichspannungsnetz GV zum Zwischenkreis des Antriebssystems FT1 übertragen. Der Strom fließt von C1 zu A1 über den Schalter Q1.1 und die Drossel L1.1. Analog fließt der Strom von D1 zu B1 über den Schalter Q1.2 und die Drossel L1.2.

2.1. Voraussetzungen:

2.1.1. Die Spannung Uc des Gleichspannungsnetzes GV muss höher als die Zwischenkreisspannung UZK1 des Antriebssystems FT1 sein um einen Stromfluss zu ermöglichen.
2.1.2. Es muss ein Mindestspannung des Gleichspannungsnetzes GV in Höhe von Uref vorhanden sein, erst dann werden die Schalter Q1.1 und Q1.2 dauerhaft eingeschaltet.

2.2. Zustand des Leistungswandlers:

2.2.1. Die Schalter Q1.1 und Q1.2 sind an und befinden sich dauerhaft in Durchlassrichtung. Die Schalter Q1.1 und Q1.2 bleibend an, bis die Spannung Uc des Gleichspannungsnetzes GV unter die Mindestspannung Uref fällt oder die Spannung UZK1 des Antriebssystems FT1 höher als die Spannung Uc des Gleichspannungsnetzes GV ist.
2.2.2. Leistungsdioden D1.1 und D1.2 befinden sich in der Sperrrichtung.
2.2.3. Der Schalter Q1.3 ist an.

3. Betriebszustand

[0037] Der Leistungswandler GS1 befindet sich in einem Wartemodus. Es wird keine Energie über den Leistungswandler GS1 übertragen.

3.1. Voraussetzungen:

3.1.1. Die Spannung Uc des Gleichspannungsnetzes GV ist kleiner als Uref.
3.1.2. Die Zwischenkreisspannung UZK1 des Antriebssystems FT1 ist kleiner als Uc.

3.2. Zustand des Leistungswandlers GS1:

3.2.1. Die Schalter Q1.1 und Q1.2 sind ausgeschaltet.
3.2.2. Leistungsdioden D1.1 und D1.2 befinden sich in der Sperrrichtung.
3.2.3. Der Schalter Q1.3 ist an.

4. Betriebsmodus

[0038] Der Leistungswandler GS1 ist ausgeschaltet.

4.1. Es sind keine Mindestvoraussetzungen notwendig.
4.2. Zustand des Leistungswandlers:
4.2.1. Der Schalter Q1.3 ist aus.
4.2.2. Die Schalter Q1.1, Q1.2 und deren Steuerung sind ausgeschaltet.

[0039] Das Ziel der Schalter Q1.1 und Q1.2 ist es, die Spannung UZK1 genauso groß oder ein wenig größer als die Ruhespannung Uref zu halten und zu

regeln. Jeder Leistungswandler GS1 bis GSn wird einzeln und identisch zur bereits beschriebenen Vorgehensweise gesteuert. Durch das Koppeln mehrerer Zwischenkreise ZK1 bis ZKn wird die Energie von einigen Zwischenkreisen ZK1 bis ZKn entnommen und über das Gleichspannungsnetz GV an andere Zwischenkreise ZK1 bis ZKn weitergegeben. Je mehr Zwischenkreise ZK1 bis ZKn gekoppelt sind, desto kleiner kann der gemeinsame Speicherkondensator CGV dimensioniert werden.

[0040] Wenn die elektrischen Antriebsmaschinen M1 bis Mm beschleunigen, benötigen sie normalerweise mehr Energie als zum Halten einer konstanten Geschwindigkeit. Beschleunigen viele Antriebsmaschinen M1 bis Mm gleichzeitig, tritt im als Wechselstromnetz ausgebildeten Energieversorgungsnetz EV eine kurzfristige, sehr hohe Leistungsspitze auf. Um alle Lastspitzen im Stromnetz abdecken zu können, ist ein hoher Aufwand, insbesondere ein hoher Kostenaufwand für eine Infrastruktur erforderlich, beispielsweise für Transformatoren und Kabel.

[0041] In einer Produktionshalle hat eine derartige Produktionsanordnung FTA mit einer Zwischenkreiskopplung den zusätzlichen Vorteil, dass ein Teil des hohen Leistungsbedarfs wegfällt, da der Energiebedarf vom lokalen Gleichspannungsnetz GV ausgeglichen wird. Der Wegfall der Energiespitzen hat einen positiven Effekt auf das sinusförmige Wechselstromnetz, d. h. auf das Energieversorgungsnetz EV, so dass die gesamte harmonische Verzerrung des Energieversorgungsnetzes EV kleiner wird.

[0042] Viele Produktionsanordnungen nach dem Stand der Technik benötigen einen gewissen Anteil ihrer Energie zur Kühlung eines eigenen Schaltschrankes, da die regenerative Energie mit Hilfe des Bremswiderstandes BW im oder am Schaltschrank in Wärme umgewandelt wird. Da die auf den Bremswiderstand BW wirkende regenerative Energie bei der erläuterten Produktionsanordnung FTA deutlich geringer ist oder sogar gegen Null geht, erwärmt sich der Schaltschrank weniger, wodurch weniger Energie für dessen Kühlung erforderlich ist. Mit einer großen Anzahl zusammengeschlossener Zwischenkreise ZK1 bis ZKn kann die gesamte regenerative Energie der Anstriebssysteme FT1 bis FTn zwischen diesen ausgetauscht werden. In diesem Fall ist es möglich, einen besonders klein dimensionierten Bremswiderstand BW einzusetzen oder diesen völlig entfallen zu lassen.

ZITATE ENTHALTEN IN DER BESCHREIBUNG

Diese Liste der vom Anmelder aufgeführten Dokumente wurde automatisiert erzeugt und ist ausschließlich zur besseren Information des Lesers aufgenommen. Die Liste ist nicht Bestandteil der deutschen Patent- bzw. Gebrauchsmusteranmeldung. Das DPMA übernimmt keinerlei Haftung für etwaige Fehler oder Auslassungen.

Zitierte Patentliteratur

- DE 102011122427 A1 [0002, 0005]

Patentansprüche

1. Produktionsanordnung (FTA) mit wenigstens zwei Antriebssystemen (FT1, FT2), welche jeweils zumindest eine elektrische Maschine umfassen, die über jeweilige bidirektionale elektrische Leistungswandler (GS1, GS2) mit einem gemeinsamen, eine Plusleitung und eine Minusleitung umfassenden Gleichspannungsnetz (GV) elektrisch gekoppelt sind, wobei jeder der bidirektionalen Leistungswandler (GS1, GS2) zumindest für eine der Leitungen ein Halbleiter-Schaltelement (Q1.1, Q2.1) und eine Induktivität (L1.1, L2.1) aufweist, **dadurch gekennzeichnet,** dass wenigstens einer der bidirektionalen Leistungswandler (GS1, GS2) auch in der anderen Leitung ein Halbleiter-Schaltelement (Q1.2, Q2.2) und eine Induktivität (L1.2, L2.2) aufweist.

2. Produktionsanordnung (FTA) nach Anspruch 1, **dadurch gekennzeichnet,** dass zumindest der wenigstens eine bidirektionale elektrische Leistungswandler (GS1, GS2), welcher auch in der anderen Leitung ein Halbleiter-Schaltelement (Q1.2, Q2.2) aufweist, zusätzlich in dieser anderen Leitung eine Induktivität (L1.2, L2.2) umfasst.

3. Produktionsanordnung (FTA) nach Anspruch 1 oder 2, **dadurch gekennzeichnet,** dass zumindest einer der elektrischen bidirektionalen Leistungswandler (GS1, GS2) in wenigstens einer der Leitungen eine elektrische Dämpferschaltung umfasst, welche parallel zu dem Halbleiter-Schaltelement (Q1.1, Q1.2, Q2.1, Q2.2) und der Induktivität (L1.1, L1.2, L2.1, L2.2) angeordnet ist.

4. Produktionsanordnung (FTA) nach einem der vorhergehenden Ansprüche, **dadurch gekennzeichnet,** dass jeder der elektrischen bidirektionalen Leistungswandler (GS1, GS2) zumindest in einer der Leitungen eine Diode (D1.1, D1.2, D2.1, D2.2) umfasst.

5. Produktionsanordnung (FTA) nach einem der vorhergehenden Ansprüche, **dadurch gekennzeichnet,** dass zumindest einer der elektrischen bidirektionalen Leistungswandler (GS1, GS2) einen elektromechanischen Schalter (Q1.3, Q2.3) umfasst, mittels welchem die entsprechende elektrische Maschine von dem Gleichspannungsnetz (GV) entkoppelbar ist.

Es folgen 2 Seiten Zeichnungen

Anhängende Zeichnungen

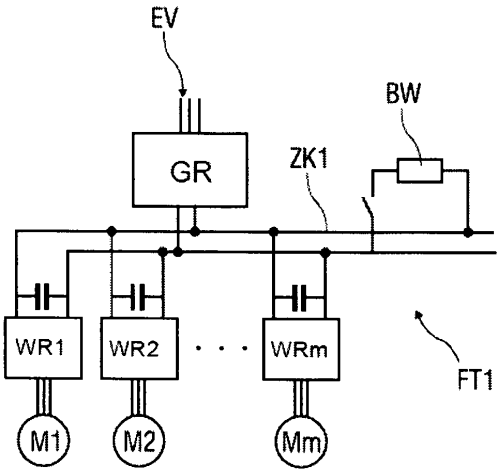

Fig.1

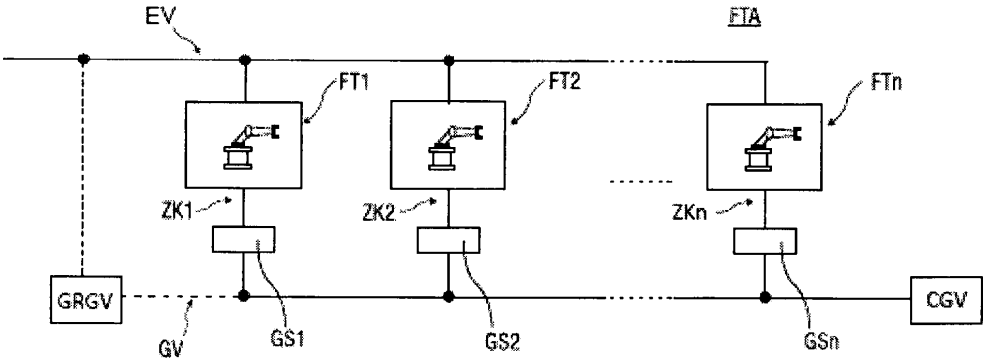

Fig.2

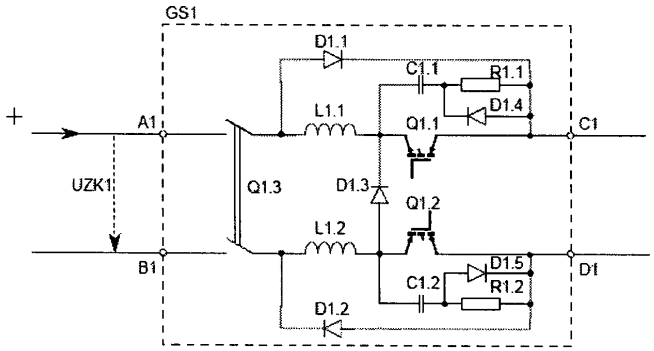
GS1
D1.1
C1.1
R1.1
D1.4
L1.1
Q1.1
C1
A1
+
UZK1
Q1.3
D1.3
Q1.2
L1.2
D1.5
C1.2
R1.2
D1
B1
D1.2

Fig.3

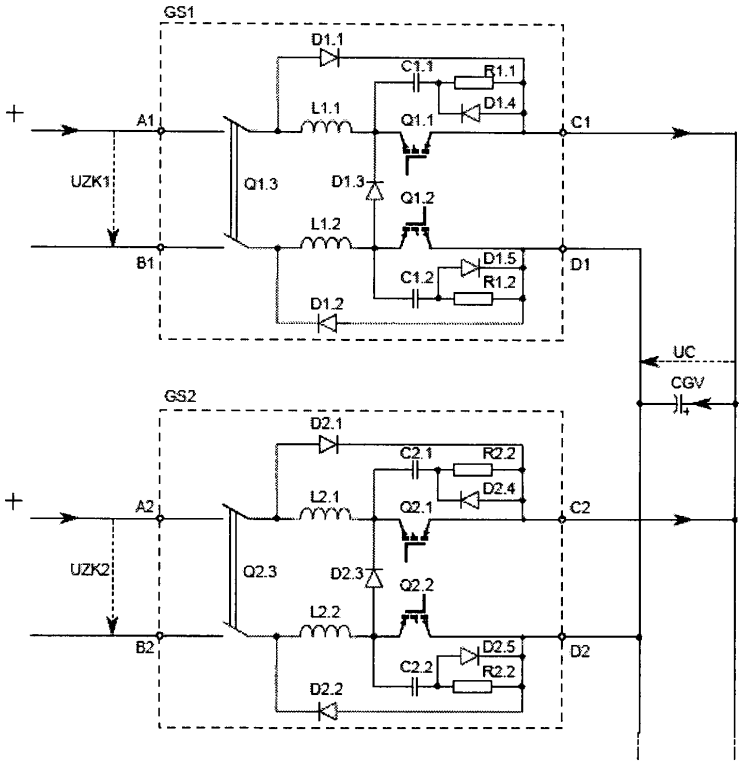
GS1
D1.1
C1.1
R1.1
D1.4
L1.1
Q1.1
C1
A1
+
UZK1
Q1.3
D1.3
Q1.2
L1.2
D1.5
C1.2
R1.2
D1
B1
D1.2
UC
CGV
GS2
D2.1
C2.1
R2.2
D2.4
L2.1
Q2.1
C2
A2
+
UZK2
Q2.3
D2.3
Q2.2
L2.2
D2.5
C2.2
R2.2
D2
B2
D2.2

Fig.4

Armands Šenfelds was born in 1986 in Riga. He received a Bachelor's degree in 2009 and a Master's degree in 2010 in Electrical Engineering from Riga Technical University (RTU), Latvia. In 2012, he received a Master's degree in Electrical Power Engineering from RWTH Aachen University, Germany. Since 2013, he has been a research assistant, researcher and lecturer at the Institute of Industrial Electronics and Electrical Engineering (IEEI) of Riga Technical University.

He has been a member of the IEEE association since 2008 and has served in various positions in the IEEE Latvian Section. He has been a Board member of the German Academic Exchange Service Alumni Club Latvia since 2013.

His research interests are related to power electronics for electrical drives, robotics, DC electrical systems, and efficient electrical energy utilization applications.